NATIONAL ADVISORY COMMITTEE FOR AERONAUTICS

TECHNICAL NOTE 3790

ANALYSIS OF WIND-TUNNEL TESTS TO A MACH NUMBER OF 0.90 OF A FOUR-ENGINE PROPELLER-DRIVEN AIRPLANE CONFIGURATION HAVING A WING WITH 40° OF SWEEPBACK AND AN ASPECT RATIO OF 10

By George G. Edwards, Donald A. Buell, Fred A. Demele, and Fred B. Sutton

Ames Aeronautical Laboratory
Moffett Field, Calif.

Washington
September 1956

1L

NATIONAL ADVISORY COMMITTEE FOR AERONAUTICS

TECHNICAL NOTE 3790

ANALYSIS OF WIND-TUNNEL TESTS TO A MACH NUMBER OF 0.90 OF A FOUR-ENGINE PROPELLER-DRIVEN AIRPLANE CONFIGURATION HAVING A WING WITH 40° OF SWEEPBACK AND AN ASPECT RATIO OF 10[1]

By George G. Edwards, Donald A. Buell, Fred A. Demele, and Fred B. Sutton

SUMMARY

An investigation has been conducted at speeds up to a Mach number of 0.90 to determine the effects of operating propellers on the longitudinal characteristics of a four-engine tractor airplane configuration having a 40° swept wing with an aspect ratio of 10. Results of wind-tunnel tests of a model representing such an airplane configuration (see NACA TN 3789) show that these effects are of most concern in the low-speed high-thrust flight regime. In the present report the low-speed data are analyzed to determine the source of the various effects and to indicate how the adverse effects can be reduced, and the high-speed data are discussed primarily from the standpoint of Mach number effects. The data on which the analysis is based were obtained in tests of a semispan model with reflection-plane mounting, representing the right-hand side of a hypothetical airplane. Single-rotation, right-hand propellers were operated at values of thrust coefficient ranging from 0 to 0.9 per propeller. The thrust coefficient was sufficient to simulate 10,000 horsepower per engine at sea level at speeds down to 120 miles per hour, assuming the model to be 1/12 scale. Variations in the model geometry included several heights and incidences of the horizontal tail as well as tail removed, two arrangements of extended split flaps, several propeller-blade angles, and independent as well as simultaneous operation of the inboard and outboard propellers.

The analysis of the low-speed data indicates that the large variations of longitudinal stability with angle of attack resulted primarily from passage of the tail into and out of the slipstream. The slipstreams also created large lift increments on the wing, particularly with flaps deflected, which resulted in increases in stability (with increasing thrust coefficient) from the outboard propeller and decreases in stability from the inboard propeller. It was concluded that the longitudinal stability characteristics of the model could be improved by moving the nacelles outward, increasing the tail height, and reducing the tail span.

[1]Supersedes NACA RM A54F14 by George G. Edwards and Donald A. Buell, 1954, and also includes the analysis from NACA RM A53J23 by Fred B. Sutton and Fred A. Demele, 1954.

Estimates of the stability with nacelles moved 0.1 of the semispan outboard of their original position are shown, along with estimates of rolling and yawing moments resulting from loss of thrust on an outboard engine.

A study of the high-speed data indicates that the effects of operating propellers on the longitudinal characteristics of the model were comparatively small at high subsonic speeds.

The propulsive characteristics of the model are presented and compared with those of the isolated propeller for both low-speed and high-speed conditions of operation.

INTRODUCTION

The potentialities of the turbine-propeller propulsion system, particularly with regard to take-off and range characteristics of multiengine airplanes, have stimulated interest in the long-range turboprop airplane designed to fly at high subsonic speeds. A practical airplane configuration for this application appears to be one utilizing a sweptback wing of high aspect ratio in combination with tractor-mounted supersonic propellers. The effects of these highly loaded propellers on the flow over the swept wing and tail surfaces and the consequent effects on the longitudinal characteristics of the airplane cannot be estimated with confidence on the basis of existing experimental data or by theoretical methods. Applicable experimental data are meager, and existing theoretical methods, developed for airplanes with low propeller-disc loadings and unswept wings, are of doubtful validity for the arrangement considered.

An investigation has been conducted in the Ames 12-foot pressure wind tunnel to determine the longitudinal characteristics of a representative multiengine airplane configuration with sweptback wing of high aspect ratio. The investigation included wind-tunnel tests of a model with and without supersonic-type propellers. The power-off longitudinal characteristics of several combinations of the components of this airplane configuration have been presented in references 1 to 4. The results of power-on tests at low and at high subsonic speeds have been presented without analysis in reference 5.

The present report is concerned with an analysis of the data presented in reference 5. The sources of the large effects of operating propellers indicated in the low-speed data are traced in an effort to indicate those design features which would reduce adverse effects of operating propellers on the longitudinal characteristics of this type of airplane. Calculated static longitudinal stability characteristics are presented for a revised airplane configuration. Also investigated is the propulsive efficiency of the configuration tested and its relation to the efficiency of the isolated propeller.

NOTATION

A	upflow angle, average angle of local flow at the 0.7 propeller radius on the horizontal center line of the propeller plane, measured with respect to the thrust axis in a plane parallel to the plane of symmetry
a	mean-line designation, fraction of chord over which design load is uniform
a'	normal acceleration
a_t	lift-curve slope of the isolated tail
a_w	lift-curve slope of the model, tail off
b/2	wing semispan perpendicular to the plane of symmetry
b'	propeller-blade width
C_L	lift coefficient, $\frac{\text{lift}}{qS}$
C_l	rolling-moment coefficient, $\frac{\text{rolling moment (for complete airplane)}}{q(2S)b}$
C_m	pitching-moment coefficient about the quarter point of the wing mean aerodynamic chord, $\frac{\text{pitching moment}}{qS\bar{c}}$
$C_{m_{cg}}$	pitching-moment coefficient about the center of gravity, $\frac{\text{pitching moment}}{qS\bar{c}}$ (See fig. 1(a).)
C_N	propeller normal-force coefficient, $\frac{N}{q\frac{\pi D^2}{4}}$
C_n	yawing-moment coefficient, $\frac{\text{yawing moment (for complete airplane)}}{q(2S)b}$
C_P	power coefficient, $\frac{P}{\rho n^3 D^5}$
$C_{P_{total}}$	sum of the power coefficients for both propellers
C_T	thrust coefficient, $\frac{T}{\rho n^2 D^4}$

$C_{T_{total}}$ propulsive thrust coefficient for complete model (both propellers operating), $-\frac{SJ^2}{2D^2}\left(C_{X_{props\ on}} - C_{X_{props\ off}}\right)_{\alpha=constant}$

C_X longitudinal force coefficient, $\frac{X}{qS}$

c local wing chord parallel to the plane of symmetry

c' local wing chord normal to the reference sweep line (See table I.)

$\bar{c}$ wing mean aerodynamic chord, $\frac{\int_0^{b/2} c^2 dy}{\int_0^{b/2} c\, dy}$

c_{l_i} wing-section design lift coefficient

D propeller diameter

g acceleration due to gravity

h maximum thickness of propeller-blade section

i_t incidence of the horizontal tail with respect to the wing-root chord

J propeller advance ratio, $\frac{V}{nD}$

l_t tail length, distance between the quarter points of the mean aerodynamic chords of the wing and the horizontal tail, measured parallel to the plane of symmetry

M free-stream Mach number

N normal force per propeller, perpendicular to the propeller shaft in a vertical plane

n propeller rotational speed

n' normal acceleration factor, $\frac{a'}{g}$

P shaft power per motor

q free-stream dynamic pressure, $\frac{\rho V^2}{2}$

q_t effective dynamic pressure at the tail

q_{ss} local dynamic pressure in the slipstream at the tail

R Reynolds number, based on wing mean aerodynamic chord

R'	propeller-tip radius
r	propeller-blade-section radius
S	area of the semispan wing, flaps off
S_t	area of semispan tail
T	thrust per propeller, parallel to free stream
T_c	thrust coefficient per propeller, $\frac{T}{\rho V^2 D^2}$
t	wing-section maximum thickness
V	free-stream velocity
$\overline{V}$	tail volume, $\frac{l_t S_t}{\bar{c} S}$
W	weight of assumed full-scale airplane
X	longitudinal force, parallel to stream and positive in a drag-wise direction
Δx	longitudinal distance from the quarter point of the mean aero-dynamic chord to a more rearward moment center
y	lateral distance from the plane of symmetry
α	angle of attack of the wing chord at the plane of symmetry (referred to herein as the wing-root chord)
α_t	angle of attack of the tail
β	propeller-blade angle measured at 0.70 tip radius
β'	propeller-blade-section angle
ϵ	effective downwash angle
δ	flap angle, measured relative to the local chord in planes normal to the reference sweep line
η	propeller or propulsive efficiency
$\eta_t \frac{q_t}{q}$	tail-efficiency factor (ratio of the lift-curve slope of the horizontal tail when mounted on the model to the lift-curve slope of the isolated horizontal tail)
ρ	mass density of air

φ angle of local wing chord relative to the wing-root chord, positive for washin, measured in planes parallel to the plane of symmetry

$\frac{dC_m}{di_t}$ tail effectiveness parameter, measured at a constant angle of attack

Subscripts

av average

trim indicates condition of C_m or $C_{m_{cg}} = 0$

w wing

t tail

SELECTION OF MODEL

Design of the model was based on some of the requirements of an assumed airplane capable of long-range operation at a cruising speed of 550 miles per hour at an altitude of 40,000 feet (M = 0.83) with wing loadings of the order of 75 to 100 pounds per square foot (C_L = 0.4 to 0.5). This section of the report will be devoted to a brief discussion of the factors which were considered in the design of the model. More detailed discussion of this subject will be found in reference 1 (wing, fuselage, fences), reference 2 (all-movable tail), reference 4 (nacelles), and reference 5 (flaps).

A semispan model was used in preference to a sting-mounted, full-span model primarily because of the larger size permissible with the semispan model, which resulted in increased Reynolds number as well as more space within the model for oil, water, electric, and air lines. Limitations of this arrangement are that only longitudinal characteristics can be determined and that the direction of rotation of the propellers of the image wing is always opposite to that on the semispan wing itself. The semispan model was designed to represent to 1/12 scale the right-hand side of a hypothetical four-engine airplane having right-hand propellers on the right wing and left-hand propellers on the left wing. Details of the model are presented in figure 1 and in table I. Photographs of the model mounted in the wind tunnel are presented in figure 2.

The wing incorporates a number of features designed to alleviate the longitudinal stability difficulties usually associated with flow separation on sweptback wings of high aspect ratio. These features include cambered wing sections having NACA four-digit thickness distribution (comparatively large leading-edge radius), twist to reduce the load on the outer portions of the wing, and chordwise fences on the upper surface

to reduce spanwise flow of the boundary layer and improve the spanwise distribution of load. The spanwise variation of twist and of section maximum thickness ratio shown in figure 1(b) was determined by the requirement that spanwise elements on the wing surfaces be linear. The wing design is therefore not necessarily optimum from an aerodynamic standpoint.

The fuselage (coordinates given in table I) was a half-body of revolution composed of a cylindrical midsection with simple fairings fore and aft. The wing was mounted high on the fuselage at 3° incidence as shown in figure 1(a). Compared to a lower position, this wing position is favorable in that it results in a higher thrust axis relative to the airplane center of gravity (more negative pitching moments due to thrust) while maintaining an under-wing mounting of the nacelle. The all-movable horizontal tail was arranged for testing at various heights (fig. 1(a)).

The shape and size of the nacelles (fig. 1(c)), as well as their locations with respect to the plane of the wing-root chord and leading edge, were governed to a considerable extent by considerations other than aerodynamic. These considerations included space requirements for electric motors and gear boxes for driving model propellers, and provisions for access and removal of these units without impairing the strength of the wing. The aerodynamic qualities of the nacelles in regard to drag and interference effects are probably adversely affected by the previously mentioned requirements which resulted in somewhat larger nacelles than would be required by the engines of the assumed airplane. As may be observed from figure 1(c), the nacelles were inclined downward at a considerable angle with respect to the wing (inboard nacelle -6.5° and outboard nacelle -7.0°). The resulting inclination of the thrust axes was intended to minimize the forces exciting first-order vibratory stresses in the propeller since, if the angles are properly selected, taking into account upwash from the wing, fuselage, and nacelles, the positive upflow angles induced at the low-speed high-gross-weight condition result in excitation forces equal in magnitude to those resulting from the negative upflow angles at the high-speed low-gross-weight condition. For the speed range of a modern high-performance airplane, this inclination of the thrust axis will result in about zero excitation for the design cruise condition. The thrust axis inclination for the model was calculated in accordance with the theoretical method described in Appendix B of reference 6 to provide zero upflow at the assumed cruise condition ($C_L = 0.40$, $M = 0.83$). The adequacy of such calculations was subsequently verified in the investigation of reference 7 wherein the actual upflow angles were measured on the model.

A three-blade supersonic propeller, designated the NACA 1.167-(0)(03)-058 and having right-hand rotation, was used in the high Mach number tests of the model. This propeller was a 1/12-scale model of a propeller for the assumed airplane, designed to absorb 5000 horsepower with an efficiency of 75 percent at a forward Mach number of 0.83 and an altitude of 40,000 feet. The high-speed tests were conducted with propellers operating at approximately full-scale Mach numbers, blade angles,

and advance ratios. For the low-speed tests, however, a thicker propeller was necessary because of the very high blade loadings accompanying operation in the wind tunnel at an air density of 6 atmospheres. This propeller, designated the NACA 1.167-(0)(05)-058, was identical to the NACA 1.167-(0)(03)-058 propeller except that the blade thicknesses were increased by a factor of 5/3 at all radial stations. Blade-form curves for these propellers are presented in figure 3. The low-speed tests were conducted with propellers operating at approximately full-scale blade angles and advance ratios, but at reduced forward speed due to load limitations of the propeller and power limitations of the model motor and gear box. It should be pointed out that in consequence the model propeller operated with section Mach numbers which were everywhere subsonic during these tests at low speeds, whereas, the full-scale constant-speed propeller would operate with supersonic local Mach numbers near the blade tip even at zero forward speed.

Two arrangements of extended split flaps were tested on the model, as illustrated in figure 1(d). In the arrangement designated "inboard flaps," the flaps extended from the fuselage to the outer nacelle, and in the second arrangement, designated "outboard flaps," they extended from the inboard nacelle to 70 percent of the semispan. The gaps between the flaps and the wing trailing edge, nacelles, and fuselage were sealed. The outboard-flap arrangement was devised after tests with inboard flaps showed severe destabilizing effects due to propeller operation.

TESTS

Test Conditions and Procedure

The majority of the low-speed tests upon which the data analysis is based were made at a Mach number of 0.082, a Reynolds number of 4,000,000, and a propeller-blade angle β of 26°. The corresponding dynamic pressure q of the air stream was approximately 57 pounds per square foot. Other low-speed tests were made at Mach numbers of 0.082 to 0.165, Reynolds numbers of 4,000,000 to 8,000,000, and with propeller-blade angles from 21° to 36°.

The major portion of the high-speed tests was made over a range of Mach numbers from 0.60 to 0.90 at a Reynolds number of 1,000,000 and a blade angle of 51°; however, data were also obtained at a Reynolds number of 2,000,000 and at a blade angle of 41°. The angle-of-attack range was 2° to 18° for the tests at low Mach numbers and 2° to 10° for the tests at the higher Mach numbers. The model was tested both with and without the horizontal tail, flaps, and propellers. The tail was mounted at various angles of incidence and at heights of the hinge axis of 0, 0.05, 0.10, or 0.15 of the wing semispan (see fig. 1(a)). Both the inboard flaps and the outboard flaps (fig. 1(d)) were attached at 30° of deflection δ.

At each angle of attack, the Mach number and the Reynolds number were held constant while data were obtained for several propeller rotational speeds from windmilling to the maximum attainable, the latter being limited by either the maximum power or the maximum rotational speed of the electric motor.

Measurements of the static pressures on the wind-tunnel walls during the tests at a Mach number of 0.90 indicated the possibility of partial choking of the wind tunnel. It is believed that the force and moment data shown for this Mach number are affected to some extent by this phenomenon.

Propeller Calibration

The propellers were calibrated on a specially constructed calibration nacelle. With this equipment the thrust and power characteristics of the propellers in the presence of the spinner and nacelle forebody were measured at several angles of attack for the range of test conditions covered in the tests of the complete model. Also measured were the normal force characteristics of the propellers which included an increment of normal force due to the effect of slipstream on the nacelle forebody.

REDUCTION OF DATA

The shaft thrust (parallel to the propeller shaft) and the normal force (perpendicular to the propeller shaft) were determined from the propeller calibration at Mach numbers, Reynolds numbers, propeller-blade angles, advance ratios, and upflow angles A corresponding to the complete-model test conditions. The upflow angle for the complete model without flaps and with power off was the average at the 0.7 propeller radius on the horizontal center line of the propeller plane and was based on the measured values presented in reference 7. These propeller forces were used to determine the thrust parallel to the free stream and hence the thrust coefficient T_c used herein. This thrust coefficient is essentially constant with upflow angle. Typical variations of thrust coefficient T_c with advance ratio J are shown in figures 4 and 5.

The results of the propeller normal-force measurements (which include the increment of normal force due to slipstream effect on the nacelle forebody) obtained during the calibration of the propellers are presented in figures 6 and 7. The conditions for matching these data to those for the complete model were similar to those for matching T_c, except that in this case, the direct use of the measured values of A presented in reference 7 for the complete model without flaps and power off was not sufficiently accurate because of the close dependence of normal force on the value of A. Modification of these measured values of A was made to allow for changes in upwash due to lift changes caused by slipstream on the wing and by deflection of the flaps. The correction was made using a theoretical value of the rate of change of upwash angle with lift

coefficient at the propeller planes, along with the increments of lift due to slipstream and due to flaps on the wing as deduced from the force data.

In several instances, data are presented herein for a constant power condition, based on an assumed model scale of 1/12. The relationships between T_c and C_L are shown in figure 8 for a 200,000-pound airplane in level flight at sea level and in figure 9 for a 150,000-pound airplane in level flight at 40,000 feet with constant-speed propellers turning at 1715 rpm. Also shown in figure 8 are the variations of propeller efficiency and blade angle with velocity, determined from the propeller calibration.

TEST RESULTS

The basic data obtained in the tests of the powered model have been presented in reference 5. Figures 10 and 11 of this report are examples of the basic data for conditions of low and high speed, respectively; that is, lift, longitudinal force, and pitching-moment coefficients, plotted in conventional form for constant values of thrust coefficient, T_c. The range of configurations and test conditions for which data are available is indicated in table II of this report.

Low-Speed Conditions

Increases in Reynolds number (to obtain flow conditions more nearly like those at full scale) and in Mach number (to increase the stream dynamic pressure and thus the accuracy of measurements) reduced the thrust coefficient which could be obtained with the model motor power available at any given propeller-blade angle. In figure 12 the longitudinal characteristics of the model (tail off) at various Reynolds numbers and Mach numbers are compared. The effects of changes in propeller-blade angle on the longitudinal characteristics of the model are shown in figure 13. It is apparent that within the range of these tests the effects of changes in Reynolds number and Mach number are of secondary importance. The data of figure 13 indicate somewhat larger effects of changes in propeller-blade angle. The differences in pitching-moment characteristics of the model may be attributed primarily to changes in propeller normal force and slipstream rotation accompanying changes in propeller-blade angle. The indicated differences in longitudinal-force coefficient C_X, however, are believed to be largely scatter resulting from inaccuracies in establishing the thrust coefficient T_c. Most of the discussion will concern data obtained at a Reynolds number of 4,000,000, a Mach number of 0.082, and a propeller-blade angle of 26°, for which conditions the highest thrust coefficients could be obtained.

High-Speed Conditions

Lift-curve slopes, pitching-moment-curve slopes, and longitudinal-force coefficients for the model are presented in figure 14 for Reynolds numbers of 1,000,000 and 2,000,000, for blade angles of 41° and 51°, and at Mach numbers from 0.70 to 0.90. At Mach numbers of 0.70 and 0.80 the effects of varying Reynolds number and blade angle were quite small. However, at a Mach number of 0.90 there were large changes in the force- and moment-curve slopes and in the longitudinal force as a result of increasing the Reynolds number from 1,000,000 to 2,000,000. It is felt, however, that the data for this Mach number might have been affected to some extent by the phenomenon of partial choking of the wind tunnel.

DISCUSSION OF LOW-SPEED CONDITIONS

The results presented in reference 5 show some rather large effects of operating propellers on the longitudinal characteristics of this airplane configuration at low speeds. In order to indicate the factors which caused the over-all observed effects, the discussion will begin with the results of an analysis of the data in terms of the various increments of lift and pitching moment derived from direct propeller forces, slipstream effects on the wing, and slipstream effects on the tail. Direct comparisons of the data are then presented to show the influence of configuration changes on the pitching-moment characteristics, followed by an analysis of static longitudinal stability in terms of several well-known parameters. The objective of this analysis is, of course, to indicate not only the magnitude of the various effects, but also the means whereby the adverse effects of propellers on static longitudinal stability can be reduced.

Components of the Lift Changes Due to Operating Propellers

The operating propellers create components of lift, either directly from the shaft thrust and normal force of the propeller or indirectly as a result of the effects of the propeller slipstream on the wing and the horizontal tail. These components of lift are important because not only do they affect the total lift but they usually influence the longitudinal stability and trim of the airplane.

Increments of lift from direct propeller forces.- The shaft-thrust and normal-force data measured in the propeller calibration were resolved into incremental lift coefficients, taking account of the upflow angles prevailing on the complete model as compared to those on the calibration nacelle (see section entitled "REDUCTION OF DATA"). The calculated incremental lift coefficients from each propeller operating on the model at several constant thrust coefficients are shown in figure 15 for a range of angles of attack. Since the over-all effect on lift is small, the data shown may be considered to apply to either the inboard or the outboard

propeller operating with wing flaps up or with either of the two flap configurations. A check showed the differences in lift-coefficient increment for these various conditions to amount to less than 0.01.

Increment of lift from slipstream on the wing.- The increments of lift coefficient attributable to the effects of the propeller slipstream on the wing and rear portion of the nacelles have been calculated from the data for various model configurations and are shown in figures 16 and 17. The method of obtaining this incremental lift coefficient, $\Delta C_{L_{wing}}$, was as follows:

$$\Delta C_{L_{wing}} = C_{L_1} - C_{L_2} - \Delta C_{L_{\substack{\text{propeller-nacelle} \\ \text{normal force}}}} - \Delta C_{L_{\substack{\text{propeller shaft} \\ \text{thrust}}}}$$

where

C_{L_1} lift coefficient of the model with tail off and with propellers operating at given thrust coefficient

C_{L_2} lift coefficient of the model with tail off and with propellers off

This increment in lift coefficient includes power effects on the rear portion of the nacelle and all wing-nacelle interference resulting from the slipstream. Referring to figure 16, it may be seen that with flaps up, $\Delta C_{L_{wing}}$ was negative at angles of attack below 4° or 5°, despite the fact that portions of the wing immersed in the slipstream were operating at section lift coefficients of the order of 0.35, power off. Comparison of $\Delta C_{L_{wing}}$ for both propellers operating (flaps up or flaps down) with the sum of values of $\Delta C_{L_{wing}}$ measured for inboard and outboard propellers operated independently generally shows some positive interference lift. In regard to figure 17, it is noted that changing from inboard flaps to outboard flaps decreased $\Delta C_{L_{wing}}$ but had little effect on the rate of change of $\Delta C_{L_{wing}}$ with angle of attack.

Increment of lift from tail.- For a constant tail incidence the increment of lift due to the effects of power on the tail is dependent upon tail height and incidence as well as on flap configuration. However, the increment of lift due to the effects of power on the tail can hardly be discussed without reference to the pitching-moment changes involved, since the lift on the tail must be that to balance the airplane. This will be discussed in succeeding paragraphs.

Components of the Pitching-Moment Changes Due to Operating Propellers

The application of power results in changes of pitching moment, due in a large measure to the fact that the centers of the lift increments previously discussed are at some distance from the reference center of moments. The various components of the change in pitching moment can therefore be classified in the same manner as the lift changes of the

previous section, that is, according to whether they arise from the direct forces of the propeller (normal force and thrust), or whether they result from the effects of the propeller slipstream on the wing or on the tail. The components will be considered in that order.

Increments of pitching moment from direct propeller forces.- The normal force of the propeller (including the increment in normal force due to slipstream effect on the nacelle forebody) can be considered to act in the plane of the propeller[2] and the pitching moment from this source is simply the normal force times the distance to the moment center. The increments of pitching-moment coefficient due to normal forces created by the operating propellers are shown in figure 18. The swept-wing configuration with tractor propellers inherently has larger pitching-moment increments from propeller normal force than a corresponding straight-wing configuration because the propeller must be farther forward to maintain a given clearance between the wing and the inboard propeller tip.

The increments of pitching-moment coefficient due to shaft thrust of the operating propellers (thrust parallel to the shaft times the distance to the moment center) are shown in figure 19. It is obvious that changes in the vertical location of the propellers with respect to the center of gravity can materially affect the magnitude of these increments in pitching-moment coefficient.

Increment of pitching moment from slipstream on the wing.- The increments of pitching-moment coefficient attributable to the effects of the propeller slipstream on the wing and on the rear portion of the nacelles have been calculated from the data for various model configurations and are shown in figures 20 and 21. The method of obtaining this incremental pitching-moment coefficient, $\Delta C_{m_{wing}}$, was as follows:

$$\Delta C_{m_{wing}} = C_{m_1} - C_{m_2} - \Delta C_{m_{\substack{\text{propeller-nacelle} \\ \text{normal force}}}} - \Delta C_{m_{\substack{\text{propeller shaft} \\ \text{thrust}}}}$$

where

C_{m_1} pitching-moment coefficient of the model with tail off and with propellers operating at the given thrust coefficient

C_{m_2} the pitching-moment coefficient of the model with tail off and with propellers off

and all pitching-moment coefficients are referred to the 1/4 point of the mean aerodynamic chord.

The increments of pitching-moment coefficient due to the effects of the slipstream on the wing are closely related to the local lift changes which occur and their location along the span of the wing. Hence, such configuration characteristics as spanwise position of the nacelles and spanwise extent of the flaps are dominant factors affecting the magnitude of this increment of pitching-moment coefficient. Referring to figure 20,

[2]The pitching moment of the propeller-nacelle combination about the intersection of the thrust axis with the plane of the propeller was found to be negligible.

it is noted that with flaps up $\Delta C_{m_{wing}}$ is positive, due almost entirely to the influence of the inboard propeller. There were no large changes in the variation of $\Delta C_{m_{wing}}$ with α due to lowering the inboard flaps. In figure 21 it can be seen that the change from inboard to outboard flaps made $\Delta C_{m_{wing}}$ much more negative but had little effect on its variation with α.

Increment of pitching moment from tail.- The increments of pitching-moment coefficient attributable to the effects of operating propellers on the tail (at constant incidence) were calculated as follows:

$$\Delta C_{m_{tail}} = \left(C_{m_{tail\ on}} - C_{m_{tail\ off}}\right)_{power\ on} - \left(C_{m_{tail\ on}} - C_{m_{tail\ off}}\right)_{power\ off}$$

Figure 22 gives values of the increment for one tail incidence, flaps up, and demonstrates the large moments that are incurred from this source. These data also illustrate the importance of the vertical location of the horizontal tail on $\Delta C_{m_{tail}}$.

The pitching moment contributed by the tail can be expressed as

$$C_{m_{tail}} = - a_t \bar{V}(\alpha + i_t - \epsilon)\ \eta_t \frac{q_t}{q} \qquad (1)$$

For a given tail incidence, the lift on the tail, and thus the pitching moment due to the tail, is dependent on the downwash and the dynamic pressure at the tail, both of which will be affected by operation of the propellers. A study of the effects of propeller slipstream on the parameters ϵ and $\eta_t(q_t/q)$ provides some insight into the flow changes at the tail which produce pitching-moment changes.

The parameter $\eta_t(q_t/q)$, calculated from the force data by means of the equation

$$\eta_t \frac{q_t}{q} = - \frac{dC_m}{di_t} \frac{1}{a_t \bar{V}} \qquad (2)$$

is presented in figure 23 as a function of angle of attack for various constant thrust conditions and for propellers off. (The value of a_t was taken as 0.059 per degree based on experimental data for the isolated tail presented in reference 2.) Data are compared for two different tail heights (0 and 0.10 b/2), approximately one propeller radius apart, with flaps up and with either the inboard or the outboard flaps deflected. The data in figure 23 are useful for ascertaining the approximate location of the slipstream relative to the tail. It is observed that deflection of the inboard flaps moved the slipstream downward to the extent that it missed the high tail even at high angles of attack; whereas, deflection of the outboard flaps moved it down only a small amount in the region of the tail.

The effective angles of downwash ϵ, calculated from the force data by means of the equation

$$\epsilon = \alpha + i_t - \frac{\left(C_{m_{\text{tail on}}} - C_{m_{\text{tail off}}}\right)_{\alpha=\text{constant}}}{\frac{dC_m}{di_t}} \qquad (3)$$

are presented in figure 24. The variation of ϵ is affected by a number of factors, some of which have opposing effects, and the relative importance of each is difficult to ascertain from the data available. The data in figures 23 and 24 indicate that the variation of ϵ with α at constant T_c and the variation of ϵ with T_c at constant α are greatly dependent on the location of the tail relative to the slipstream. Also very important in its effect on ϵ is the location of the tail in the field of downwash from the wing itself. Over most of the angle-of-attack range, an increase of T_c increased the lift on the wing (see fig. 16) which by itself would increase the downwash and also move downward the point of maximum downwash. However, it can be seen in figure 24 that there is a general reduction in the effect of increasing T_c on ϵ for those instances where the tail is in the slipstream (see fig. 23).

Comparison of pitching-moment increments.- The relative magnitude of the various pitching-moment-coefficient increments due to the effects of power and an indication of the effects on static longitudinal stability are shown in figure 25 (flaps up) and figure 26 (inboard flaps deflected). In these figures only, the pitching-moment coefficients have been referred to a new moment center which is more representative of the vertical height of the center of gravity for the assumed full-scale airplane. The longitudinal location of this assumed center of gravity is maintained at the quarter point of the mean aerodynamic chord but its vertical location is lowered $0.10\bar{c}$ (see fig. 1(a)). The effect of this change of moment center is to nearly eliminate the shaft thrust contribution to pitching moments without materially changing any of the other increments. From figures 25 and 26 it may be observed that the propeller normal force contributed a general increase in slope of the pitching-moment-coefficient curve, even at zero thrust, and the effect was, as might be expected, essentially independent of changes of flap configuration or tail height. For constant T_c the slipstream on the wing contributed an increase in moment, but no general change in slope of the pitching-moment-coefficient curve. The tail contribution as a function of angle of attack was extremely variable compared to the other components. This was, of course, due to the variation in tail lift as the tail moved into or out of the slipstream. Changes of tail height and deflection of flaps strongly influenced the pitching moment contributed by the tail.

In figures 27 and 28 similar data are presented with the inboard and the outboard propellers operating independently (that is, with one propeller removed). These data show that the inboard propeller caused most

of the effects of power on the pitching-moment coefficient (flaps up or flaps down), due primarily to the effects of the slipstream on the wing and on the tail.

Effect of Configuration Changes on the Pitching-Moment Characteristics of the Model

The various components of pitching-moment and lift coefficients discussed in the previous sections combine to give the characteristics evident in the basic data (ref. 5). In the following discussion the over-all effects of configuration changes on the pitching-moment characteristics will be considered in the light of what is known concerning the component effects.

Effects of variations of tail height and incidence.- The position of the horizontal tail with respect to the slipstream is an important factor affecting the tail contribution to the pitching moment, as was evident from figures 25 through 28. The effects of changes in tail height on the over-all pitching-moment characteristics of the model with flaps up and propellers operating at several constant thrust coefficients are shown in figure 29. Observing the changes in the pitching-moment-coefficient curves for the tail-off condition (fig. 29), it is seen that an increase in thrust coefficient resulted in a moderate positive increase in dC_m/dC_L. The linearity of these curves was, however, little affected by an increase in power. With the tail on, the pitching-moment characteristics were decidedly nonlinear at thrust coefficients above zero, due to passage of the outer portion of the tail into and out of the slipstream (refer to fig. 23(a)). The abrupt change in the slope dC_m/dC_L to a more negative value indicates entry of the tail into the slipstream. Increasing the tail height increased the lift coefficient at which this reduction in dC_m/dC_L began.

The pitching-moment characteristics of the model with the horizontal tail at various heights are further compared in figure 30 where the pitching-moment curves are arranged to show the effect of increasing thrust coefficient for each tail height. The constant-power curve superimposed thereon shows how dC_m/dC_L for constant power differed from that for constant thrust coefficient.

While comparable data for all four tail heights were obtained at thrust coefficients T_c to only 0.4 (figs. 29 and 30), the range of thrust coefficients was extended to 0.80 for two tail heights, 0 and 0.10 b/2. Figure 31(a) compares the pitching-moment characteristics for the model with the flaps up and figure 31(b) compares the data for the model with the inboard flaps deflected. The chief effect of the inboard flaps was to deflect the slipstream downward (see fig. 23), resulting in

pitching-moment characteristics with the low tail that resemble those with the higher tail, flaps up.

The various factors affecting the tail contribution to dC_m/dC_L will now be examined to provide the basis for explaining and interpreting the large changes in power-on pitching-moment characteristics accompanying changes in tail height or deflection of the flaps. Using the relation expressing the pitching-moment coefficient due to the tail, equation 1, the following expression can be written (for a constant thrust or power condition and a constant angle-of-tail incidence):

$$\frac{dC_{m_{tail}}}{dC_{L_w}} = \frac{1}{a_w}\frac{dC_{m_{tail}}}{d\alpha} = -\frac{a_t}{a_w}\bar{V}\left\{\left(1-\frac{d\epsilon}{d\alpha}\right)\eta_t\frac{q_t}{q}+\alpha_t\frac{d[\eta_t(q_t/q)]}{d\alpha}\right\} \quad (4)$$

where

$$\alpha_t = \alpha + i_t - \epsilon$$

and the subscript w refers to the complete model less tail. It is ordinarily assumed that $\frac{dC_{m_{tail}}}{dC_L} \approx \frac{dC_{m_{tail}}}{dC_{L_w}}$; that is, the tail lift is neglected. A more accurate expression is

$$\frac{dC_{m_{tail}}}{dC_L} = \frac{\frac{dC_{m_{tail}}}{dC_{L_w}}}{1-\left[\frac{\bar{c}}{l_t}\left(\frac{dC_{m_{tail}}}{dC_{L_w}}\right)\right]} \quad (5)$$

The values of a_t/a_w, $1-(d\epsilon/d\alpha)$, and $\eta_t(q_t/q)$ which appear in equation 4 and are assumed independent of tail incidence, are presented in figure 32 for various thrust conditions, flaps up. Similar information is given in figures 33 and 34 for two cases of flaps deflected. The effect of power-induced lift changes on $\frac{dC_{m_{tail}}}{dC_L}$ was significant as shown by the changes in a_t/a_w with T_c (which reflect the changes in a_w). For example, at an angle of attack of 5°, flaps up, a_t/a_w decreased from 0.74 to 0.52 as T_c increased from 0 to 0.80. By itself, this represents a 30-percent change in $\frac{dC_{m_{tail}}}{dC_L}$. The value of a_t/a_w with flaps up was about the same as that with flaps deflected except at high angles of attack.

The effect of power on the effective-downwash term, $1-(d\epsilon/d\alpha)$, was erratic (figs. 32, 33, and 34), depending as it does on such diverse factors as changes in wing-generated downwash, changes in downwash from

the propeller, changes in velocity of the slipstream, and changes in the position of wing wake and slipstream relative to the tail. An indication of the location of the slipstream with respect to the tail is provided by the curves of $\eta_t(q_t/q)$ vs. α presented in figure 23 and repeated for convenience in figures 32, 33, and 34. It is important to note that with the high tail and with the inboard flaps deflected (a condition for which the curves of $\eta_t(q_t/q)$ indicate that the tail was out of the slipstream except at the higher angles of attack) the value of $1-(d\epsilon/d\alpha)$ decreased with increasing thrust coefficient at angles of attack up to about 10° (a destabilizing effect). With the low tail, the opposite effect occurred in that $1-(d\epsilon/d\alpha)$ increased.

The term $d[\eta_t(q_t/q)]/d\alpha$ which expresses the dependency of the tail contribution to stability on the tail load (eq. 4), has been evaluated from the test data and is presented in figures 35, 36, and 37 as a function of α. The value of α_t is also shown since it is the product of the terms α_t and $d[\eta_t(q_t/q)]/d\alpha$ which affects $dC_{m_{tail}}/d\alpha$ (eq. 4). The magnitude of the effect is dependent not only on thrust coefficient and tail position relative to the slipstream (these factors affecting $d[\eta_t(q_t/q)]/d\alpha$ primarily) but also on tail incidence through its effect on α_t. The effect of tail incidence on the pitching-moment curves is shown in figure 38 for tail heights of 0 b/2 and 0.10 b/2, flaps up. Similar data for the model with the flaps deflected are presented in figures 39 and 40. The effect of tail incidence is important at moderate to high thrust coefficients but only when the tail is entering or leaving the propeller slipstream where $d[\eta_t(q_t/q)]/d\alpha$ assumes the largest numerical values (figs. 35, 36, and 37). For such cases, the constant tail incidence pitching-moment curve is obviously a poor indicator of the longitudinal stability except at the trim lift coefficient.

Effects of changing flap configuration.- The power-on pitching-moment characteristics of the model with two arrangements of flaps and a tail height of 0.10 b/2 are presented in figure 41. Note that test data are compared at different tail incidences for the two flap configurations in order that similar trim conditions exist in the two cases. It is observed that with inboard flaps, the pitching-moment curves are nearly linear over the greater portion of the lift-coefficient range, but there is a progressive increase in dC_m/dC_L with increasing T_c. The linear portions of these curves extend over a lift range for which the curves of $\eta_t(q_t/q)$ vs. α (fig. 33) indicate that there was little, if any, direct contact of the slipstream with the tail surfaces. The increase in dC_m/dC_L with increasing T_c was due largely to the propeller normal forces (see fig. 18(b)).

The pitching-moment curves for the model with outboard flaps (fig. 41) are not linear, showing a distinct change of slope dC_m/dC_L

at lift coefficients well below the maximum. Comparison of these data with the curves of $\eta_t(q_t/q)$ vs. α (fig. 34) indicates that dC_m/dC_L became more negative because the tail entered the slipstream. Moving the flaps from the inboard to the outboard location moved the effective center of pressure of wing sections affected by them out along the span, which not only produced more negative pitching moments at a given C_L and T_c (apparent in fig. 41 in spite of the change of tail incidence) but also, at a given C_L, reduced the change of pitching moment with increasing T_c. The latter effect can be explained on the basis of the data in figure 21 which show that the pitching-moment increment due to slipstream on the wing with outboard flaps became more negative with increasing T_c; whereas, with inboard flaps, it became more positive. Moving the flaps outboard also caused a large reduction in effective downwash ϵ at all thrust coefficients (as may be seen from fig. 24). This effect in combination with the more negative pitching moments from the wing caused the large negative tail incidence required to trim the model at moderate lift coefficients.

Effect of single-propeller operation.- The data obtained with the inboard and the outboard propellers operating independently are of considerable interest, not only because they help to explain the large effects of operating propellers on the model as tested, but because they can be used as the basis for estimating the effects of configuration changes such as moving the nacelles to other spanwise positions.

In figure 42 the pitching-moment characteristics of the model with the tail off and both propellers operating are compared with similar data with the inboard and outboard propellers operating independently. Data are presented for the model with the flaps up and with the inboard flaps deflected. The translation of the pitching-moment curves with increasing T_c, evident in all of these data, is primarily the result of positive pitching moments contributed by the propeller thrust. (As may be seen from fig. 19, this increment of pitching-moment coefficient was essentially independent of angle of attack at a given thrust coefficient.) The data of figure 42 for the case of only the inboard propeller operating show an increase in dC_m/dC_L with increasing T_c. This effect was caused by the contributions of propeller normal force and slipstream effect on the wing (see figs. 18 and 20). With outboard propeller only, the slope of the pitching-moment curves decreased with increasing T_c. In this case the portion of the wing affected by the slipstream lies behind the moment center. Consequently, the moment due to slipstream effect on the wing opposed the moment created by the outboard propeller normal force, the latter moment being of considerably less magnitude than that from the inboard propeller because of the more rearward location of the propeller disc (see figs. 18 and 20). The changes in slope of the pitching-moment curves caused by inboard and outboard propellers appear to be

approximately compensating since the data of figure 42 for both propellers operating show little change in slope with increasing T_c and are nearly linear.

Data similar to those in figure 42 are presented in figure 43 for the model with tail at 0.10 b/2. It is seen that with outboard propeller only, the pitching-moment curves were linear and dC_m/dC_L did not change with T_c. On the other hand, with inboard propeller only, the linearity and slope of the pitching-moment curves were greatly affected by increases in T_c. Comparison of the data in figures 42 and 43 leads to the conclusion that the major part of the adverse effects of propeller operation on the pitching-moment characteristics of the model was due to the effects of the slipstream from the inboard propeller on the flow at the tail.

Stick-Fixed Longitudinal Stability of the Model

The discussion up to this point has been concerned only with the changes in lift and pitching moment due to power at arbitrary angles of tail incidence. However, stick-fixed longitudinal stability is a function of the lift and pitching moment for the particular tail incidence which will trim the model at a given lift coefficient. In the ensuing discussion the effects of operating propellers on the longitudinal stability will be presented for trim conditions.

Unless the subscript cg is used with the various parameters, it is to be understood that the center of moments is at the quarter point of the mean aerodynamic chord.

Effects of power on various longitudinal stability parameters.- Each of the stability parameters in general use portrays the effects of power in varying degrees depending on which parameter is used. The longitudinal stability of the model with flaps up is presented in figure 44 in terms of three of these parameters. The tail incidence for trim $(i_t)_{trim}$ was determined from the test data by straight-line fairing of C_m vs. i_t for constant lift coefficient, extrapolating where necessary. The slope of the pitching-moment curve $(dC_m/dC_L)_{trim}$ and the static margin (i.e., the distance in mean aerodynamic chords from the center of moments to the neutral point) were determined by means of straight-line fairings of dC_m/dC_L vs. C_m/C_L at constant lift coefficient, following the method of reference 8 for the neutral point. In some instances data were not available at a sufficient number of tail incidences in the proper range to avoid some rather long extrapolations. Although the order of accuracy under such circumstances is not high, the results are considered adequate for discerning gross effects.

The variation of $(i_t)_{trim}$ with C_L, figure 44(a), shows effects of power similar to the pitching-moment curves (fig. 31(a), for example). A negative slope of the curves in figure 44(a) indicates positive stability; thus, at high T_c, the model was marginally stable at high lift coefficients with the low tail and at low lift coefficients with the high tail. The sources of the power effects are indicated by the following expressions developed from elementary considerations:

$$(i_t)_{trim} \equiv (\alpha_t - \alpha + \epsilon)_{trim} \tag{6}$$

and since

$$(\alpha_t)_{trim} = \frac{(C_m)_{tail\ off}}{\eta_t(q_t/q)\ a_t \overline{V}} \tag{7}$$

$$(i_t)_{trim} = \frac{(C_m)_{tail\ off}}{\eta_t(q_t/q)\ a_t \overline{V}} - (\alpha - \epsilon)_{trim} \tag{8}$$

The parameter $(dC_m/dC_L)_{trim}$ shown in figure 44(b), is the slope of the pitching-moment curve with the tail incidence for trim. It gives the same information as the $(i_t)_{trim}$ curve of figure 44(a) but is more directly associated with the pitching-moment curves and is thus somewhat easier to use when discussing pitching-moment components. A negative value indicates positive stability, as did the slope of the $(i_t)_{trim}$ curve. The sources of the power effects on this parameter may be observed in the terms of the following expressions for $(dC_m/dC_L)_{trim}$ which neglect the lift from the tail.

$$\left(\frac{dC_m}{dC_L}\right)_{trim} = \left(\frac{dC_m}{dC_L}\right)_{tail\ off} + \frac{dC_{m_{tail}}}{dC_L} \tag{9}$$

and using equations 4 and 7,

$$\left(\frac{dC_m}{dC_L}\right)_{trim} = \left(\frac{dC_m}{dC_L}\right)_{tail\ off} - \frac{a_t}{a_w}\left\{\overline{V}\left(1 - \frac{d\epsilon}{d\alpha}\right)\eta_t(q_t/q) + \frac{C_{m_{tail\ off}} \dfrac{d[\eta_t(q_t/q)]}{d\alpha}}{a_t[\eta_t(q_t/q)]}\right\} \tag{10}$$

It is evident from equation (10) that the magnitude of the pitching-moment coefficient, tail off, can affect the tail contribution to stability if $d[\eta_t(q_t/q)]/d\alpha$ is not negligible. Figures 32 to 37 show the quantities making up the tail contribution as they are affected by power changes while figures 15 to 21 indicate the effects of power on the tail-off components of stability. The nonlinearities in the variation of $(dC_m/dC_L)_{trim}$ with C_L, shown in figure 44(b), are due largely to changes in the tail-load term.

The static margin, shown in figure 44(c), represents the maximum distance the center of gravity may be moved rearward without making the airplane unstable. It is normally the most convenient stability parameter where center-of-gravity travel is to be considered. It may be noted from figures 44(b) and 44(c) that for this configuration there were in some cases large differences between $(dC_m/dC_L)_{trim}$ and the static margin. The differences can be explained by means of the following equations which describe the moment relationship between the existing center of moments and a more rearward center of moments (indicated by a prime) separated by the distance Δx:

$$C_{m'} \cong C_m + \frac{\Delta x}{\bar{c}} C_L \tag{11}$$

$$\frac{dC_{m'}}{dC_L} \cong \frac{dC_m}{dC_L} + \frac{\Delta x}{\bar{c}} \tag{12}$$

It is understood that all derivatives are for constant tail incidence. If the model were trimmed about the original center of moments, these become:

$$C_{m'} \cong \frac{\Delta x}{\bar{c}} C_L \tag{13}$$

$$\frac{dC_{m'}}{dC_L} \cong \left(\frac{dC_m}{dC_L}\right)_{trim} + \frac{\Delta x}{\bar{c}} \tag{14}$$

Thus, $\Delta x/\bar{c}$ is the change in slope of the pitching-moment curve at the original tail incidence. Now, an additional increment of slope may occur when the model is retrimmed since this involves a change in α_t which, as may be seen from equation 4, can change the tail contribution to the slope of the pitching-moment curve if $d[\eta_t(q_t/q)]/d\alpha$ is not zero. Neglecting tail lift, this increment may be expressed

$$\Delta\left(\frac{dC_{m'}}{dC_L}\right) = -\Delta\alpha_t \frac{a_t}{a_w} \bar{V} \frac{d[\eta_t(q_t/q)]}{d\alpha} \tag{15}$$

but since

$$\Delta\alpha_t = \frac{C_m'}{\eta_t(q_t/q)\ a_t\bar{V}} = \frac{C_L(\Delta x/\bar{c})}{\eta_t(q_t/q)\ a_t\bar{V}} \tag{16}$$

$$\Delta\left(\frac{dC_m'}{dC_L}\right) = -\frac{C_L}{a_w}\frac{\Delta x}{\bar{c}}\frac{\frac{d[\eta_t(q_t/q)]}{d\alpha}}{\eta_t(q_t/q)} \tag{17}$$

For trimmed conditions about the new moment center

$$\left(\frac{dC_m'}{dC_L}\right)_{trim} \cong \left(\frac{dC_m}{dC_L}\right)_{trim} + \frac{\Delta x}{\bar{c}} - \frac{C_L}{a_w}\frac{\Delta x}{\bar{c}}\frac{\frac{d[\eta_t(q_t/q)]}{d\alpha}}{\eta_t(q_t/q)} \tag{18}$$

Setting $(dC_m'/dC_L)_{trim}$ equal to zero makes $\Delta x/\bar{c}$ the static margin, expressed as follows:

$$\text{static margin} = \left(\frac{\Delta x}{\bar{c}}\right)_{\substack{\text{neutral}\\ \text{point}}} \cong \frac{-(dC_m/dC_L)_{trim}}{1 - \frac{C_L}{a_w}\frac{\frac{d[\eta_t(q_t/q)]}{d\alpha}}{\eta_t(q_t/q)}} \tag{19}$$

This expression illustrates why the degree of longitudinal stability indicated by the static margin was at times much larger than that indicated by the slope of the pitching-moment curve (see data for the high tail, figs. 44(b) and 44(c)). For example, figures 44(b) and 44(c) indicate that at $C_L = 1.1$ and $T_c = 0.6$, the value of $(dC_m/dC_L)_{trim}$ is -0.31 whereas the static margin is 0.80.

Effects of flaps on the longitudinal stability.- The stability characteristics of the model with various flap configurations are presented in terms of $(dC_m/dC_L)_{trim}$ in figure 45 for tail heights of 0 b/2 and 0.10 b/2. The stability changes due to deflection of flaps (at constant thrust coefficient T_c) indicated in figure 45 can be correlated with changes in the various parameters appearing in equation (10) by reference to figures 32 to 37 and to the $C_{m_{tail\ off}}$ data in figures 38, 39, and 40. For example, consider the stability curves of figure 45 for a tail height of zero. With flaps up, there was a decrease of stability with increasing lift coefficient at lift coefficients above 0.4 (and thrust coefficients other than zero) due primarily to a decrease in $\eta_t(q_t/q)$ (fig. 32) as the tail moved out of the slipstream, and to

the negative values of $d[\eta_t(q_t/q)]/d\alpha$ (fig. 35) combined with increasing values of $C_{m_{tail\ off}}$ (fig. 38(a)).

With deflection of the inboard flaps, the slipstream was moved downward. Reference to figures 33 and 36 reveals that in this case $\eta_t(q_t/q)$ increased with increasing lift coefficient and $d[\eta_t(q_t/q)]/d\alpha$ became positive as the tail moved into the slipstream, both trends tending to increase stability according to equation (10).

Considering next the stability curves in figure 45 for the model with a tail height of 0.10 b/2, it may be noted that with flaps up, the stability increased with increasing lift coefficient (at constant thrust coefficients other than zero). This increase in stability was due primarily to the increase in $\eta_t(q_t/q)$ (fig. 32) and the positive value of $d[\eta_t(q_t/q)]/d\alpha$ (fig. 35) combined with positive values of $C_{m_{tail\ off}}$ (fig. 38). With inboard flaps deflected, the slipstream was deflected downward so that the tail remained out of the slipstream over most of the angle-of-attack range. Consequently, $\eta_t(q_t/q)$ did not change with lift coefficient and $d[\eta_t(q_t/q)]/d\alpha$ approached zero. There was also a sizeable reduction in $1-(d\epsilon/d\alpha)$ due to deflection of the flaps as may be seen in figures 32 and 33. The result was a loss of stability due to deflection of the inboard flaps (fig. 45, 0.10 b/2).

The stability curves in figure 45 for the model with outboard flaps may be interpreted in a manner similar to that outlined for the other cases, noting that in this case, $C_{m_{tail\ off}}$ was negative according to figure 40. It should be observed that with the outboard flaps deflected, a large negative angle of tail incidence (i_t to -14°) was required to trim the model at high angles of attack.

Effects of vertical movement of the center of moments on the longitudinal stability.- The effects on longitudinal stability of displacing the center of moments, or center of gravity, a distance $0.1\bar{c}$ below the original moment center (located at $\bar{c}/4$) are shown in figure 46 for the case of flaps up. It is observed that with the low tail the effect of lowering the center of gravity was to increase the longitudinal stability; whereas, with the high tail, the effect was either much reduced or actually destabilizing. In both instances a change of tail incidence was required to retrim about the new center of gravity. The influence of tail height results from differences in the effect of tail load changes on stability which, as may be seen in equation (10), are in turn dependent upon the values of $d[\eta_t(q_t/q)]/d\alpha$.

Reduction of Adverse Effects of Propellers on Longitudinal Stability

The longitudinal characteristics of the subject model demonstrate some of the undesirable effects of propeller operation which should be suppressed or eliminated. There is, of course, a need for theoretical methods of calculating these effects of operating propellers on the longitudinal stability. However, the results of attempts to calculate power effects for this model entirely by means of existing theory have been discouraging. Such calculations may be considered in three parts which treat separately the effects due to direct propeller forces normal to and along the thrust axis, those due to slipstream action on the wing and nacelles, and those due to slipstream action on the flow at the tail. Obviously, the pitching moment due to propeller thrust can be calculated accurately. It has been found that the propeller normal force, and therefore the pitching moment due to it, can be calculated with fair accuracy for the isolated propeller using a method based on the oscillating aerodynamic forces associated with blades rotating in an inclined flow field. However, since a sizable portion of the measured normal force was attributable to slipstream effect on the forward portion of the nacelle, correlation between experiment and theory was not very satisfactory. Actually, an attempt was made to predict the normal force due to slipstream on the nacelle, but the agreement with experiment was not good.

An attempt was made to calculate the pitching moments arising from slipstream effects on the wing by consideration of the lift increments on the portions of the wing immersed in the slipstream. The calculations followed the method of reference 9 in which the propeller is regarded as an actuator disc (no rotation in the slipstream). Lift due to slipstream on the nacelles was neglected. The total lift increment due to propeller slipstream effects was predicted with adequate accuracy but the pitching-moment increment, which depends on the center of pressure of the lift increments on portions of the wing behind each propeller, was not predicted satisfactorily. The latter result is not surprising in view of the experimental pressure-distribution results presented in reference 10 which show a large effect of slipstream rotation on the distriubtion of incremental lift due to slipstream on the wing. Some of the discrepancy was, of course, due to neglect of slipstream effects on the nacelles.

Finally, with regard to prediction of the pitching-moment contribution of the tail, a strictly theoretical approach seems quite impractical for configurations such as considered herein where the tail passes into and out of the slipstream with changing angle of attack. Such predictions would require not only satisfactory estimates of the dynamic pressure and of the flow angles in the slipstream, but equally as important and probably more difficult, satisfactory estimates of the location of the slipstream relative to the tail. On the other hand, the longitudinal stability changes associated with slipstream effects on the tail have

been shown to be so serious that a more practical approach indicates the need for configuration changes to prevent the slipstream from striking the tail.

Assuming that the basic nature of the configuration (that is, a swept wing, four-engine tractor type) is to be retained, it appears that there are three ways of reducing or eliminating direct contact of the propeller slipstream with the horizontal tail and the associated large changes in longitudinal stability. The tail could be moved to a very high or a very low position, or the propellers could be moved farther outboard, or the tail span could be reduced. Since there are limitations on all three, a combination of these might be required.

When inboard flaps are used, a high tail position is more favorable than a low position from the standpoint that the flaps deflect the slipstream downward, and in the case of the high tail, away from it. With the high tail it is also possible that the tail would remain out of the slipstream when the airplane is yawed. No large increase in the directional and lateral control problems would be anticipated from increased tail height. However, a simple increase in the height of the tail will not in itself correct all deficiencies of this configuration. The tail operates in a downwash field which, even though the slipstream does not strike the tail, is responsive to power changes. It has been shown that the effect of power on the effective downwash was quite destabilizing in those instances when there were no compensating effects due to slipstream striking the tail. Additional configuration changes are therefore indicated.

An outward shift of the nacelles (with an accompanying rearward shift) produces favorable changes in the pitching moments arising from the propeller normal forces and from wing lift due to the slipstream (as well as decreasing the likelihood that the slipstream will strike the horizontal tail). For the tractor configuration considered, the pitching moment due to propeller normal force increases with angle of attack (at constant T_c) to produce a destabilizing effect and this can be reduced by outward shift of the nacelles. The pitching moment resulting from wing lift due to slipstream is approximately a linear function of α (at constant T_c) but is stabilizing or destabilizing, depending upon the location of the effective center of pressure of this lift relative to the moment center. If the nacelles are moved sufficiently far outward, the effect of power on the pitching moment arising from slipstream on the wing can be made stabilizing and thus can be used as a means of counteracting the destabilizing effects from other sources. The amount that the nacelles can be moved outward is restricted by the accompanying increase in the lateral and directional control required to cope with engine failure.

Estimate of longitudinal stability with the nacelles moved outward.- In the absence of flow surveys at the position of the tail, some rough

approximations were used to establish the position of the slipstream with respect to the tail. This was necessary in order to judge how far outward the nacelles need be moved to prevent the slipstream from striking the tail. The calculations involved the determination of how much of the outer portion of the tail would have to be immersed in the slipstream to produce the observed increase in the maximum value of $\eta_t(q_t/q)$ from $T_c = 0$ to $T_c = 0.8$. The assumption was made that the dynamic-pressure distribution in the slipstream could be approximated with sufficient accuracy for this purpose by that given in reference 11 for a counter-rotating propeller ahead of a straight wing. It was further assumed that the dynamic pressure due to the slipstream at each spanwise station of the tail influenced the over-all effective value of $\eta_t(q_t/q)$ in proportion to the tail loading at that station as determined by the Weissinger method. (Note that η_t is assumed to be independent of T_c.) The results of these rough calculations are given in figure 47 for high angles of attack where the slipstream effect is indicated to extend farthest inboard. The figure indicates that an outward movement of the nacelles of 0.1 b/2 would result in a small effect of power on $\eta_t(q_t/q)$ even with no alterations to the plan form of the horizontal tail. Further improvement could be gained by a reduction of tail span.

Even though the slipstream does not actually strike the tail when the nacelles are moved outward, it is likely that there would be some changes in effective downwash due to power. The nature of these changes is illustrated in figure 48 where calculated effective downwash is presented for inboard and outboard propellers at their original spanwise positions. In the absence of force data for several tail incidences with propellers operating independently, values of dC_m/di_t for calculating ϵ were taken from power-off data for the case of outboard propeller only and from data with both propellers operating for the case of inboard propeller only. The data of figure 48 indicate that, with the outboard propeller operating, an increase in thrust coefficient T_c produced a decrease in the rate of change of ϵ with α. This stabilizing effect of T_c on ϵ can be attributed partially to the spanwise variations of wing lift which are caused by propeller operation. The data in reference 10 show that, for the model used in the present investigation, there were large increments in normal force on those portions of the wing behind the propeller due to propeller operation. These increments can be expected to increase the downwash to the rear of and to decrease the downwash to the side of the affected wing sections, due to trailing vortices shed as a result of the large and concentrated changes in span loading. For the present model having right-hand propellers, this effect would be expected to be largest on the portion of the wing inboard of the nacelle where the lift increment is the greatest. With the outboard propeller operating, the resultant effect on the tail will depend on the proximity of the tail to the trailing vortex from the section of the wing behind the upgoing propeller blades, as well as on other factors such as the rotation that remains in the slipstream and the interaction of the slipstream and the wing-downwash field. The fact that a propeller as far

from the tail as the outboard propeller can produce a decrease in ϵ attests to the possible strength of the effect. This fact also points up the possibility that a propeller situated between the present inboard and outboard positions may give a large stabilizing effect of downwash if the major portion of the tail area lies inboard of the wing sections immersed in the slipstream and if the rotation of the propeller has the same direction as those on the model. Since the magnitude of the effect is uncertain, it is neglected in present estimates of stability with the nacelles moved outward. However, if the tail is no longer subjected to the high dynamic pressure of the slipstream and if the tail-off stability can be improved, the stability contributed by the tail will be a smaller part of the model stability than was the case with the existing model, and the importance of the effect of power on downwash will be diminished.

On the basis of the foregoing considerations, the assumption will be made that if the nacelles are moved to stations 0.35 b/2 and 0.60 b/2, to a first approximation the effects of power on the tail contribution to stability can be neglected, leaving only the pitching-moment contributions of the direct propeller forces and the slipstream effect on the wing to be considered. It will be assumed that the nacelles are moved outward to stations 0.35 b/2 and 0.60 b/2, the longitudinal position of the nacelles being established by maintaining the distance between the propeller planes and the reference sweep line, and the vertical position of the thrust line being established on the basis of linear variation with spanwise position. The calculation of the pitching moments due to propeller normal force and shaft thrust for the new nacelle locations was made simply by changing the previous values in proportion to the changes in the lengths of the moment arms. These data are presented in figures 49 and 50.

The calculation of the new values of pitching-moment contribution of the slipstream on the wing involved the use of the increments of lift and pitching moment due to slipstream derived from the experimental data, adjusted for changes in the areas of the wing immersed in the slipstream and for changes in the moment arm resulting from outward movement of the nacelles. It was assumed that for a given thrust coefficient the distribution of incremental lift over each wing area in the slipstream was unaltered by moving the propeller outward. The latter assumption implies that for the case of flaps deflected, the flaps were moved outward with the nacelles. The estimated pitching-moment contribution of the wing derived on the above assumptions is presented in figure 51.

The estimated longitudinal stability of the model with nacelles moved to stations 0.35 b/2 and 0.60 b/2 was calculated using the data in figures 49 to 51 and equation 10 (the tail lift was not neglected, however). The slope of the pitching-moment curve, tail off and power off, was assumed unchanged by movement of the nacelles and flaps. The factors $1-(d\epsilon/d\alpha)$ and $\eta_t(q_t/q)$ were assumed equal to those measured with power off, while $d[\eta_t(q_t/q)]/d\alpha$ was taken as zero. The results of these

calculations are given in figure 52 in terms of $(dC_m/dC_L)_{trim}$ for both the new and the original configurations. It is indicated that the revised configuration would have more nearly constant longitudinal stability than the original and would show little variation with thrust. Note that although the model with outboard flaps loses very little stability with increasing thrust, the tail incidence for trim is even more negative than on the original configuration (estimated at approximately -16° at $C_L = 1.6$, $T_c = 0.40$).

Estimates of lateral and directional moments due to asymmetric loss of power.- An outward shift of the nacelles, which has been suggested as one means of alleviating adverse effects of propellers on longitudinal stability, would be detrimental to the lateral and directional characteristics. Within the limitations of the data which have been obtained with the semispan model, estimates have been made of the rolling moments and yawing moments created by loss of thrust on the right outboard nacelle and are shown in figure 53 for an angle of attack of 14°. The lateral center of pressure of the lift increment on each area of the wing affected by slipstream was estimated, on the basis of the pressure data in reference 10, to be located at a distance of one-half the radius of the propeller inboard of the thrust axis. This lateral center of pressure was used for all flap configurations. The direct propeller forces were assumed to act at the thrust axes.

The values of rolling-moment coefficient that are shown in figure 53 are, of course, only part of that which the ailerons may have to counteract in case of engine failure. The large yawing-moment coefficient caused by loss of thrust on an outboard engine (see fig. 53) may be expected to result in additional rolling moment due to yawing. The estimates in figure 53 show that moving the nacelles outward produces an increase of about 15 percent in rolling-moment coefficient for the engine-out condition. The increase in yawing moment amounts to about 20 percent.

Propulsive Characteristics

The propeller thrust, denoted by T_c, was not available in its entirety as propulsive thrust on the model. The propulsive thrust of the two propellers (i.e., the longitudinal force of the semispan model with power on minus the longitudinal force with power off, at a constant angle of attack) was calculated and converted to the propeller-thrust coefficient $C_{T_{total}}$ (note that $C_{T_{total}}$ is for two propellers). Figure 54(a) presents the propulsive-thrust characteristics of the model with flaps up (tail off) at two angles of attack, along with the power characteristics for both propellers. Also shown in figure 54(a) for comparison are the thrust and power characteristics of a pair of isolated propellers operating at approximately zero inclination to the airstream. At the

lower angle of attack (6.1°) the propellers on the model also operated at approximately zero inclination.

In the calculation of propulsive efficiency, it has been suggested by Betz in reference 12 that the propellers be credited for the lift created by their operation. This can be done in several ways and with varying results. In the present study, the propellers were credited with an increment of thrust equal to the change in induced drag associated with the change in lift attributable to the propellers. This induced drag was calculated for an assumed elliptic span load distribution and was added to the propulsive thrust $C_{T_{total}}$ presented in figure 54(a) (both determined at constant angle of attack). Propulsive efficiencies, calculated using propulsive thrust coefficients with and without this adjustment for lift created by the propellers, are presented in figure 54(b) as functions of advance ratio J. Also shown for comparison is the efficiency of the isolated propeller. Data are presented for three propeller-blade angles and for two angles of attack of the model. Note that figure 54(b) also gives the thrust coefficient T_c (used previously in the discussion of stability) in order to relate the efficiency curves to this parameter. At an angle of attack of 6.1°, the propulsive efficiency of the model with flaps up was less than 3 percent below the efficiency of the isolated propellers at thrust coefficients of 0.1 or larger. A larger loss in efficiency is indicated at 14.3° angle of attack, although roughly half is offset by the lift creditable to the propeller.

The variation of the propulsive efficiencies with angle of attack is shown in figure 54(c) for constant values of advance ratio in the higher thrust regime. Data are presented for several flap configurations. Also shown for comparison are the isolated-propeller efficiencies measured at angles of attack corresponding to the upflow angles A existing on the model. It is indicated that the flaps generally caused a loss in efficiency at a given angle of attack, though not necessarily at a given lift coefficient. The general decrease of efficiency with increasing angle of attack is lessened, particularly at the low values of J, by crediting the propellers with lift created by their operation.

DISCUSSION OF HIGH-SPEED CONDITIONS

Effects of Operating Propellers on the Longitudinal Characteristics

The longitudinal characteristics of the model at high speeds, with and without operating propellers, have been presented in reference 5. Typical of these results are the data shown in figure 11. In general, the effects of the operating propellers were not large compared to the propeller effects at low speed. Compared to the model without propellers, operation of the propellers at constant thrust coefficients generally increased the lift-curve slopes and decreased the static longitudinal stability as inferred from the slopes of the curves of pitching-moment coefficient as

a function of lift coefficient. Generally, the trim lift coefficients increased with increasing thrust coefficient but at any constant thrust coefficient they decreased with increasing Mach number. There was no large effect of operating propellers on the variation of longitudinal force coefficient with lift coefficient at lift coefficients less than about 0.40 or 0.50.

The variations of the longitudinal characteristics with Mach number are presented in figures 55, 56, and 57. These variations are shown at lift coefficients of 0.20 and 0.40 for the model with the propellers off and with the propellers operating at several constant values of thrust coefficient.

Operation of the propellers increased the lift-curve slopes (fig. 55) but, in general, had only small effects on the variation of lift-curve slope with Mach number. At a lift coefficient of 0.40, operating the propellers at a thrust coefficient of 0.03 increased the Mach number for lift divergence from approximately 0.83 to approximately 0.86.

Figure 56 shows the variation with Mach number of the increment of longitudinal force coefficient above its value at a Mach number of 0.70 for several values of propeller thrust coefficient and with propellers removed. It was anticipated that the Mach number of longitudinal force divergence would be decreased as a result of the increased velocity behind the operating propellers. However, this effect did not occur, and the Mach number for drag divergence was little affected by operation of the propellers. At supercritical speeds, the drag rise with increasing Mach number was reduced considerably with increase in propeller thrust coefficient. This reduction was due, in part, to increases in the wing lift-curve slope with the propellers operating. Thus, the same lift coefficient can be obtained at a lower angle of attack and this fact tended to reduce the shock-induced losses over the outer portion of the wing span. It is also thought that some of the effect stemmed from increases in the effective Reynolds numbers of the wing sections immersed in the propeller slipstreams. It is doubtful that a favorable Reynolds number phenomenon would prevail at full-scale Reynolds numbers.

The effects of Mach number on the slopes of the pitching-moment curves are presented in figure 57 at lift coefficients of 0.20 and 0.40 for the model with the propellers off and with the propellers operating at several constant values of thrust coefficient. The effects of Mach number were generally greater with the propellers operating than with the propellers off. In general, the static longitudinal stability decreased slightly with Mach number when the tail was on and increased slightly when the tail was off up to a Mach number of approximately 0.82. At higher speeds, changes in stability due to Mach number were inconsistent and more pronounced.

Effects of the Operating Propellers on the Longitudinal Stability

As discussed previously, the factors which determine the static longitudinal stability of a propeller-driven airplane are the stability with the propellers removed, the direct propeller forces normal to and along the thrust axis, and the effects of the propeller slipstream on the flow on the wing and at the horizontal tail. Figures 58 and 59 show for several Mach numbers these various effects of the operating propellers on tail-on and tail-off static longitudinal stability at zero thrust, at a comparatively high constant thrust coefficient, and at the conditions of constant horsepower shown in figure 9. The data presented were obtained by adding pitching-moment increments, referred to the center of gravity, due to propeller thrust and normal force (from the propeller calibration data) to the propellers-off pitching-moment data. This total was then subtracted from the power-on pitching moments to ascertain approximately the slipstream effects. For both constant thrust and constant power, the various effects of the operating propellers on the pitching-moment characteristics of the model were small.

Figure 60 presents, for a Mach number of 0.80 and a constant thrust coefficient of 0.04, a comparison of the predicted and measured variations with angle of attack of the incremental pitching-moment coefficient due to propeller normal force. The measured variations of increments of pitching-moment coefficient with angle of attack due to propeller thrust and propeller slipstream on the wing and tail are also shown. The effect of propeller normal force on the pitching moment was calculated by a method based on the oscillating aerodynamic forces associated with blades rotating in an inclined flow field. The predicted pitching-moment increments due to the propeller normal force are in good agreement with the measured effects. The small discrepancy at the lower angles of attack is believed due to lift stemming from the asymmetry of the nacelle forebody. The theoretical computations did not account for any lift contribution due to the nacelle forebody.

The effects of propeller slipstream on the pitching-moment characteristics of the wing and tail could not be predicted to any acceptable degree of accuracy with existing methods. It is believed that the combination of the effects of wing sweepback, of viscous separation, of propeller slipstream rotation, and of wing-nacelle interference makes the estimation of slipstream effects on the pitching-moment characteristics of the wing and tail virtually impossible for the present model.

Figure 61 shows the variation with Mach number of the various effects of the operating propellers on the pitching-moment-curve slopes $\Delta(dC_m/dC_L)$. The data are presented for a representative lift coefficient for level flight ($C_L = 0.40$) and for constant thrust coefficient and constant simulated horsepower. The effects of slipstream on the horizontal tail were assumed to be the differences between tail-on and tail-off slipstream effects. The effect of propeller normal force varied with Mach number

at constant horsepower because of the relationship of thrust coefficient and lift coefficient used in calculating the conditions (fig. 9). The variations of the effects of the propeller slipstream with Mach number were small, generally amounting to a change in pitching-moment-curve slope of less than ±0.05.

Effects of the Operating Propellers on the Stability Contribution of the Horizontal Tail

The horizontal-tail contribution to stability is a function of the downwash factor $1 - (d\epsilon/d\alpha)$, the tail-efficiency factor $\eta_t(q_t/q)$, and the ratio $\frac{a_t}{a_w}$. As in the low-speed case, calculations were made to evaluate the effective downwash characteristics and the tail efficiency factor with and without operating propellers. The force data presented in reference 5 and the isolated tail-force data presented in reference 2 were used for the computations and the results are shown for several Mach numbers in figures 62, 63, and 64 as functions of angle of attack. It was assumed for the computation of downwash angle ϵ and tail-efficiency factor $\eta_t(q_t/q)$ that the Mach number at the tail was the same as the free-stream Mach number. The effect of the propellers on downwash amounted to a change in downwash angle of 0.5° or less. At high angles of attack the effects of the operating propellers on the factors $\eta_t(q_t/q)$ and $\frac{a_t}{a_w}$ were sizable, however, these effects were compensating and their overall effect on tail effectiveness was small.

The variations with Mach number of the tail-effectiveness parameter, dC_m/di_t, the isolated tail lift-curve slope, and the various factors affecting the stability contribution of the tail are shown in figures 65, 66, and 67 for a representative level flight, high-speed attitude ($\alpha = 4^\circ$). The effects of Mach number on dC_m/di_t were small with and without the operating propellers. For the selected condition, operation of the propellers had little effect on the variations of the factors $1 - (d\epsilon/d\alpha)$, $\eta_t(q_t/q)$, and $\frac{a_t}{a_w}$ with Mach number.

The effects of horizontal-tail height on the pitching-moment-curve slopes of the model with and without operating propellers are shown in figure 68 for several Mach numbers. Raising the horizontal tail increased the static longitudinal stability slightly with the propellers off at Mach numbers less than 0.90, but was destabilizing over the Mach number range of the investigation with the propellers operating.

Longitudinal Characteristics of an Assumed Airplane

Figure 69 presents a summation of the longitudinal characteristics, as calculated from the results of the subject investigation, of an assumed airplane operating with the power required for level flight at an altitude of 40,000 feet. These characteristics are presented as functions of Mach number or normal-acceleration factor. The lift coefficients shown are computed values based on a wing loading of 65 pounds per square foot and the assumed airplane altitude.

The effects of propeller operation at the power for level flight on the static longitudinal stability of the airplane were small (fig. 69). Compared to propellers-off stability a maximum decrease in pitching-moment-curve slope of 0.04 was indicated at a Mach number of 0.70. Only a small change was indicated in the stable variation of tail incidence for trim with Mach number between the conditions of propellers off and propellers operating at the power required for level flight. At constant Mach number, the variation of tail incidence for trim with normal acceleration was not greatly affected by the operation of the propellers at the power required for level flight.

Propulsive Characteristics

Figure 70 presents, for an upflow angle of approximately 0° and a Mach number of 0.80, a comparison of the characteristics of the isolated propeller with the propulsive characteristics of the model. Also shown is a comparison of the variations with Mach number of the efficiency of the isolated propeller and the propulsive efficiency of the model at a constant thrust coefficient of 0.04.

The propulsive characteristics include the lift due to the propeller slipstream (ref. 12) and the effects of the operating propellers on longitudinal force characteristics previously discussed. The method of crediting the propellers for these effects differs from the method applied in the low-speed case in that the effective thrust is determined on the basis of constant lift coefficient. This is permissible whenever the effects of operating propellers on the wing lift are small. The following relationships were used in determining the effective thrust coefficients and propulsive efficiencies of the model:

$$C_{T_{eff}} = -\left(\frac{S}{4D^2}\right)J^2\left(C_{X_{\text{props on}}} - C_{X_{\text{props off}}}\right)_{C_L=\text{const.}}$$

$$\eta = \frac{C_{T_{eff}}\, J}{C_P}$$

Figure 70 indicates that the effective thrust coefficients for the conditions selected for the comparison were greater than the thrust coefficients measured for the isolated propeller, and that the corresponding propulsive efficiencies, consequently, exceeded the efficiencies indicated for the isolated propeller. Generally, the propulsive efficiency increased with increasing Mach number while the efficiency of the isolated propellers decreased slightly. This effect is believed to be associated with the decrease in the rate of change of longitudinal force coefficient with Mach number indicated in figure 56.

In computing propulsive efficiencies, no distinction was made between the effects of propeller slipstream and the effects of propeller direct forces. However, for the range of Mach numbers and propeller thrust coefficients considered, the effects of propeller direct forces on lift were negligible.

CONCLUSIONS

The effects of operating propellers on the longitudinal characteristics of a representative four-engine tractor airplane configuration with a 40° sweptback wing have been investigated in wind-tunnel tests of a semispan model.

An analysis of the data for low-speed, high-thrust conditions indicates the following conclusions:

1. The over-all effects of operating propellers on the static longitudinal stability of the model at low speeds were generally large but varied considerably throughout the lift-coefficient range.

2. Most of the objectionable static longitudinal stability variation with lift coefficient observed with the configuration tested was due to large changes in the pitching-moment contribution of the tail originating from passage of the tail into and out of the slipstream.

3. Large lift increments due to slipstream may be expected on the sections of the wing which are immersed in the slipstream, particularly when the sections are equipped with flaps. Because of sweepback, the lateral disposition of wing areas so affected determines whether the slipstream effect on the wing will be stabilizing or destabilizing.

4. Although the effects of propeller normal force and thrust on the longitudinal stability of this configuration could be predicted with fair accuracy, available theoretical methods failed to predict satisfactorily the effects of propeller slipstream on the wing, nacelles, and horizontal tail. However, for configurations similar to that used in the present investigation, the available experimental data seem to furnish a good starting point for making such predictions.

5. To avoid large longitudinal stability variation with lift coefficient, the slipstream should not impinge on the tail. It is indicated that one way to accomplish this with the configuration tested is by moving the propellers outward about 0.1 of the wing semispan. This modification would also make the effect of propeller slipstream on the wing more stabilizing and reduce the destabilizing effects of the propeller normal forces. Calculations indicate great improvement of the longitudinal stability characteristics both with flaps up and flaps down. The lateral control required to offset the increase in rolling moment associated with loss of the outboard propeller is estimated to be 15 percent more than for the original configuration and the directional control, 20 percent more.

6. Other design changes tending to prevent the slipstream from striking the tail and which do not affect the lateral and directional control problem are reduction of the tail span and raising the horizontal tail. The experimental results indicate that if the tail is placed high enough to avoid the slipstream, the effect of power on the tail contribution to stability will be destabilizing. This indicates that for the configuration tested, some outward shift of the propellers would still be required to produce satisfactory longitudinal stability characteristics.

7. Propulsive efficiencies for the complete configuration were approximately equal to the efficiency of the isolated propeller if, in calculating propulsive efficiency, the propellers were credited with the lift they produced.

For the high-speed conditions, that is, for Mach numbers of 0.60 to 0.90, the following conclusions were indicated:

1. The over-all effects of operating propellers on the longitudinal characteristics at high subsonic speeds were not large when compared to the effects of operating propellers at low speeds. The propellers operating at constant thrust coefficients generally resulted in a reduction in the longitudinal stability. Increasing the propeller thrust coefficient while maintaining a constant Mach number increased both the longitudinal stability and the trimmed lift coefficient.

2. Operation of the propellers at constant thrust coefficient increased the wing lift-curve slope but had little effect on the variation of lift-curve slope with Mach number.

3. Operation of the propellers had little effect on the Mach number for longitudinal force divergence at a constant lift coefficient but resulted in a decrease in the rate of change of longitudinal force coefficient with Mach number at supercritical speeds. This effect increased with increasing propeller thrust coefficient and with increasing lift coefficient.

4. It was possible to predict the effects of propeller normal force on the longitudinal stability of the model with good accuracy. However, the propeller slipstream effects on the wing and horizontal tail could not be predicted with existing methods to any acceptable degree of accuracy.

5. Raising the horizontal tail had little effect on the longitudinal stability with the propellers removed but was destabilizing with the propellers operating.

6. For an assumed airplane, operating at the power required for level flight at an altitude of 40,000 feet, calculations indicate only a small change in the stable variation of tail incidence for trim with either Mach number or normal acceleration compared to the propellers-off condition.

7. Propulsive efficiencies for the complete model were generally somewhat higher than the efficiencies of the isolated propeller and increased with increasing Mach number while the efficiency of the isolated propeller decreased slightly.

Ames Aeronautical Laboratory
National Advisory Committee for Aeronautics
Moffett Field, Calif., June 14, 1954

REFERENCES

1. Edwards, George G., Tinling, Bruce E., and Ackerman, Arthur C.: The Longitudinal Characteristics at Mach Numbers Up to 0.92 of a Cambered and Twisted Wing Having 40° of Sweepback and an Aspect Ratio of 10. NACA RM A52F18, 1952.

2. Tinling, Bruce E.: The Longitudinal Characteristics at Mach Numbers Up to 0.9 of a Wing-Fuselage-Tail Combination Having a Wing With 40° of Sweepback and an Aspect Ratio of 10. NACA RM A52I19, 1952.

3. Boltz, Frederick W., and Shibata, Harry H.: Pressure Distribution at Mach Numbers Up to 0.90 on a Cambered and Twisted Wing Having 40° of Sweepback and an Aspect Ratio of 10, Including the Effects of Fences. NACA RM A52K20, 1953.

4. Tinling, Bruce E., and Lopez, Armando E.: The Effects of Nacelles and of Extended Split Flaps on the Longitudinal Characteristics of a Wing-Fuselage-Tail Combination Having a Wing With 40° of Sweepback and an Aspect Ratio of 10. NACA RM A53D06, 1953.

5. Edwards, George G., Dickson, Jerald K., Sutton, Fred B., and Demele, Fred A.: The Results of Wind-Tunnel Tests to a Mach Number of 0.90 of a Four-Engine Propeller-Driven Airplane Configuration Having a Wing With 40° of Sweepback and an Aspect Ratio of 10. NACA TN 3789, 1956.

6. Rogallo, Vernon L.: Effects of Wing Sweep on the Upwash at the Propeller Planes of Multiengine Airplanes. NACA TN 2795, 1952.

7. Lopez, Armando E., and Dickson, Jerald K.: The Effects of Compressibility on the Upwash at the Propeller Planes of a Four-Engine Tractor Airplane Configuration Having a Wing With 40° of Sweepback and an Aspect Ratio of 10. NACA TN 3675, 1956.

8. Schuldenfrei, Marvin: Some Notes on the Determination of the Stick-Fixed Neutral Point From Wind-Tunnel Data. NACA WRL-344, 1943. (Formerly NACA RB 3I20)

9. Smelt, R., and Davies, H.: Estimation of Increase in Lift Due to Slipstream. R. & M. No. 1788, British A.R.C., 1937.

10. Kolbe, Carl D., and Boltz, Frederick W.: Effects of Operating Propellers on the Wing-Surface Pressures of a Four-Engine Tractor Airplane Configuration Having a Wing With 40° of Sweepback. NACA RM A53L29, 1954.

11. Sleeman, William C., Jr., and Linsley, Edward L.: Low-Speed Wind-Tunnel Investigation of the Effects of Propeller Operation at High Thrust on the Longitudinal Stability and Trim of a Twin-Engine Airplane Configuration. NACA RM L52D04, 1952.

12. Betz, A.: Considerations on Propeller Efficiency. NACA TM 481, 1928.

TABLE I.- GEOMETRIC PROPERTIES OF THE MODEL

Wing	
Reference sweep line: Locus of the quarter chords of sections inclined 40° to the plane of symmetry	
Aspect ratio (full-span wing)	10.0
Taper ratio	0.4
Sweepback	40°
Twist	-5°
Reference sections (normal to reference sweep line)	
Root	NACA 0014, a=0.8 (modified) c_{l_i}=0.4
Tip	NACA 0011, a=0.8 (modified) c_{l_i}=0.4
Area (semispan model)	6.944 ft^2
Mean aerodynamic chord	1.251 ft
Flaps, extended from trailing edge	0.20 c'
Incidence (measured in the plane of symmetry)	3°
Fences are located at y/(b/2)=0.33, 0.50, 0.70, and 0.85.	
Nacelles	
Frontal area (each)	0.208 ft^2
Inclination (see fig. 1(c))	
Inboard	-6.5°
Outboard	-7.0°
Propellers	
Diameter	1.167 ft
Number of blades	3
Propeller-activity factor (per blade)	188.4
Propeller-blade thickness-chord ratio (0.70 radius)	0.03, 0.05
Solidity (per blade)	0.058
Blade sections	symmetrical NACA 16 series
Horizontal Tail	
Reference sweep line: Locus of quarter chords of sections inclined 40° to the plane of symmetry	
Aspect ratio (full-span tail)	4.5
Taper ratio	0.4
Sweepback	40°

TABLE I.- GEOMETRIC PROPERTIES OF THE MODEL - Concluded

Horizontal tail (Continued)

Reference section (normal to reference sweep line)	NACA 0010
Tail length, l_t	$3.25\bar{c}$
Area (semispan model)	1.387 ft^2
Mean aerodynamic chord	0.833 ft
Tail volume, $l_t/\bar{c}$ (S_t/S)	0.65
Tail heights (measured vertically from the fuselage center line to the hinge axis of the horizontal tail in wing semispans (see fig. 1(a))	0, 0.05, 0.10, 0.15

Fuselage

Fineness ratio	12.6
Frontal area (semispan model)	0.273 ft^2

Fuselage coordinates:

Distance from nose, in.	Radius, in.
0	0
1.27	1.04
2.54	1.57
5.08	2.35
10.16	3.36
20.31	4.44
30.47	4.90
39.44	5.00
50.00	5.00
60.00	5.00
70.00	5.00
76.00	4.96
82.00	4.83
88.00	4.61
94.00	4.27
100.00	3.77
106.00	3.03
126.00	0

TABLE II.- RANGE OF TEST VARIABLES

(a) Low speed; NACA 1.167-(0)(05)-058 propeller

Tail height	Type flaps	δ, deg	M	R, million	β, deg	i_t, deg	Tail height	Type flaps	δ, deg	M	R, million	β, deg	i_t, deg
tail off	none	---	0.082	4	21	---	0.15 b/2	none	---	0.123	4	31	-4
↓	↓	---	.082	4	26	---							
		---	.082	4	[a]26	---	tail off	Inbd.	30	.082	4	26	---
		---	.082	4	[b]26	---	↓	↓	↓	.082	4	[a]26	---
		---	.082	4	31	---				.082	4	[b]26	---
		---	.123	4	21	---				.082	4	31	---
		---	.123	4	31	---	↓	↓	↓	.123	4	31	---
		---	.123	4	36	---							
		---	.123	6	31	---	0	Inbd.	30	.082	4	26	0
		---	.165	8	31	---	↓	↓	↓	.082	4	26	-2
↓	↓	---	.165	8	36	---	↓	↓	↓	.082	4	26	-4
0	none	---	.082	4	26	0	0.10 b/2	Inbd.	30	.082	4	26	0
↓	↓	---	.082	4	26	-4	↓	↓	↓	.082	4	[a]26	0
		---	.082	4	26	-8				.082	4	[b]26	0
		---	.123	4	31	-4				.082	4	26	-2
							↓	↓	↓	.082	4	26	-4
0.05 b/2	none	---	.082	4	21	-4							
↓	↓	---	.082	4	31	-4	tail off	Outbd.	30	.082	4	26	---
		---	.123	4	21	-4							
		---	.123	4	31	-4	0.10 b/2	Outbd.	30	.082	4	26	0
		---	.123	4	36	-4				.082	4	[a]26	0
		---	.123	6	31	-4	↓	↓	↓	.082	4	[b]26	0
		---	.165	8	31	-4				.082	4	26	-8
↓	↓	---	.165	8	36	-4							
							tail off	Inbd.	60	.082	4	26	---
0.10 b/2	none	---	.082	4	26	-4				.082	4	31	---
↓	↓	---	.082	4	[c]26	-4	↓	↓	↓	.123	4	31	---
		---	.082	4	[a]26	-4							
		---	.082	4	[b]26	-4	0.10 b/2	Inbd.	60	.082	4	26	0
		---	.082	4	26	0							
		---	.082	4	26	-8							
		---	.123	4	26	-4							
		---	.123	4	[c]26	-4							
		---	.123	4	31	0							
		---	.123	4	31	-4							
↓	↓	---	.123	4	31	-8							

(b) High speed; NACA 1.167-(0)(03)-058 propeller

Tail height	Type flaps	δ, deg	M	R, million	β, deg	i_t, deg
tail off	none	---	0.70 to 0.90	1	51	---
↓	↓	---	0.70 to 0.90	2	51	---
		---	0.60 to 0.80	2	41	---
0		---	0.70 to 0.90	1	51	-2
↓	↓	---	↓	1	51	-4
		---		1	51	-6
		---	↓	2	51	-4
		---	0.60 to 0.80	2	41	-4
0.10 b/2	↓	---	0.70 to 0.90	1	51	-4

[a]Inboard propeller only.
[b]Outboard propeller only.
[c]Negative thrust.

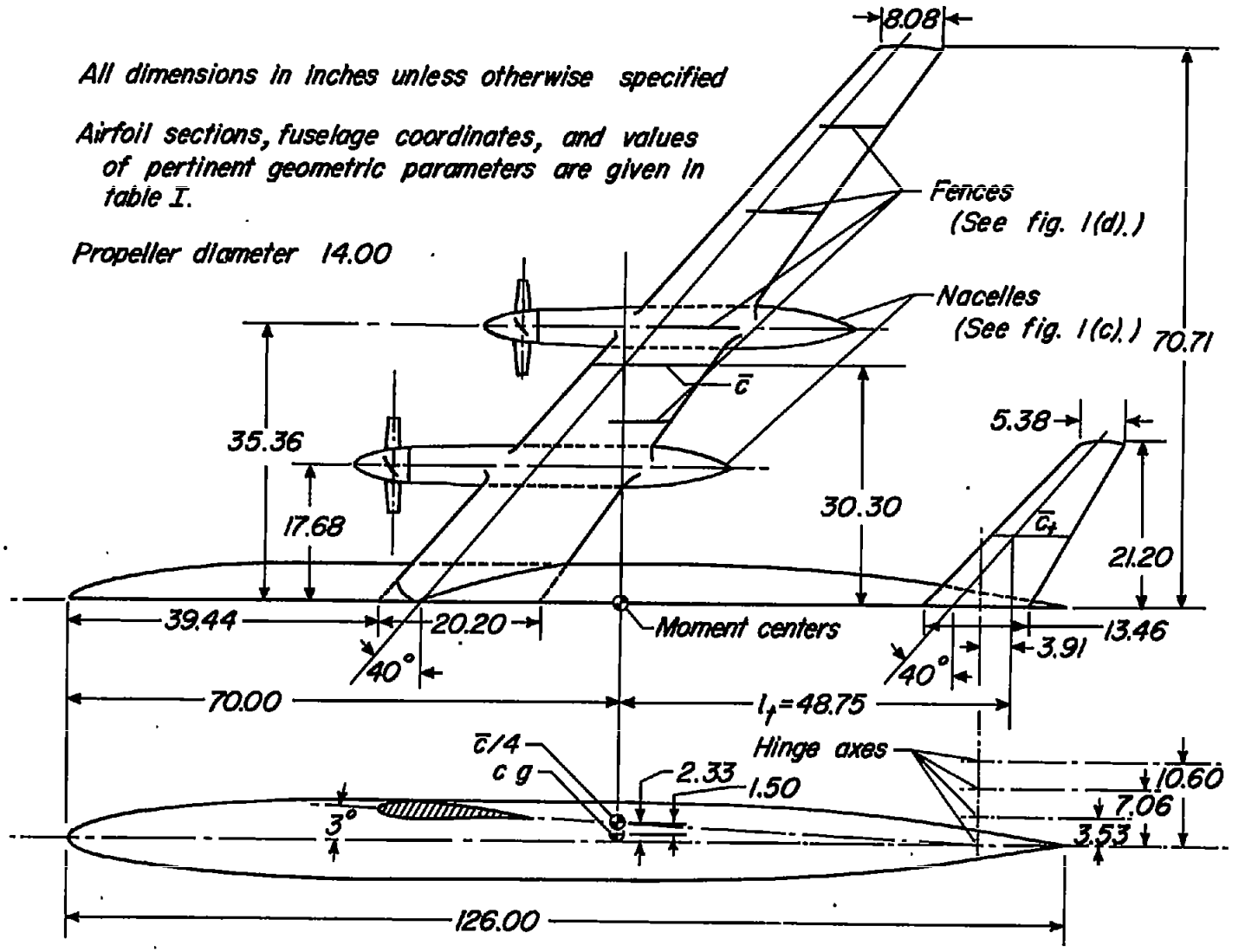

(a) Dimensions.

Figure 1.- Geometry of the model.

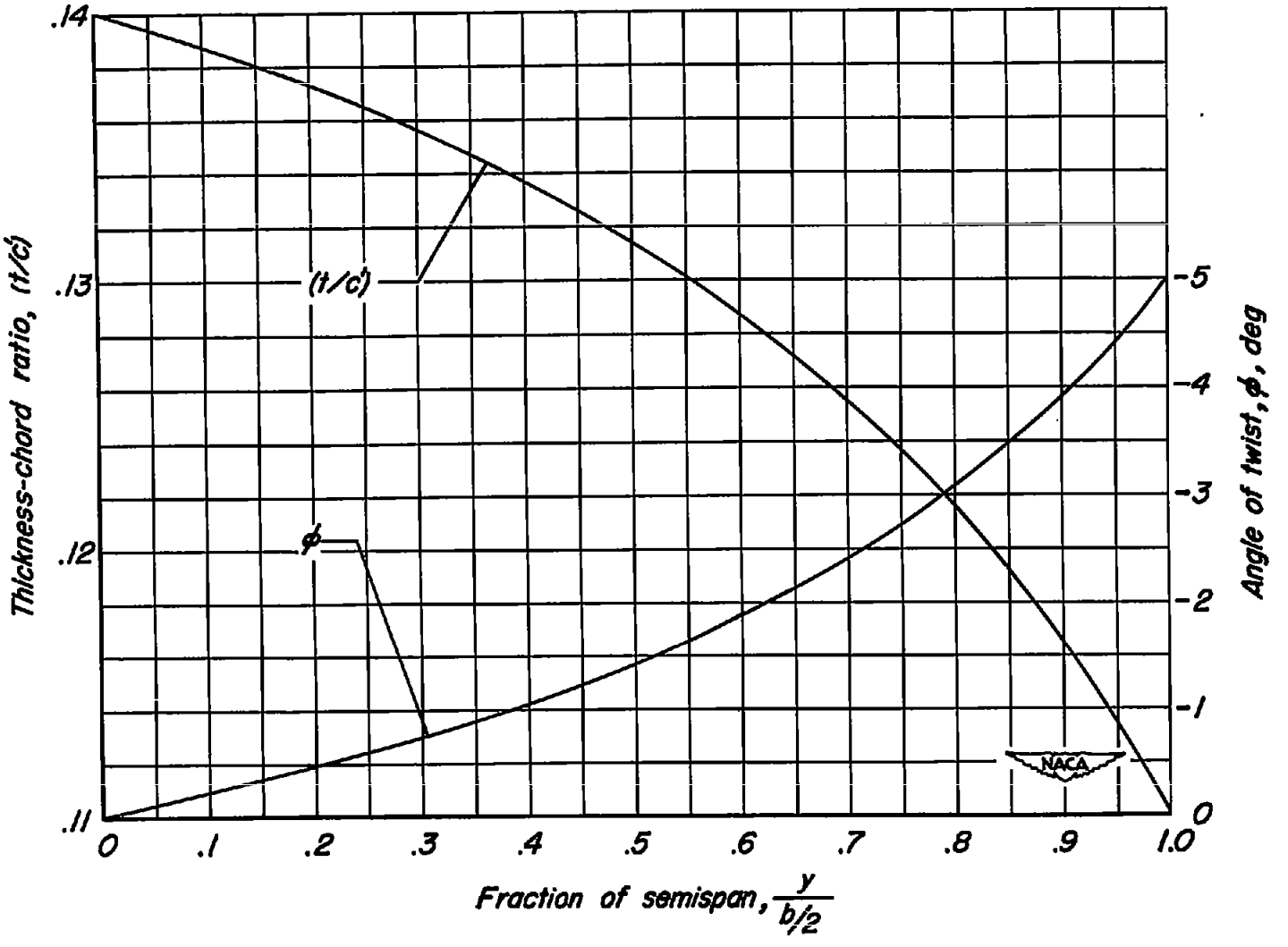

(b) Wing twist and thickness-chord ratio.

Figure 1.- Continued.

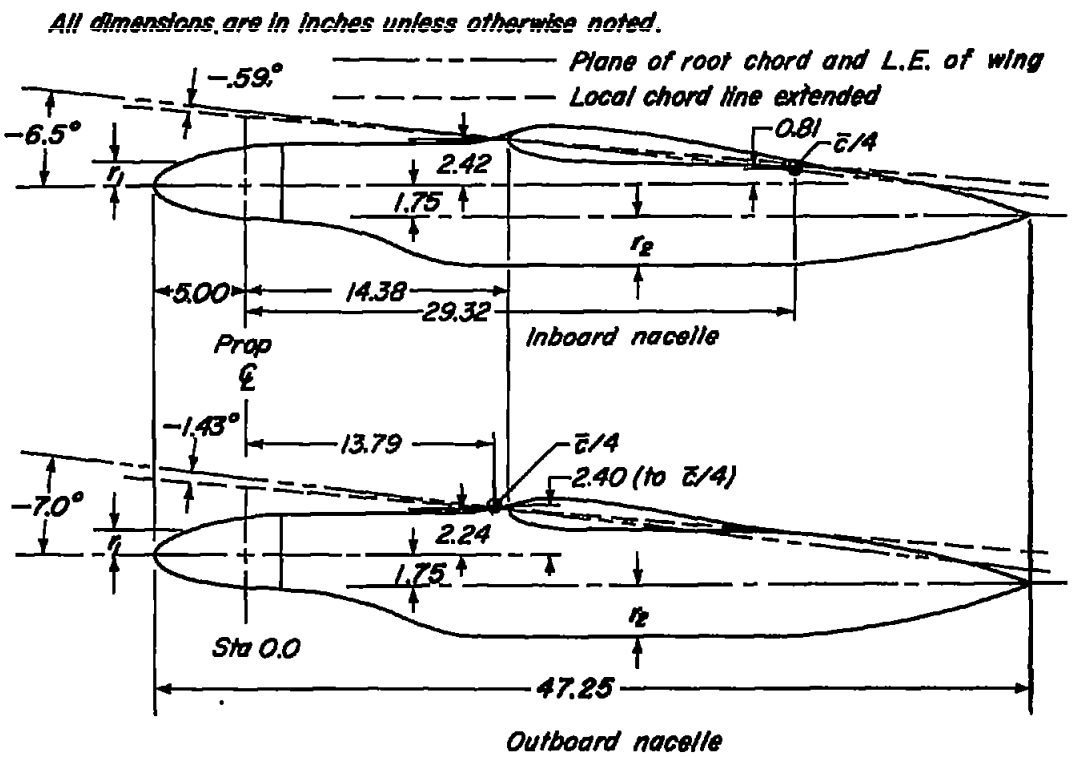

Nacelle coordinates

Sta	r_1	Sta	r_2
-5.00	0	2.00	0.350
-4.79	.385	3.00	.419
-4.58	.567	4.00	.616
-4.25	.788	5.00	.919
-3.95	.951	6.00	1.290
-3.25	1.242	7.00	1.685
-2.55	1.472	8.00	2.056
-1.80	1.670	9.00	2.359
- .80	1.871	10.00	2.556
0	1.985	11.00	2.625
2.00	2.100	30.50	2.625
12.00	2.100	32.50	2.450
		34.50	2.220
		36.50	1.825
		38.50	1.270
		40.50	.675
		41.50	.275
		42.25	0

(c) Dimensions of the nacelles.

Figure 1.- Continued.

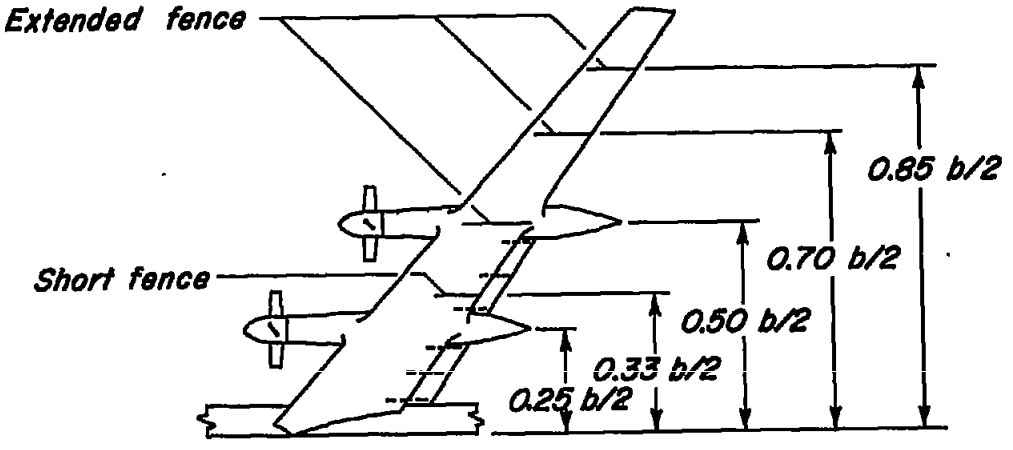

Model with inboard flaps

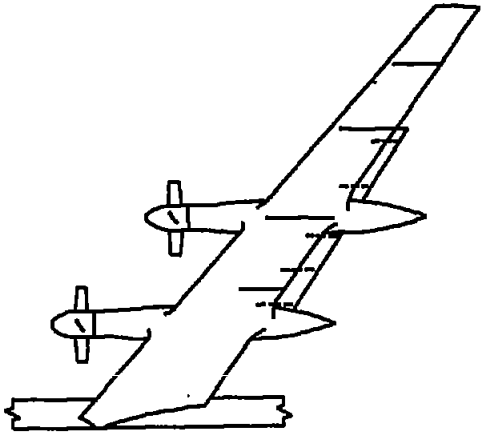

Model with outboard flaps

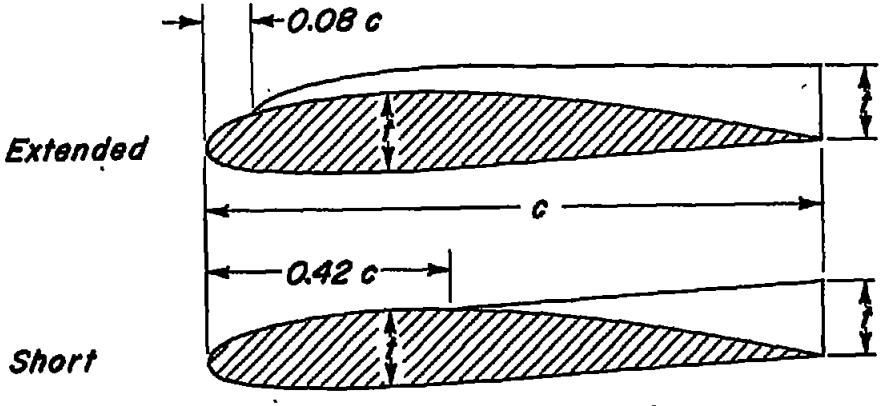

Typical sections through fences

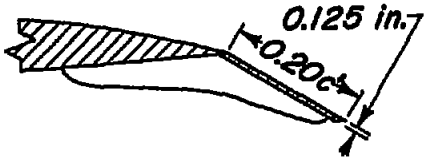

Typical section through flap and normal to reference sweep line

(d) Fence and flap details.

Figure 1.- Concluded.

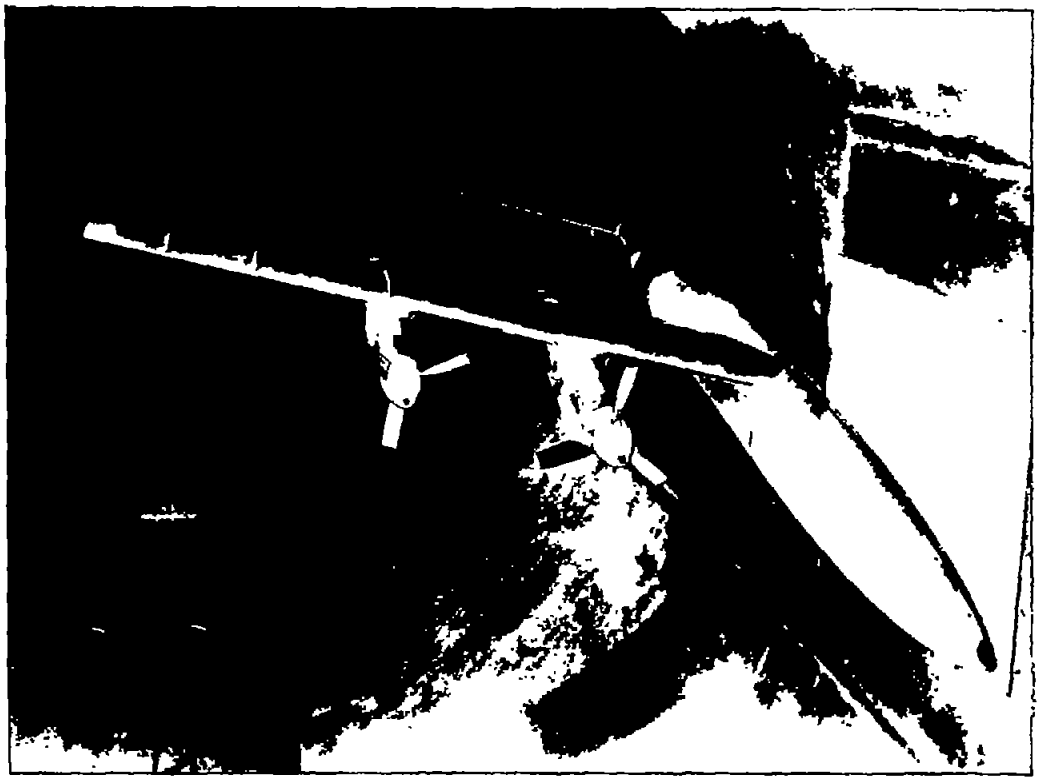

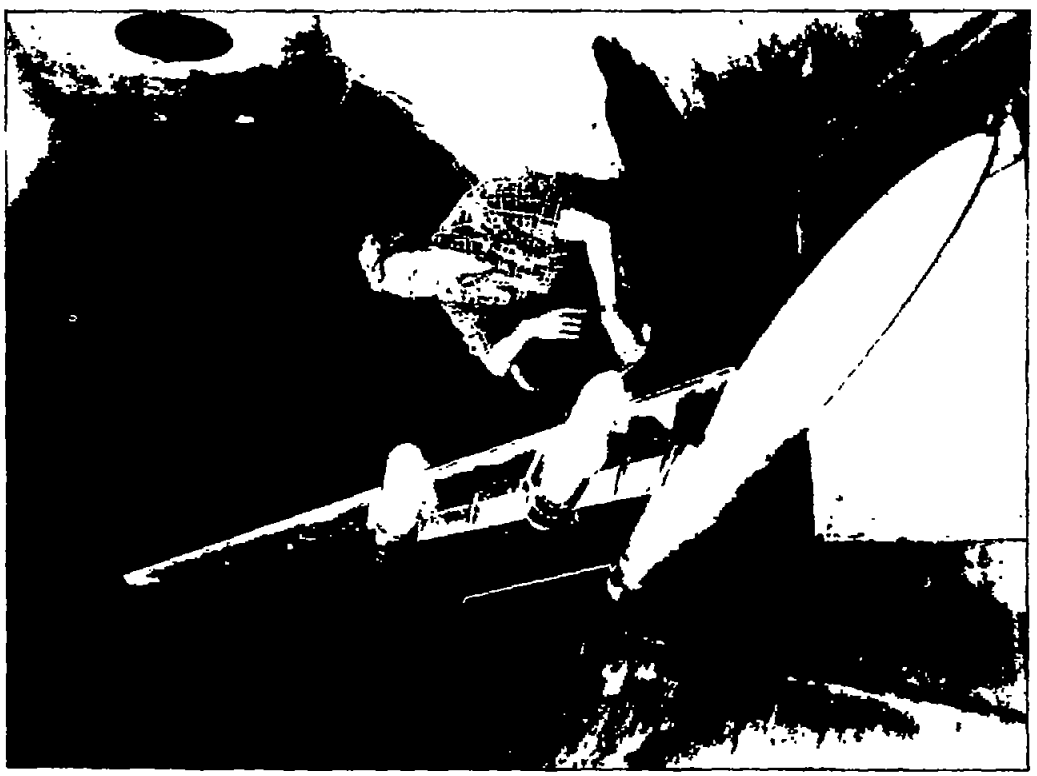

Figure 2.- Model mounted in the wind tunnel.

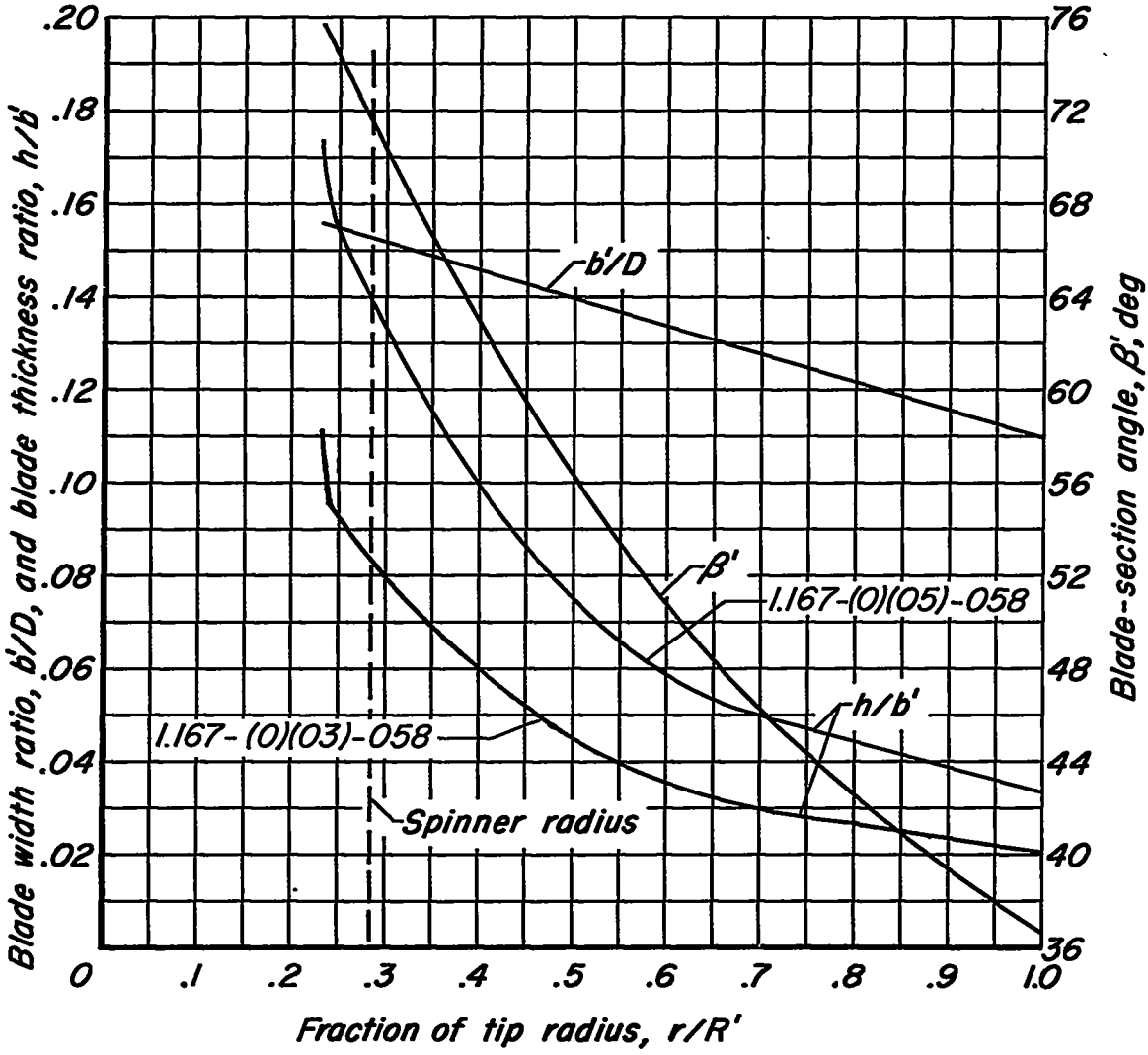

Figure 3.- Blade-form curves for the NACA 1.167-(0)(05)-058 and the NACA 1.167-(0)(03)-058 three-blade propellers.

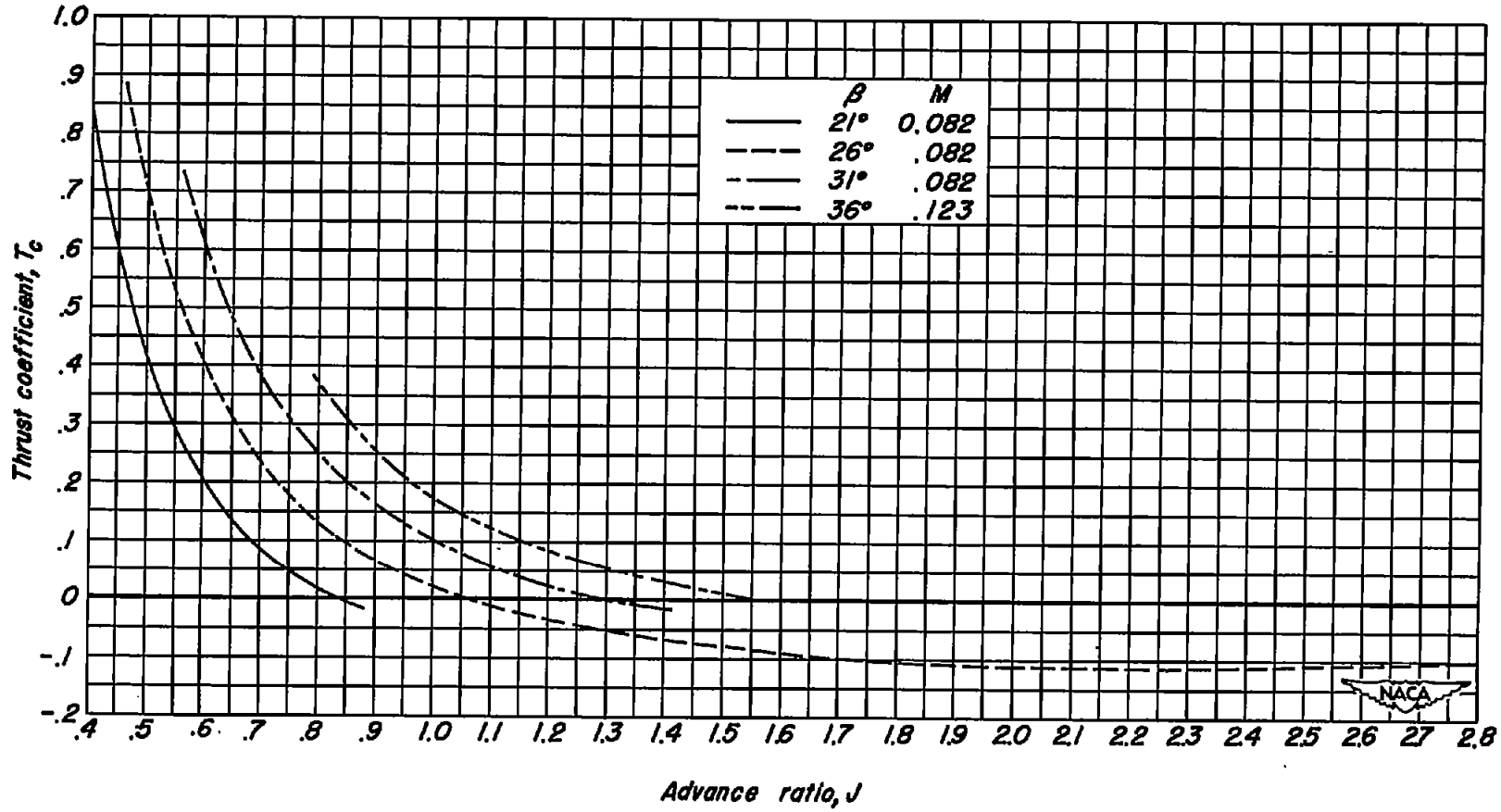

Figure 4.- The variation of T_c with J for the NACA 1.167-(0)(05)-058 propeller; A = 0°; R = 4,000,000.

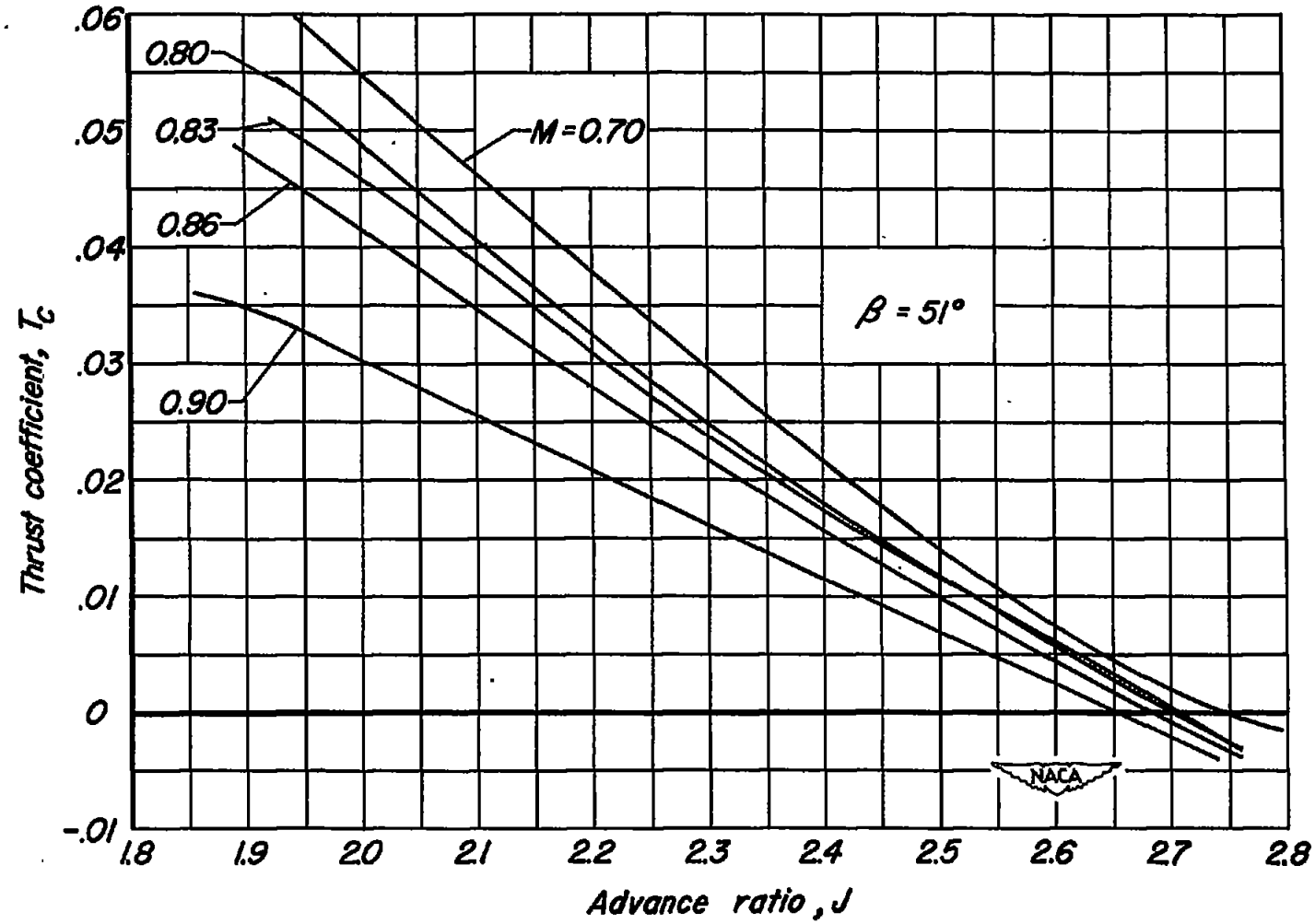

(a) R = 1×10^6

Figure 5.- The variation of T_c with J for the NACA 1.167-(0)(03)-058 propeller; A = 0°.

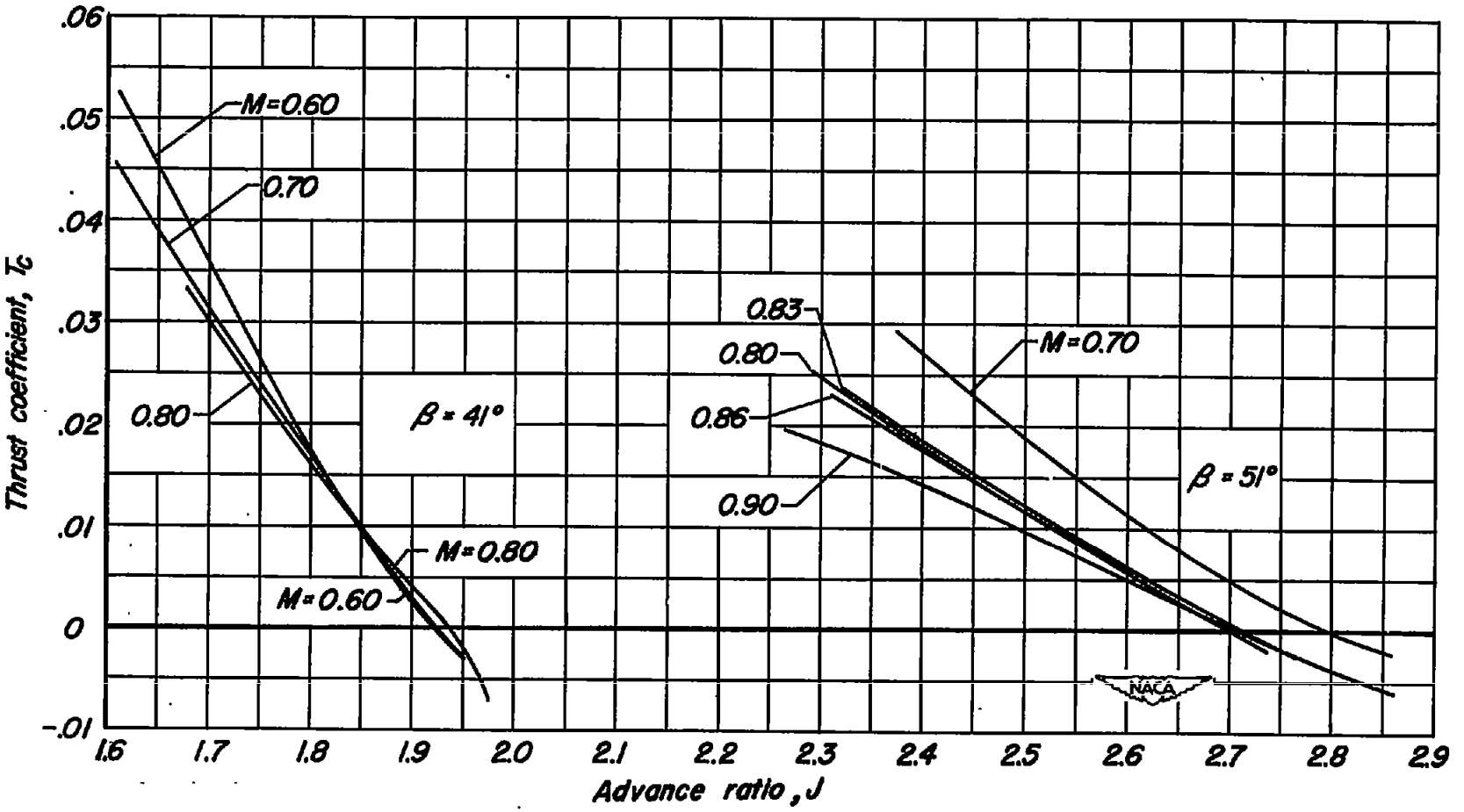

(b) R = 2×10^6

Figure 5.- Concluded.

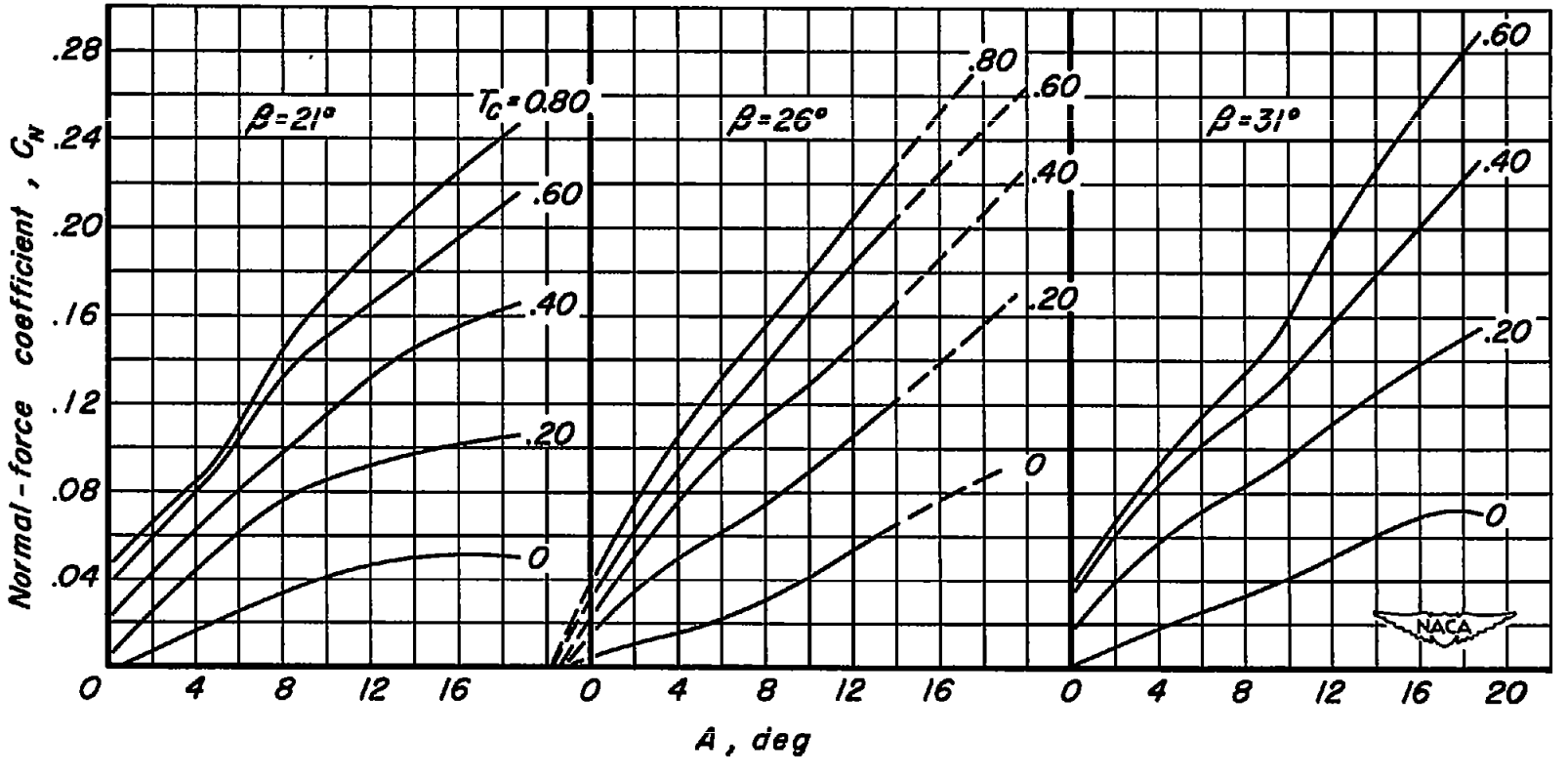

Figure 6.- Normal-force characteristics of the NACA 1.167-(0)(05)-058 propeller; M = 0.082; R = 4,000,000.

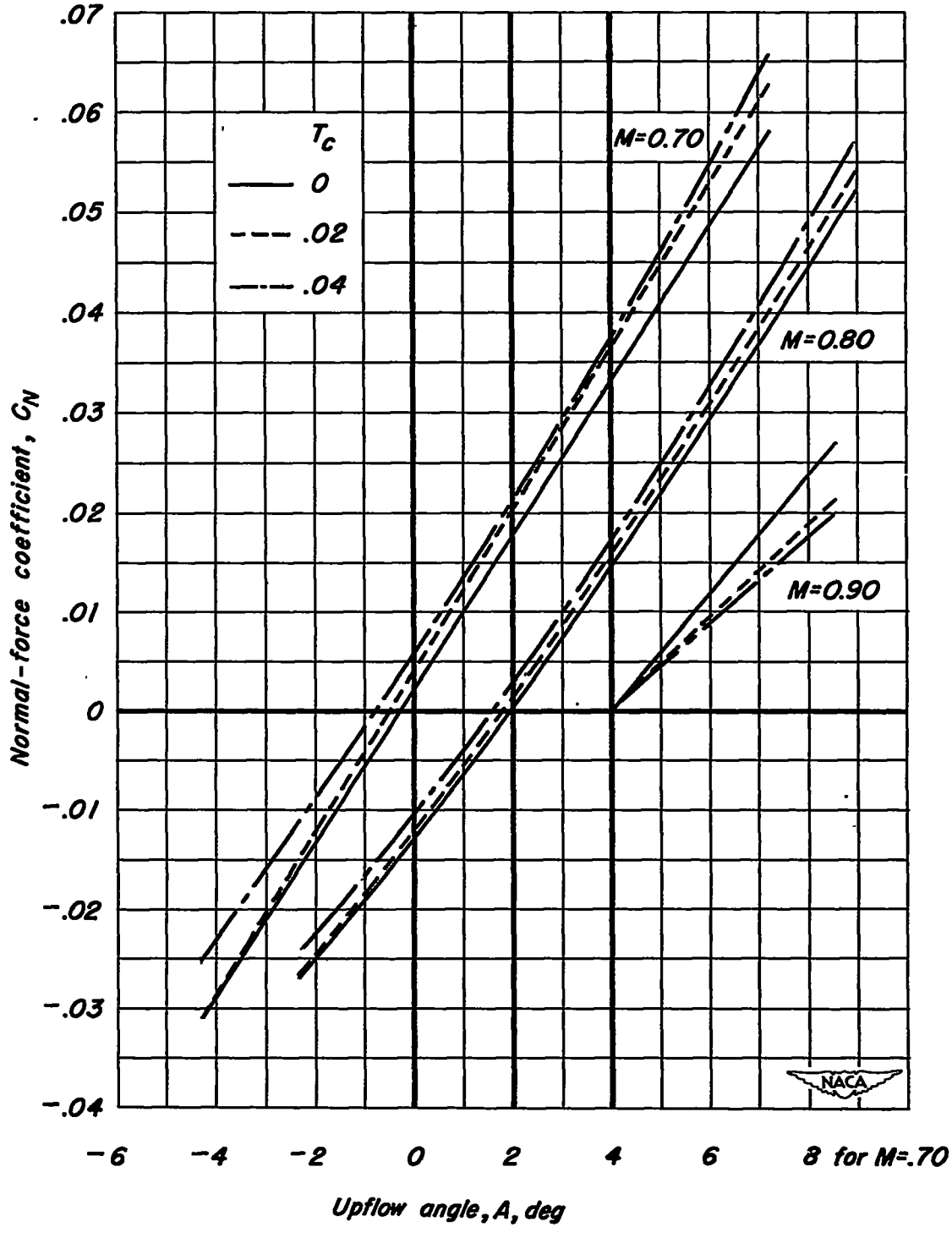

Figure 7.- Normal-force characteristics of the NACA 1.167-(0)(03)-058 propeller; $\beta = 51^{\circ}$, R = 1,000,000.

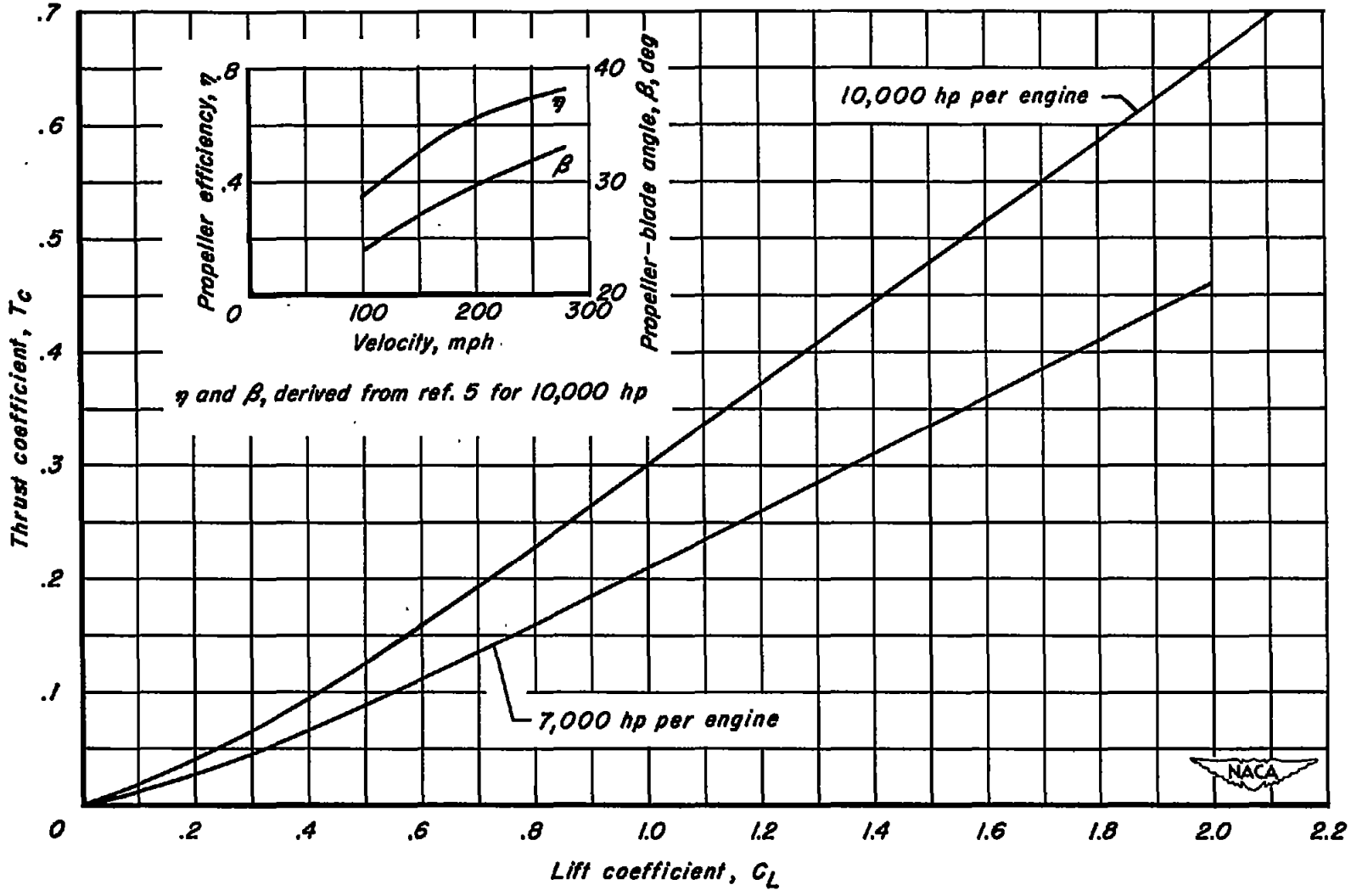

Figure 8.- The T_c vs. C_L relationship for simulated take-off full-scale constant power conditions; wing loading = 100 lb/sq ft; propeller rotational speed = 1715 rpm; propeller diameter = 14 ft; propeller efficiency and blade angle as shown; sea level.

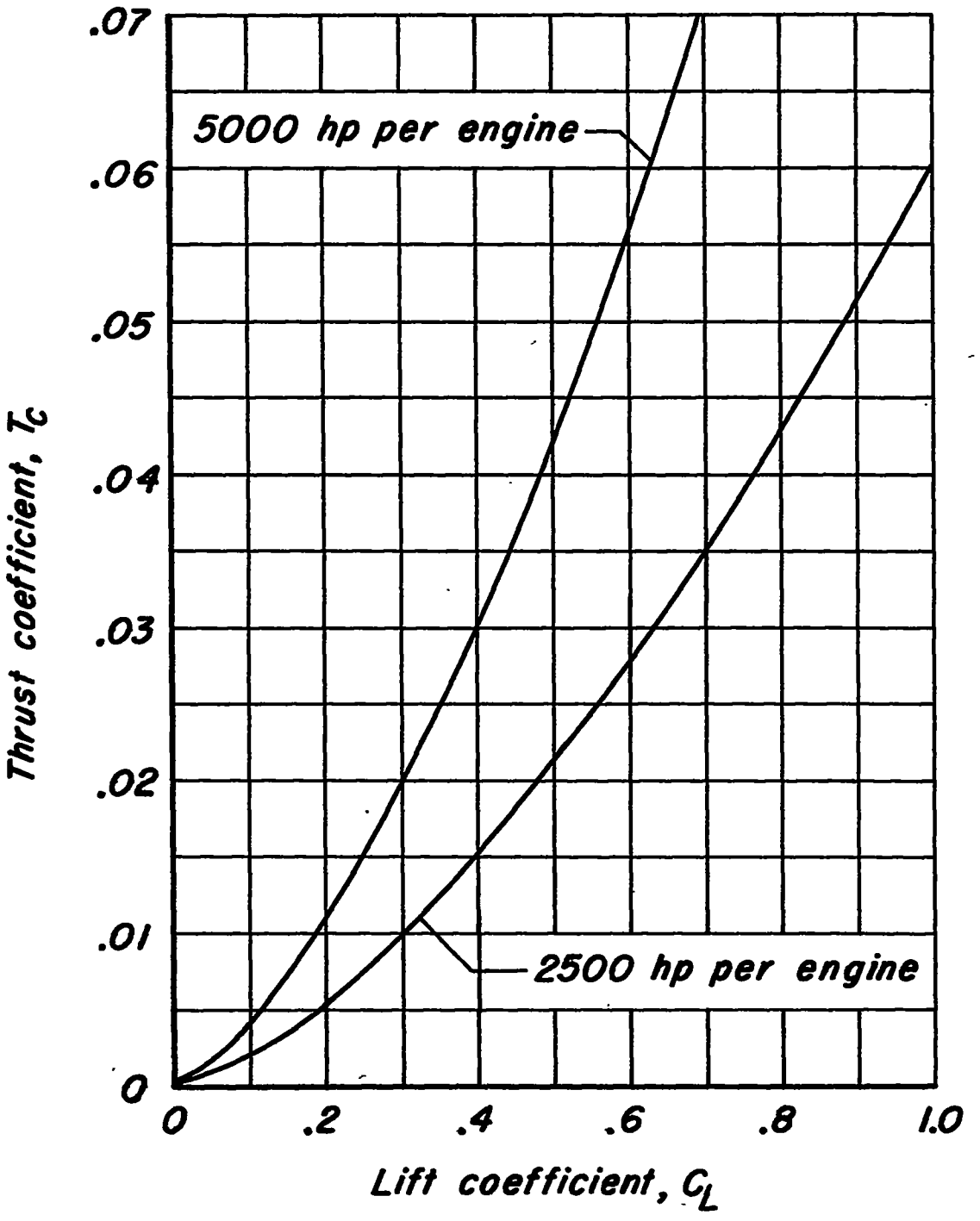

Figure 9.- The T_c vs. C_L relationship for simulated high-speed full-scale constant power conditions; wing loading = 75 lb/sq ft; propeller rotational speed = 1715 rpm; propeller diameter = 14 ft; assumed propeller efficiency = 0.65; altitude = 40,000 ft.

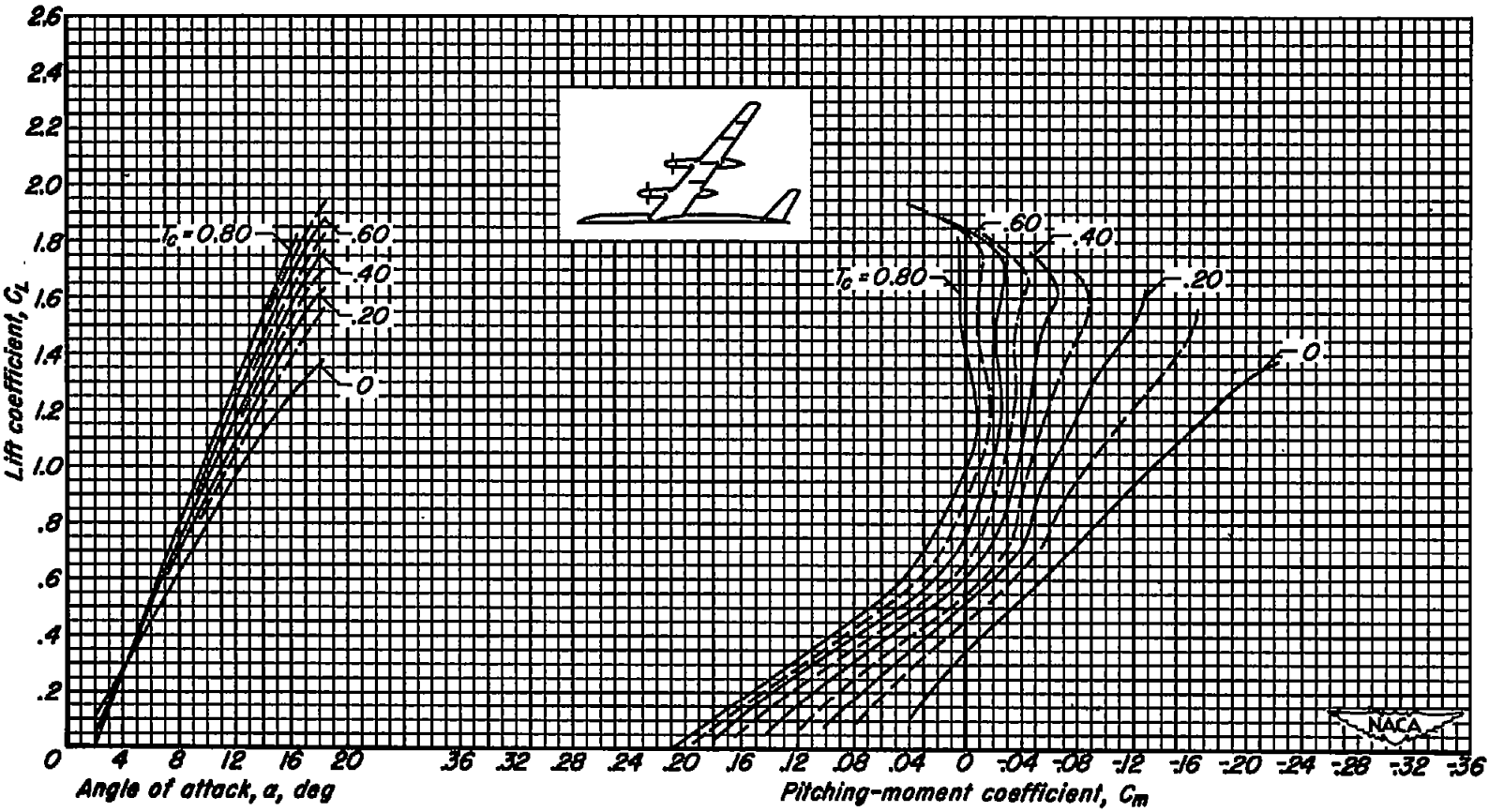

(a) C_L vs. α and C_m

Figure 10.- Example of low-speed data from reference 5 showing the longitudinal characteristics of the model; tail height = 0; flaps up; M = 0.082; R = 4,000,000; $\beta = 26^\circ$; $i_t = -4^\circ$.

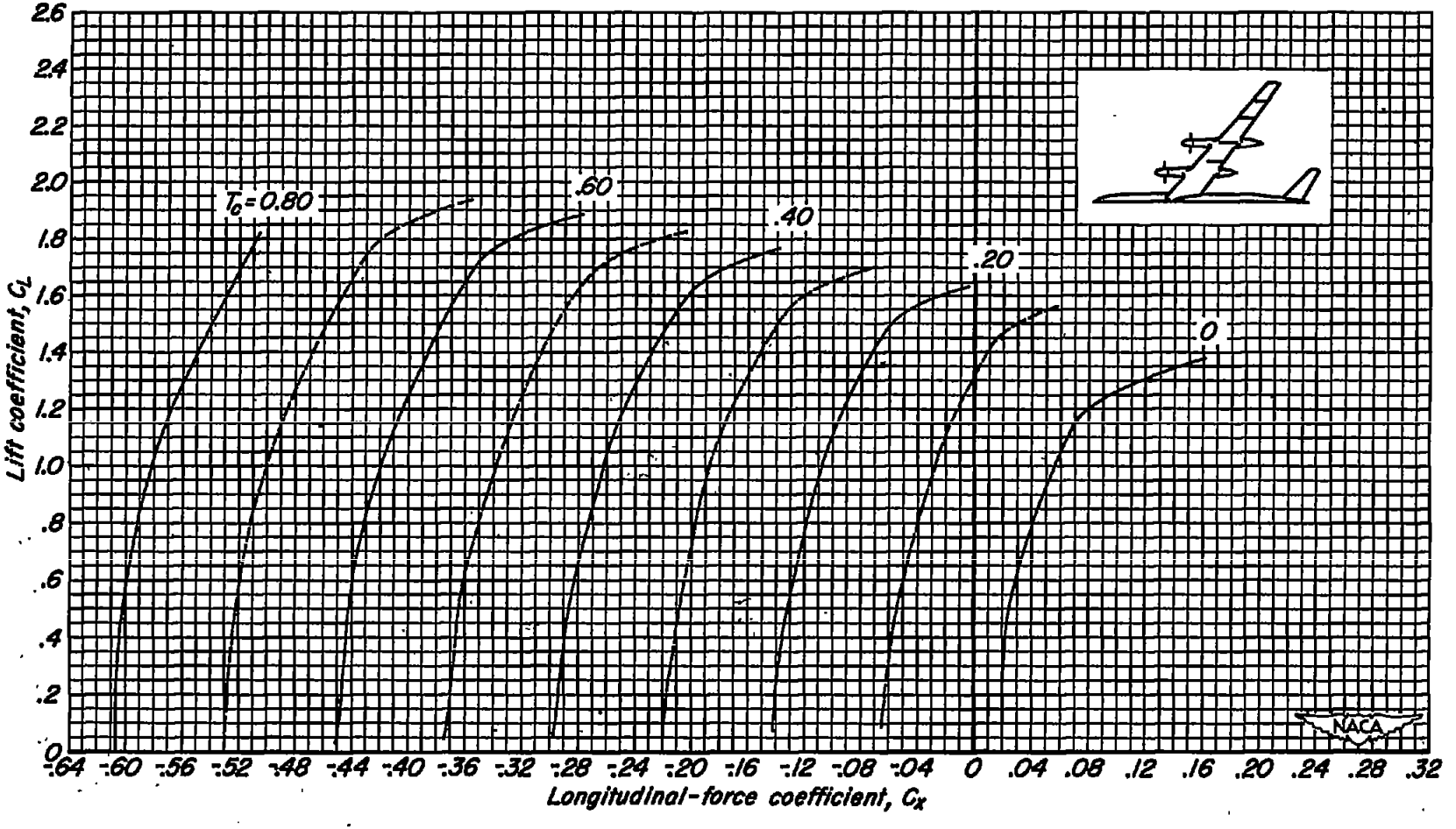

(b) C_L vs. C_X

Figure 10.- Concluded.

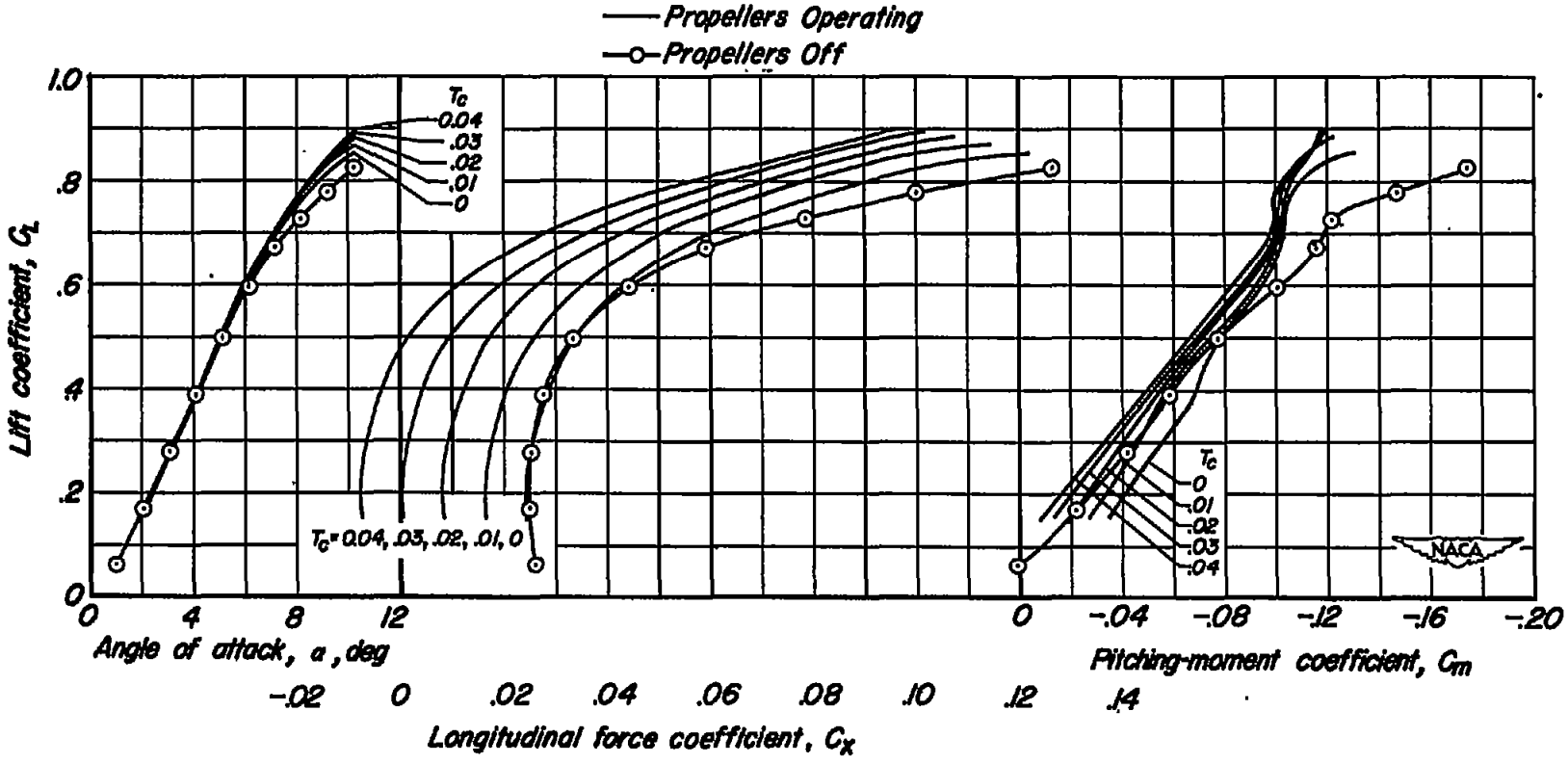

Figure 11.- Example of high-speed data from reference 5 showing the longitudinal characteristics of the model; tail height = 0; M = 0.80; R = 1,000,000; $\beta = 51^\circ$; $i_t = -2^\circ$.

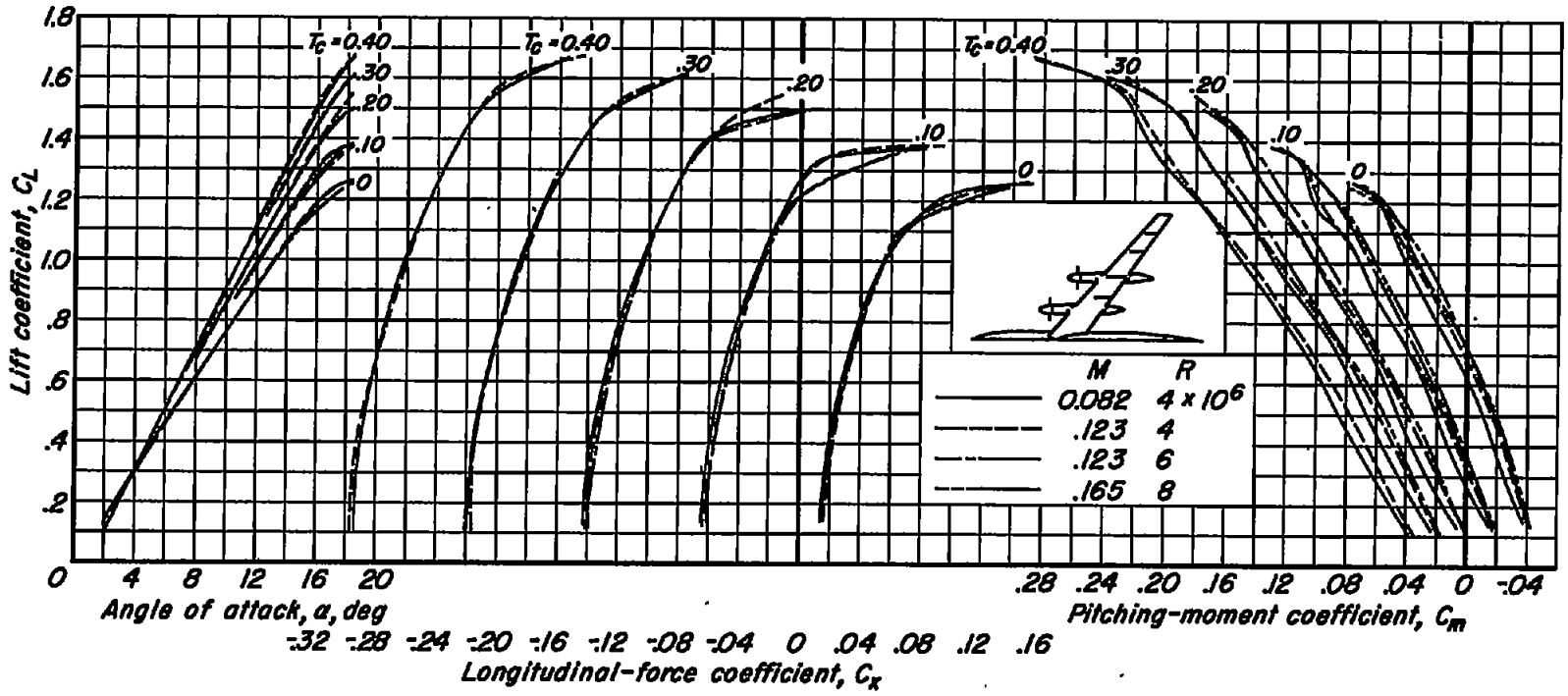

Figure 12.- The effects of Mach number and Reynolds number on the longitudinal characteristics of the model; tail removed; flaps up; $\beta = 31^\circ$.

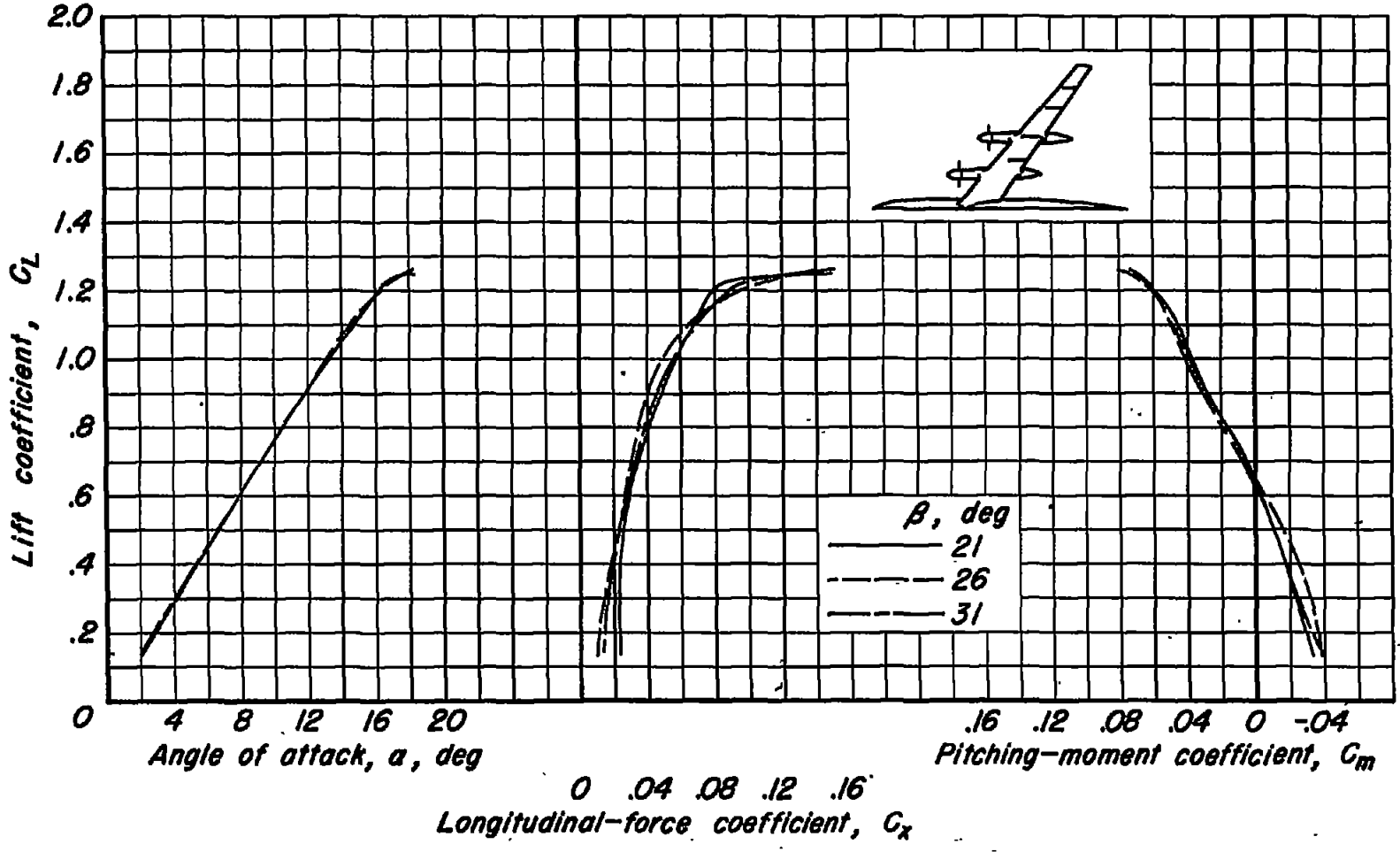

(a) $T_c = 0$

Figure 13.- The effects of propeller-blade angle on the longitudinal characteristics of the model; tail removed; flaps up; M = 0.082; R = 4,000,000.

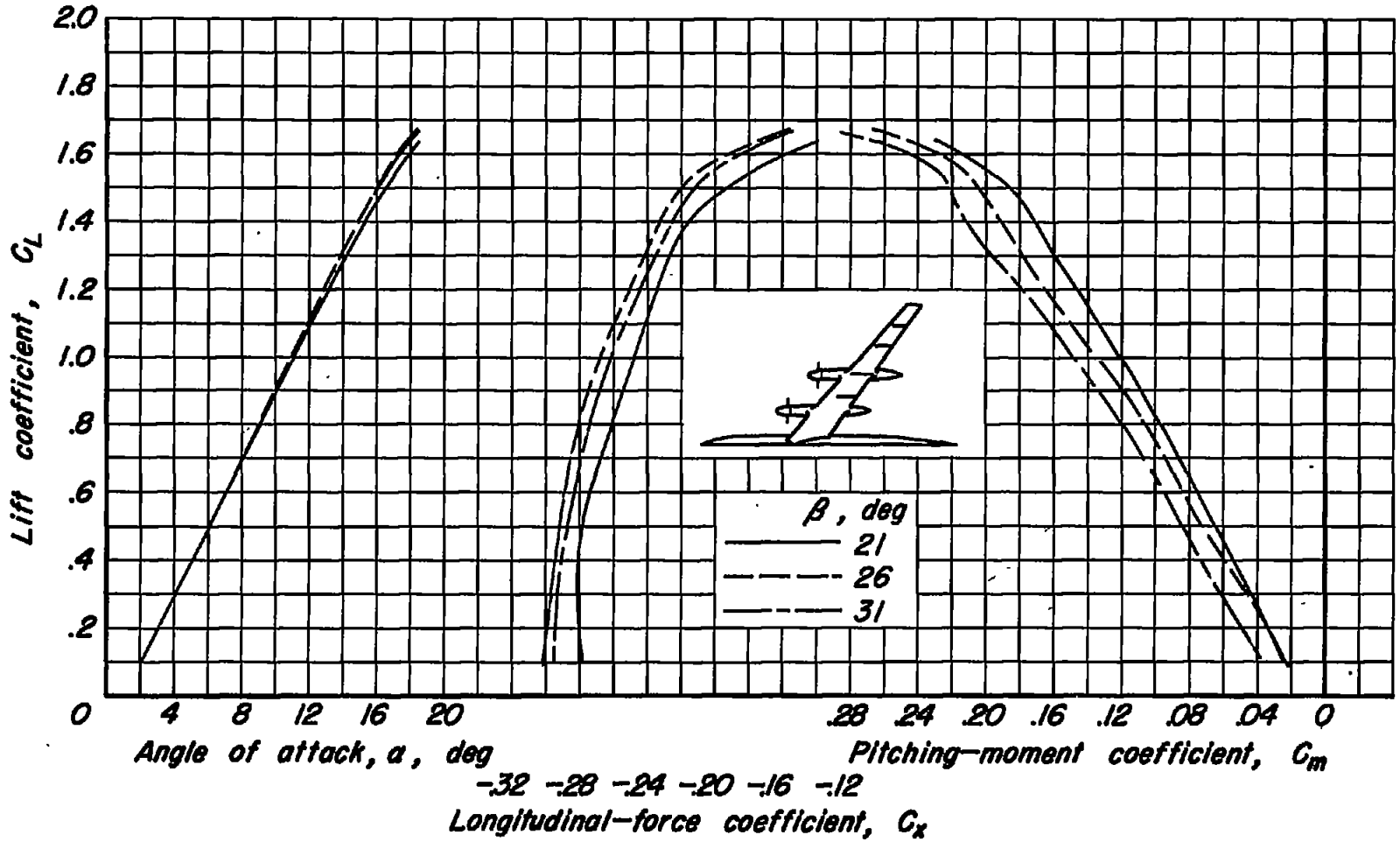

(b) $T_c = 0.40$

Figure 13.- Continued.

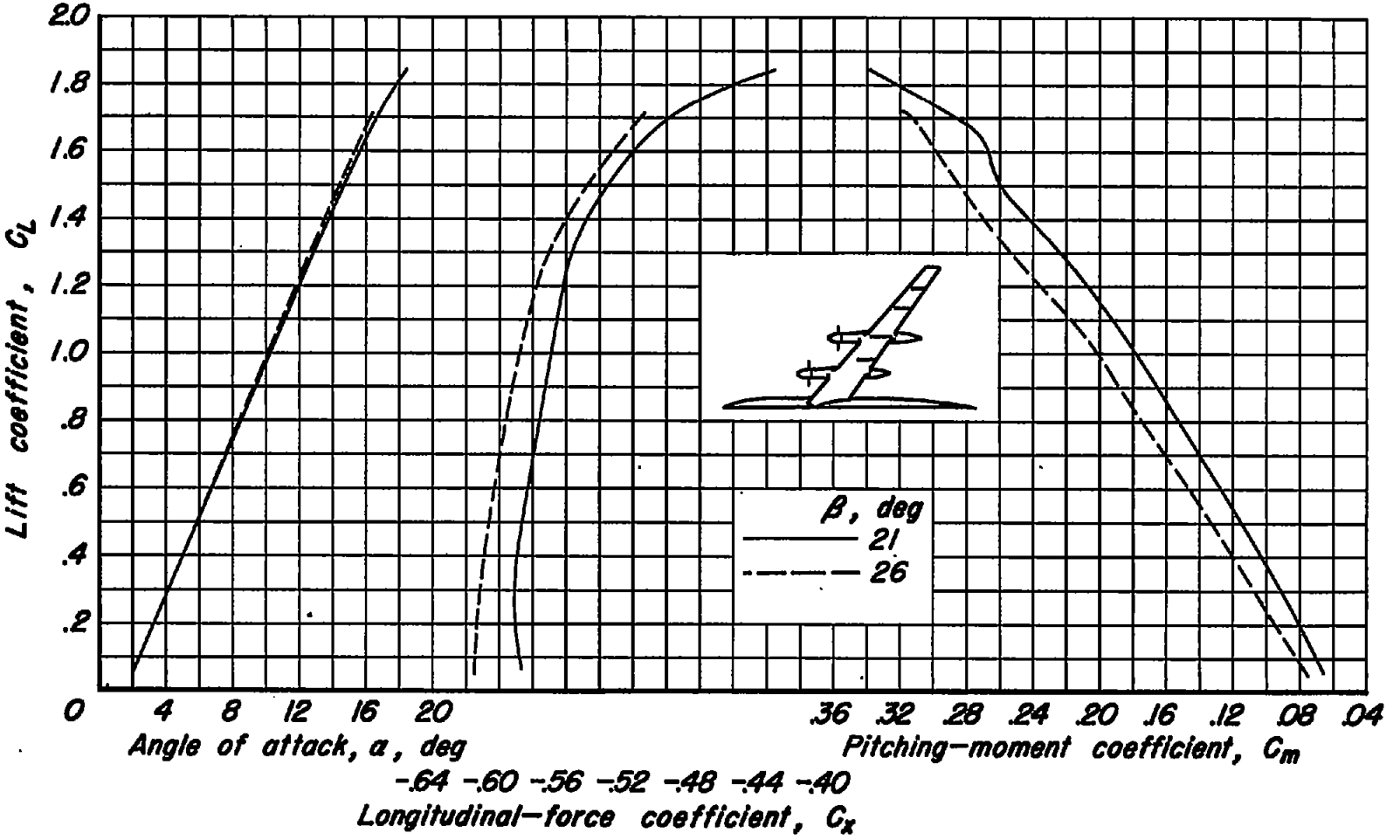

(c) T_c = 0.80

Figure 13.- Concluded.

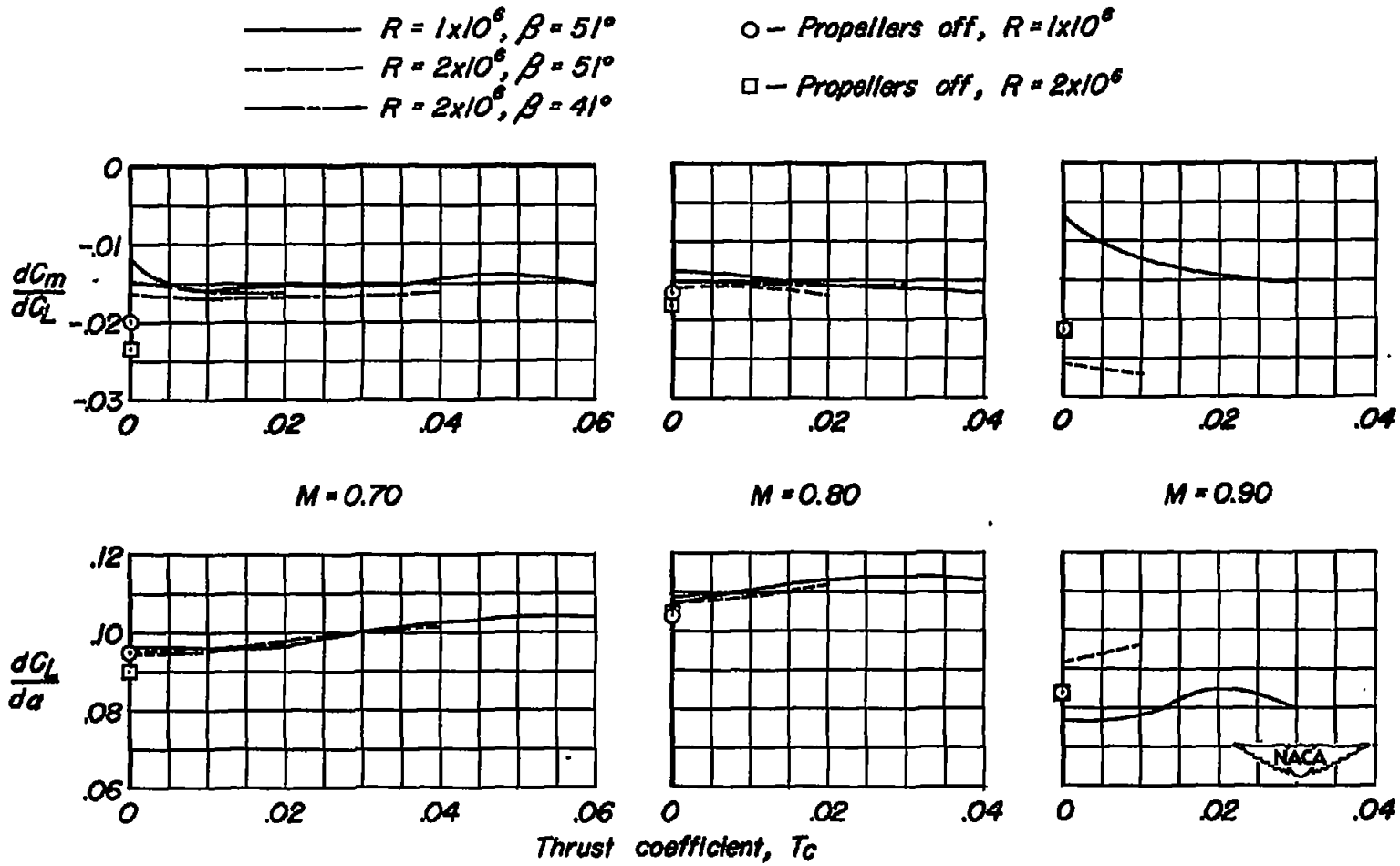

(a) Lift-curve and pitching-moment-curve slopes.

Figure 14.- The variation of the longitudinal characteristics of the model with thrust coefficient for two propeller blade angles and Reynolds numbers with and without operating propellers. C_L = 0.40, tail height = 0 b/2, i_t = -4°.

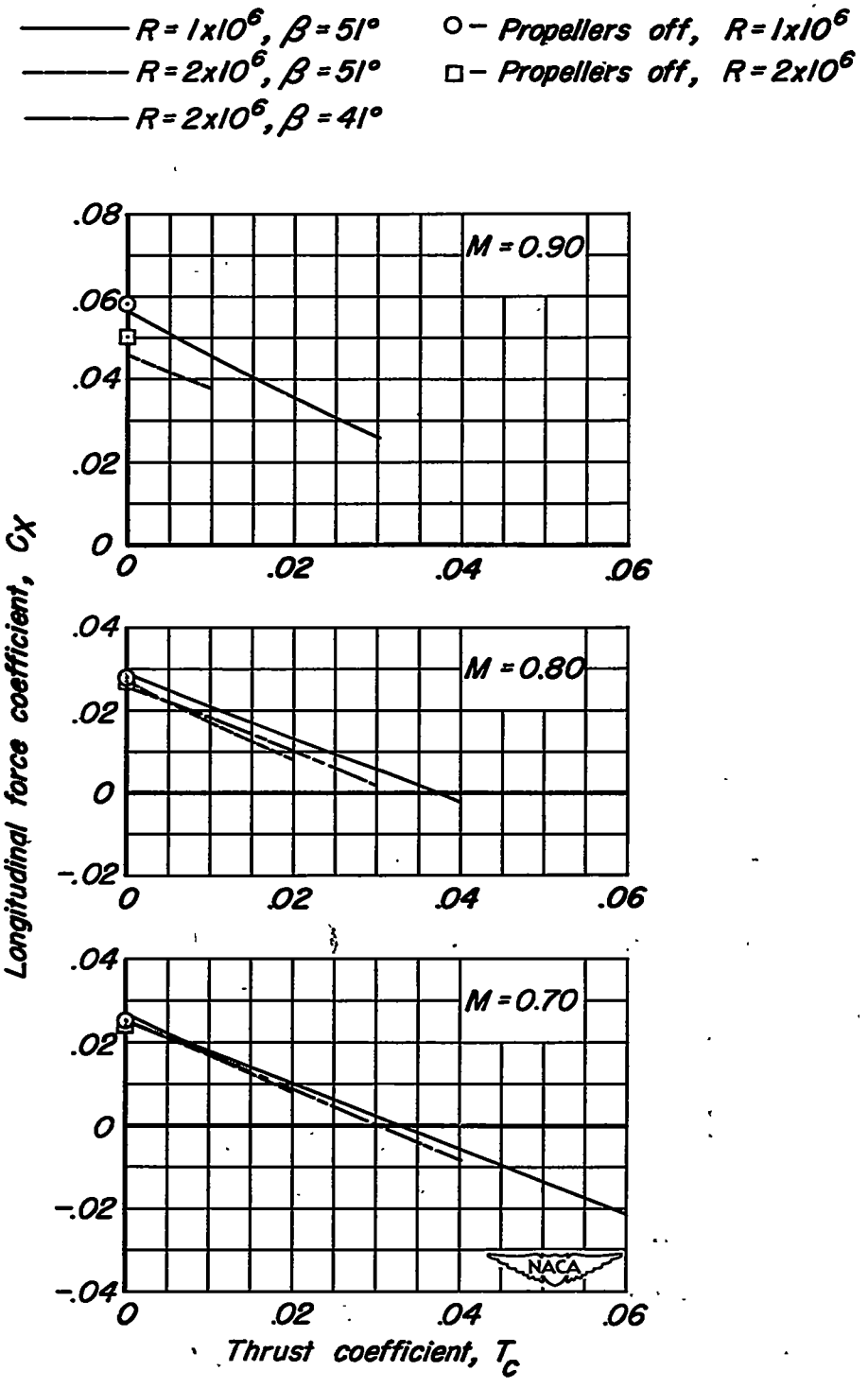

(b) Longitudinal force.

Figure 14.- Concluded.

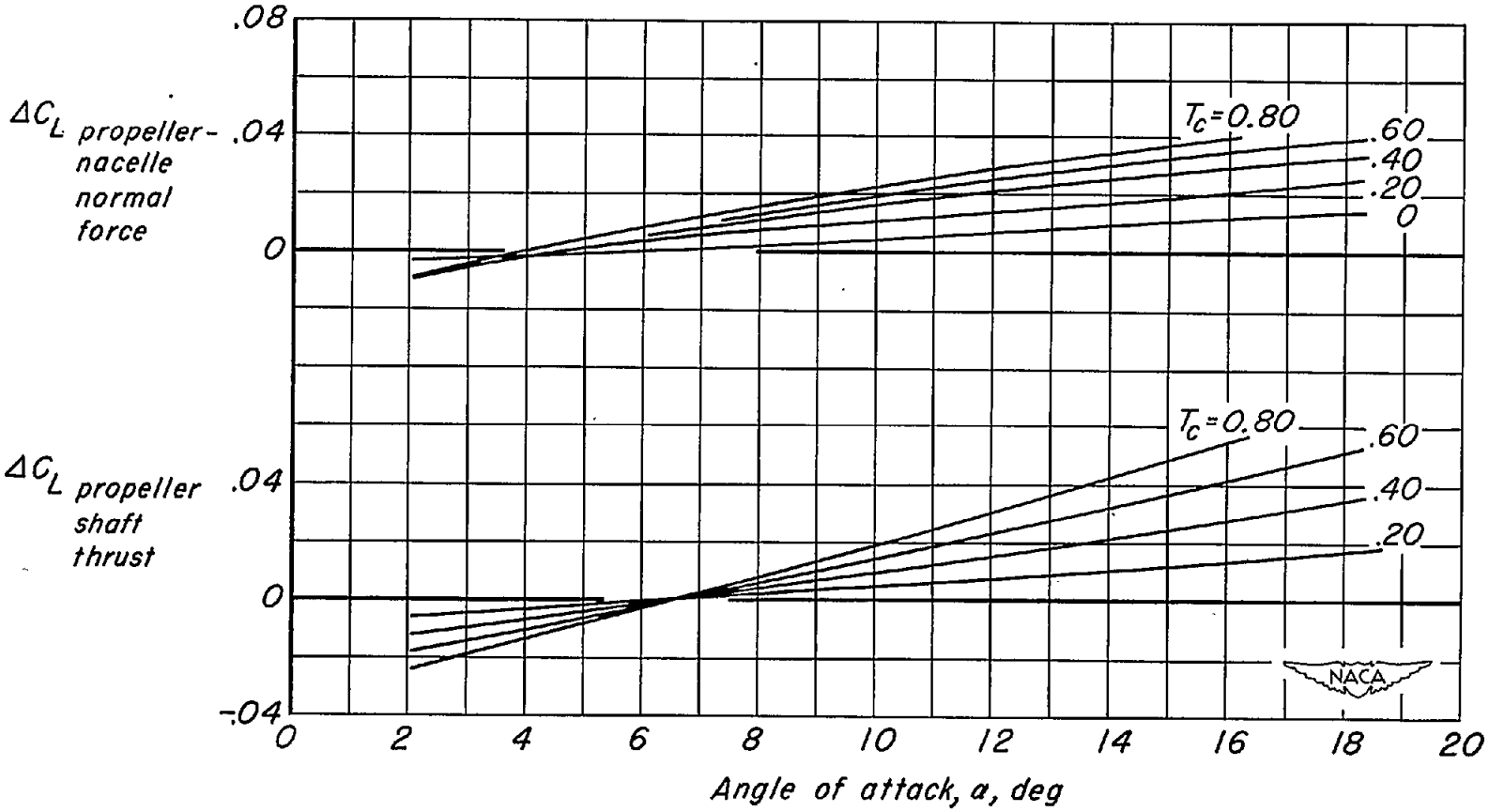

Figure 15.- The increments of lift coefficient of the model due to the normal force and shaft thrust of each propeller, including the effects of slipstream on the nacelle forebody; M = 0.082; R = 4,000,000; $\beta = 26^\circ$.

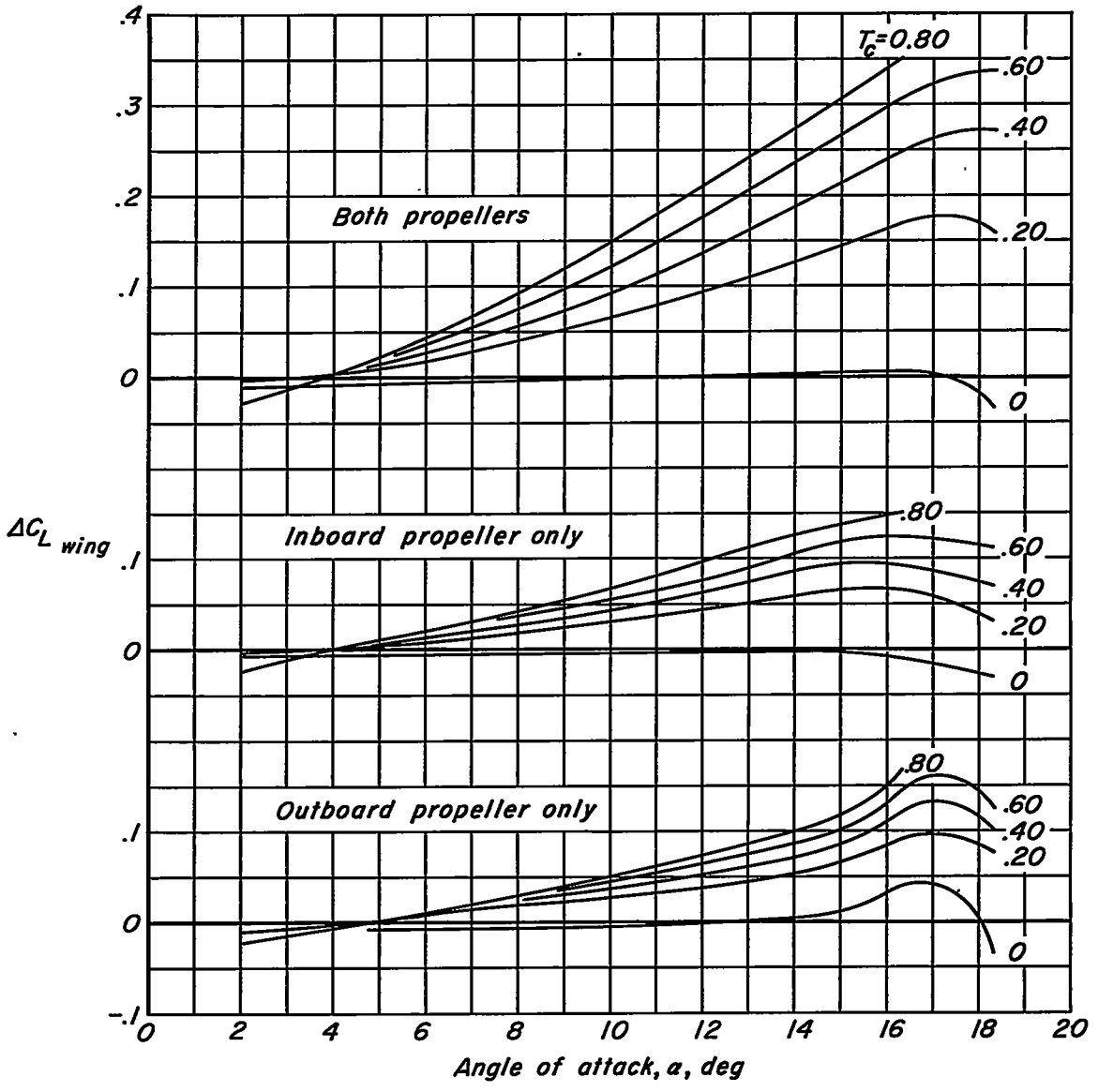

(a) Flaps up.

Figure 16.- The increments of lift coefficient due to the slipstreams on the wing; M = 0.082; R = 4,000,000; $\beta = 26^{\circ}$.

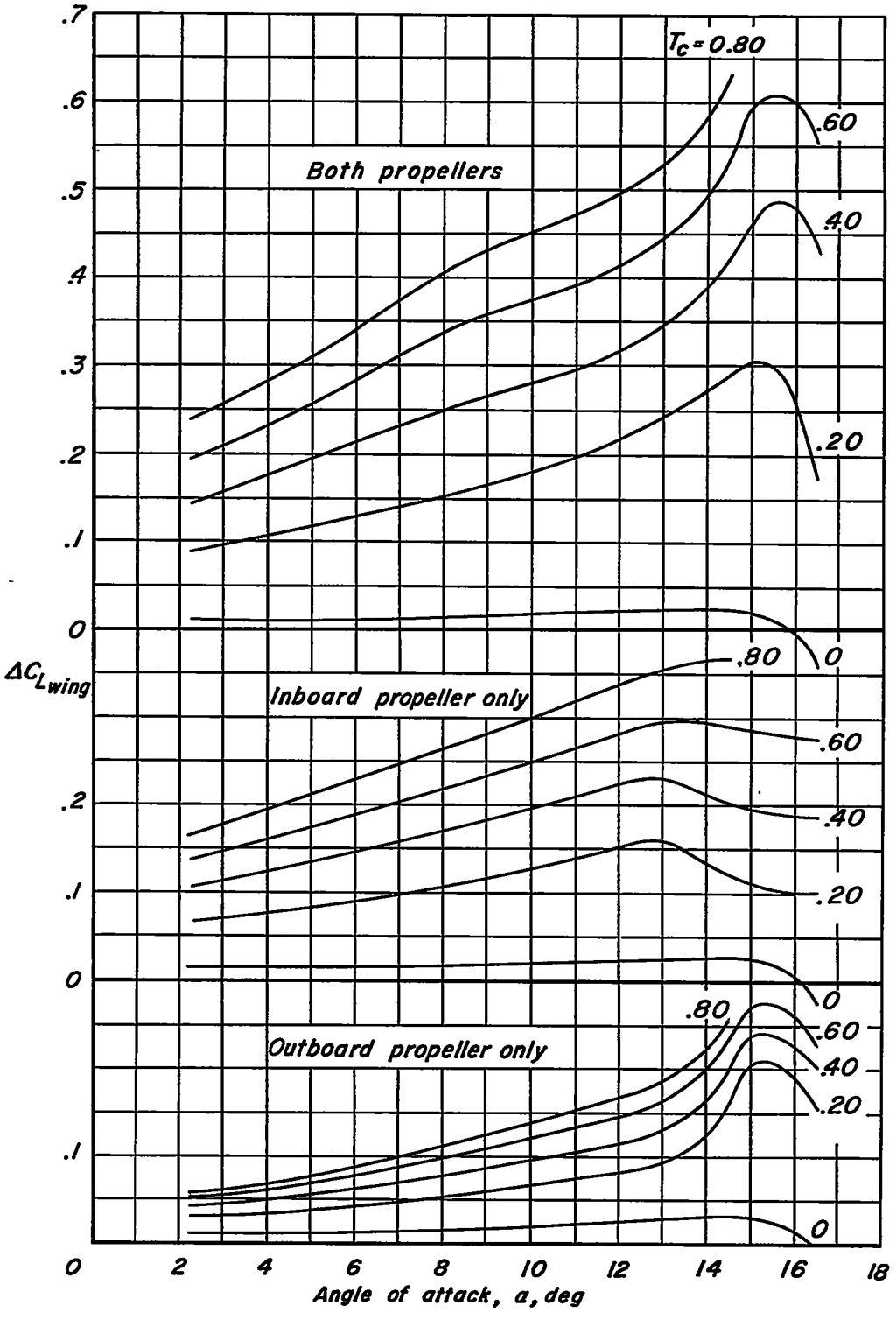

(b) Inboard flaps deflected.

Figure 16.- Concluded.

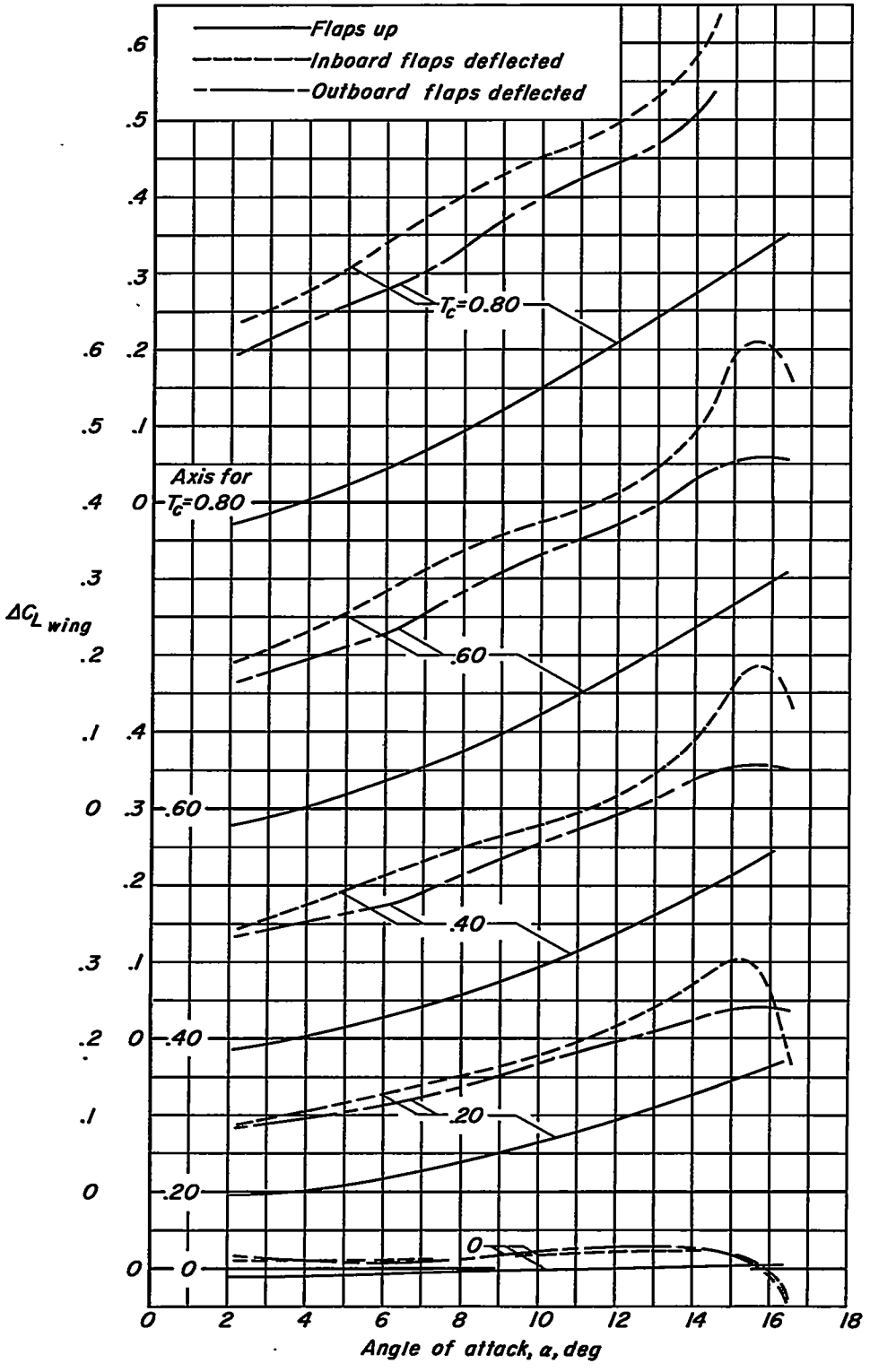

Figure 17.- The effects of flaps on the increments of lift coefficient due to the slipstreams on the wing; M = 0.082; R = 4,000,000; $\beta = 26^{\circ}$.

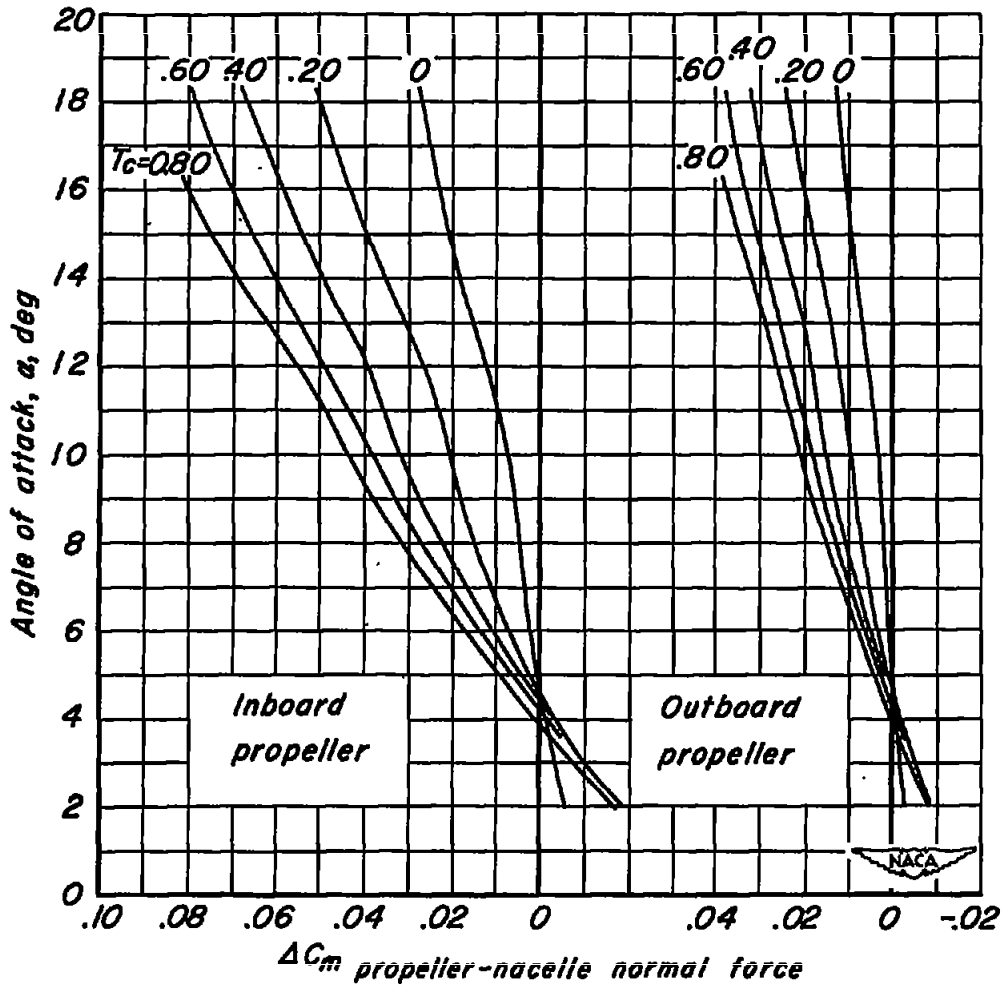

(a) Flaps up.

Figure 18.- The increments of pitching-moment coefficient of the model due to the normal force of each propeller, including the effects of slipstream on the nacelle forebody; M = 0.082; R = 4,000,000; $\beta = 26^\circ$.

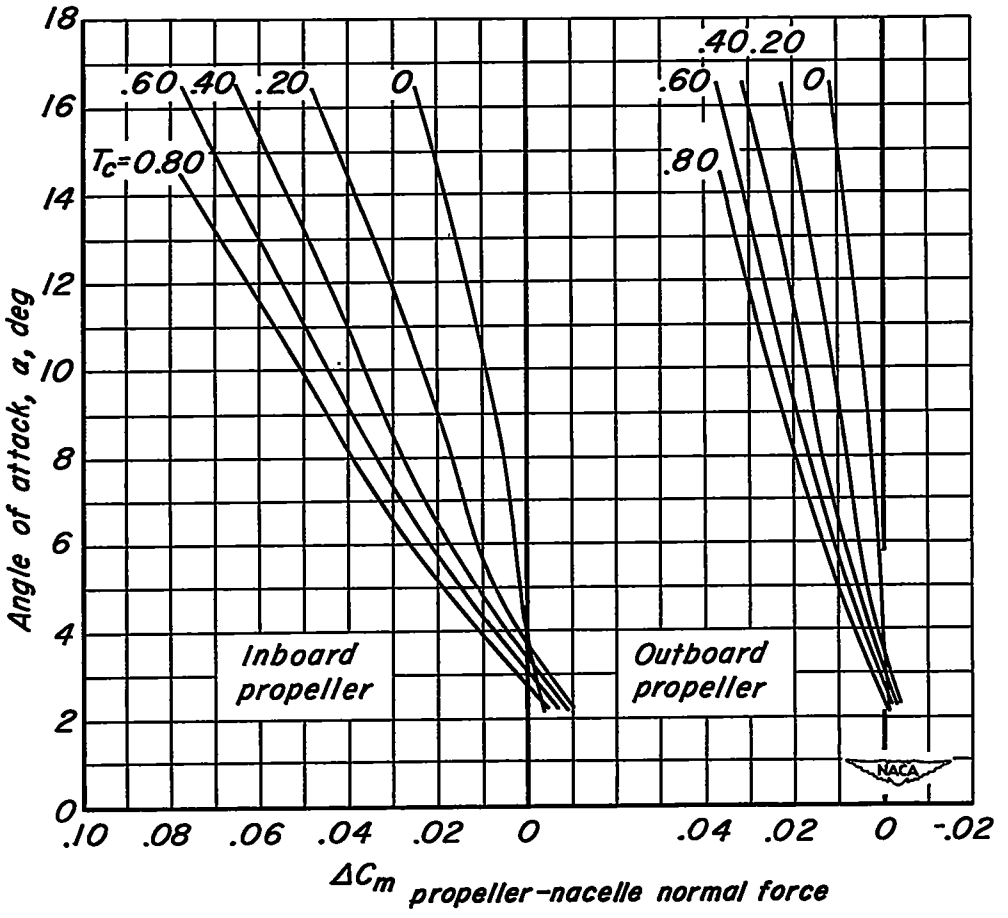

(b) Inboard flaps deflected.

Figure 18.- Concluded.

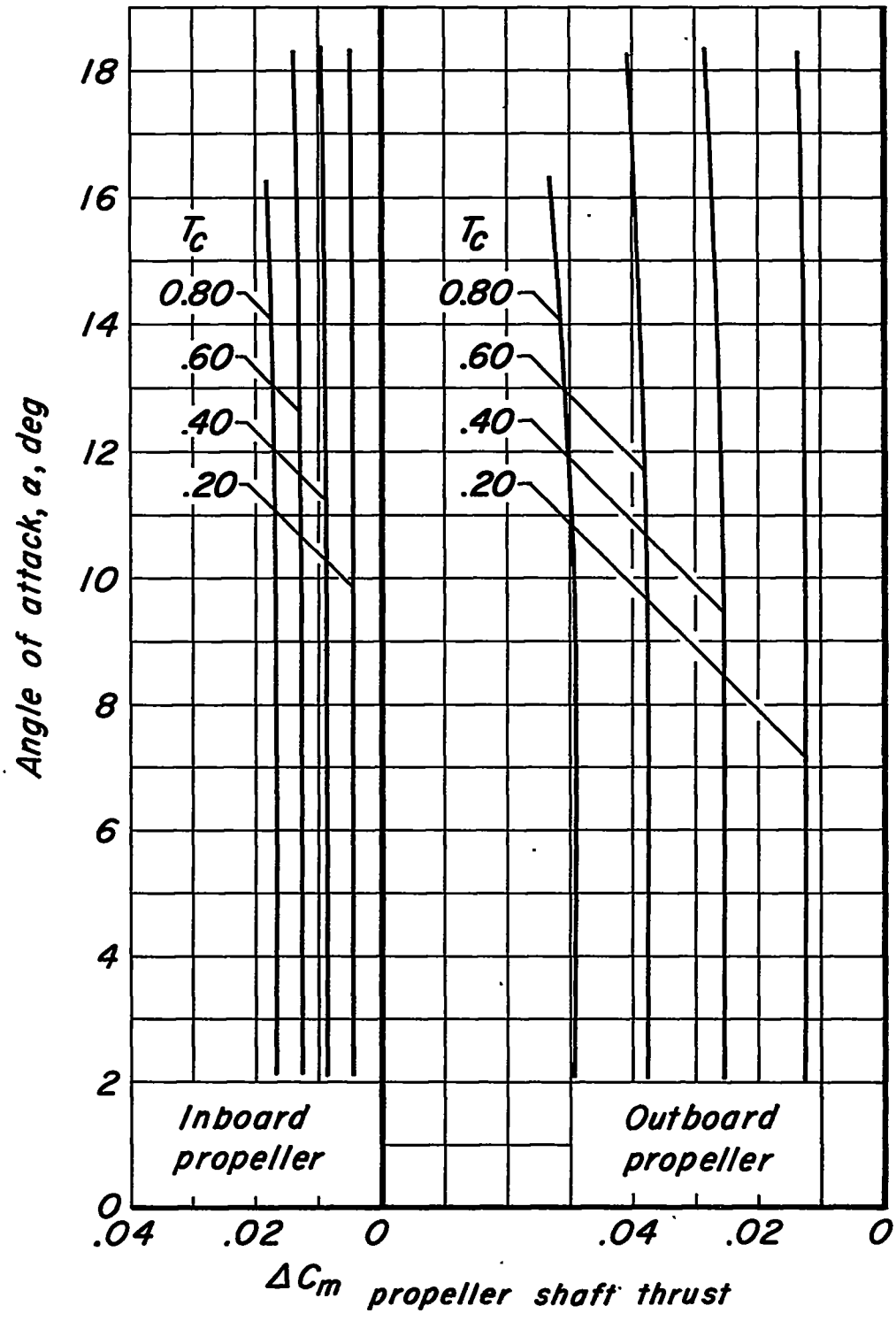

Figure 19.- The increments of pitching-moment coefficient of the model due to the shaft thrust of each propeller, including the effects of slipstream on the nacelle forebody; M = 0.082; R = 4,000,000; $\beta = 26^{\circ}$.

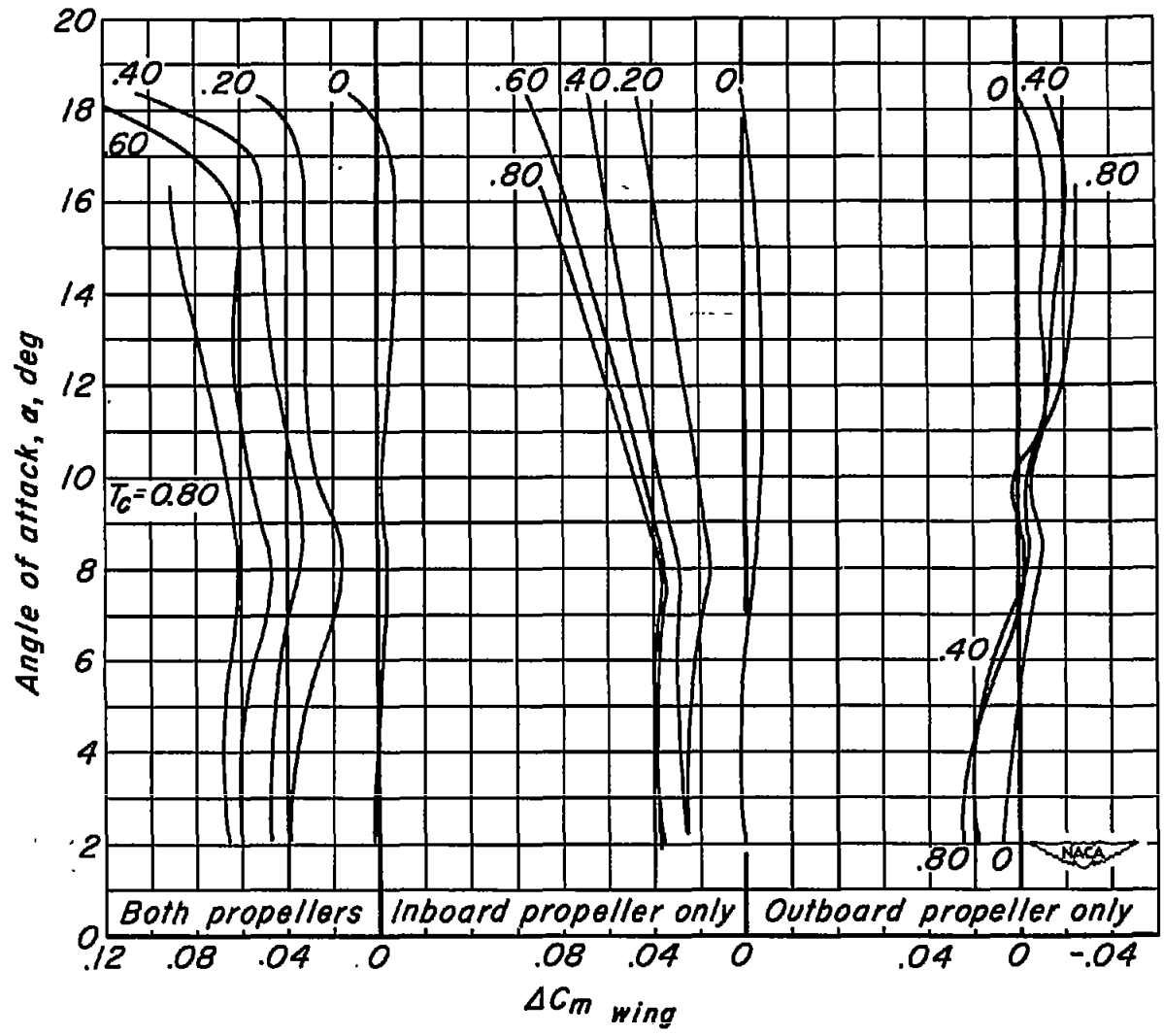

(a) Flaps up.

Figure 20.- The increments of pitching-moment coefficient due to the slipstreams on the wing; M = 0.082; R = 4,000,000; $\beta = 26^{\circ}$.

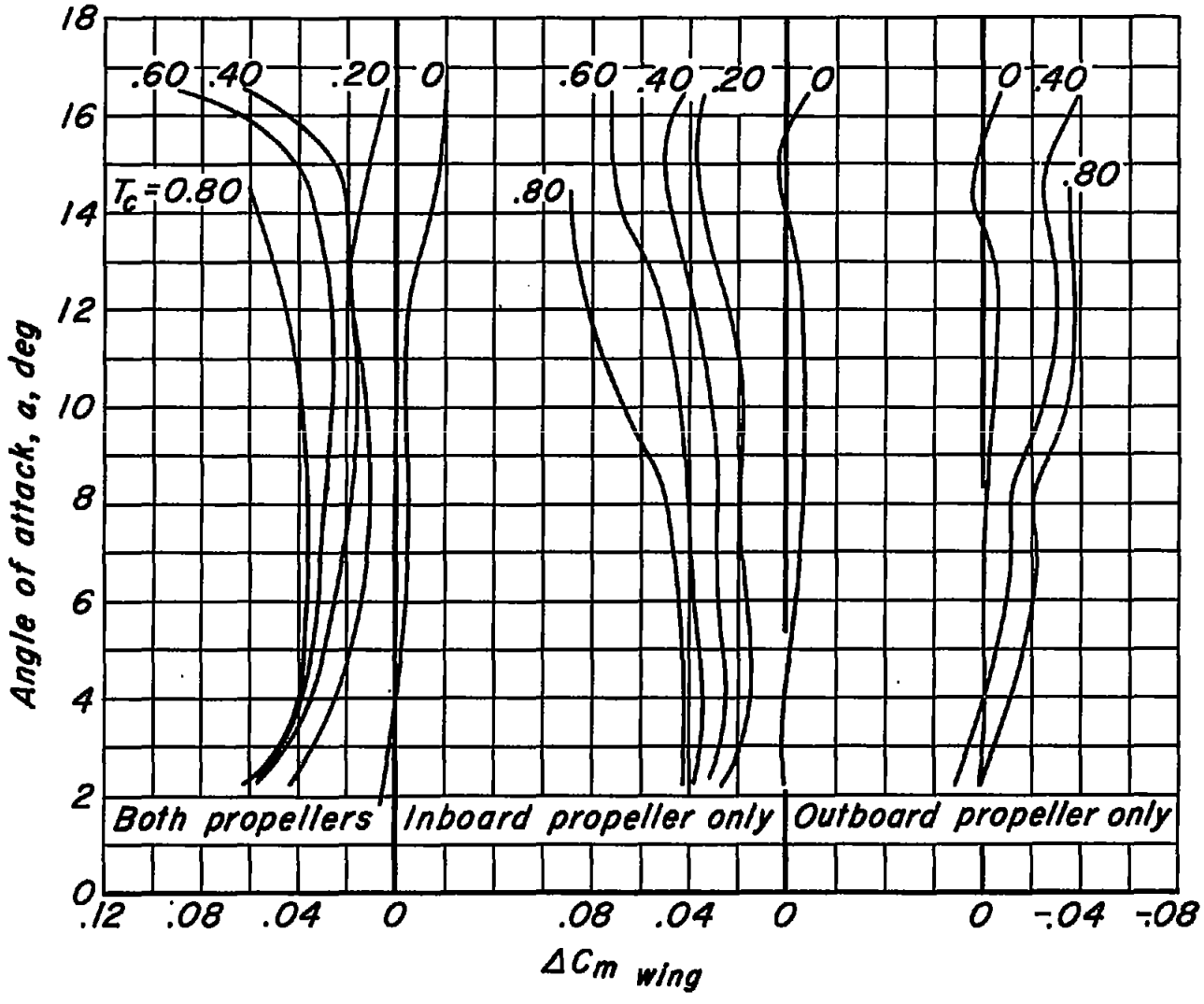

(b) Inboard flaps deflected.

Figure 20.- Concluded.

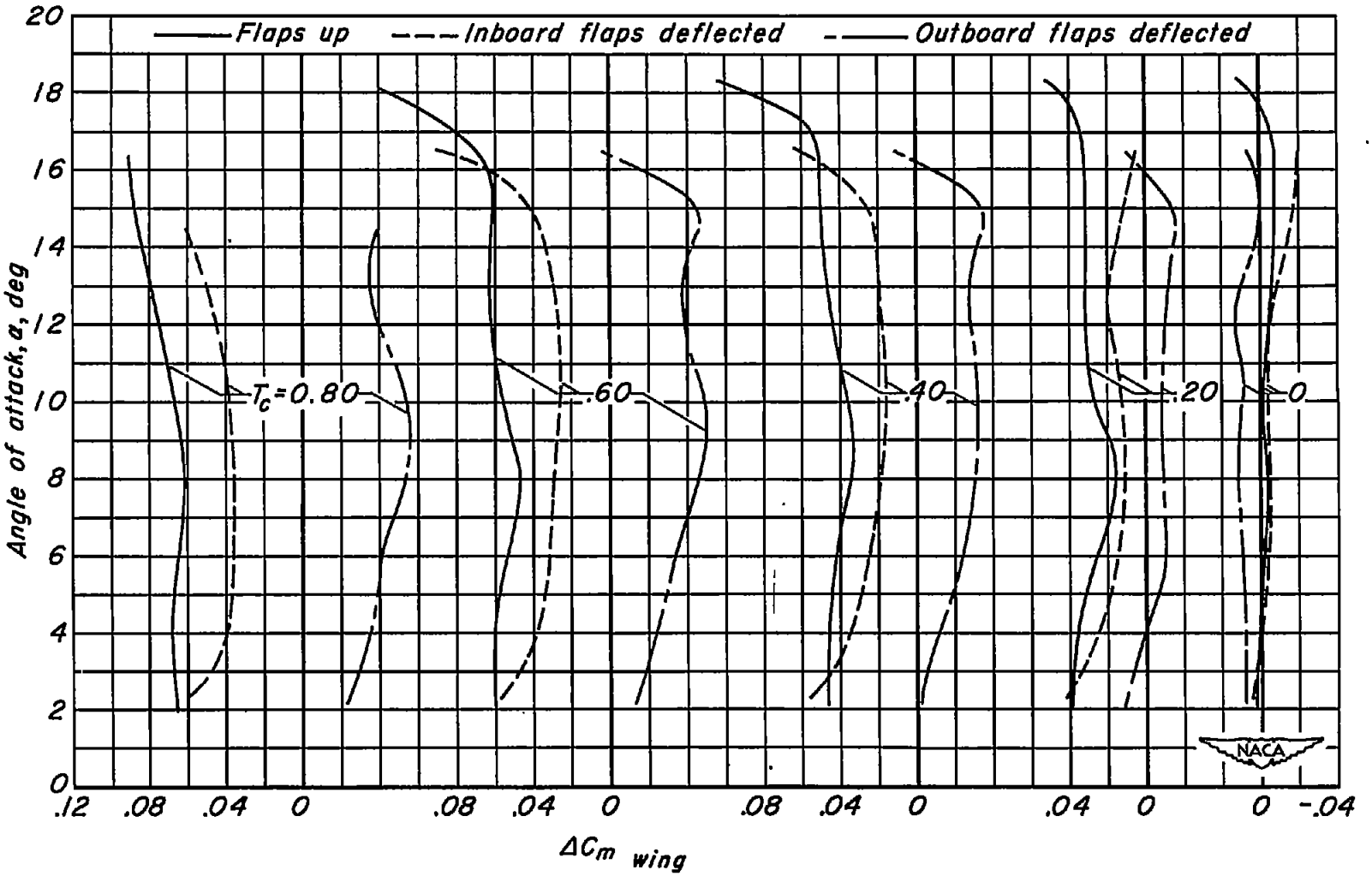

Figure 21.- The effects of flaps on the increments of pitching-moment coefficient due to the slipstreams on the wing; M = 0.082; R = 4,000,000; β = 26°.

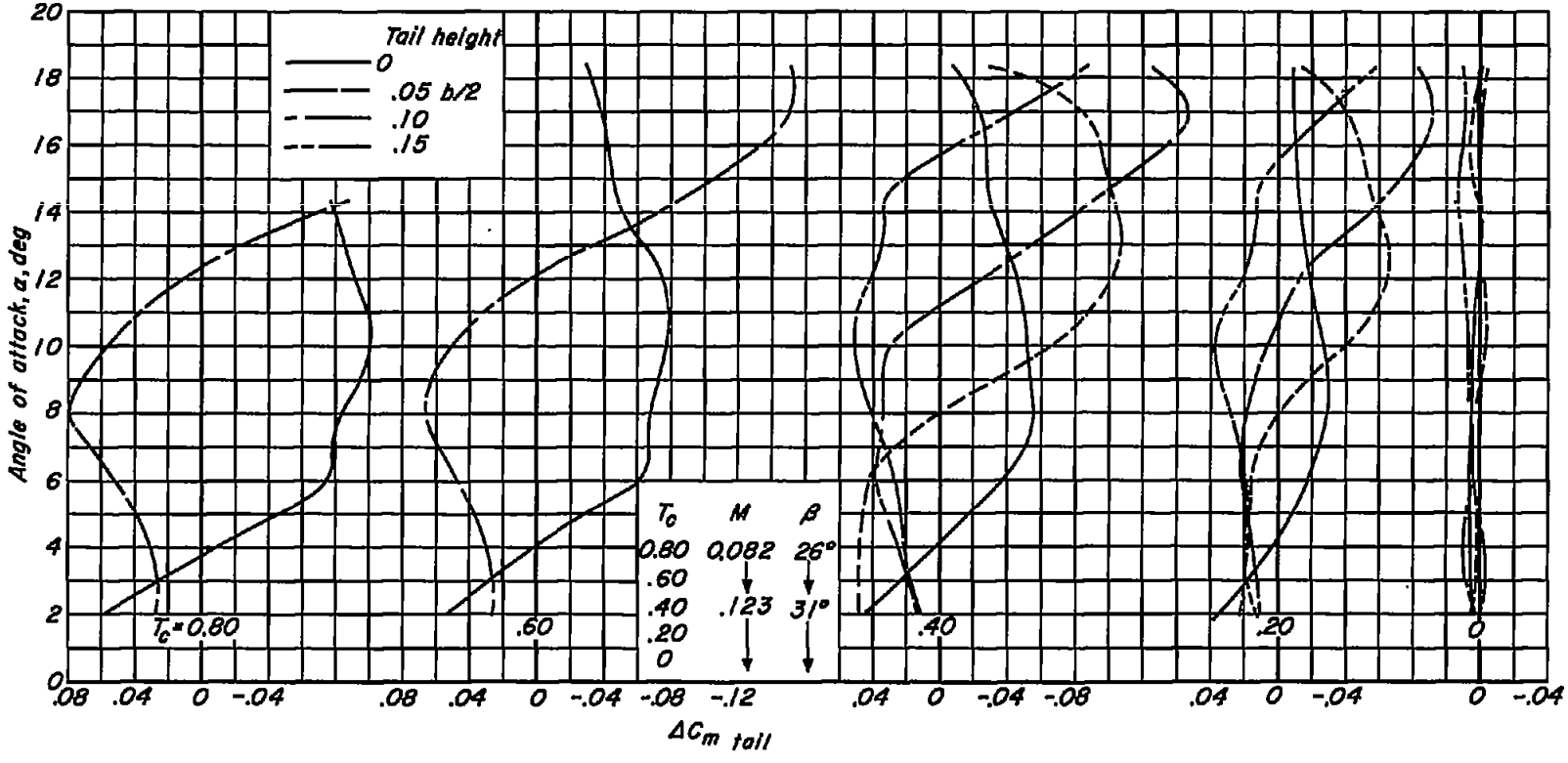

Figure 22.- The increments of pitching-moment coefficient from the tail due to operation of the propellers; flaps up; M and β as noted; R = 4,000,000; i_t = -4°.

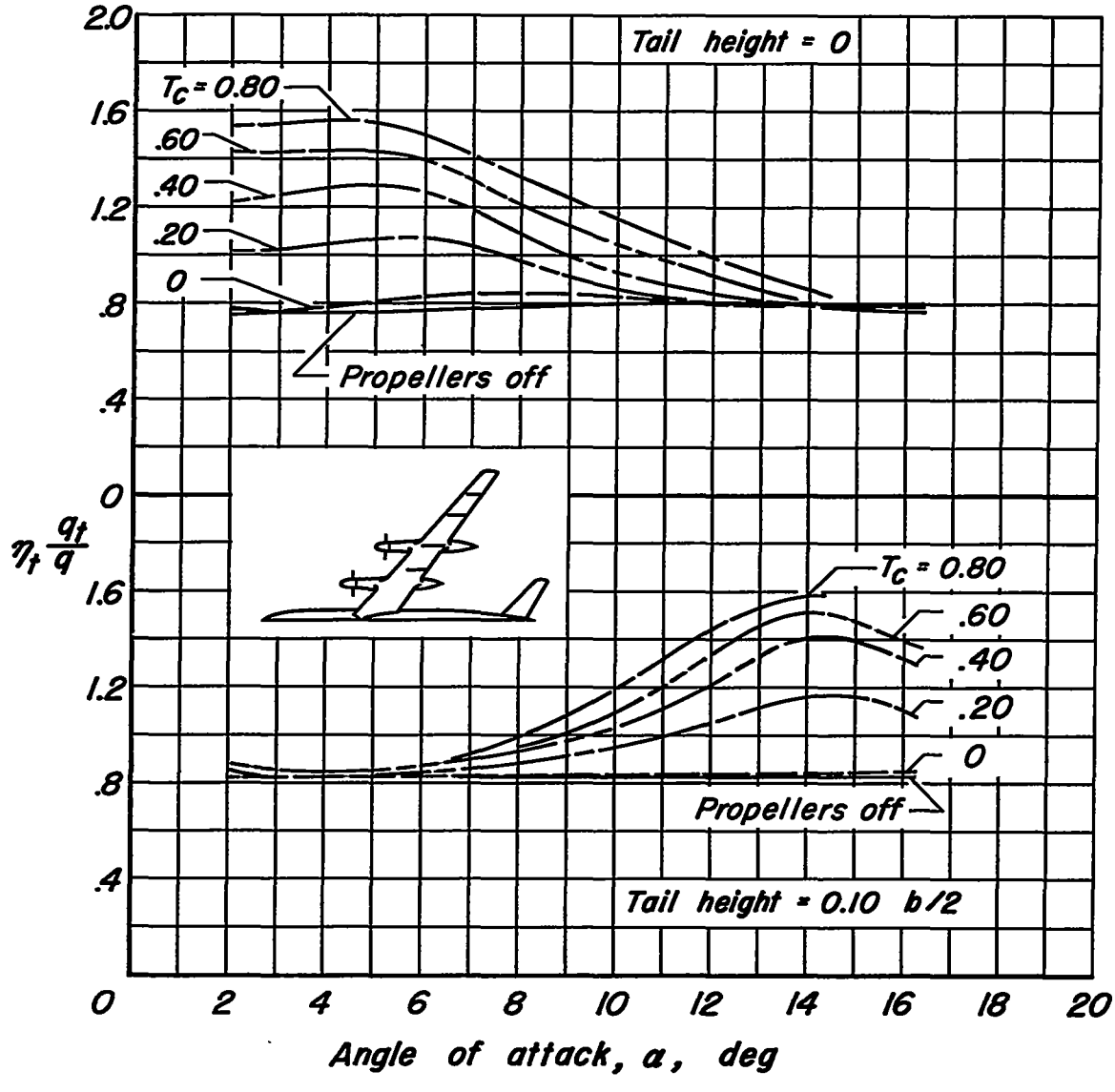

(a) Flaps up.

Figure 23.- The effects of operating propellers on the tail-efficiency factor; M = 0.082; R = 4,000,000; β = 26°.

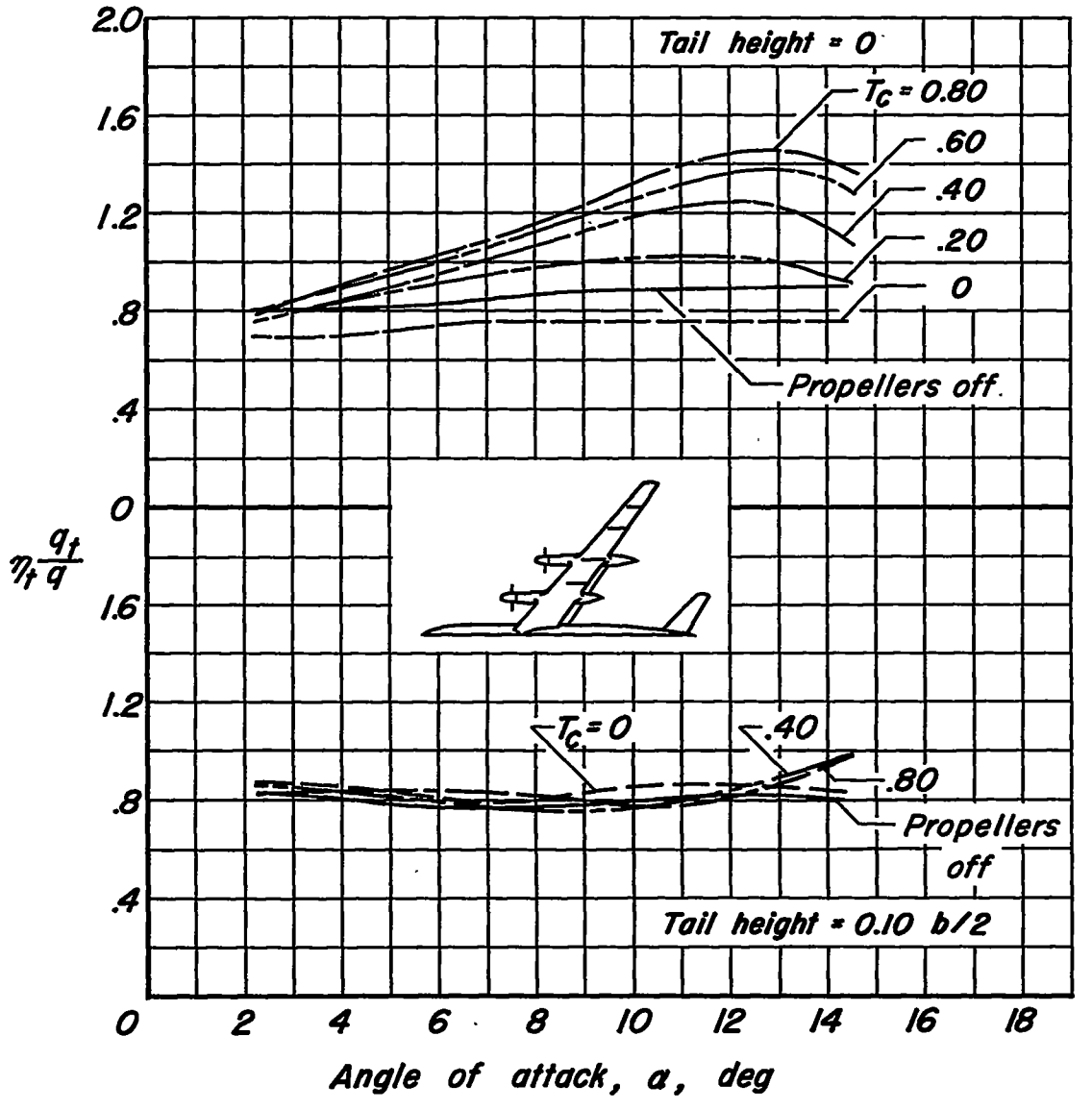

(b) Inboard flaps deflected.

Figure 23.- Continued.

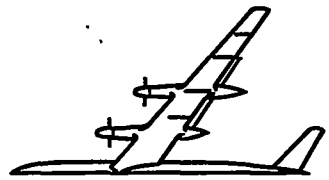

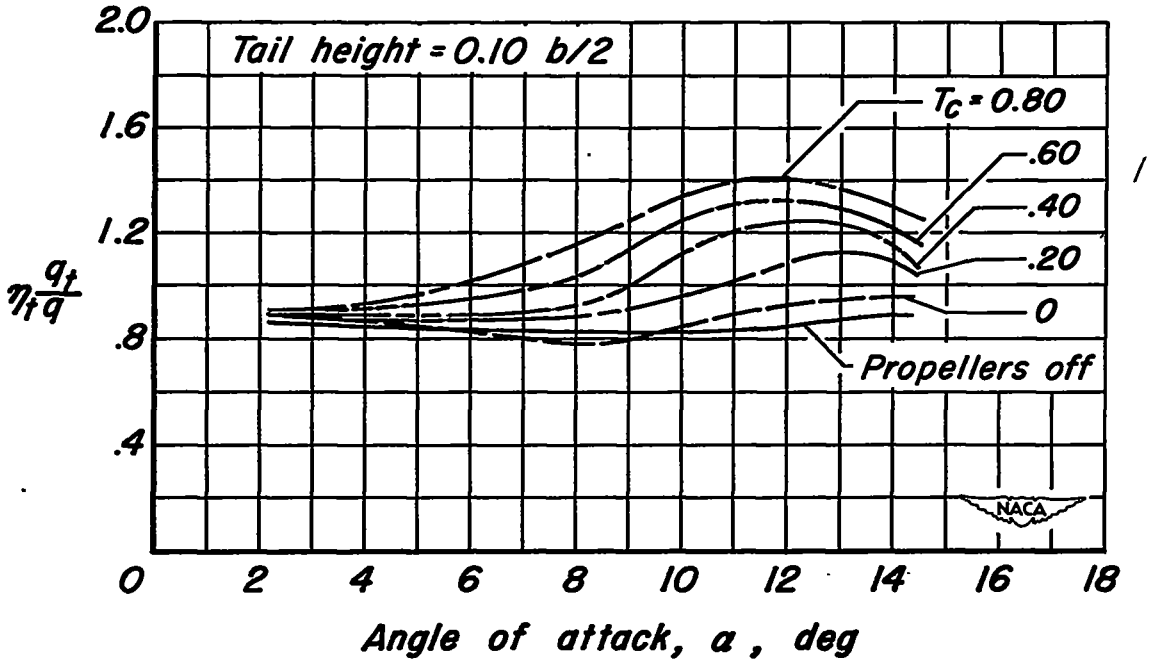

(c) Outboard flaps deflected.

Figure 23.- Concluded.

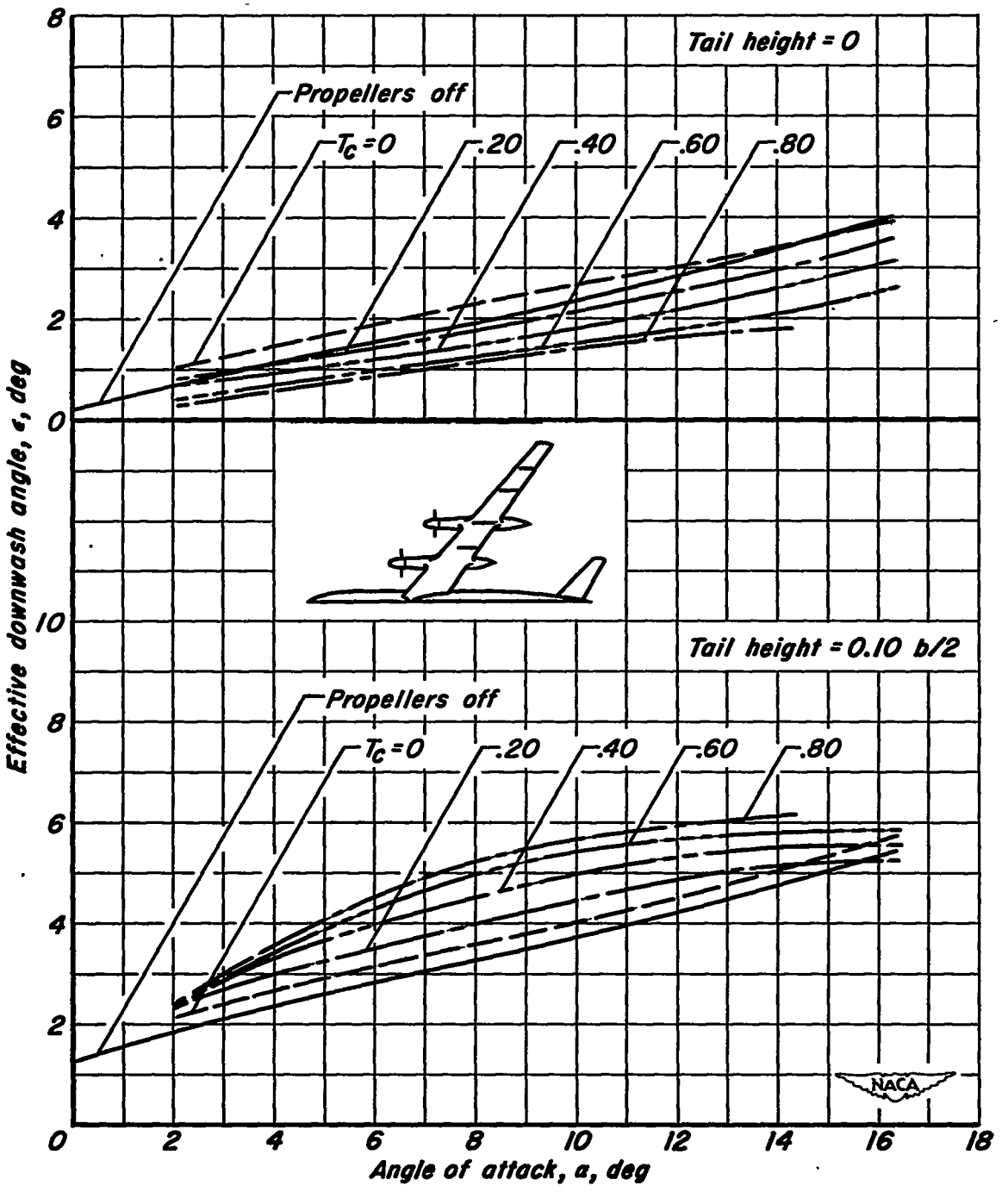

(a) Flaps up.

Figure 24.- The effects of operating propellers on the effective downwash at the tail; M = 0.082; R = 4,000,000; β = 26°.

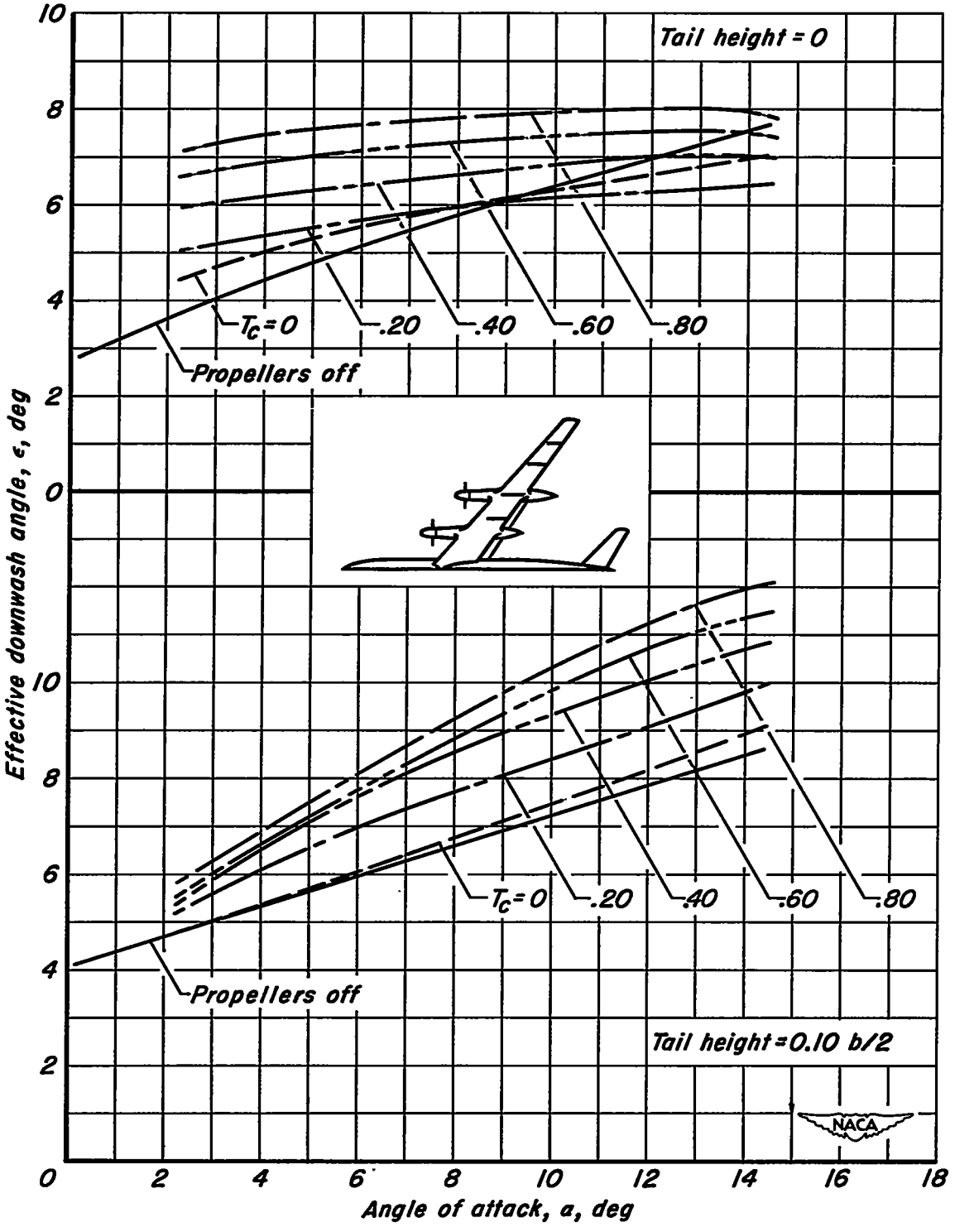

(b) Inboard flaps deflected.

Figure 24.- Continued.

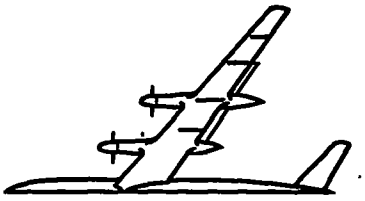

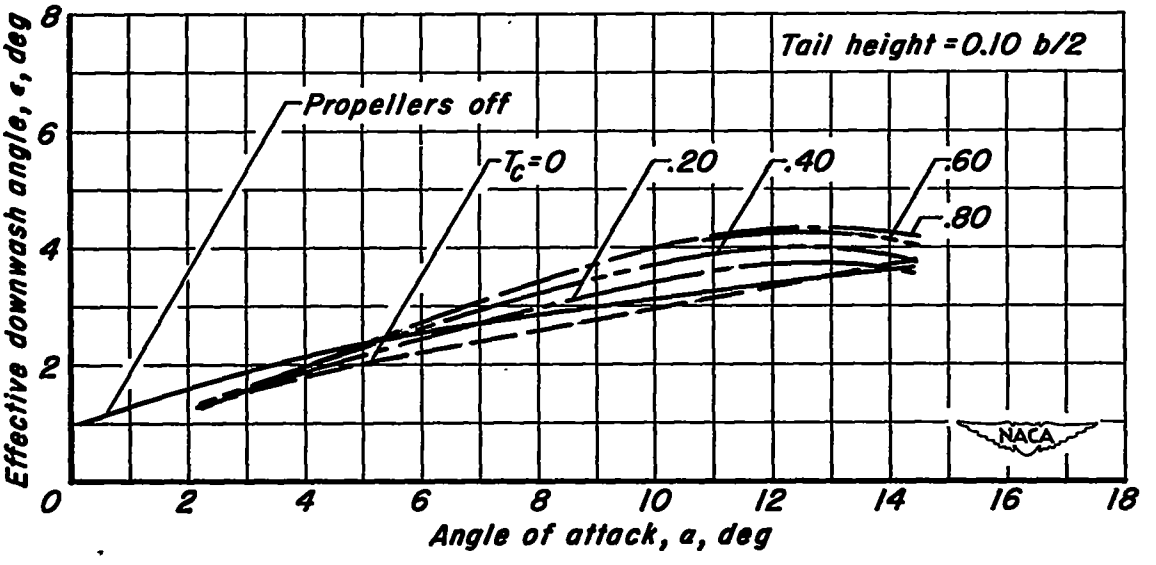

(c) Outboard flaps deflected.

Figure 24.- Concluded.

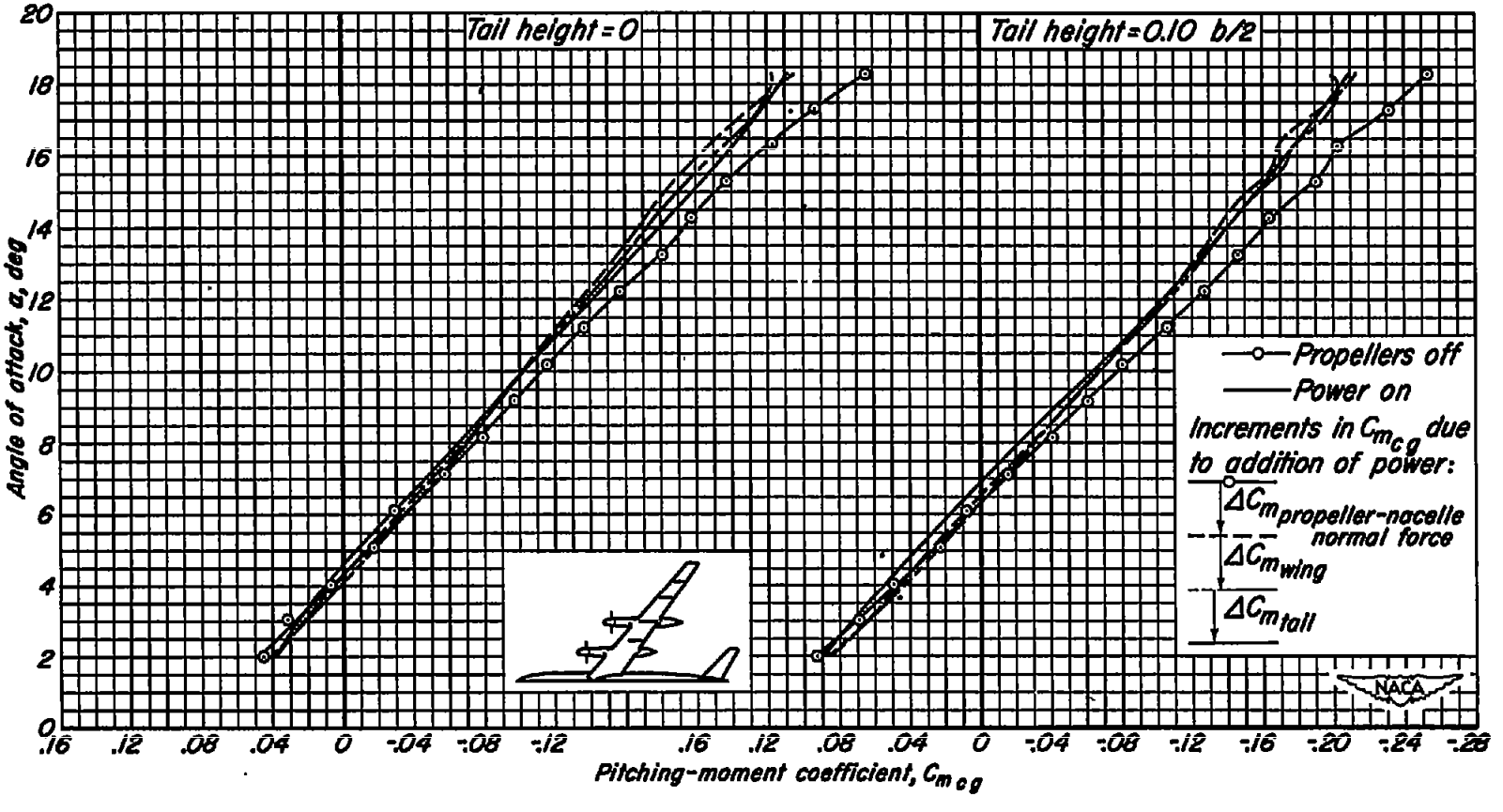

(a) $T_c = 0$

Figure 25.- The various effects of operating propellers on the pitching-moment characteristics of the model; flaps up; M = 0.082; R = 4,000,000; $\beta = 26^\circ$; $i_t = -4^\circ$.

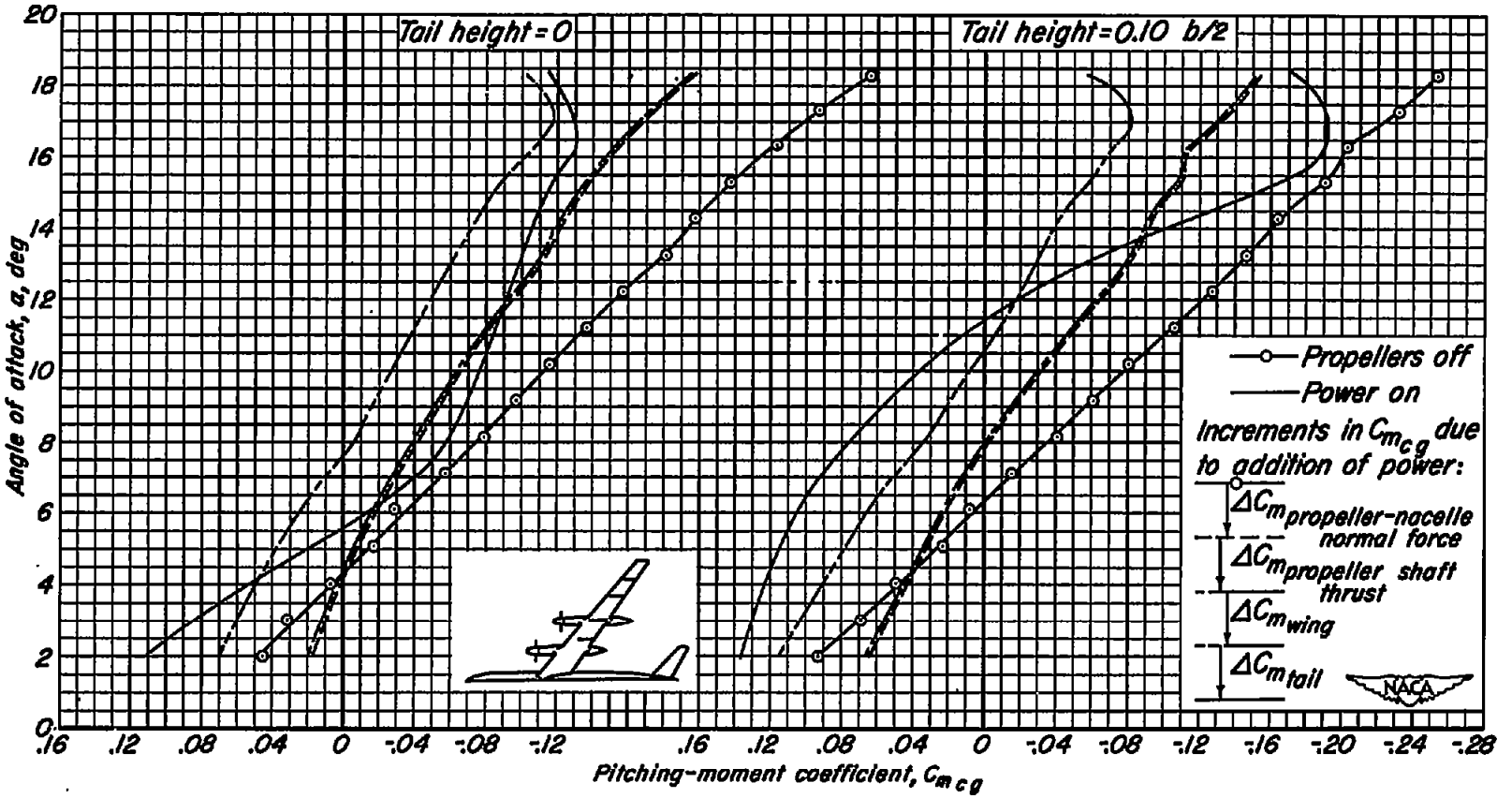

(b) $T_c = 0.40$

Figure 25.- Continued.

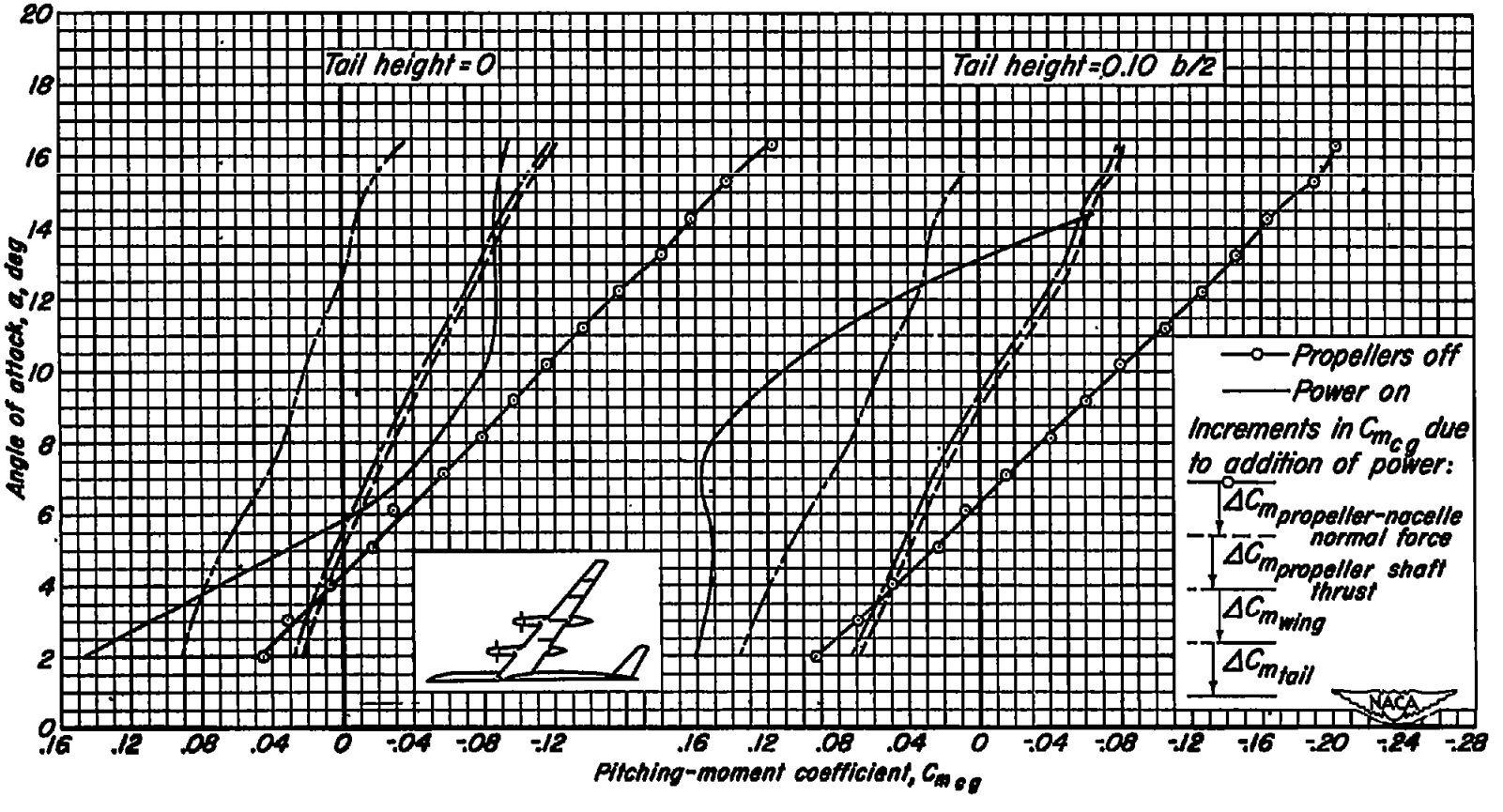

(c) T_c = 0.80

Figure 25.- Continued.

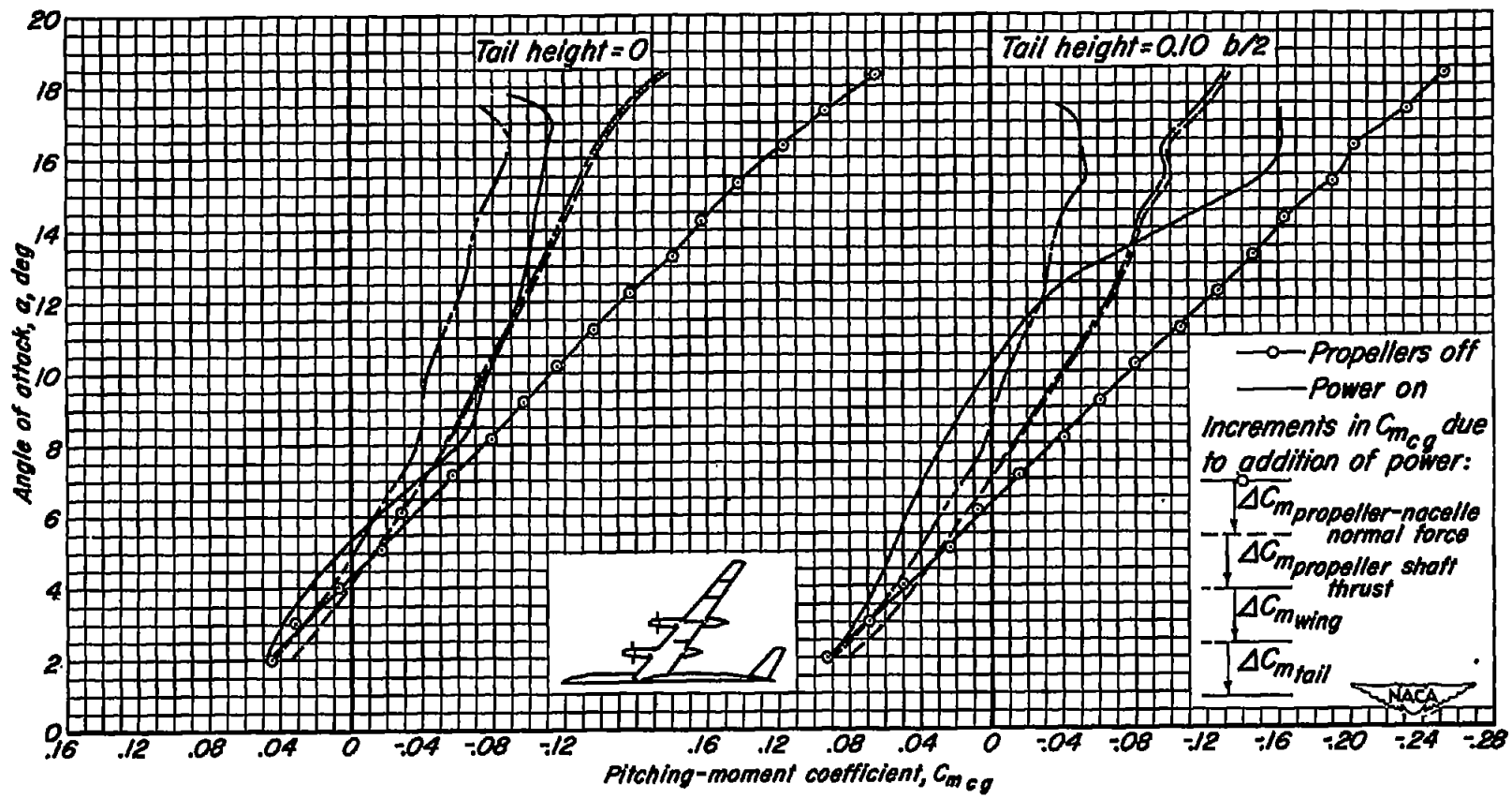

(d) 10,000 simulated hp

Figure 25.- Concluded.

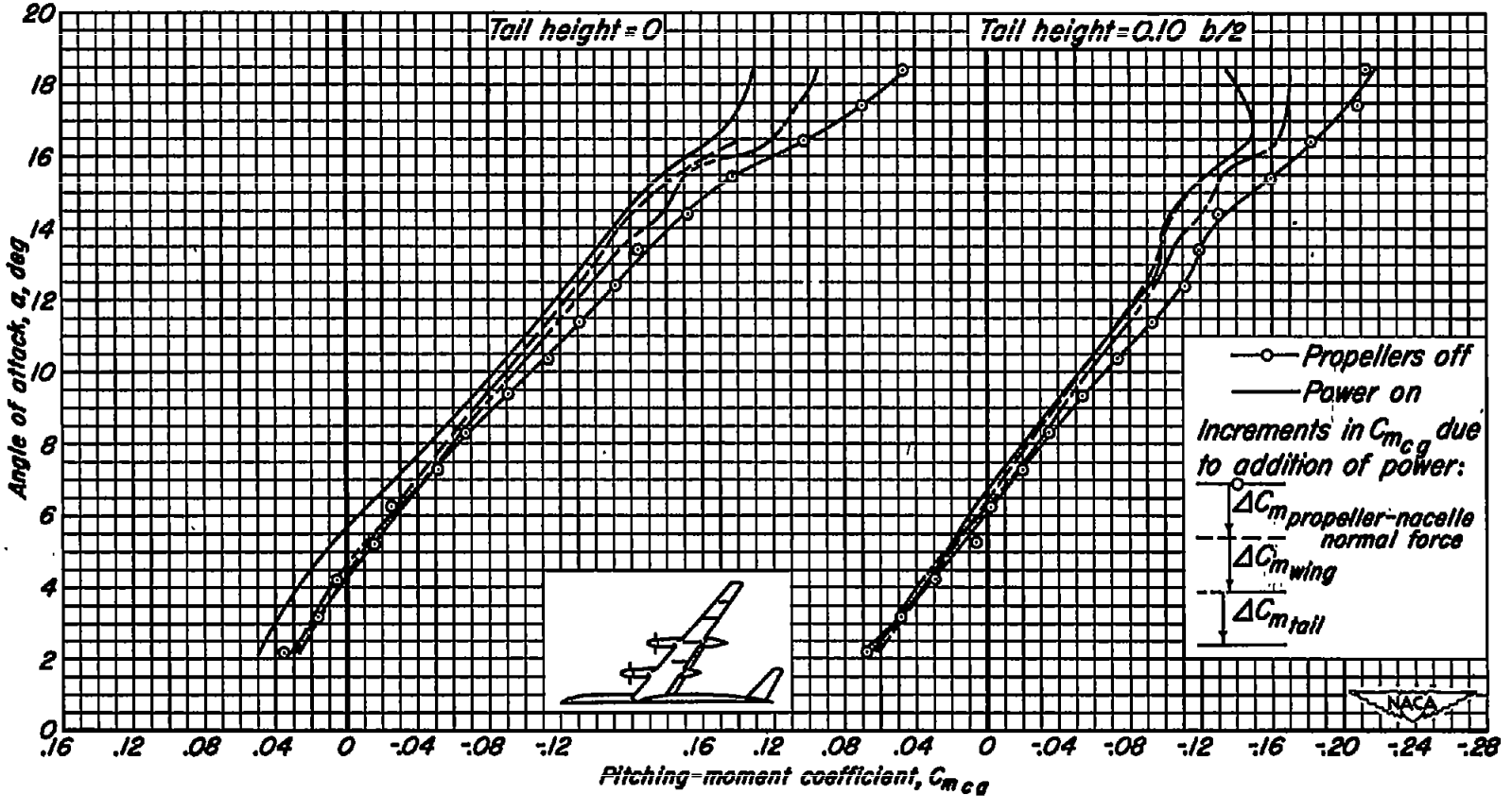

(a) $T_c = 0$

Figure 26.- The various effects of operating propellers on the pitching-moment characteristics of the model; inboard flaps deflected; M = 0.082; R = 4,000,000; $\beta = 26^\circ$; $i_t = 0^\circ$.

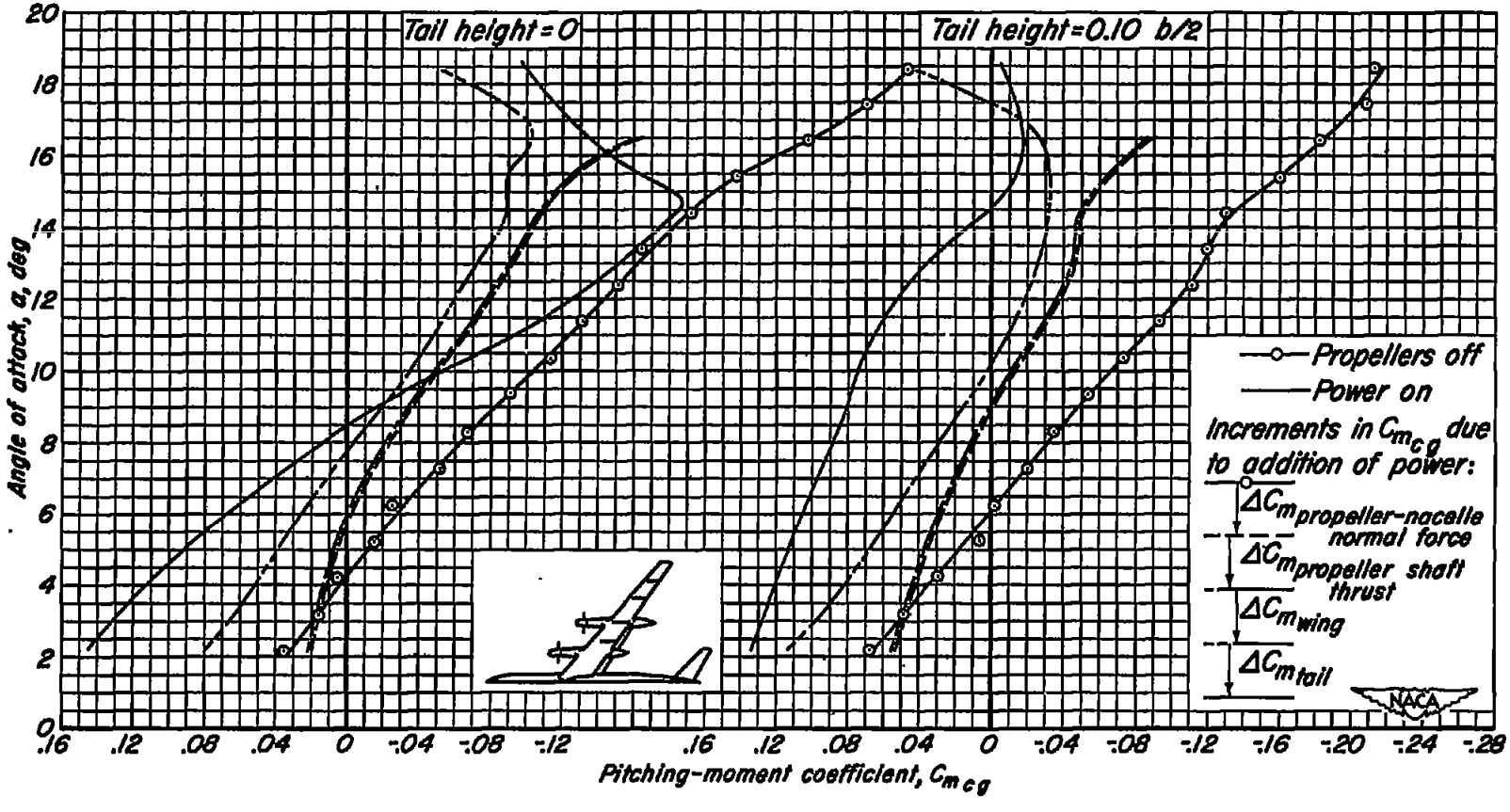

(b) $T_c = 0.40$

Figure 26.- Continued.

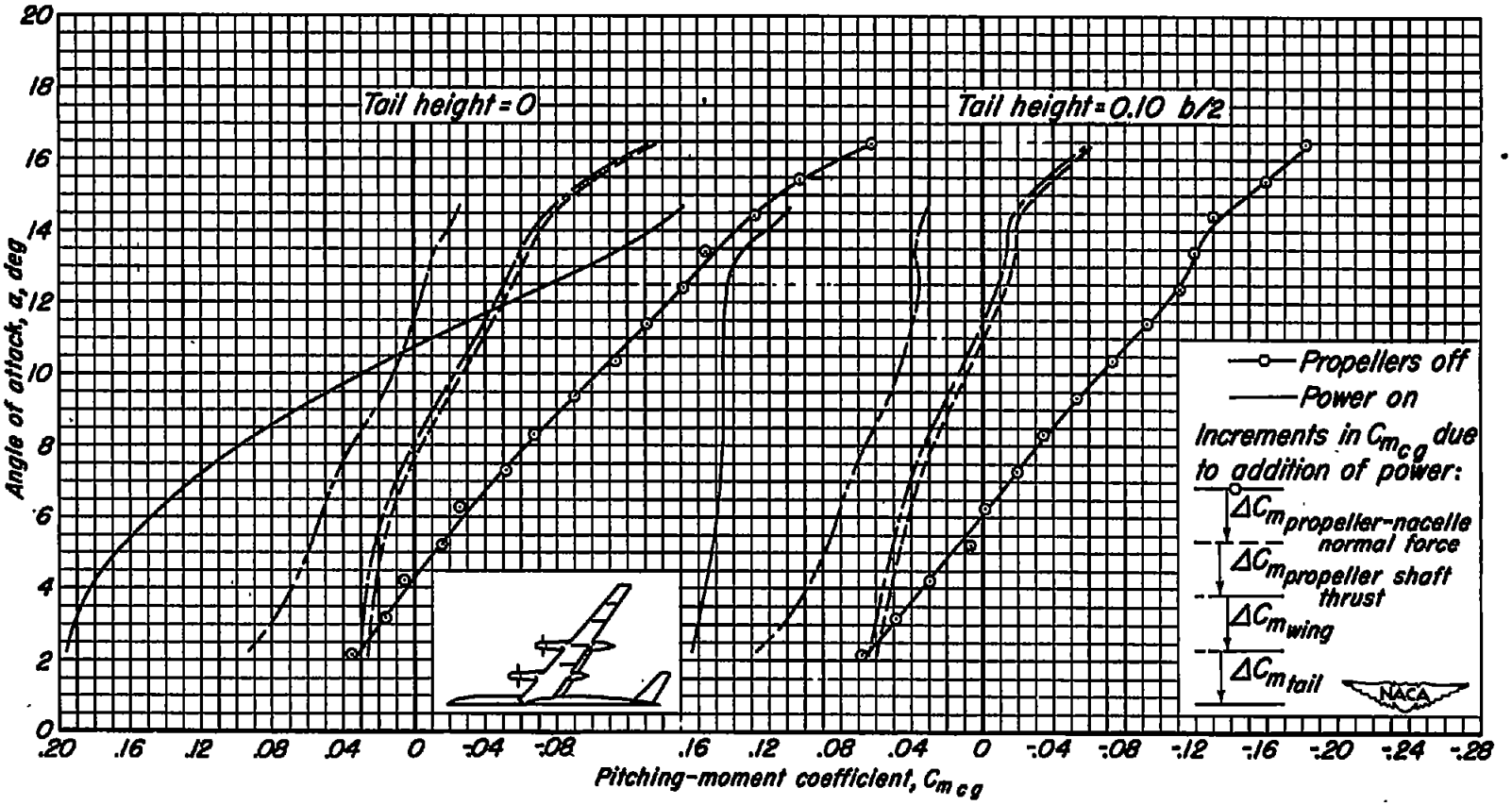

(c) $T_c = 0.80$

Figure 26.- Continued.

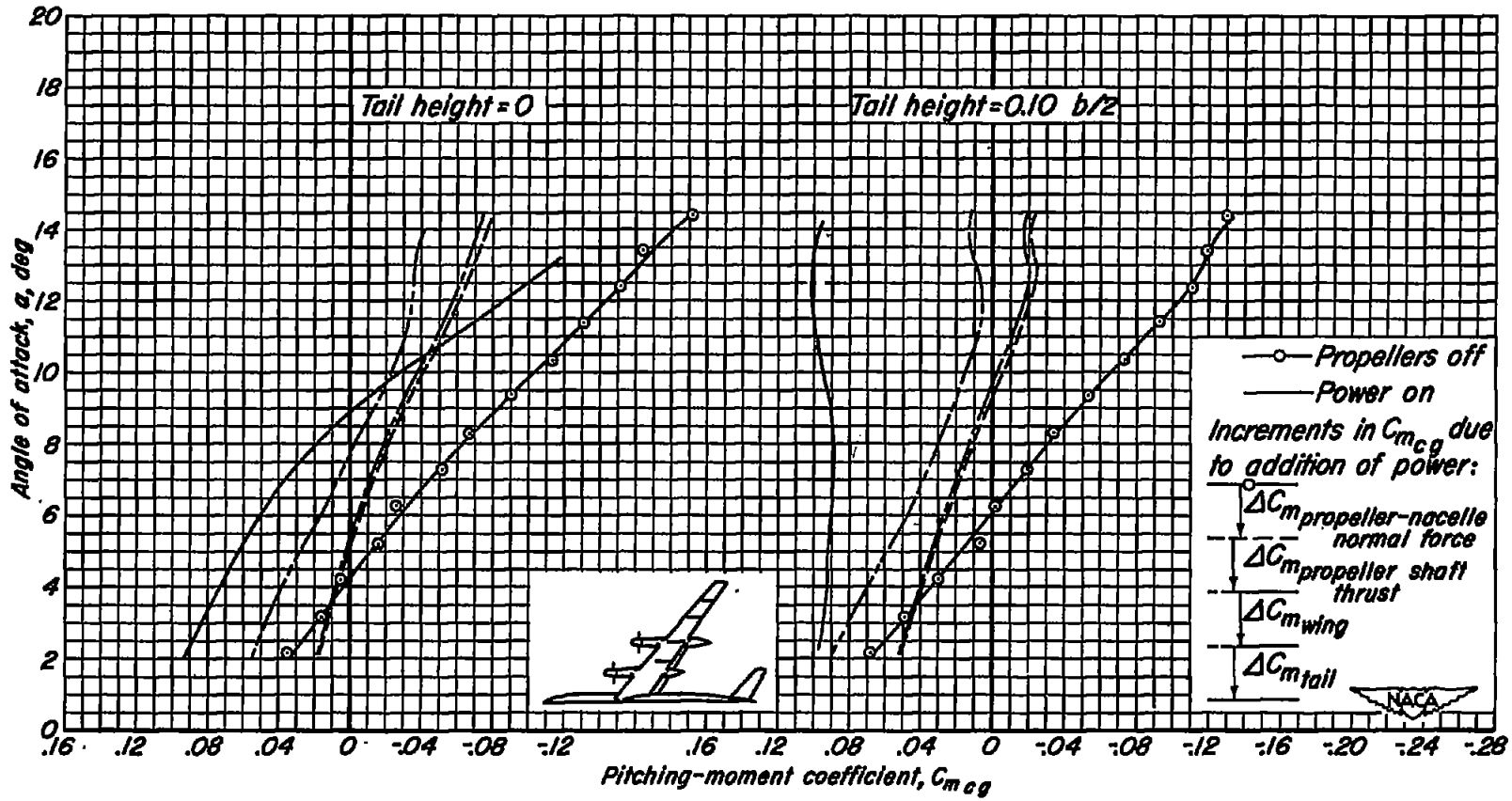

(d) 10,000 simulated hp

Figure 26.- Concluded.

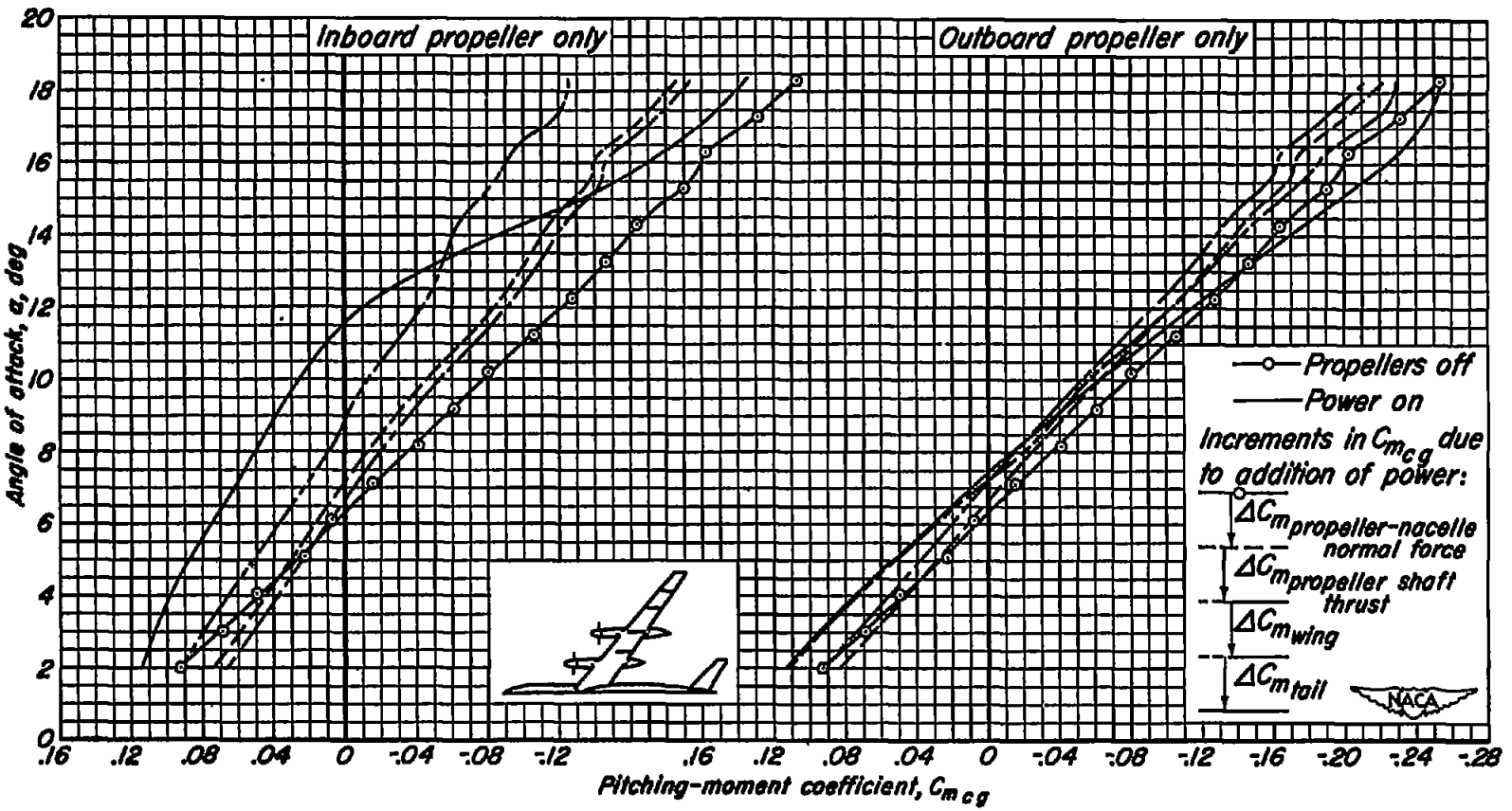

(a) $T_c = 0.40$

Figure 27.- A comparison of the various effects of the inboard propeller on the pitching-moment characteristics of the model with those of the outboard propeller; tail height = 0.10 b/2; flaps up; M = 0.082; R = 4,000,000; $\beta = 26^\circ$; $i_t = -4^\circ$.

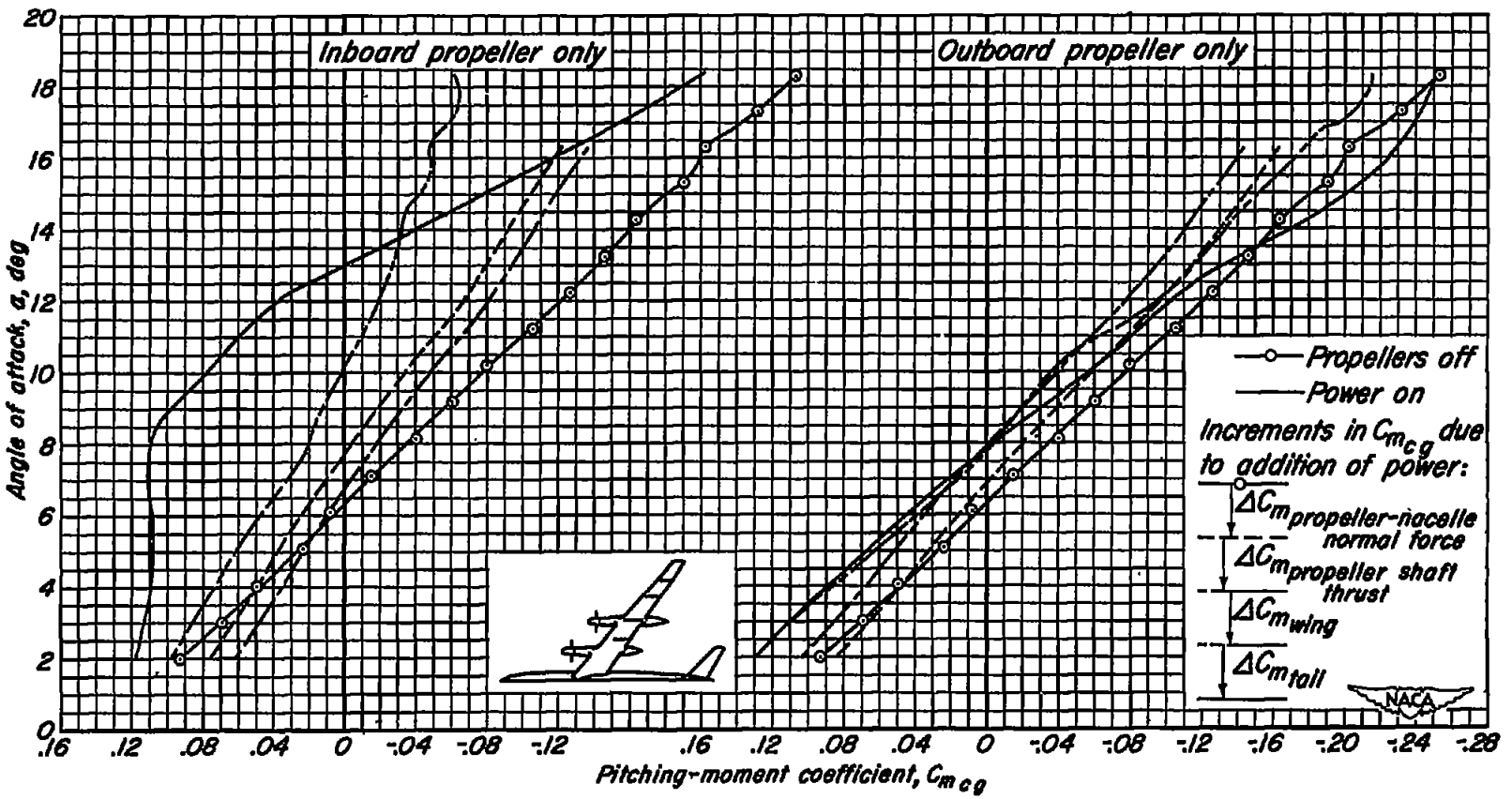

(b) T_c = 0.80

Figure 27.- Continued.

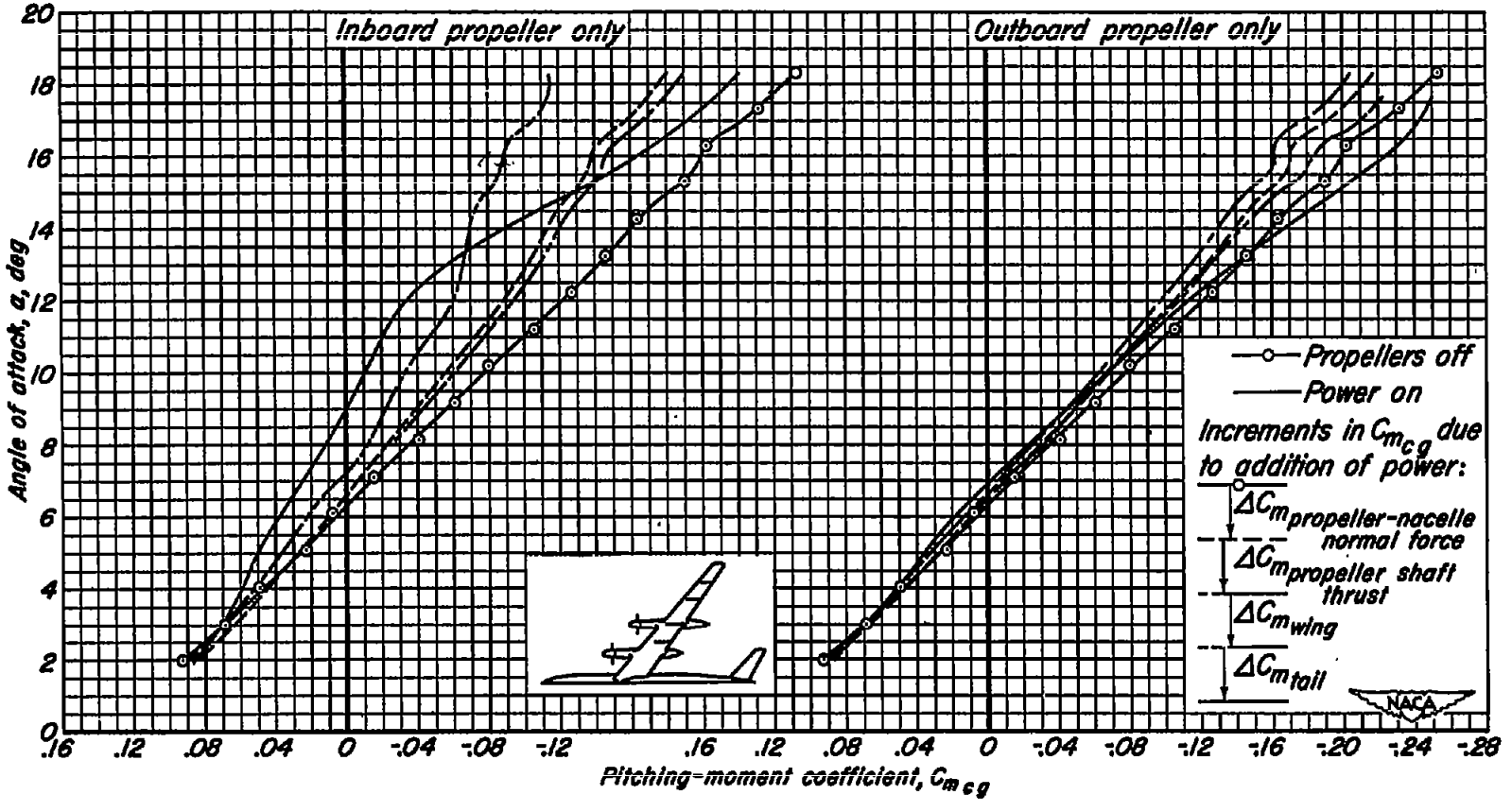

(c) 10,000 simulated hp

Figure 27.- Concluded.

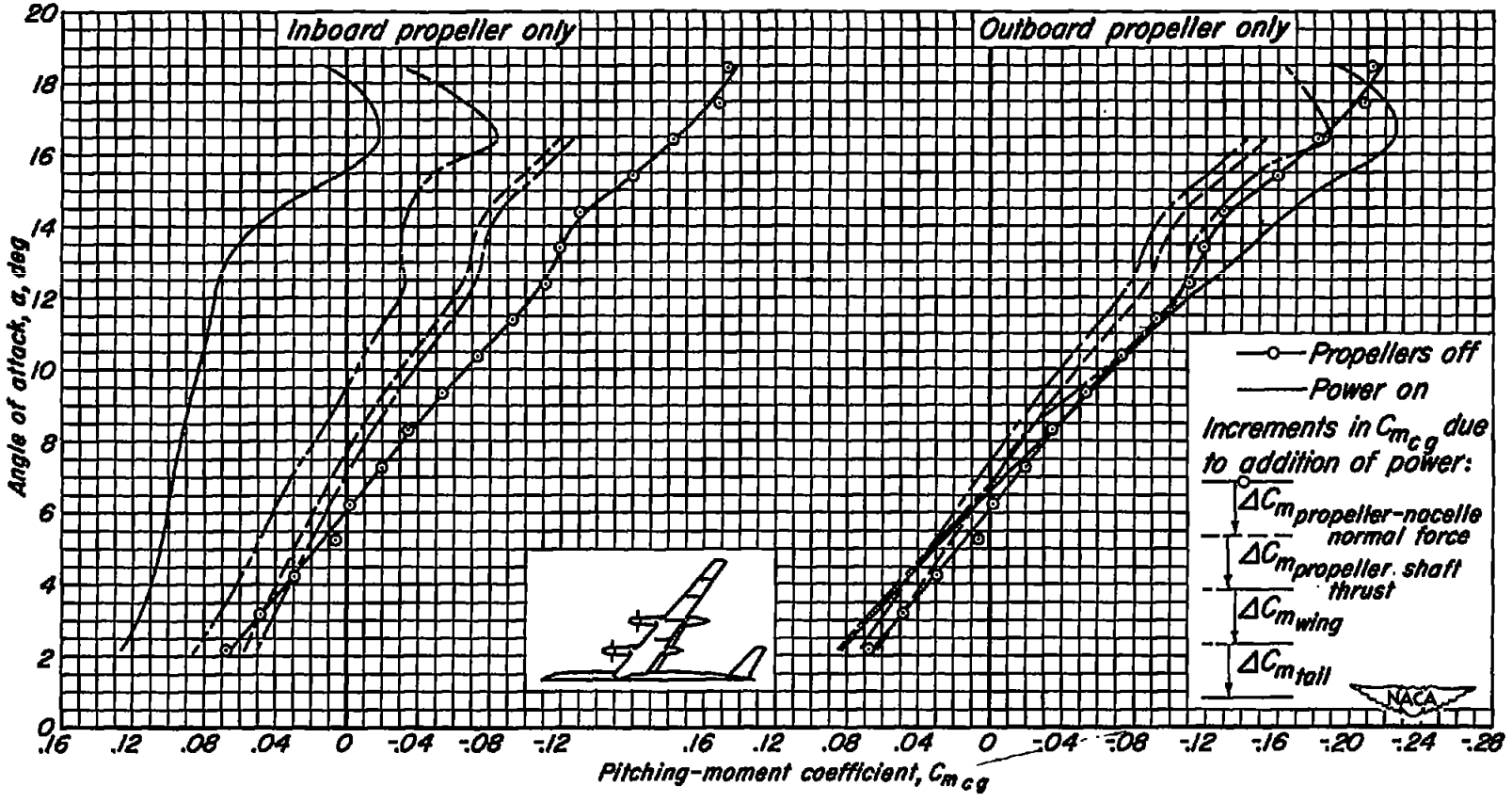

(a) $T_c = 0.40$

Figure 28.- A comparison of the various effects of the inboard propeller on the pitching-moment characteristics of the model with those of the outboard propeller; tail height = 0.10 b/2; inboard flaps deflected; M = 0.082; R = 4,000,000; $\beta = 26^\circ$; $i_t = 0^\circ$.

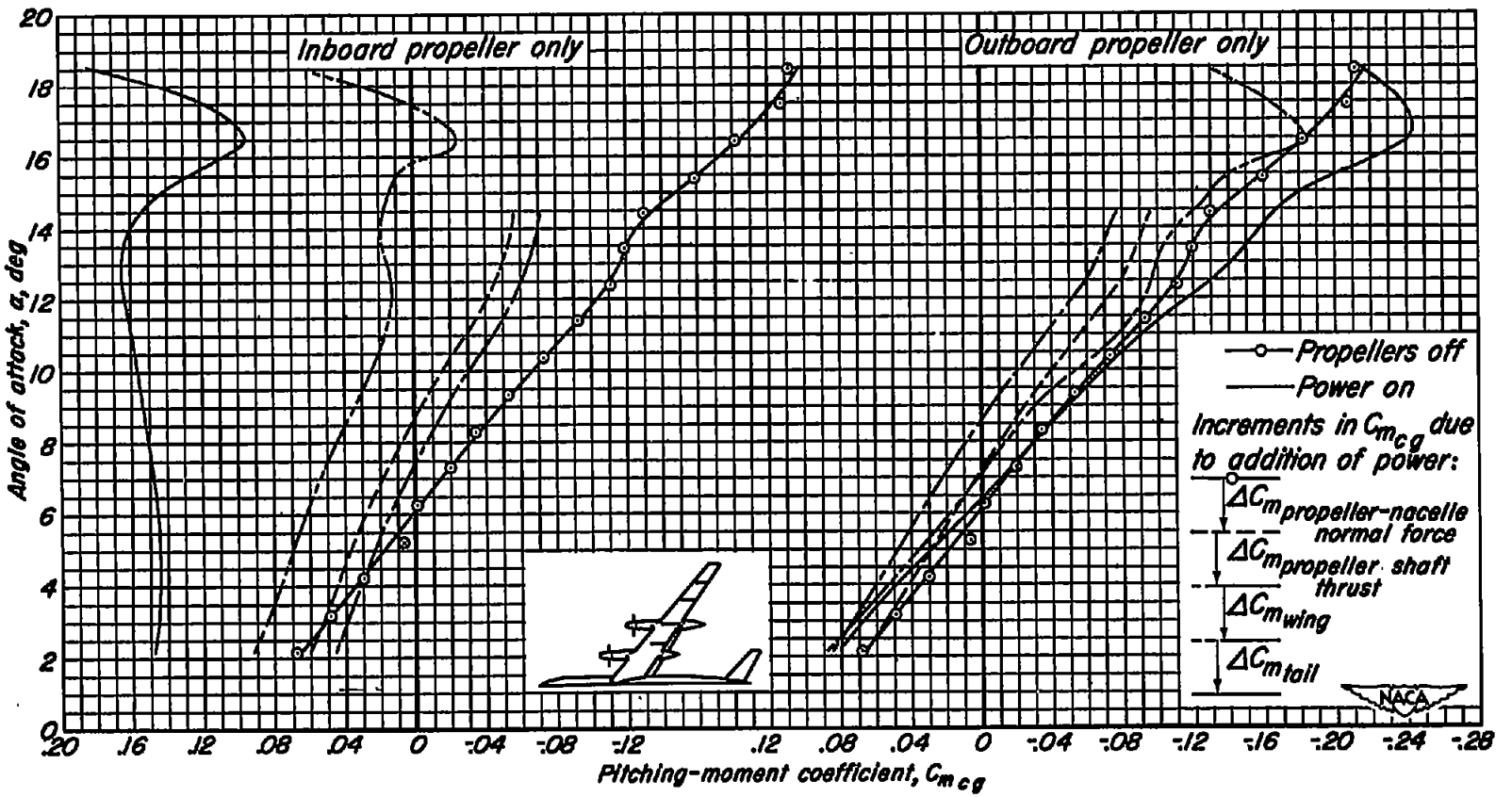

(b) $T_c = 0.80$

Figure 28.- Continued.

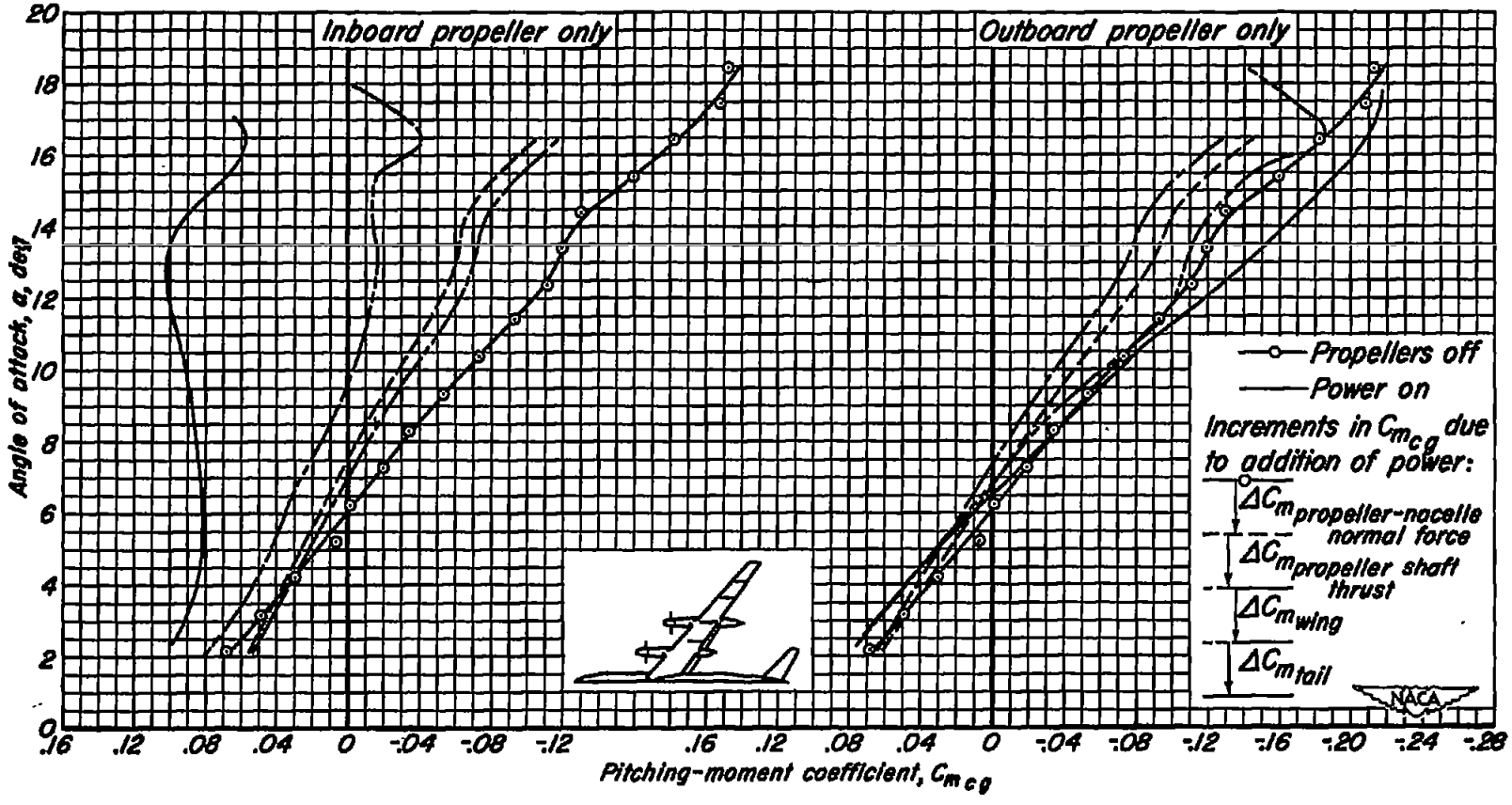

(c) 10,000 simulated hp

Figure 28.- Concluded.

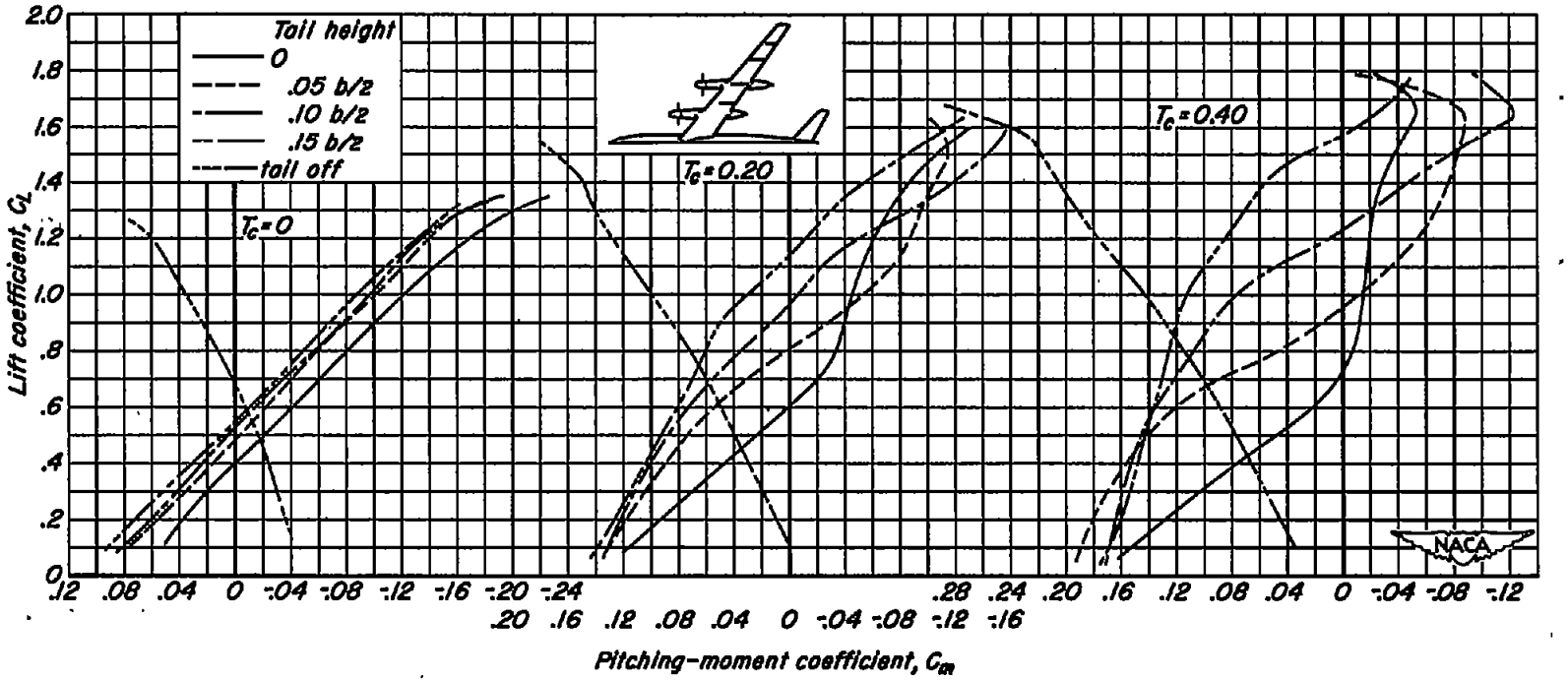

Figure 29.- The effects of tail height on the pitching-moment characteristics of the model; flaps up; M = 0.123; R = 4,000,000; $\beta = 31^\circ$; $i_t = -4^\circ$.

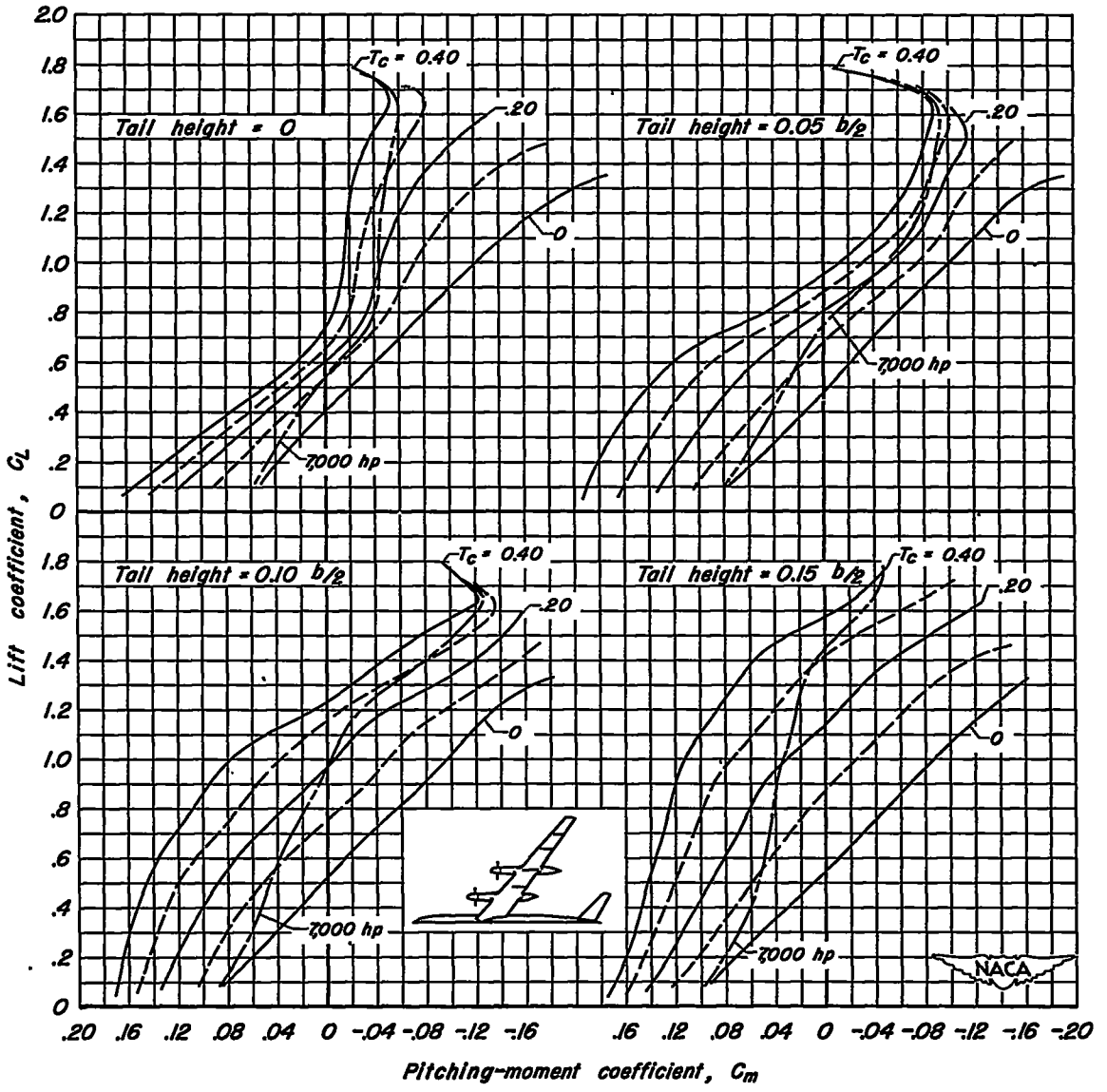

Figure 30.- A comparison at various tail heights of the effects of operating propellers on the pitching-moment characteristics of the model; flaps up; M = 0.123; R = 4,000,000; $\beta = 31^\circ$; $i_t = -4^\circ$.

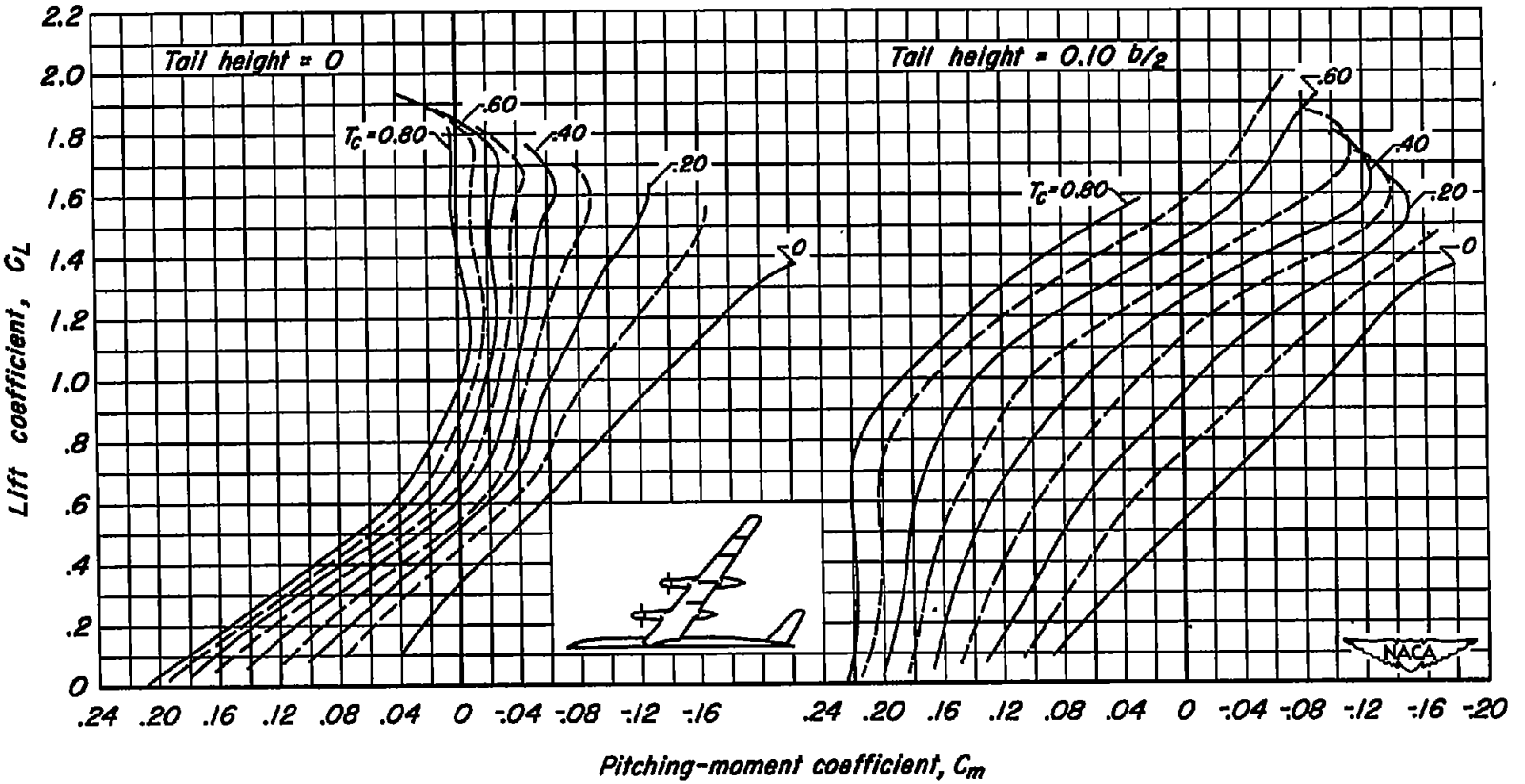

(a) Flaps up; $i_t = -4^\circ$

Figure 31.- A comparison for two tail heights of the effects of operating propellers on the pitching-moment characteristics of the model; M = 0.082; R = 4,000,000; $\beta = 26^\circ$.

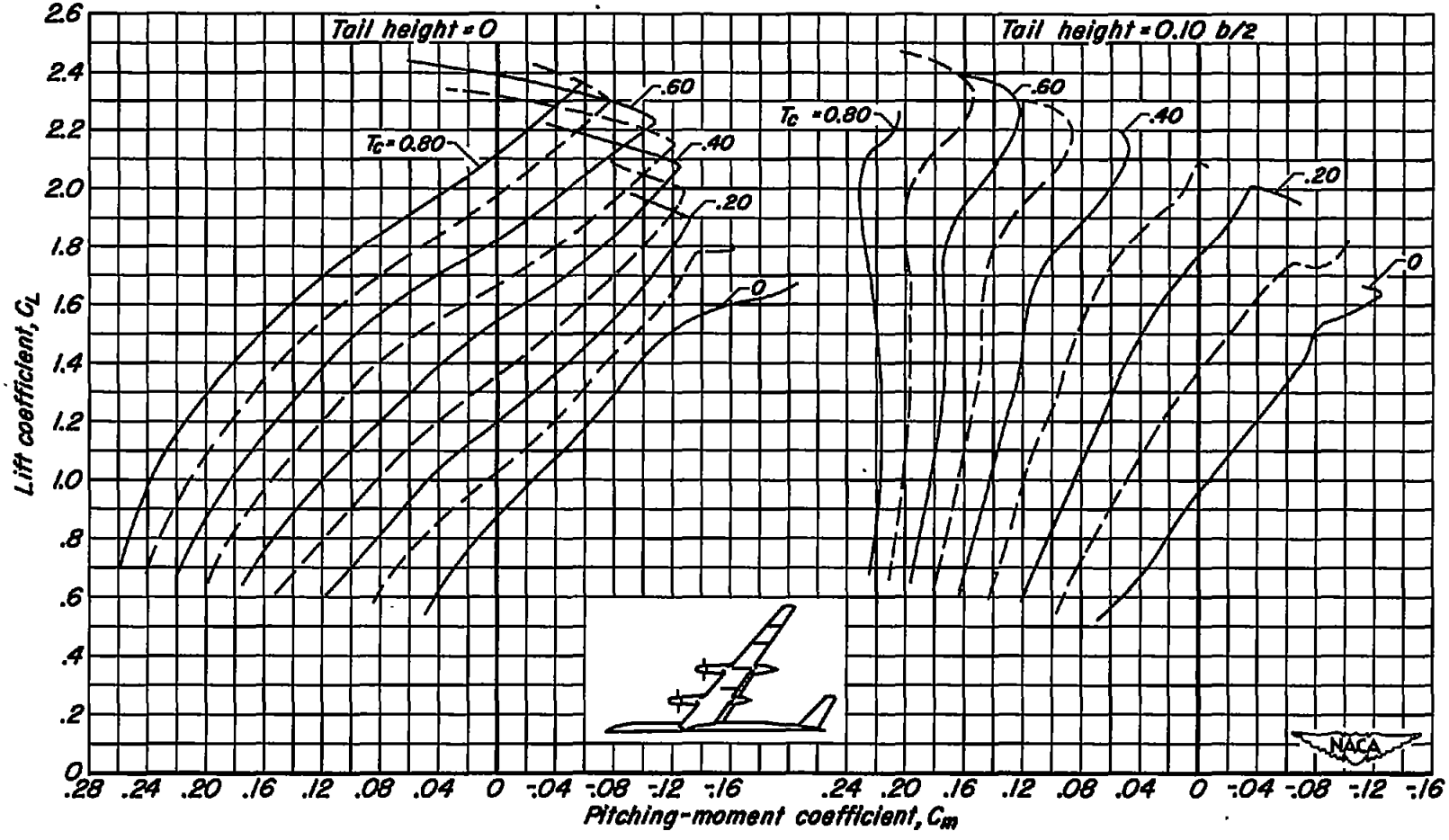

(b) Inboard flaps deflected; $i_t = 0^\circ$

Figure 31.- Concluded.

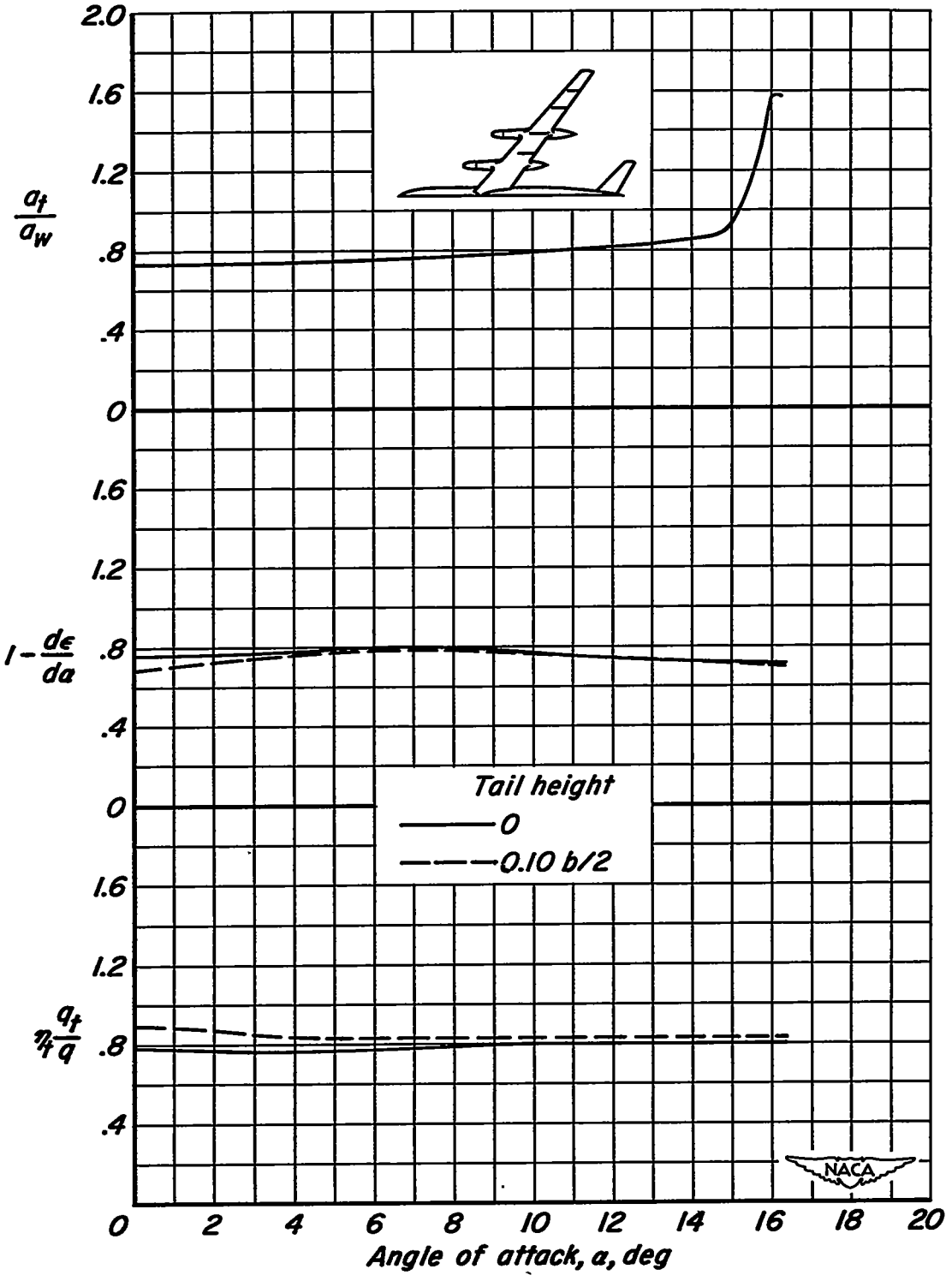

(a) Propellers off.

Figure 32.- The variation of a_t/a_w, $1-(d\epsilon/d\alpha)$, and $\eta_t(q_t/q)$ with α; flaps up; M = 0.082; R = 4,000,000; $\beta = 26^\circ$.

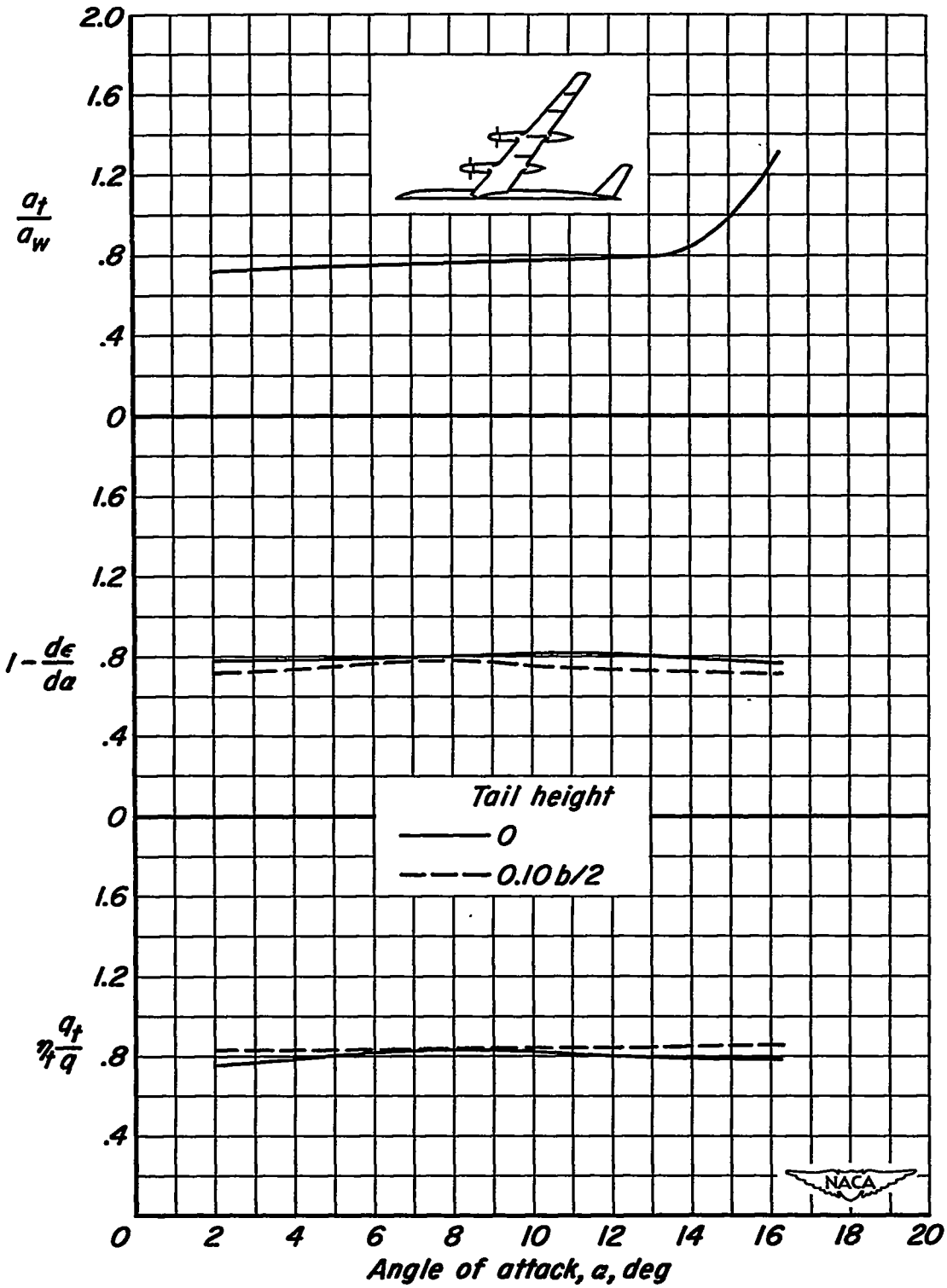

(b) $T_c = 0$

Figure 32.- Continued.

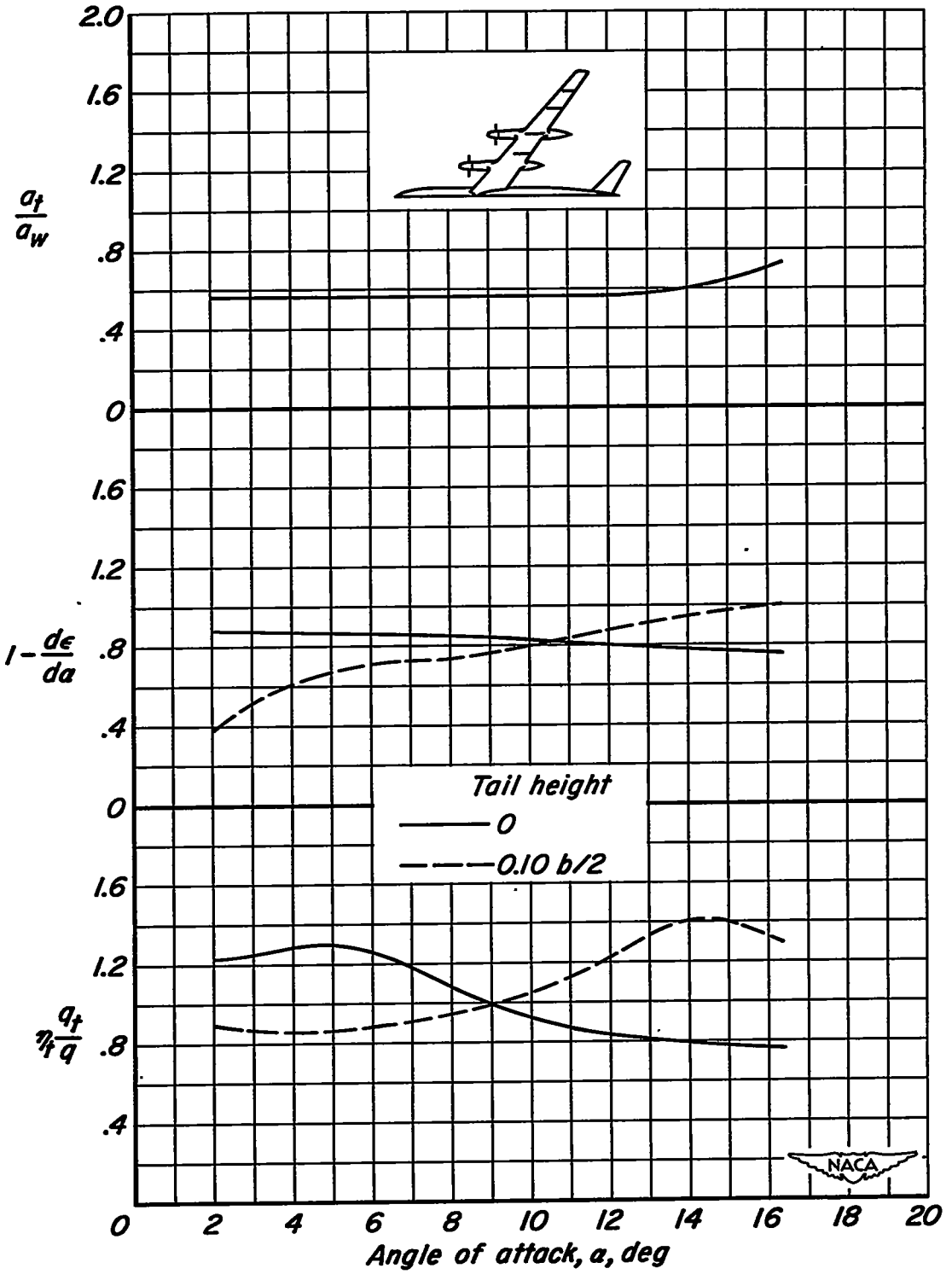

(c) $T_c = 0.40$

Figure 32.- Continued.

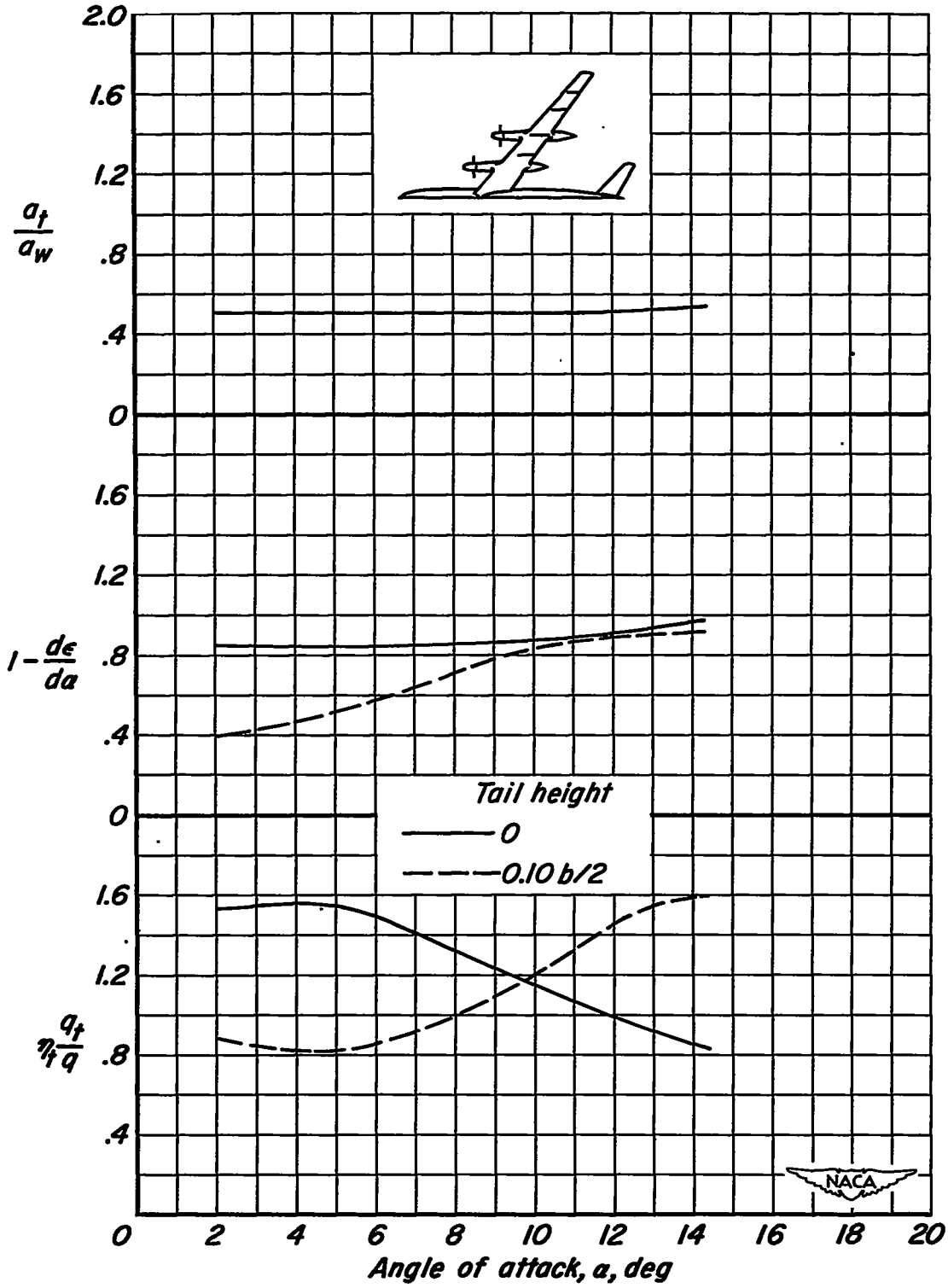

(d) $T_c = 0.80$

Figure 32.- Concluded.

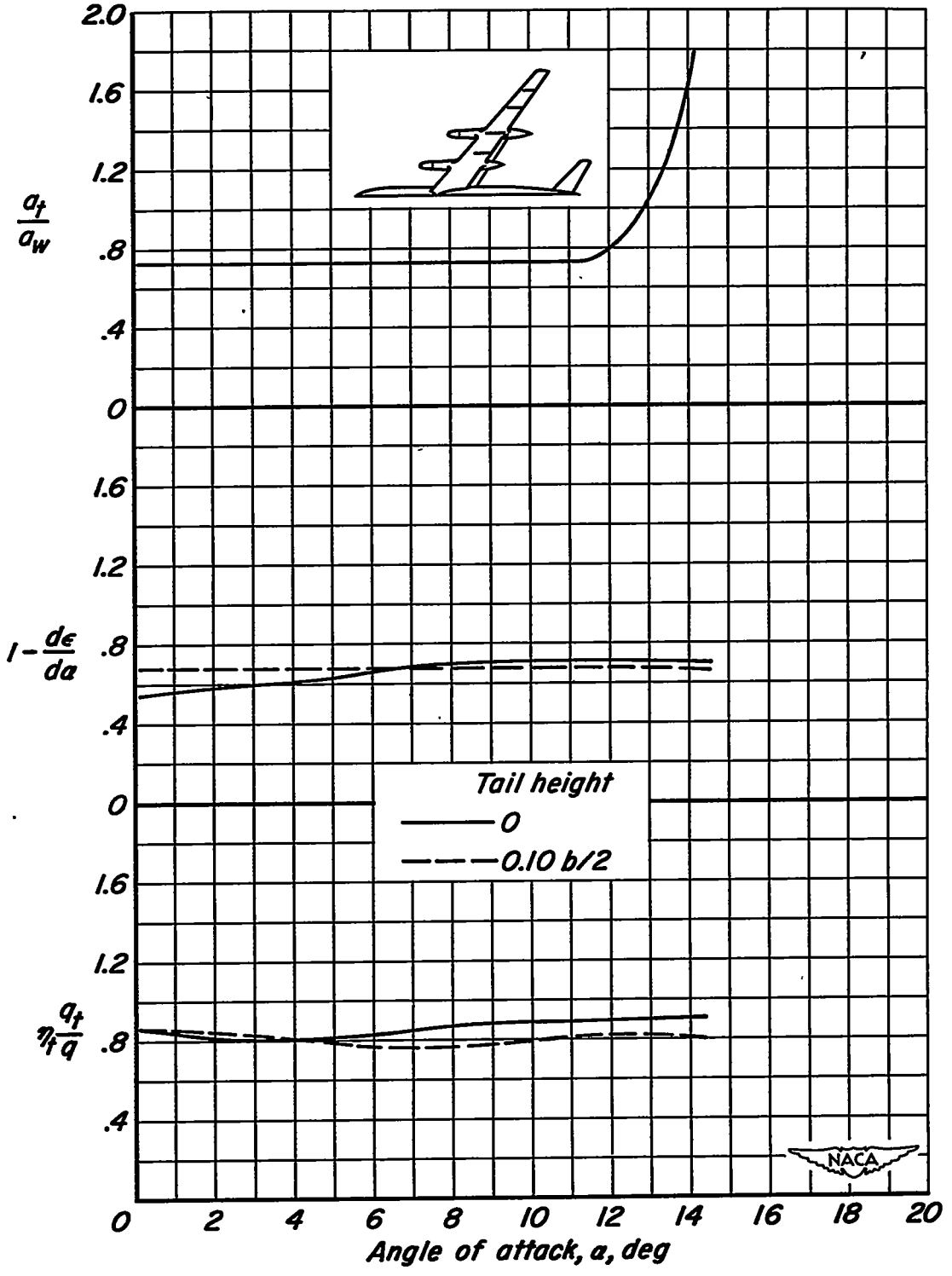

(a) Propellers off.

Figure 33.- The variation of a_t/a_w, $1-(d\epsilon/d\alpha)$, and $\eta_t(q_t/q)$ with α; inboard flaps-deflected; M = 0.082; R = 4,000,000; $\beta = 26^\circ$.

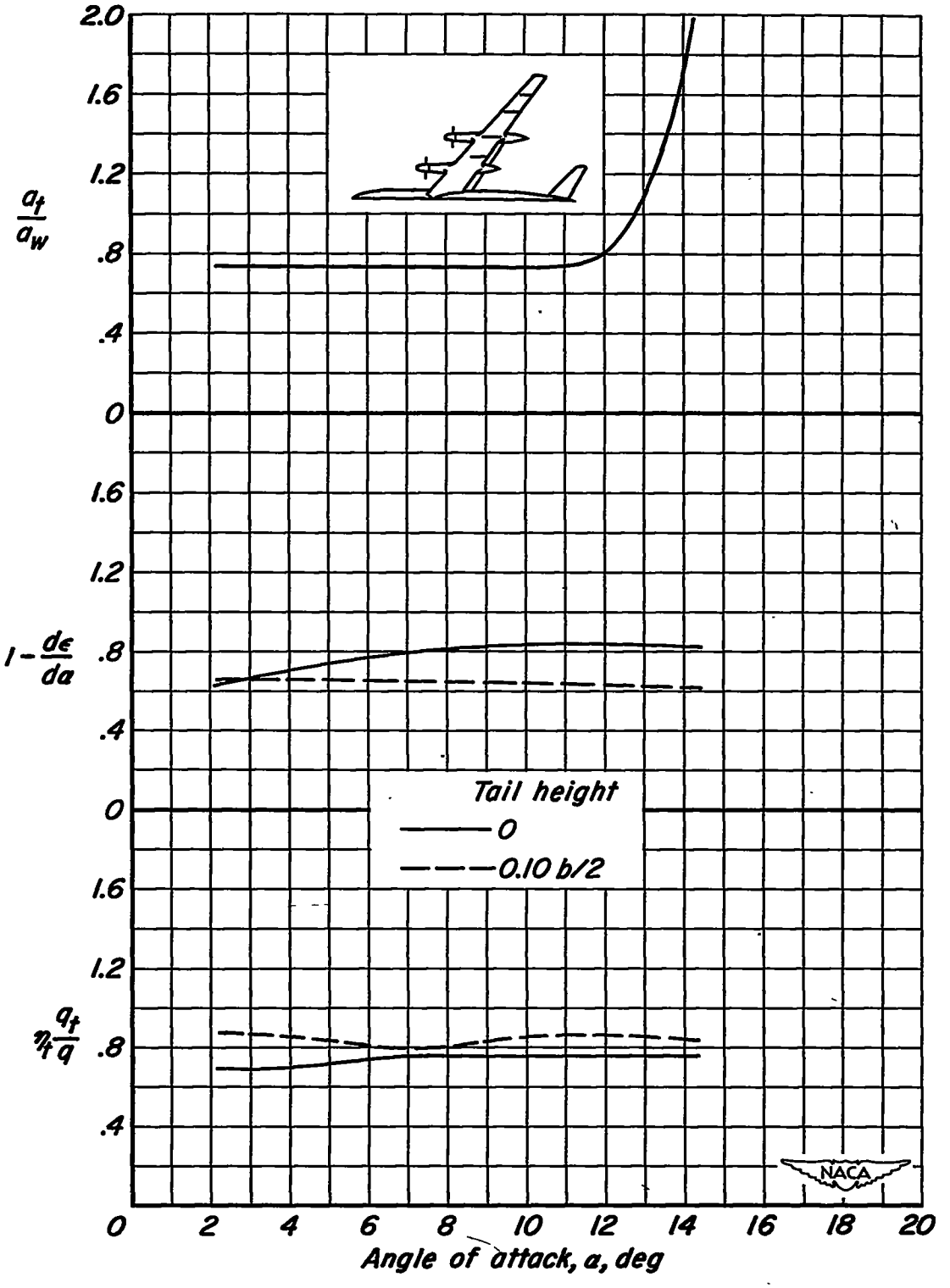

(b) $T_c = 0$

Figure 33.- Continued.

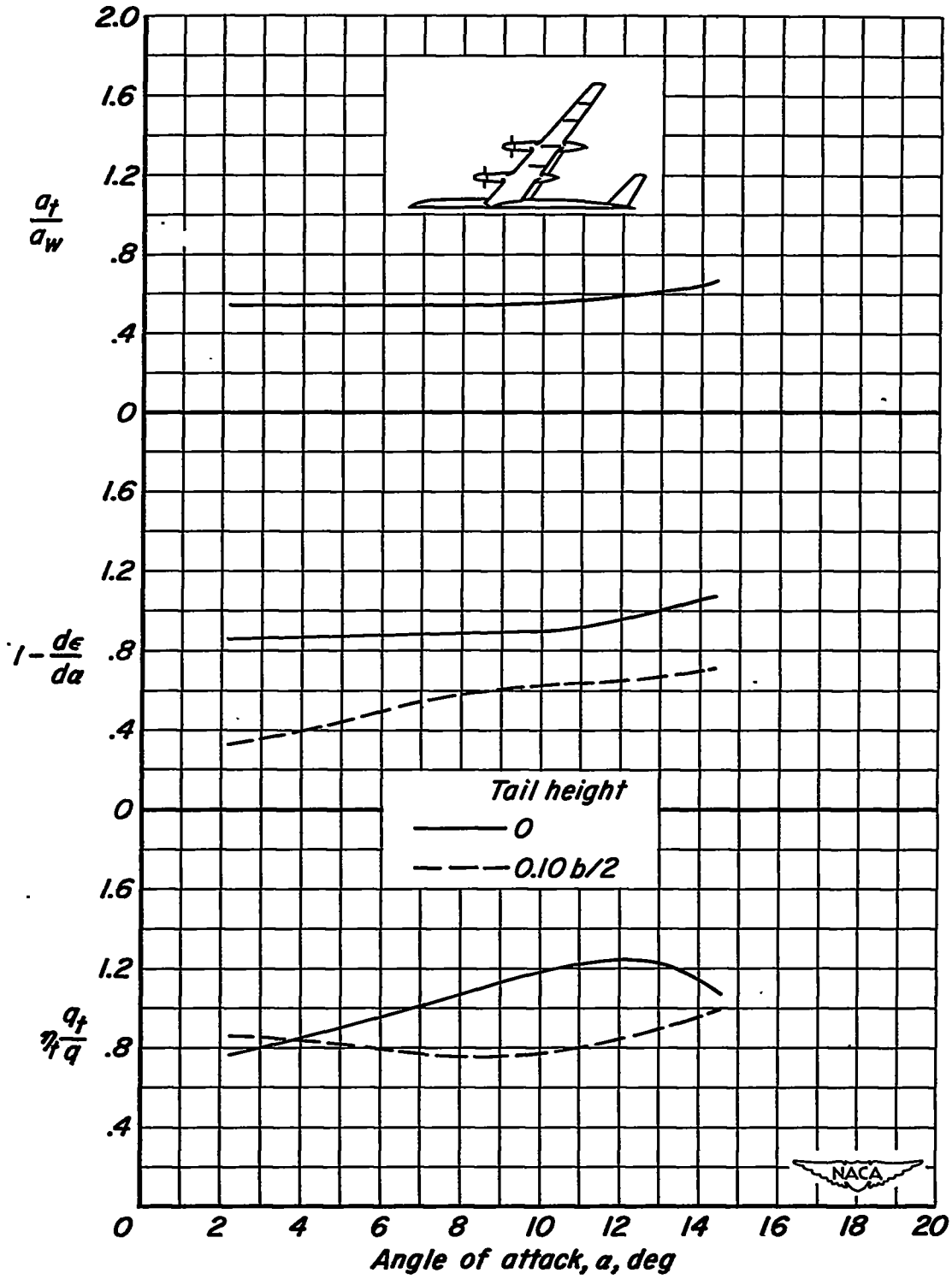

(c) $T_c = 0.40$

Figure 33.- Continued.

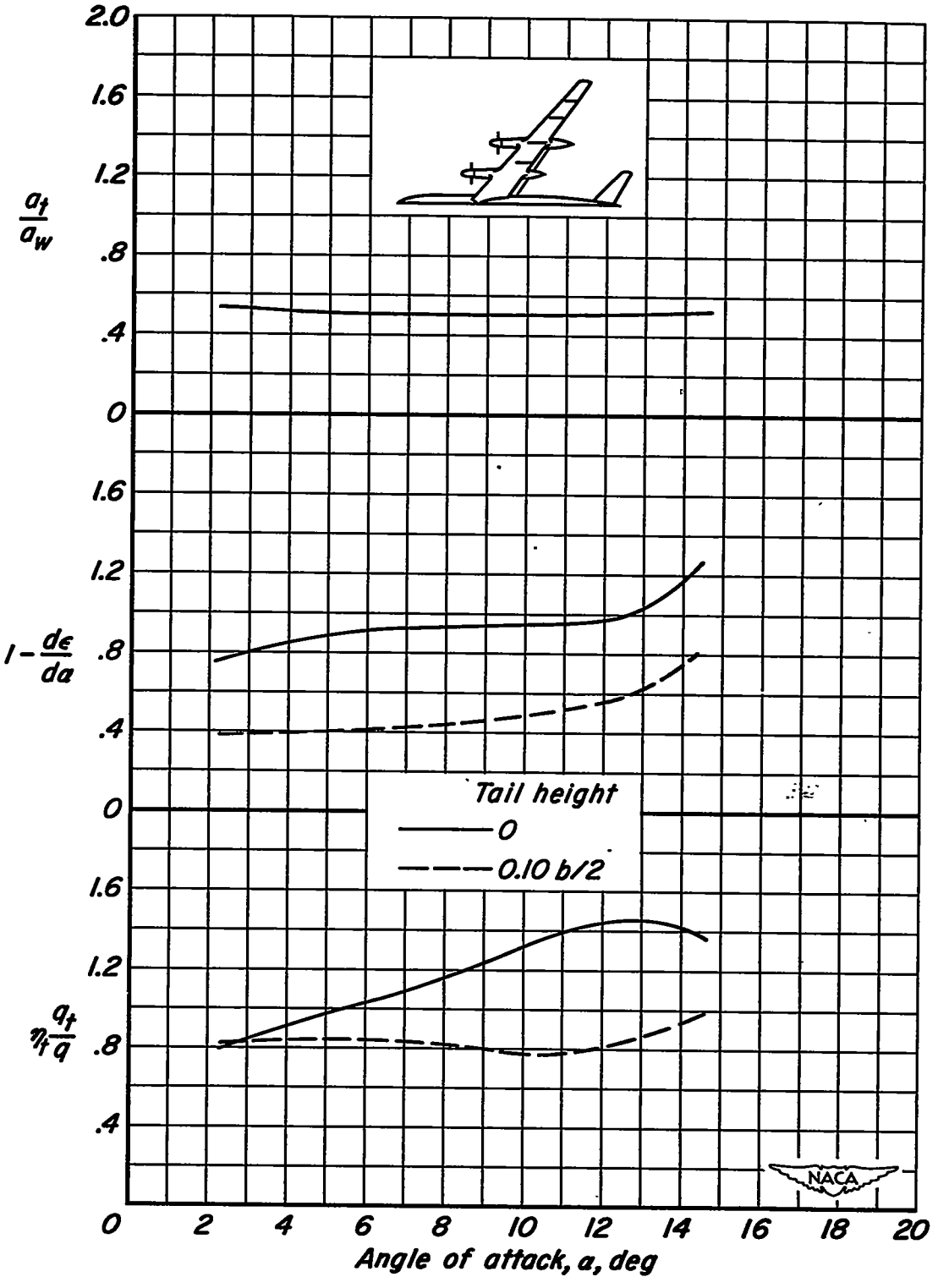

(d) $T_c = 0.80$

Figure 33. - Concluded.

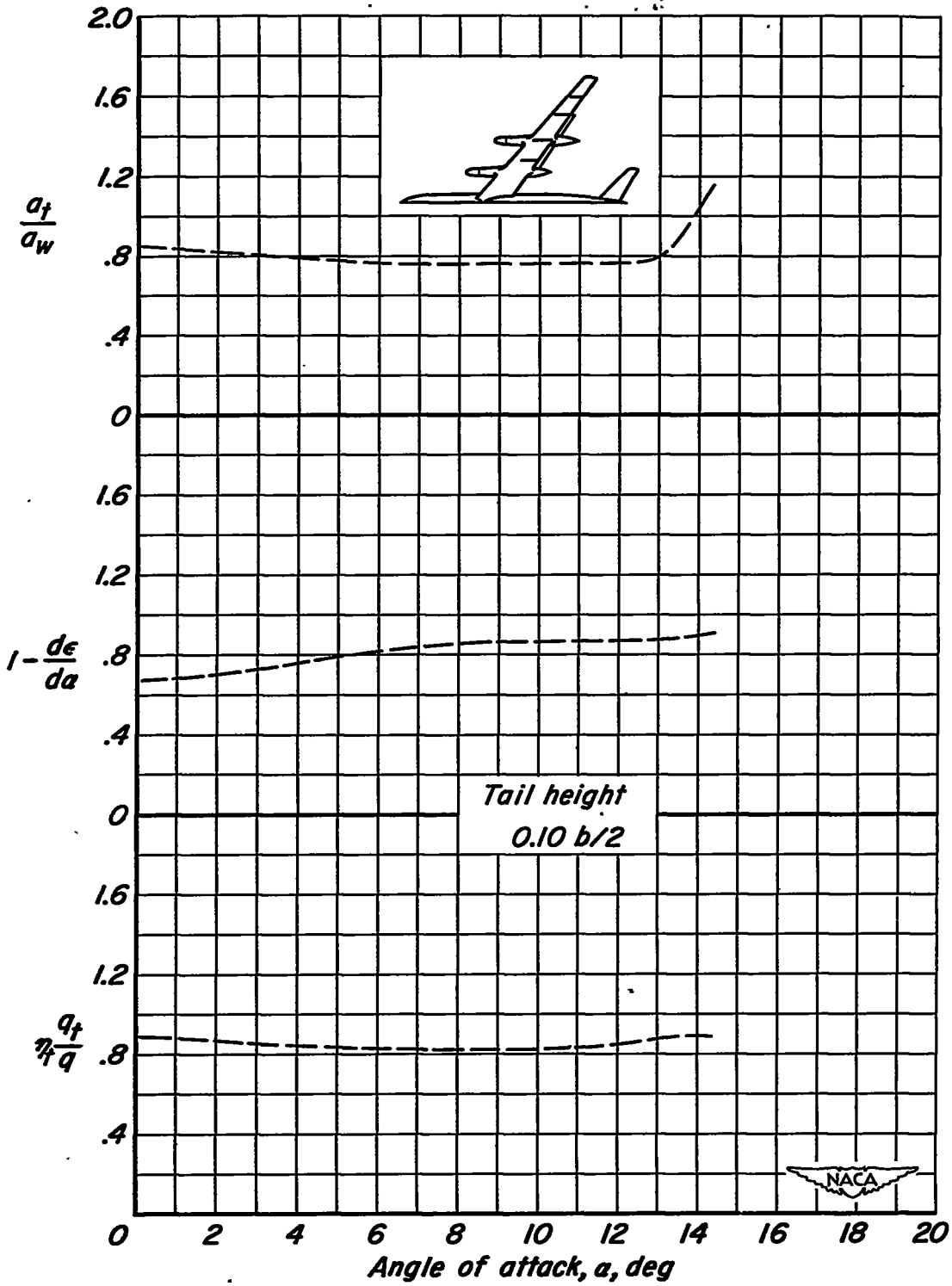

(a) Propellers off.

Figure 34.- The variation of a_t/a_w, $1-(d\epsilon/d\alpha)$, and $\eta_t(q_t/q)$ with α; outboard flaps deflected; M = 0.082; R = 4,000,000; $\beta = 26^\circ$.

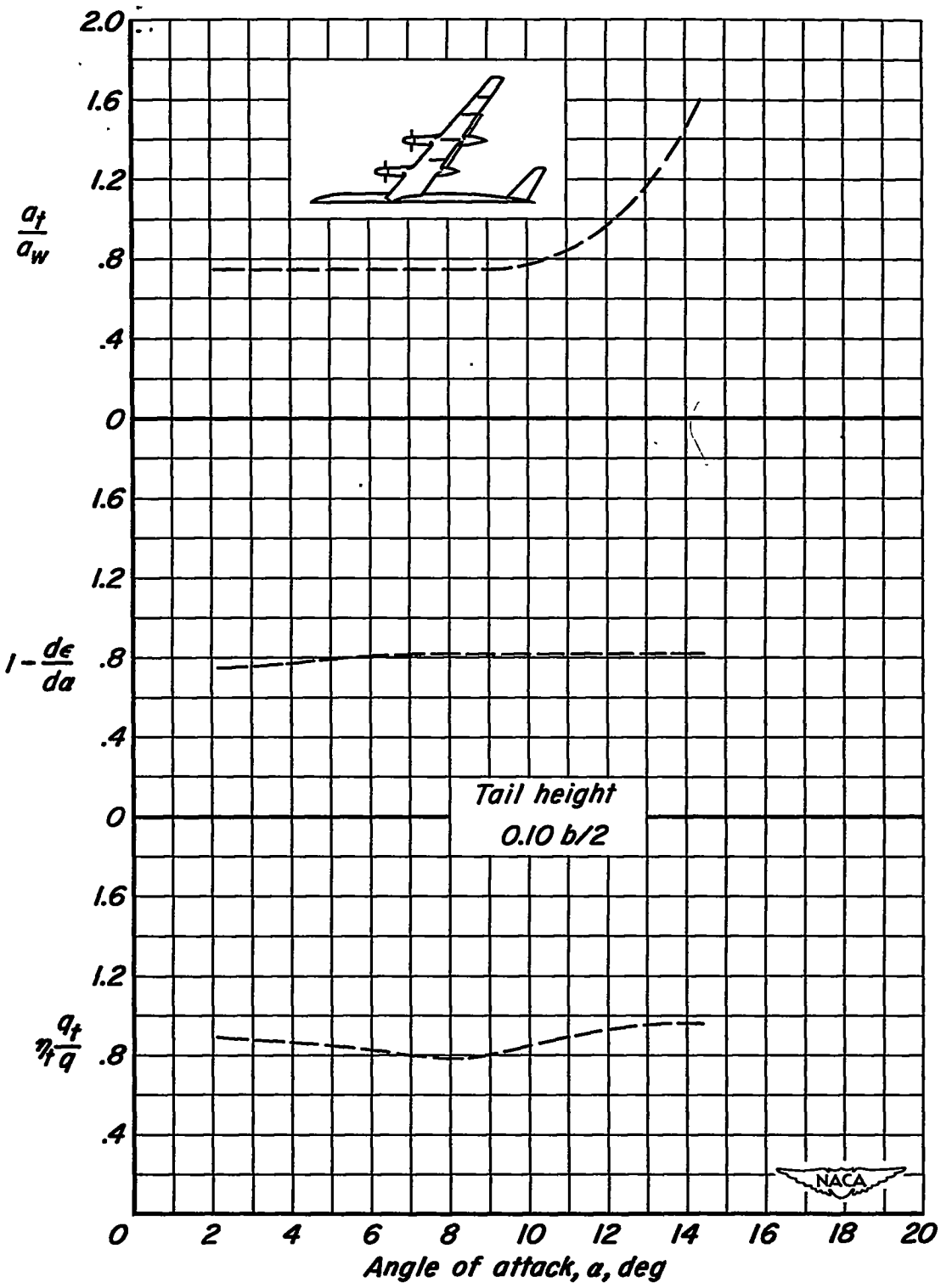

(b) $T_c = 0$

Figure 34.- Continued.

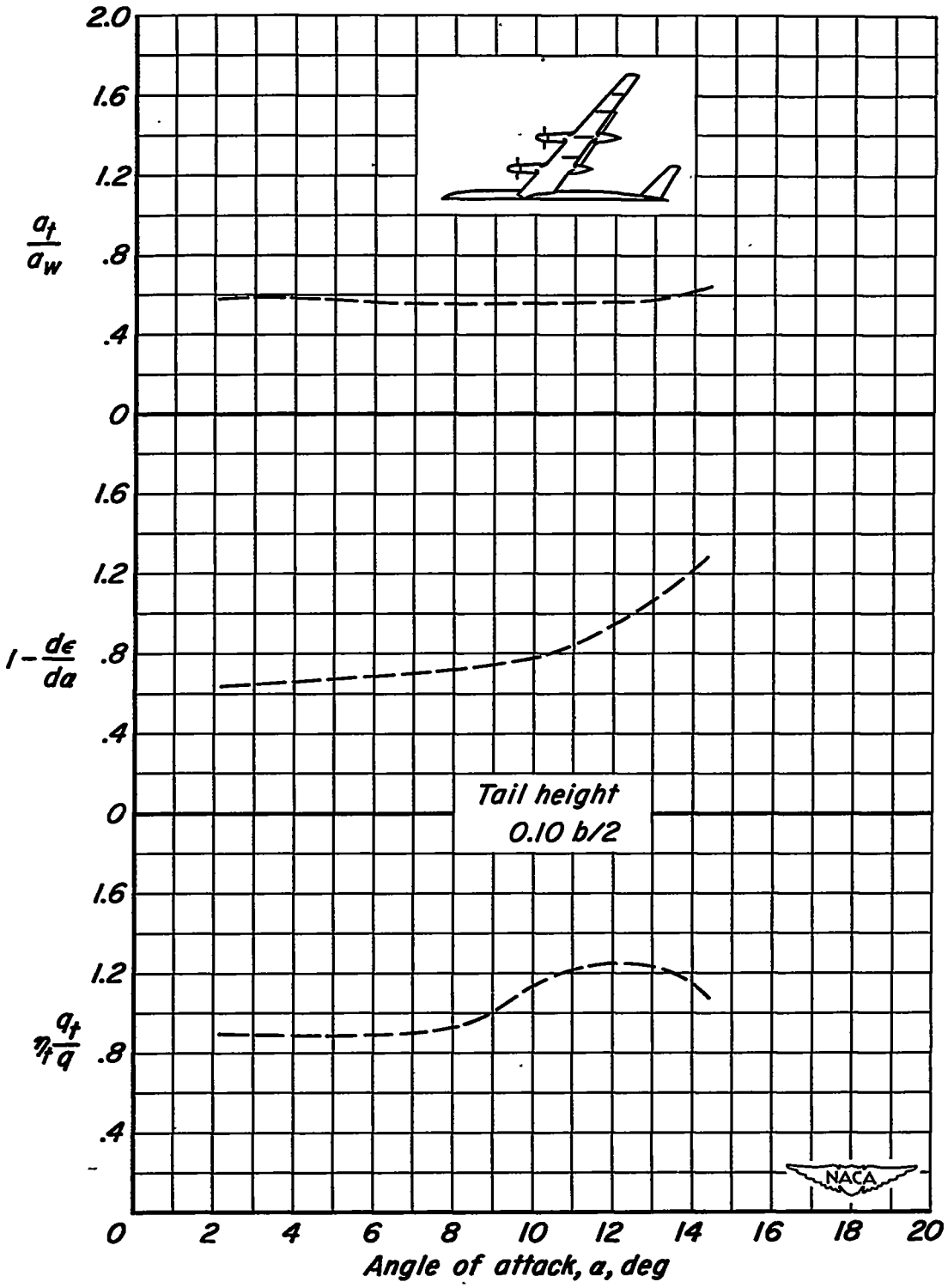

(c) $T_c = 0.40$

Figure 34.- Continued.

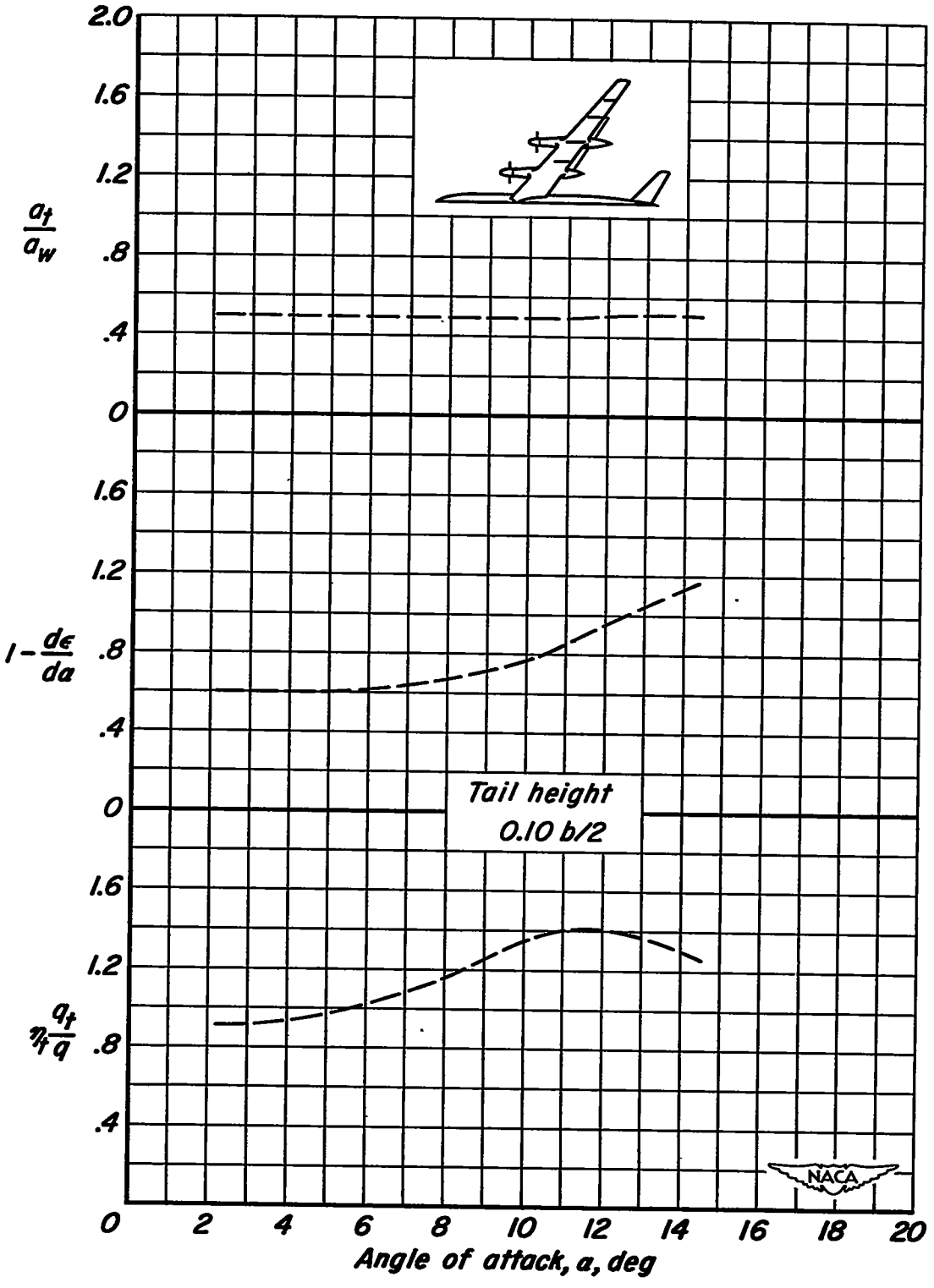

(d) $T_c = 0.80$

Figure 34.- Concluded.

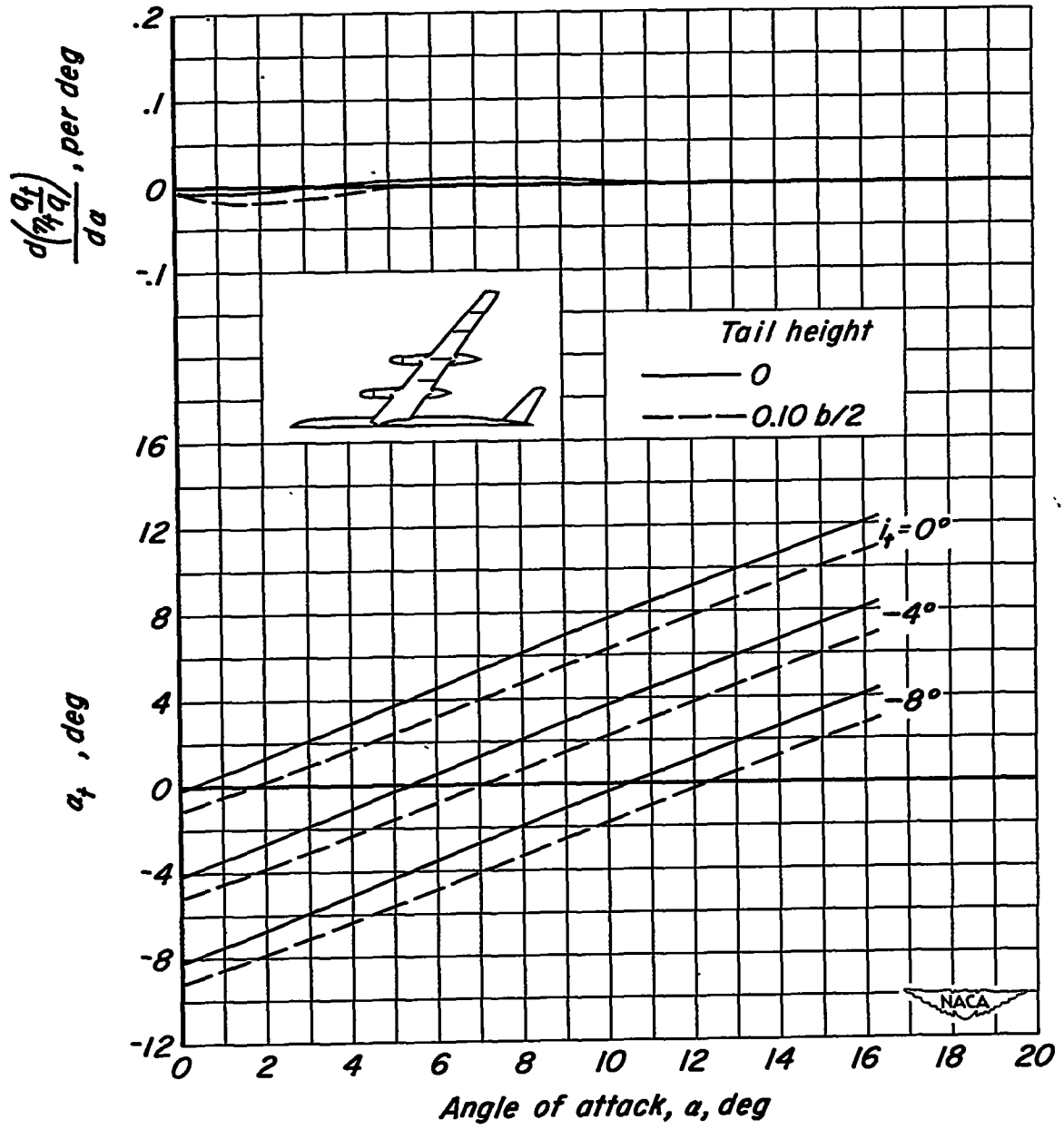

(a) Propellers off.

Figure 35.- The variation of $\frac{d(\eta_t q_t/q)}{d\alpha}$ and α_t with α; flaps up; M = 0.082; R = 4,000,000; β = 26°.

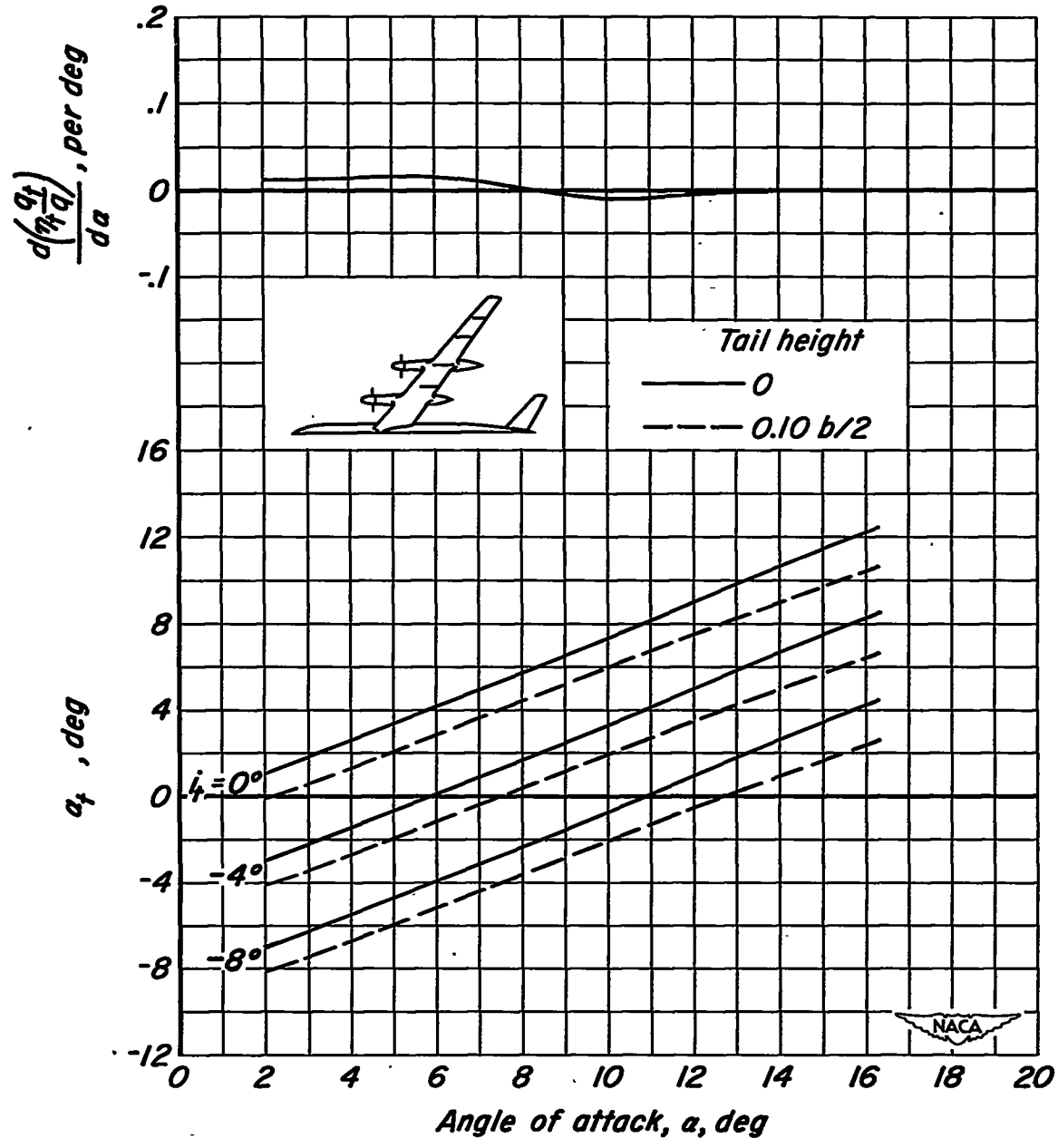

(b) $T_c = 0$

Figure 35.- Continued.

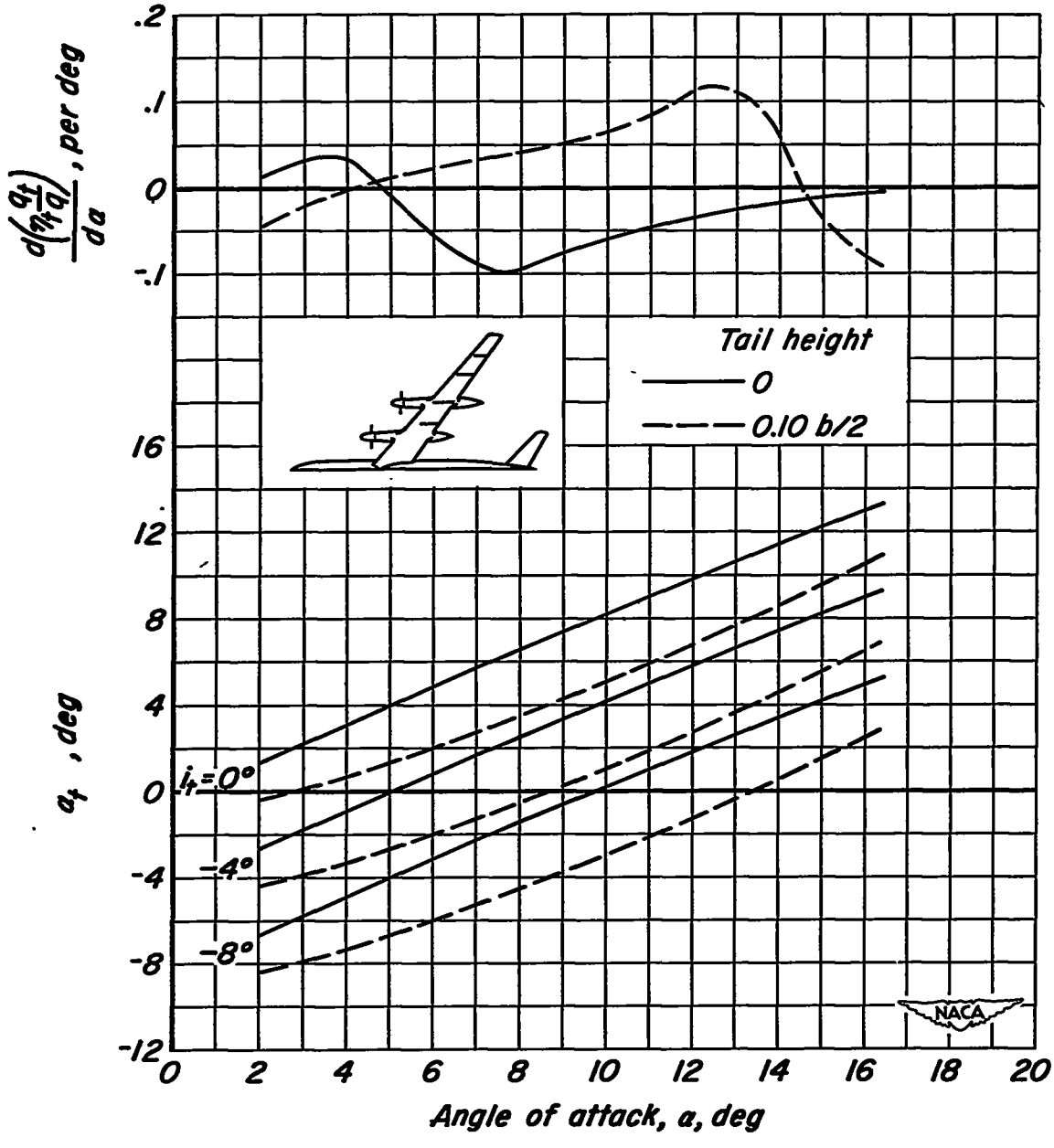

(c) T_c = 0.40

Figure 35.- Continued.

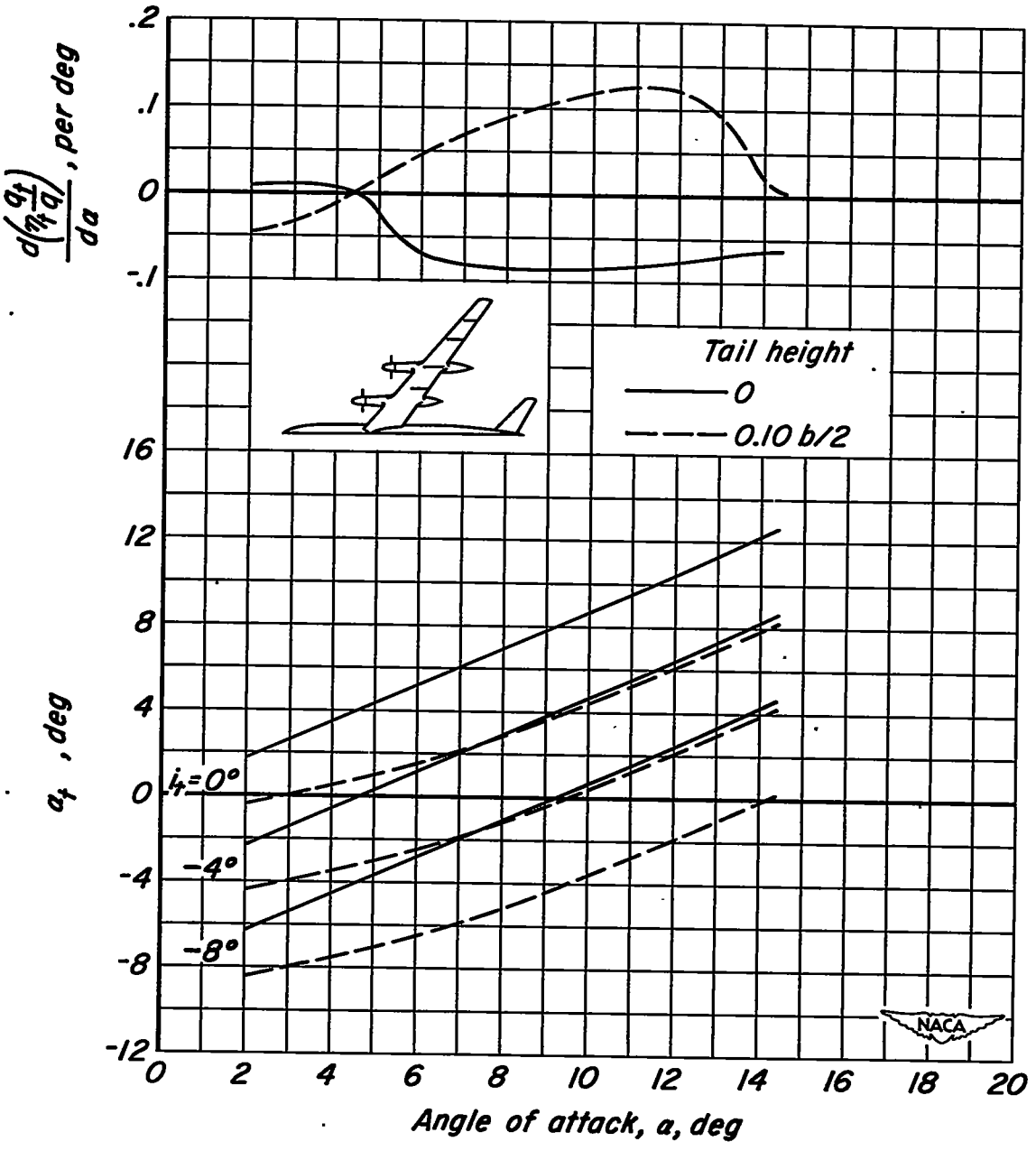

(d) T_c = 0.80

Figure 35.- Concluded.

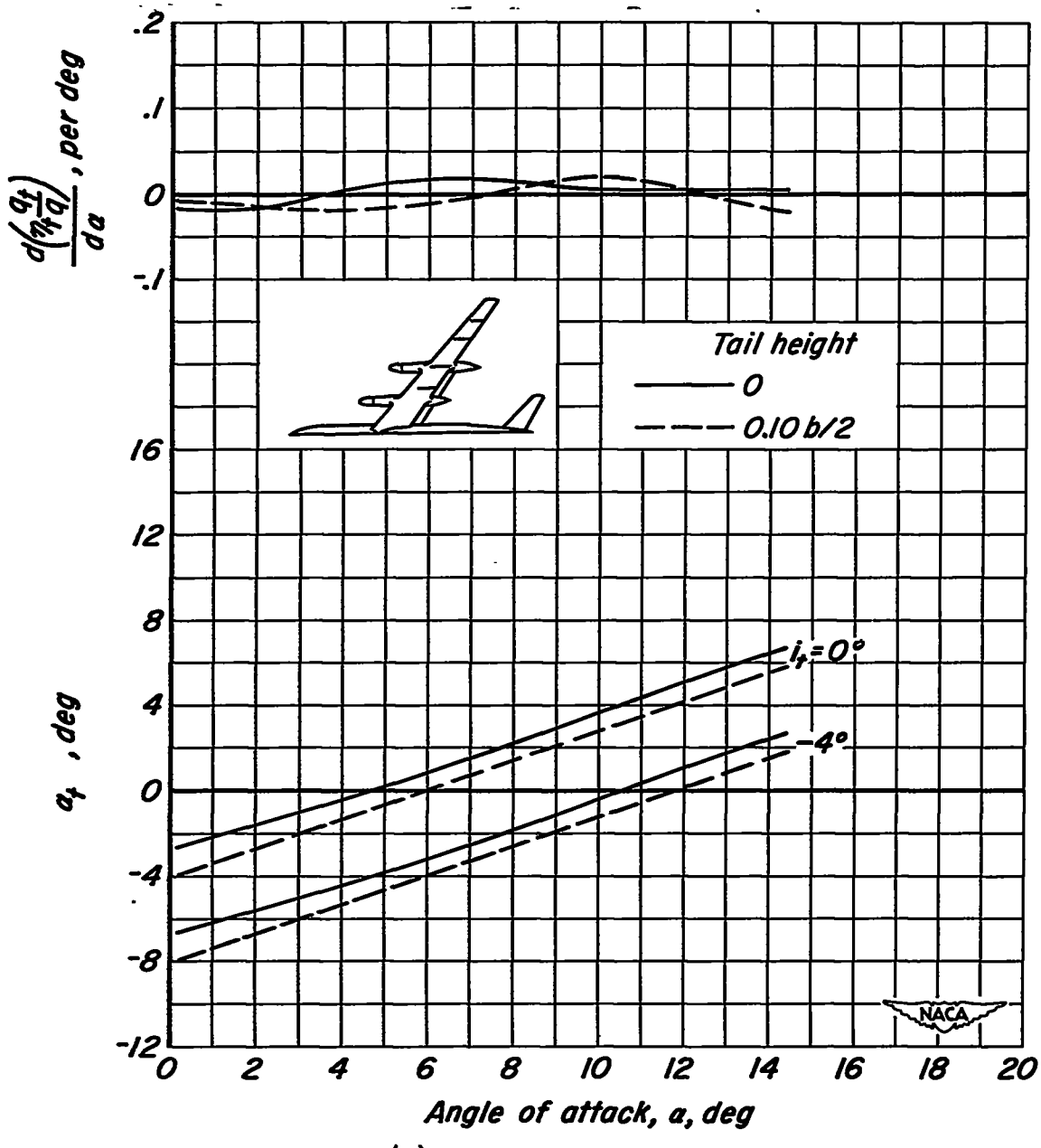

(a) Propellers off.

Figure 36.- The variation of $\frac{d(\eta_t q_t/q)}{d\alpha}$ and α_t with α; inboard flaps deflected; M = 0.082; R = 4,000,000; $\beta = 26^\circ$.

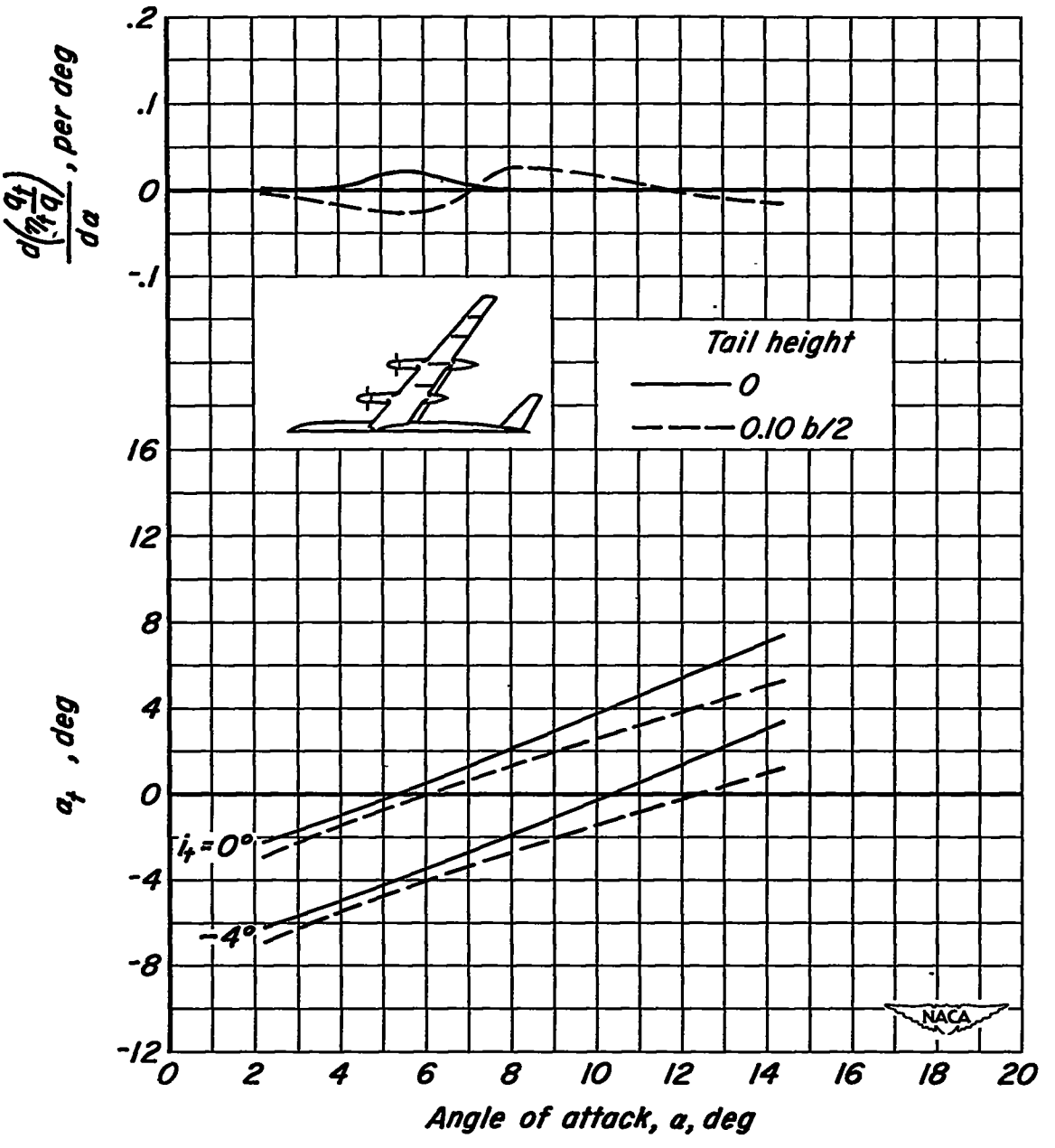

(b) $T_c = 0$

Figure 36.- Continued.

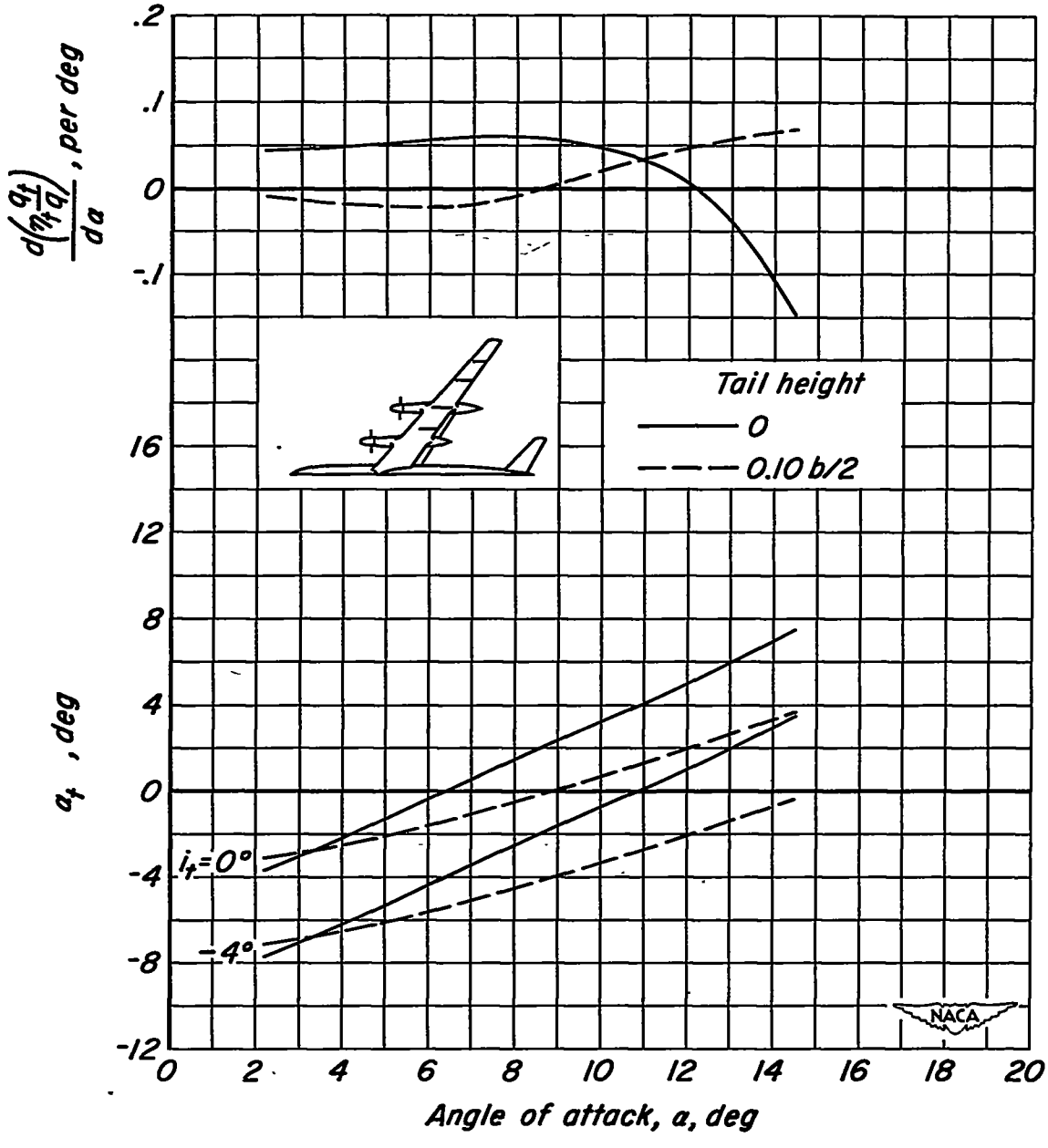

(c) T_c = 0.40

Figure 36.- Continued.

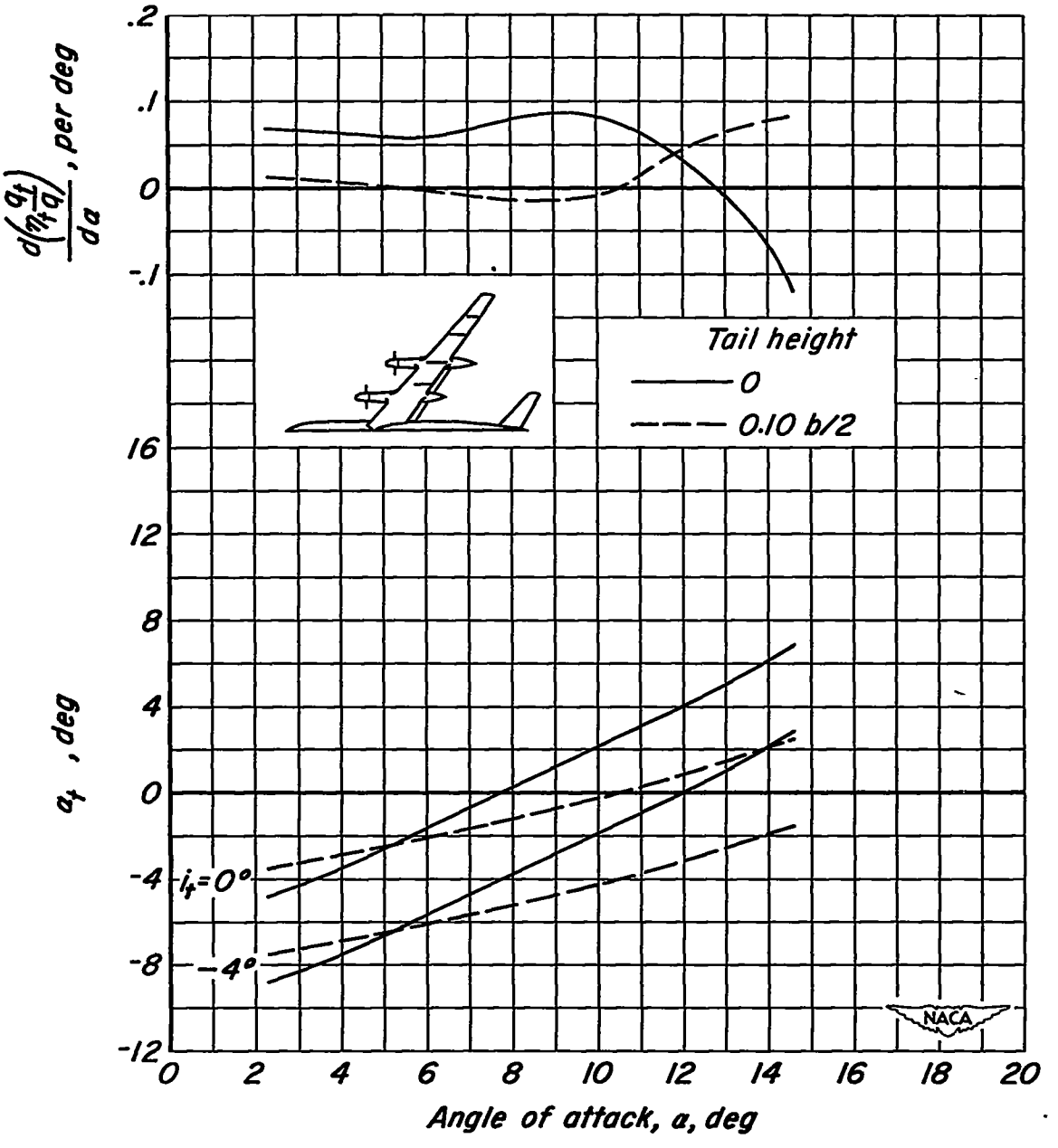

(d) T_c = 0.80

Figure 36.- Concluded.

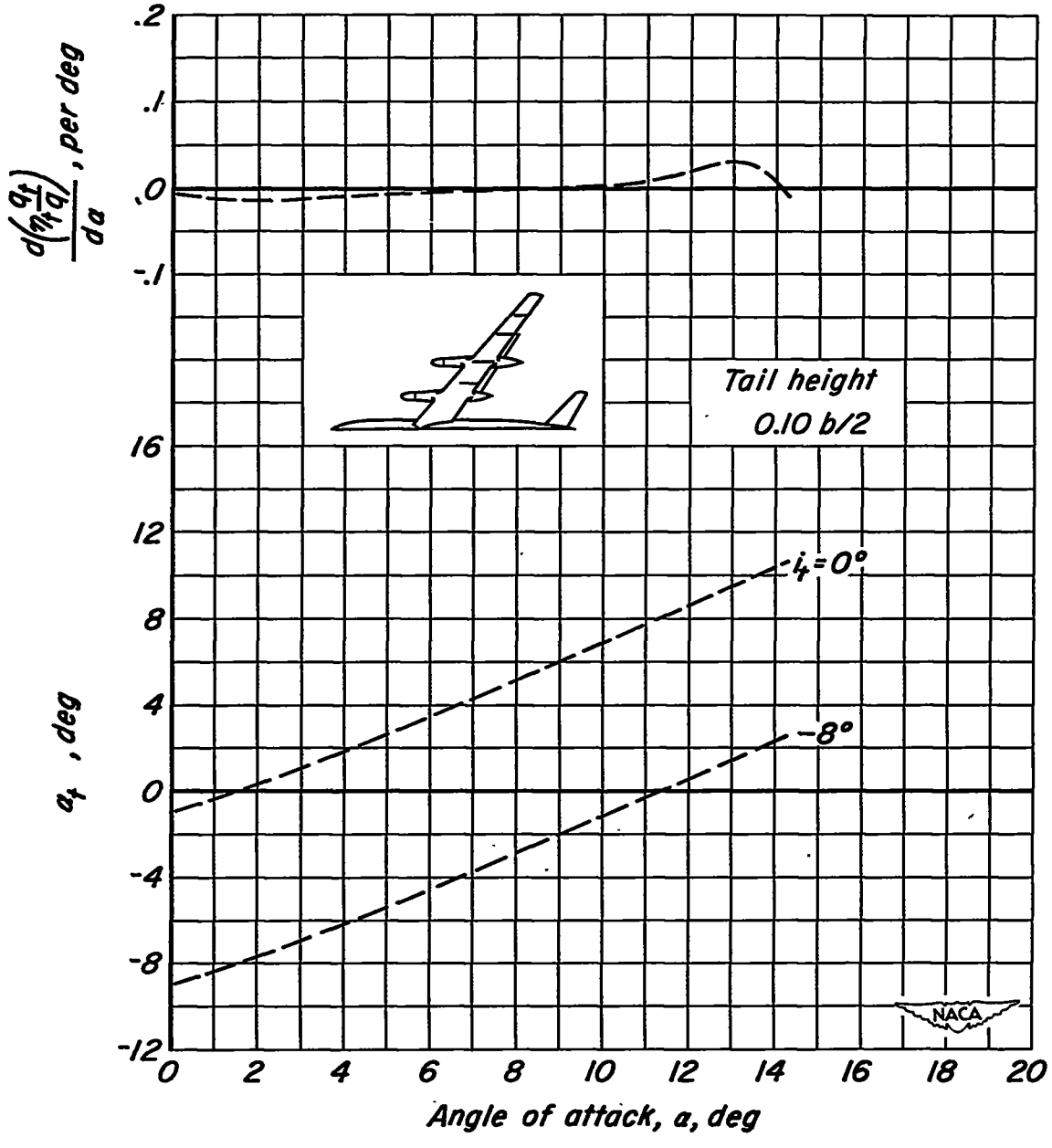

(a) Propellers off.

Figure 37.- The variation of $\frac{d(\eta_t q_t/q)}{d\alpha}$ and α_t with α; outboard flaps deflected; M = 0.082; R = 4,000,000; $\beta = 26^\circ$.

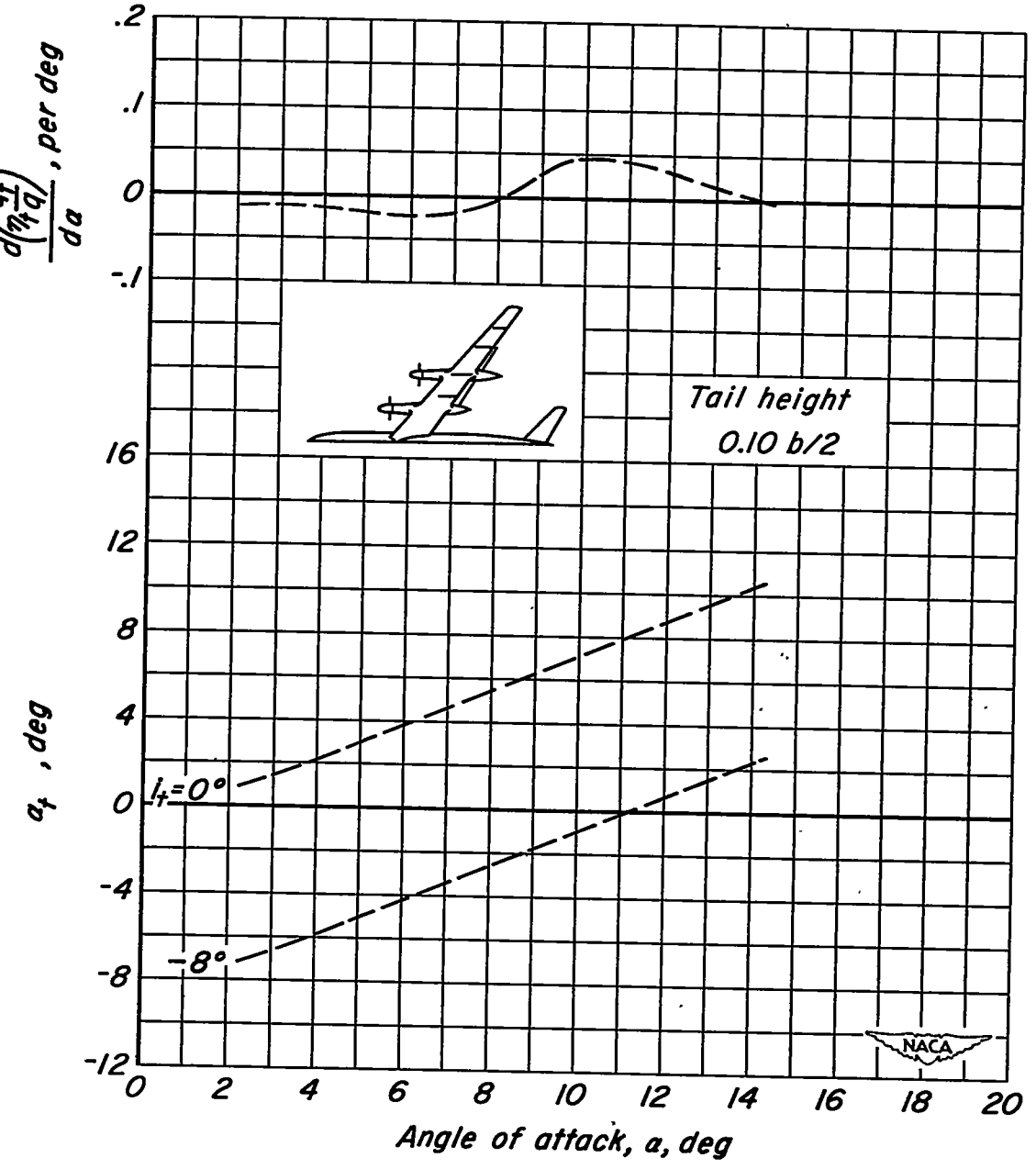

(b) $T_c = 0$

Figure 37.- Continued.

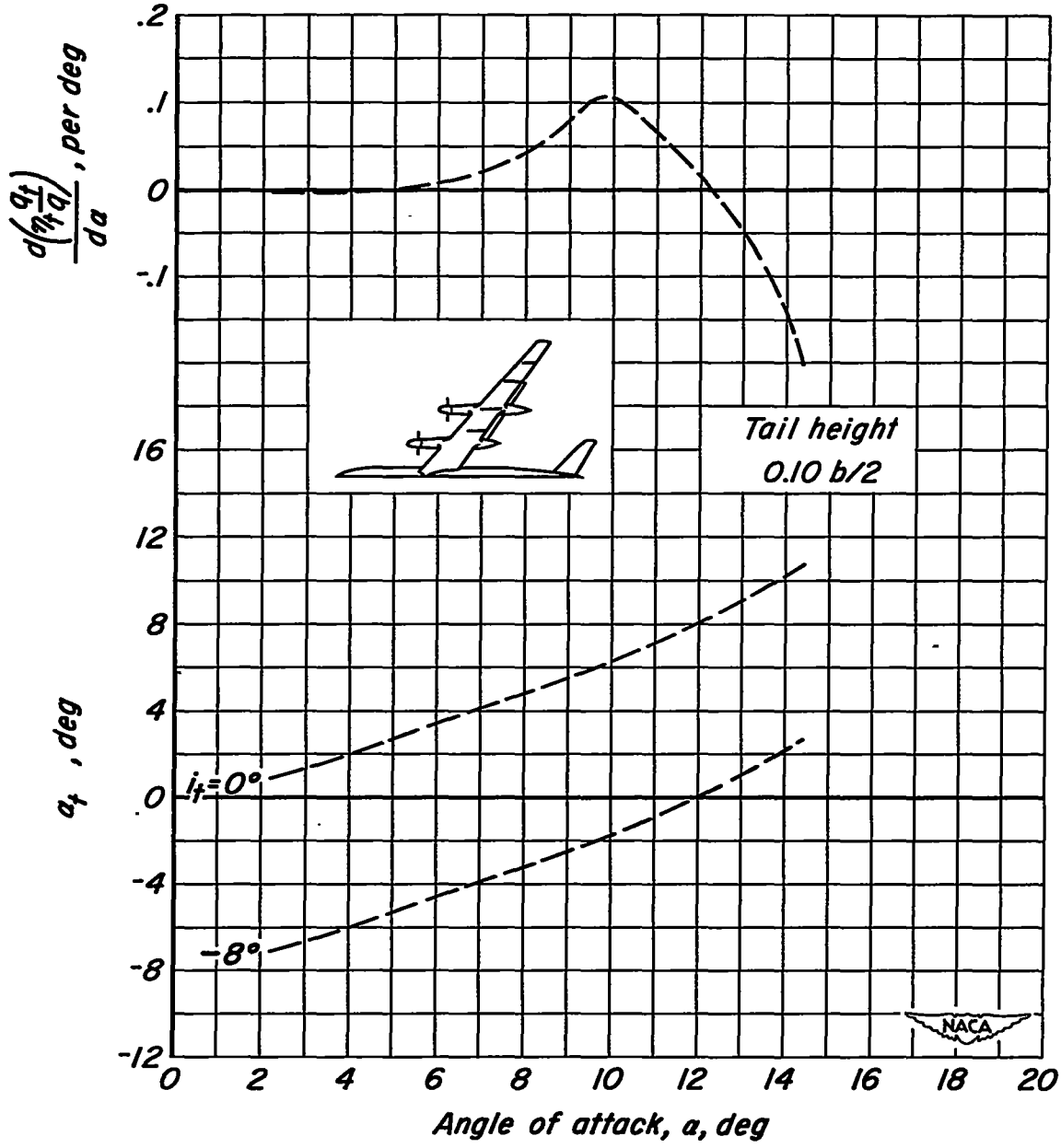

(c) T_c = 0.40

Figure 37.- Continued.

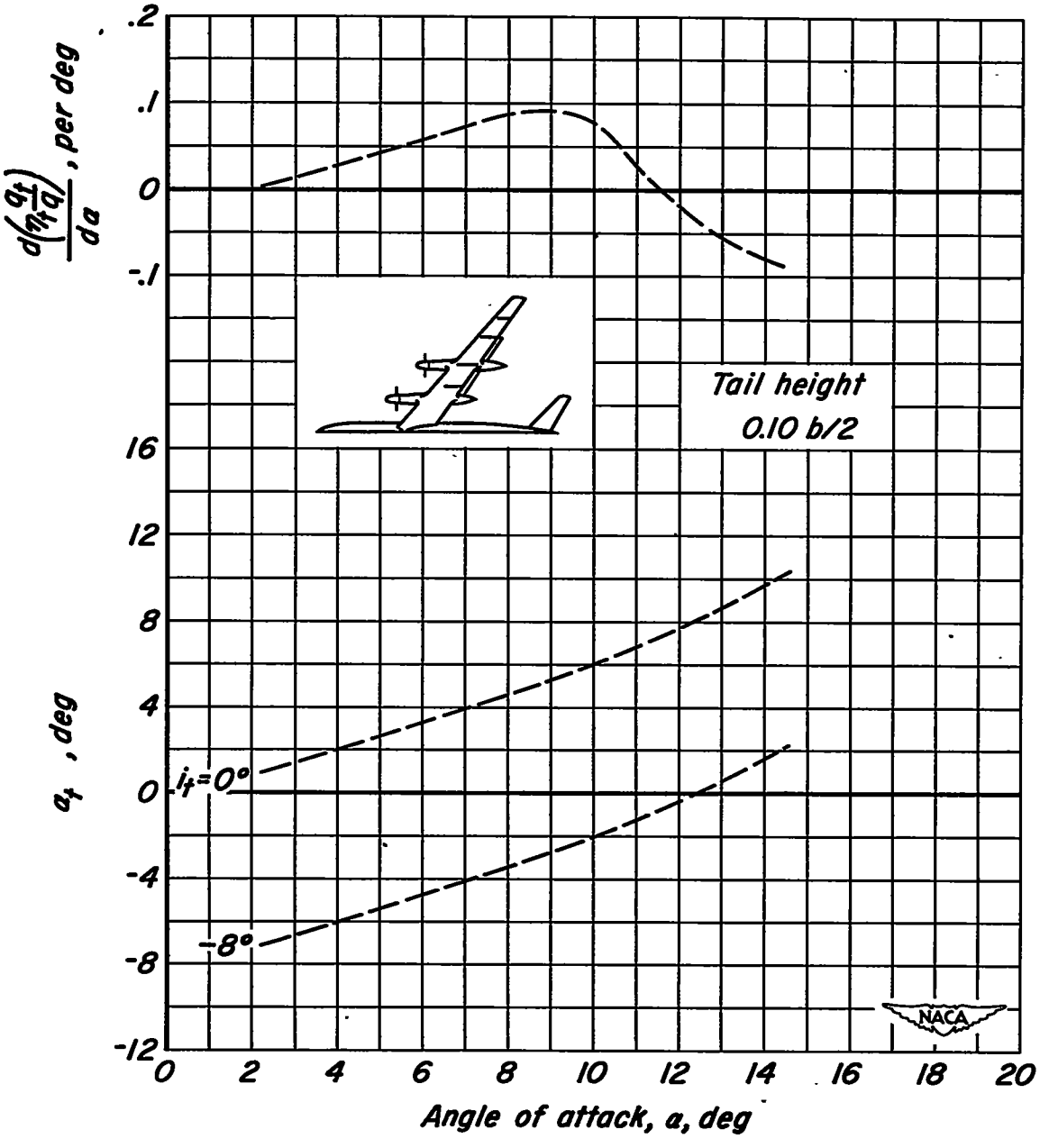

(d) T_c = 0.80

Figure 37.- Concluded.

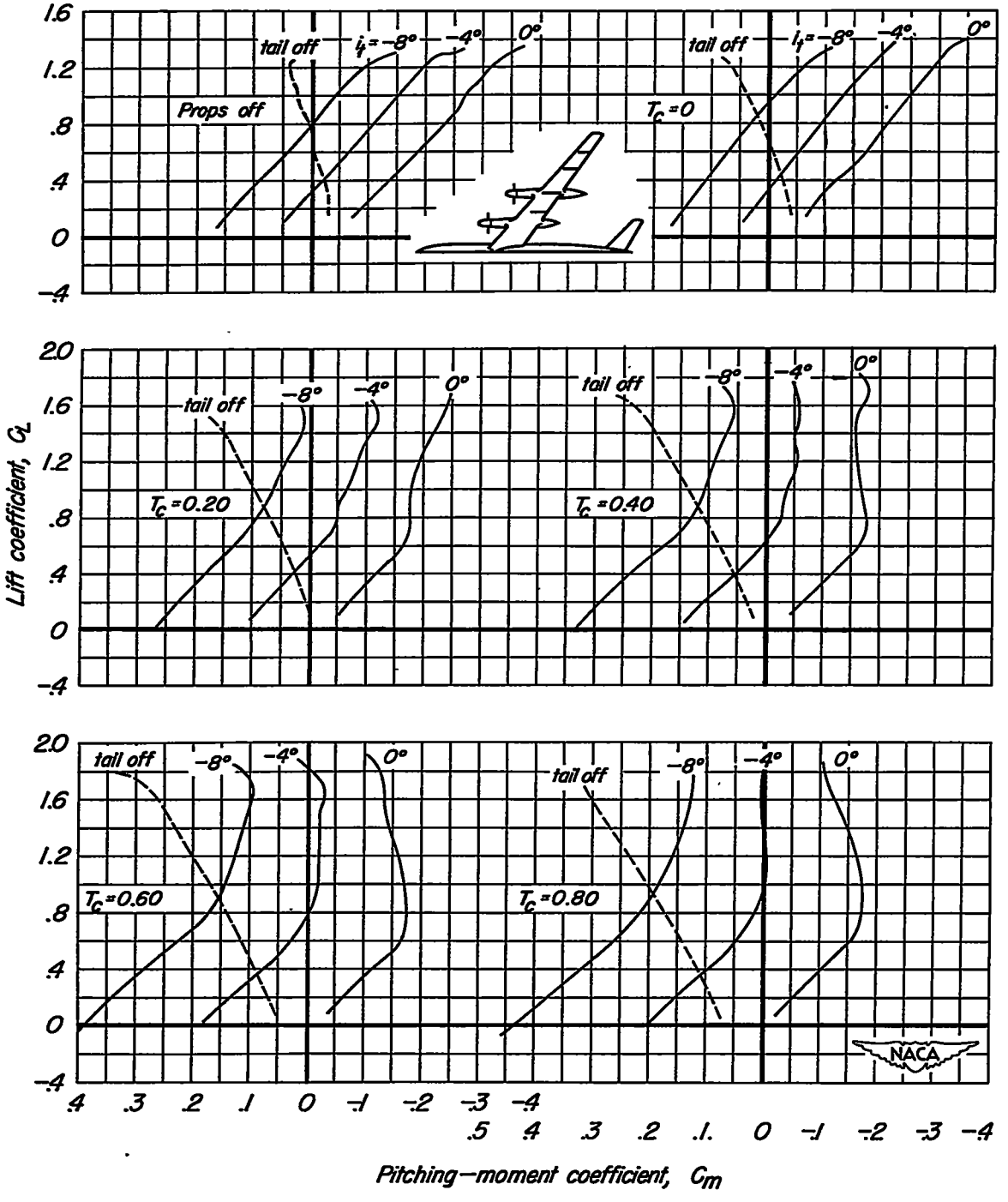

(a) Tail height = 0

Figure 38.- The effects of tail incidence on the pitching-moment characteristics of the model; flaps up; M = 0.082; R = 4,000,000; $\beta = 26^\circ$.

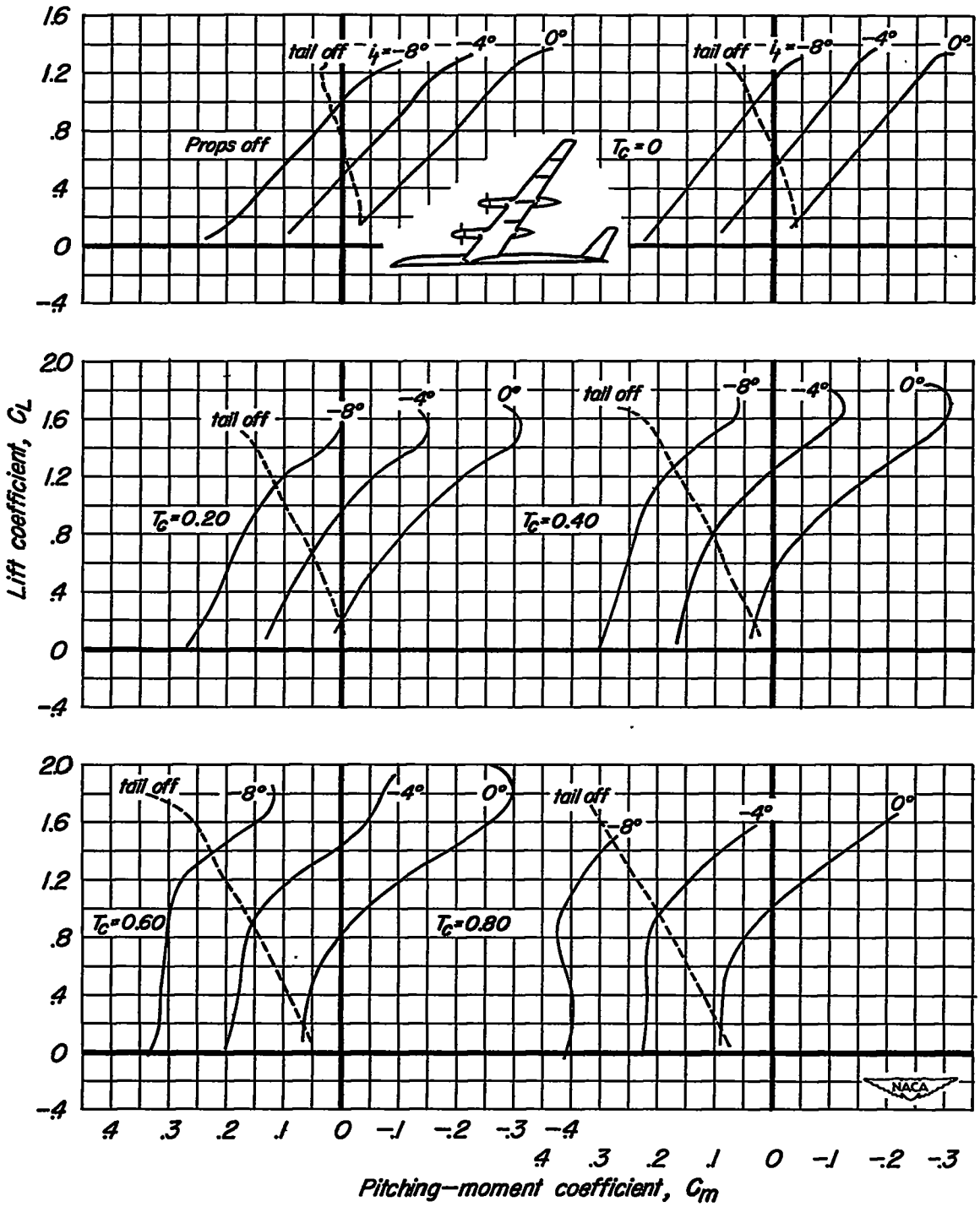

(b) Tail height = 0.10 b/2

Figure 38.- Concluded.

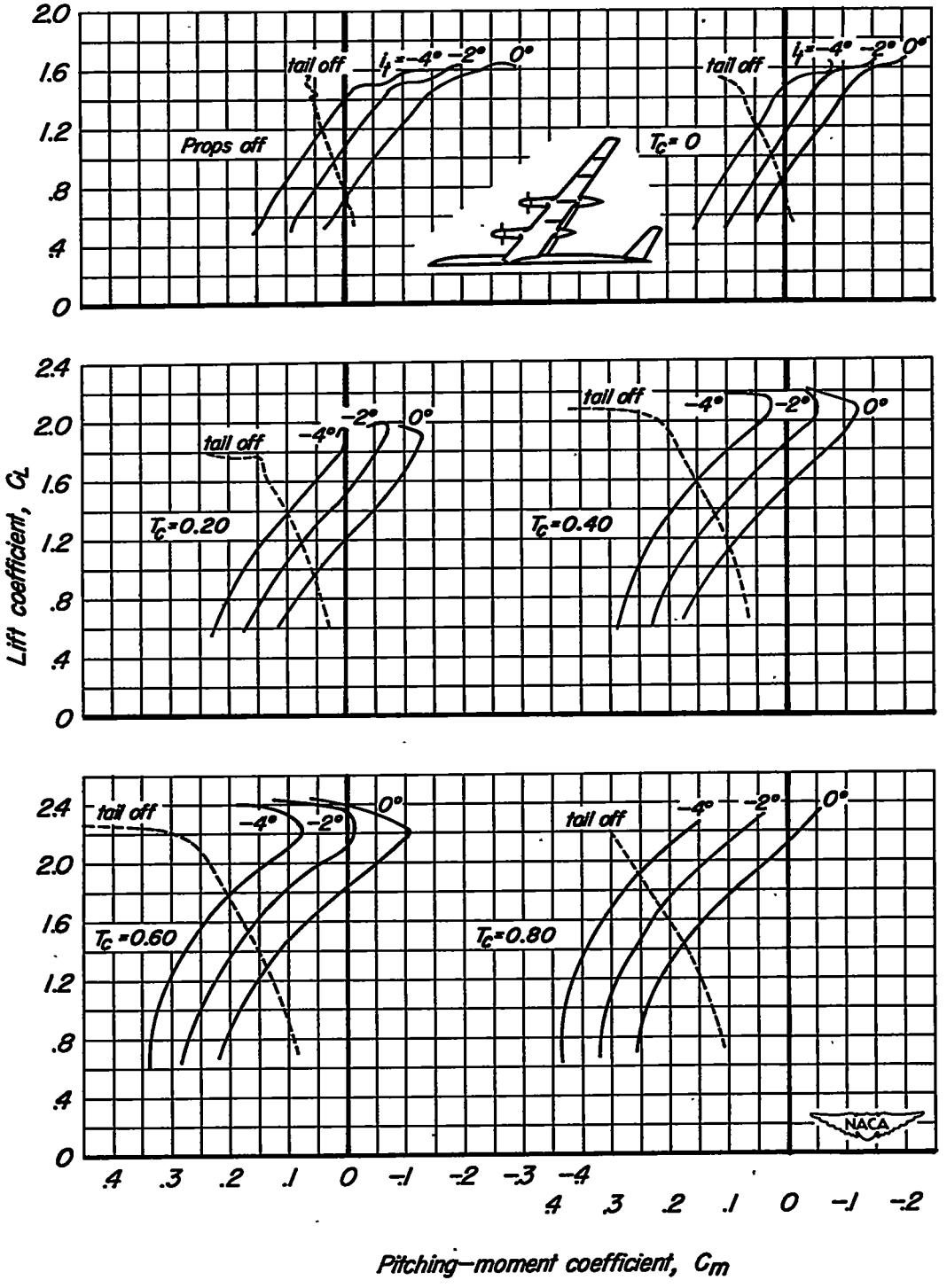

(a) Tail height = 0

Figure 39.- The effects of tail incidence on the pitching-moment characteristics of the model; inboard flaps deflected; M = 0.082; R = 4,000,000; $\beta = 26^{\circ}$.

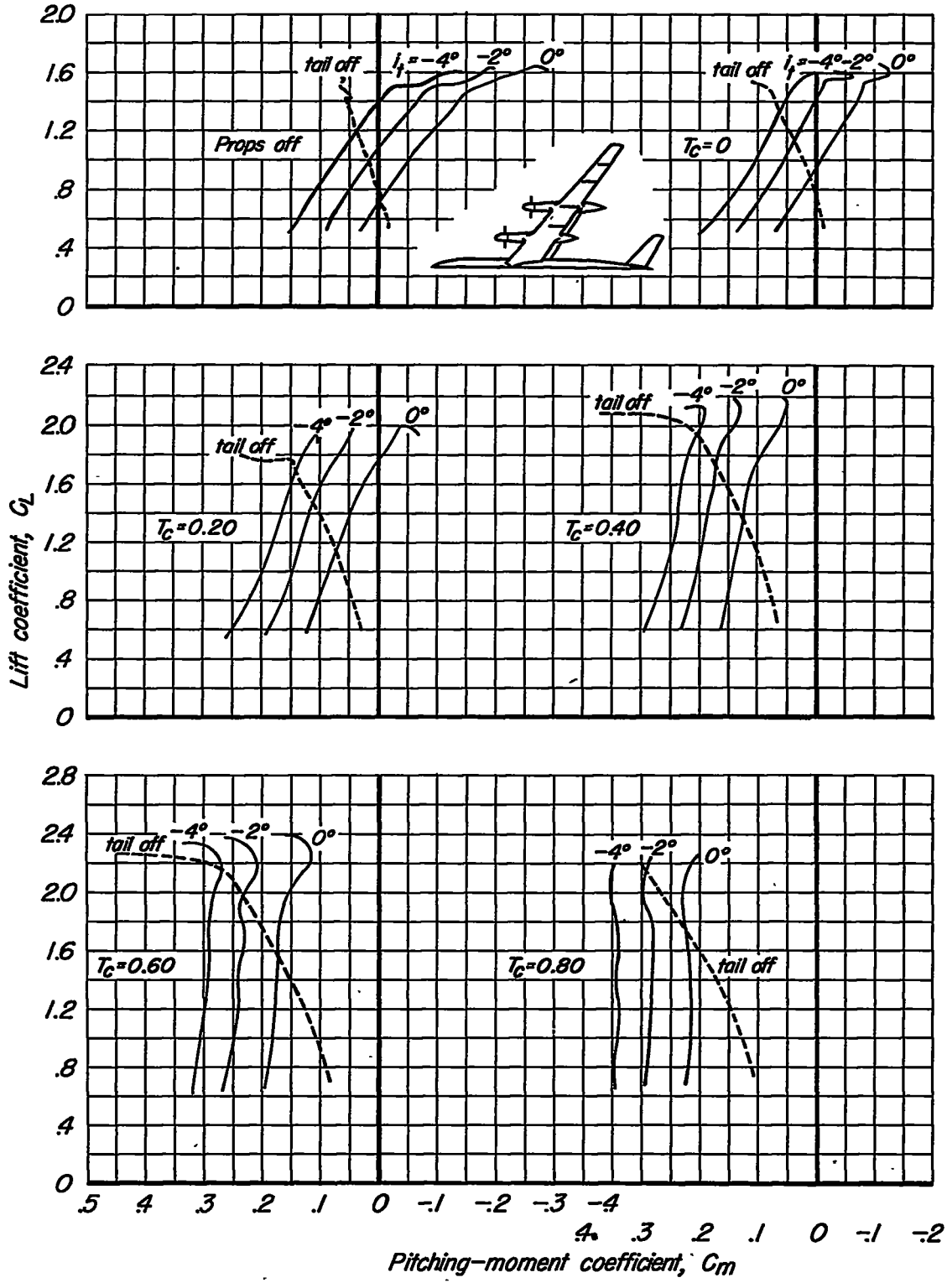

(b) Tail height = 0.10 b/2

Figure 39.- Concluded.

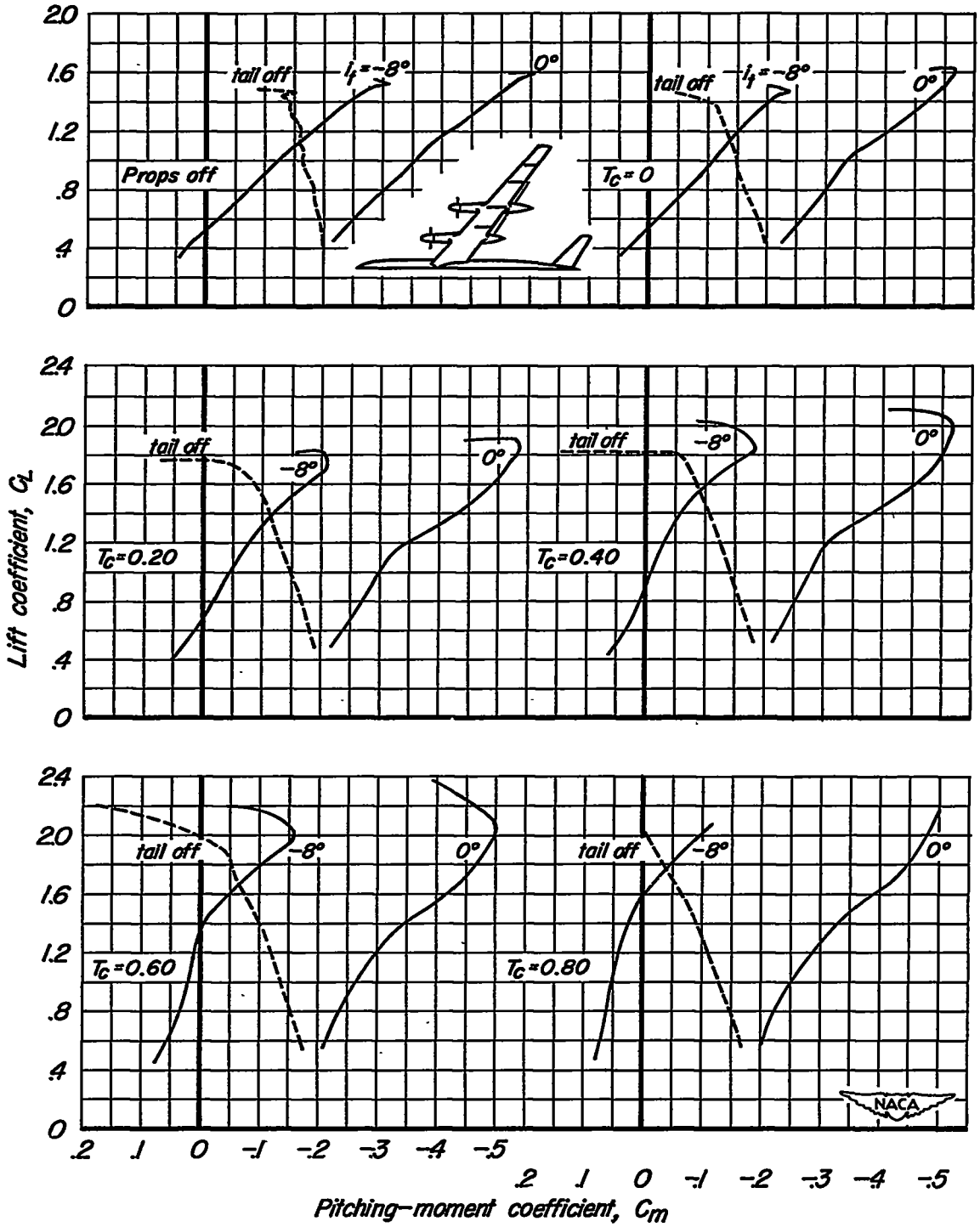

Figure 40.- The effects of tail incidence on the pitching-moment characteristics of the model; tail height = 0.10 b/2; outboard flaps deflected; M = 0.082; R = 4,000,000; $\beta = 26^{\circ}$.

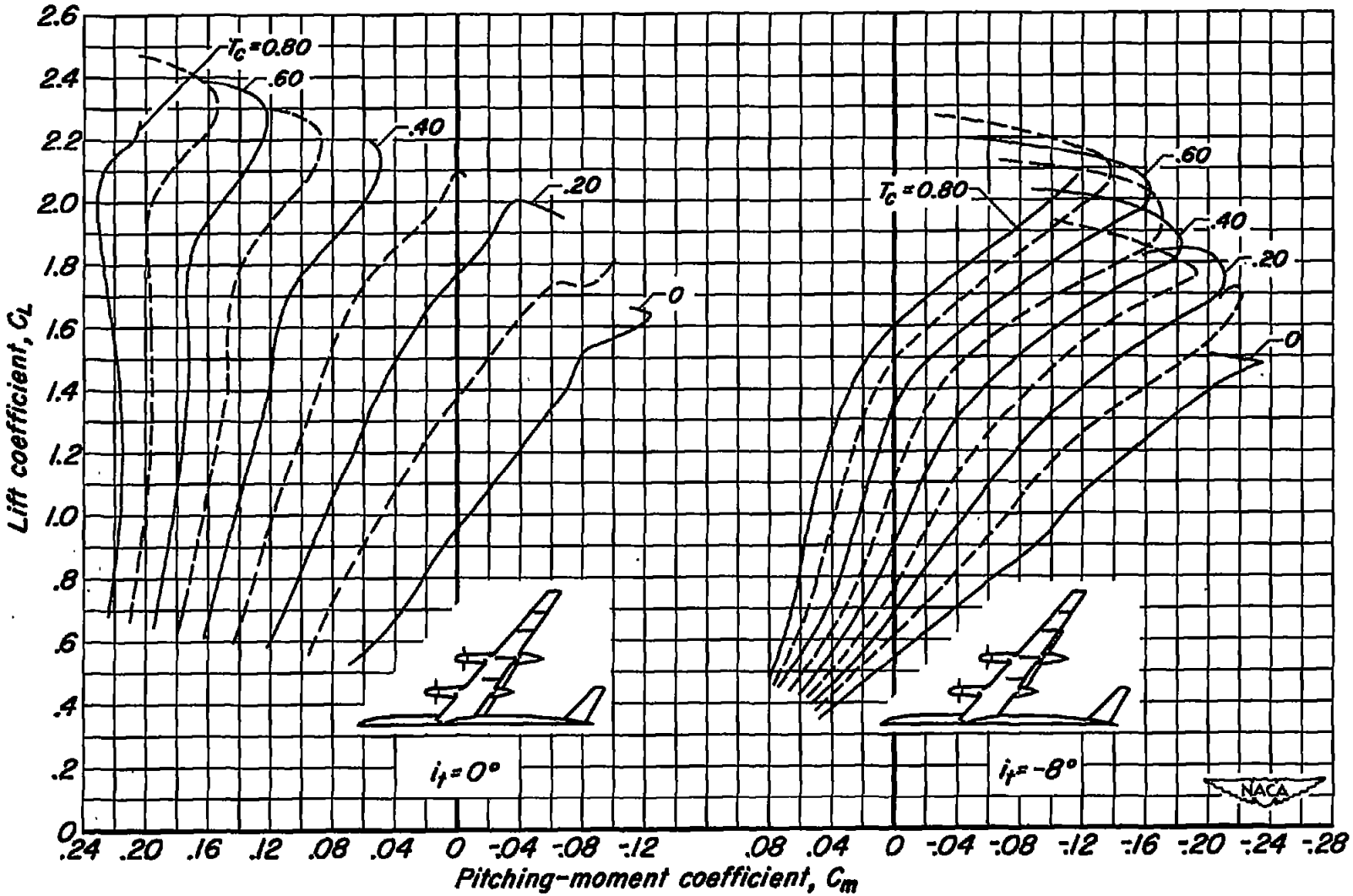

Figure 41.- A comparison of the pitching-moment characteristics of the model having inboard flaps with those of the model having outboard flaps; tail height = 0.10 b/2; M = 0.082; R = 4,000,000; $\beta = 26^{\circ}$.

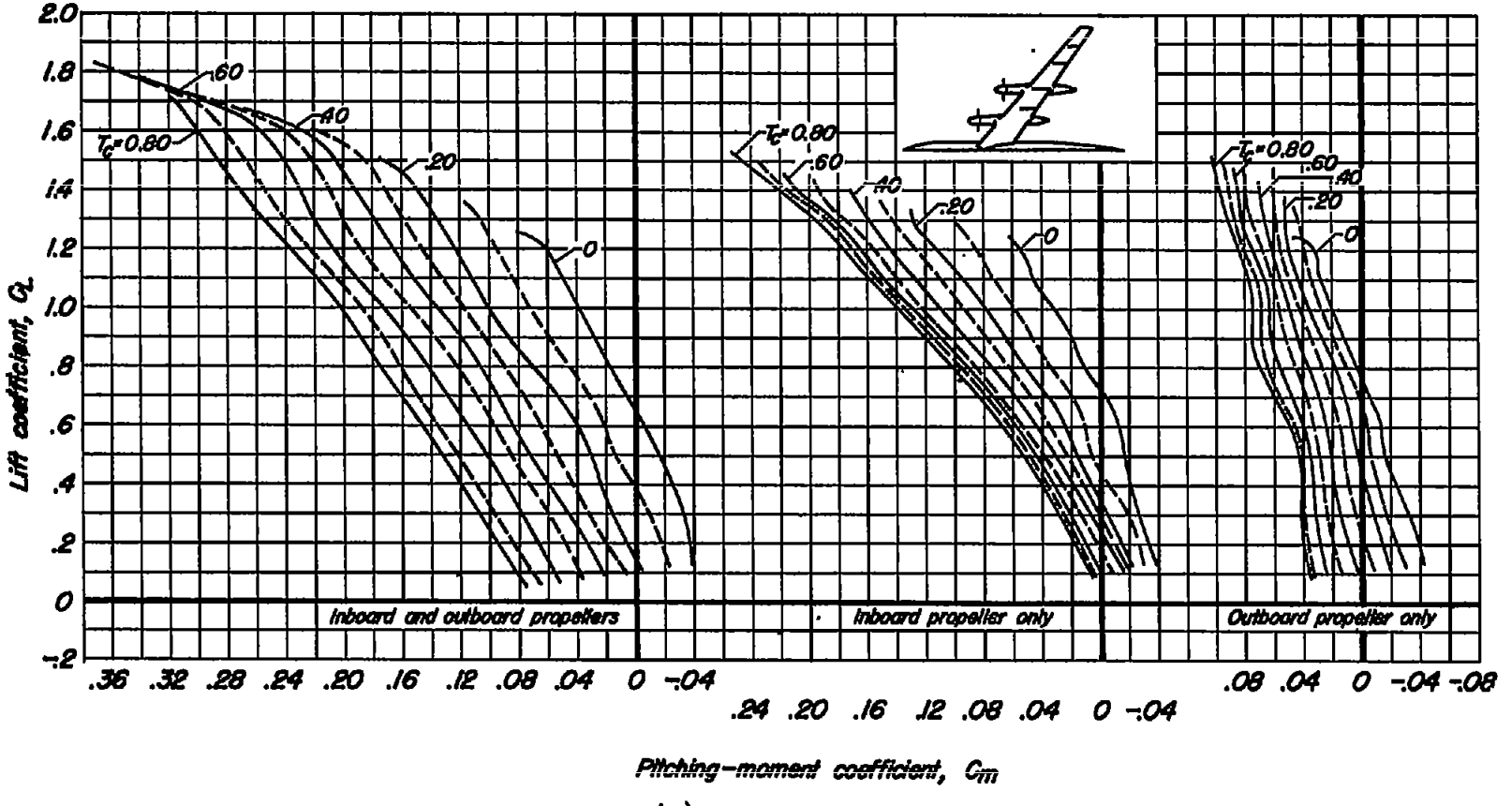

(a) Flaps up.

Figure 42.- A comparison of the pitching-moment characteristics of the model for independent and simultaneous operation of the propellers; tail removed; M = 0.082; R = 4,000,000; β = 26°.

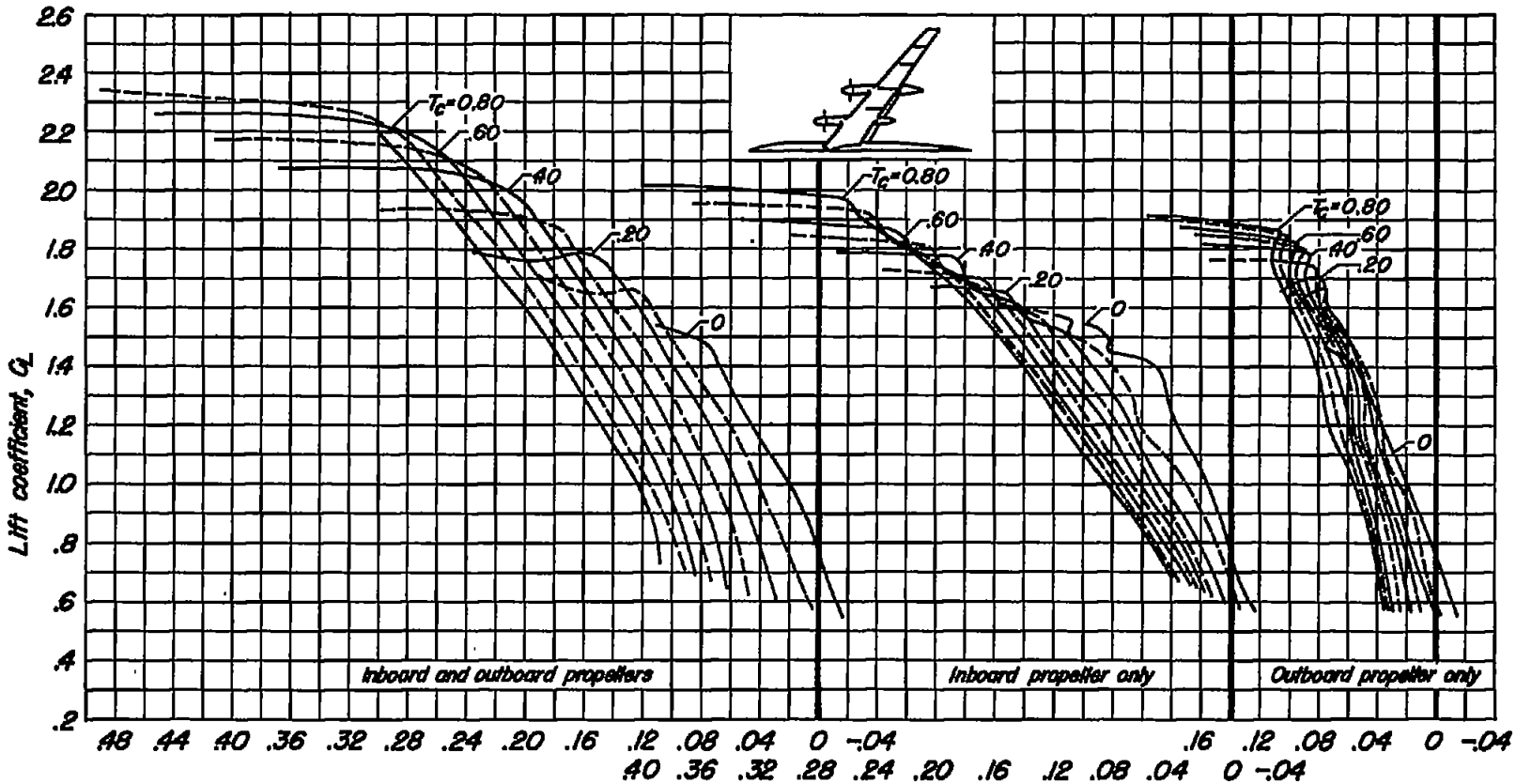

(b) Inboard flaps deflected.

Figure 42.- Concluded.

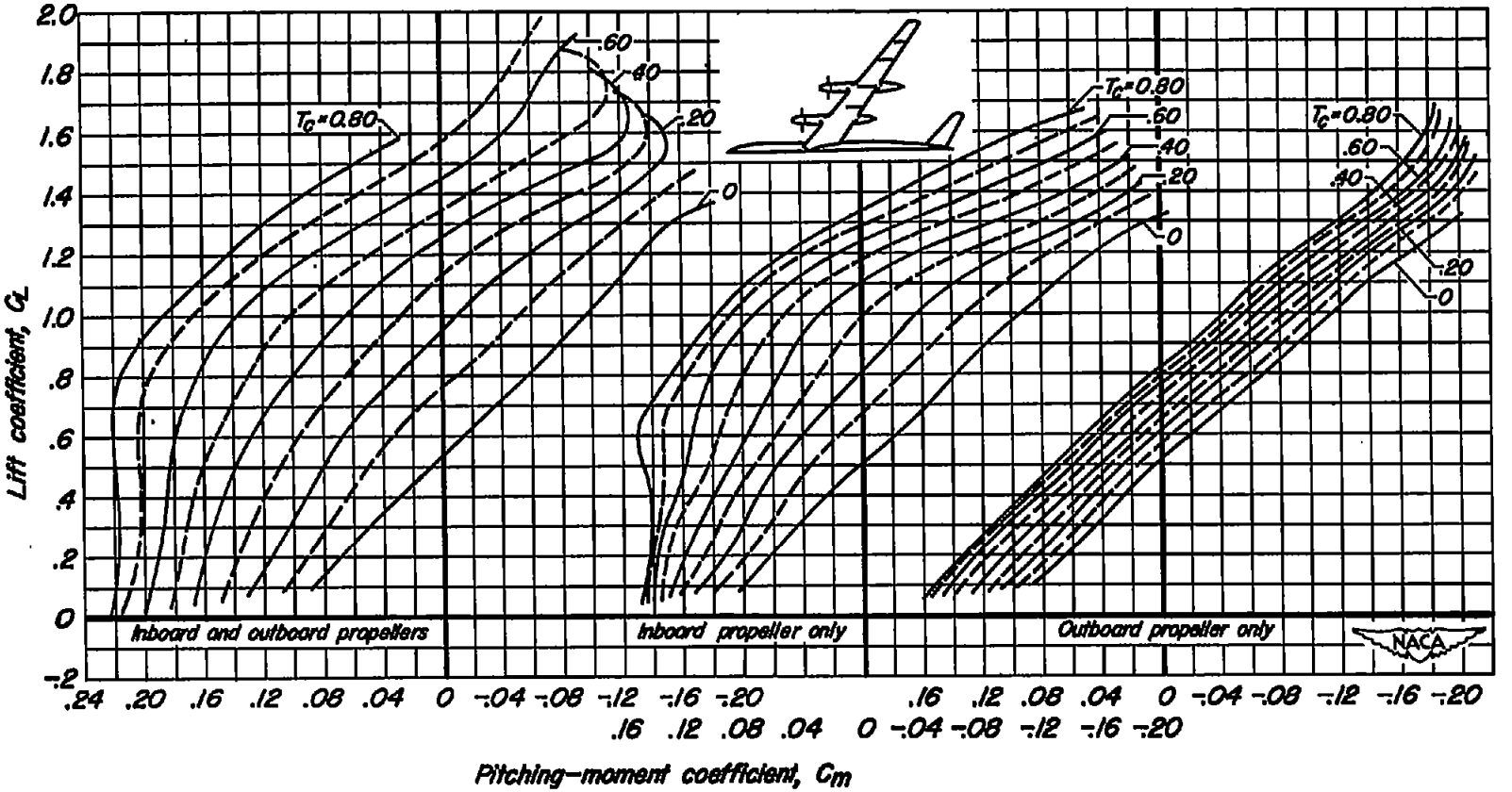

(a) Flaps up; $i_t = -4^\circ$.

Figure 43.- A comparison of the pitching-moment characteristics of the model for independent and simultaneous operation of the propellers; tail height = 0.10 b/2; M = 0.082; R = 4,000,000; B = 26°.

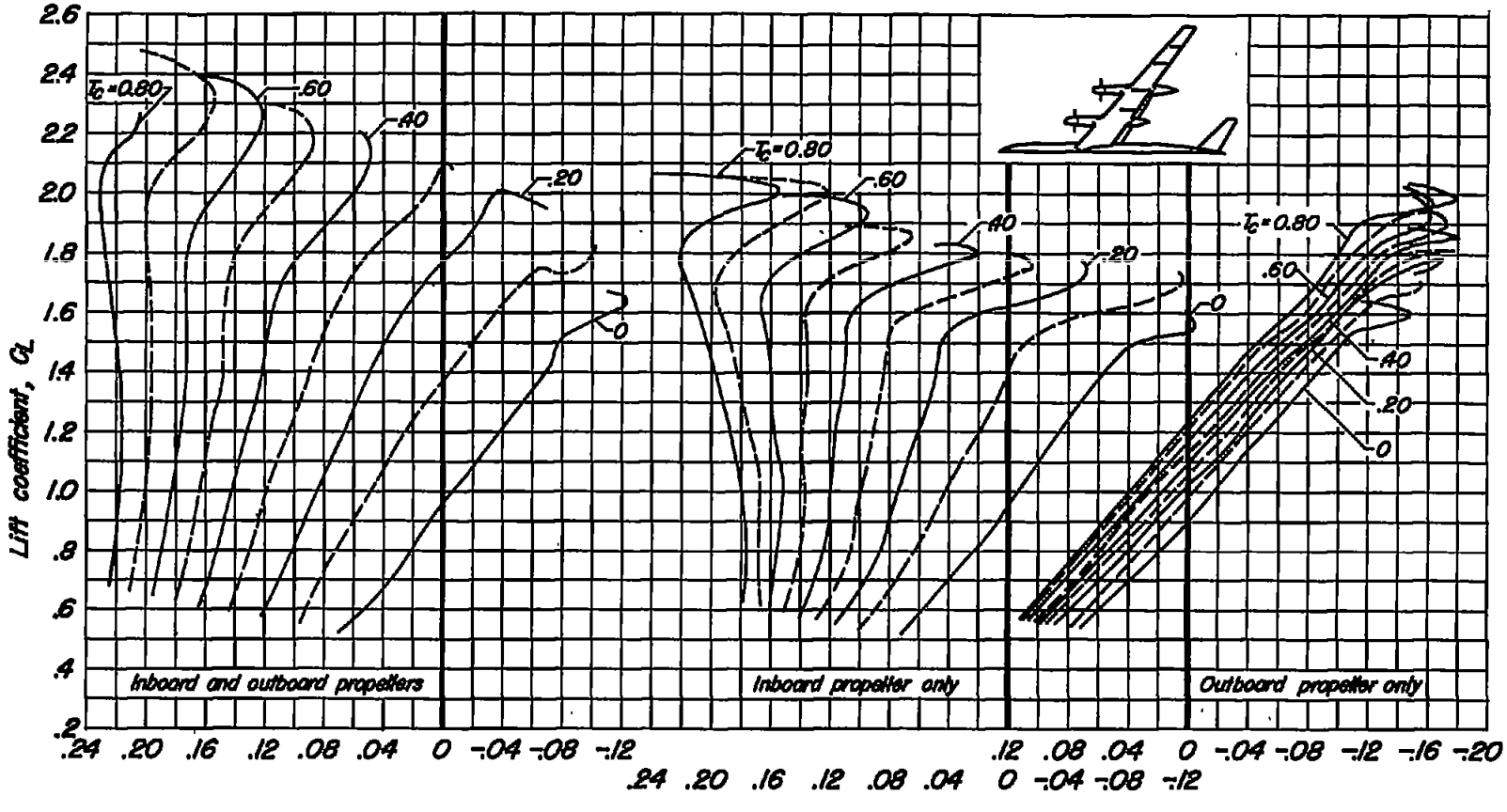

(b) Inboard flaps deflected; $i_t = 0^\circ$.

Figure 43.- Concluded.

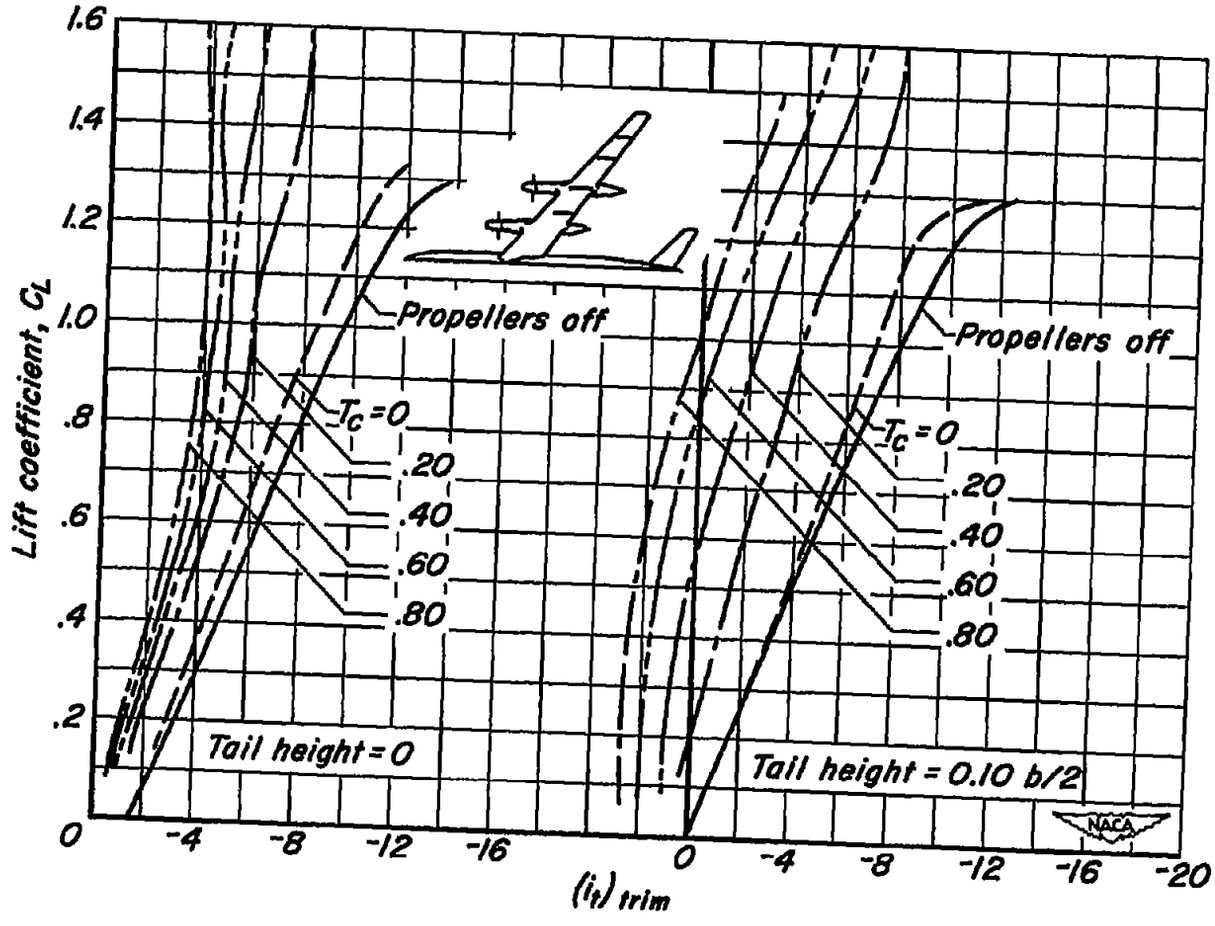

(a) $(i_t)_{trim}$ vs. C_L

Figure 44.- A comparison for two tail heights of the effects of operating propellers on the longitudinal stability of the model; flaps up; M = 0.082; R = 4,000,000; $\beta = 26^\circ$.

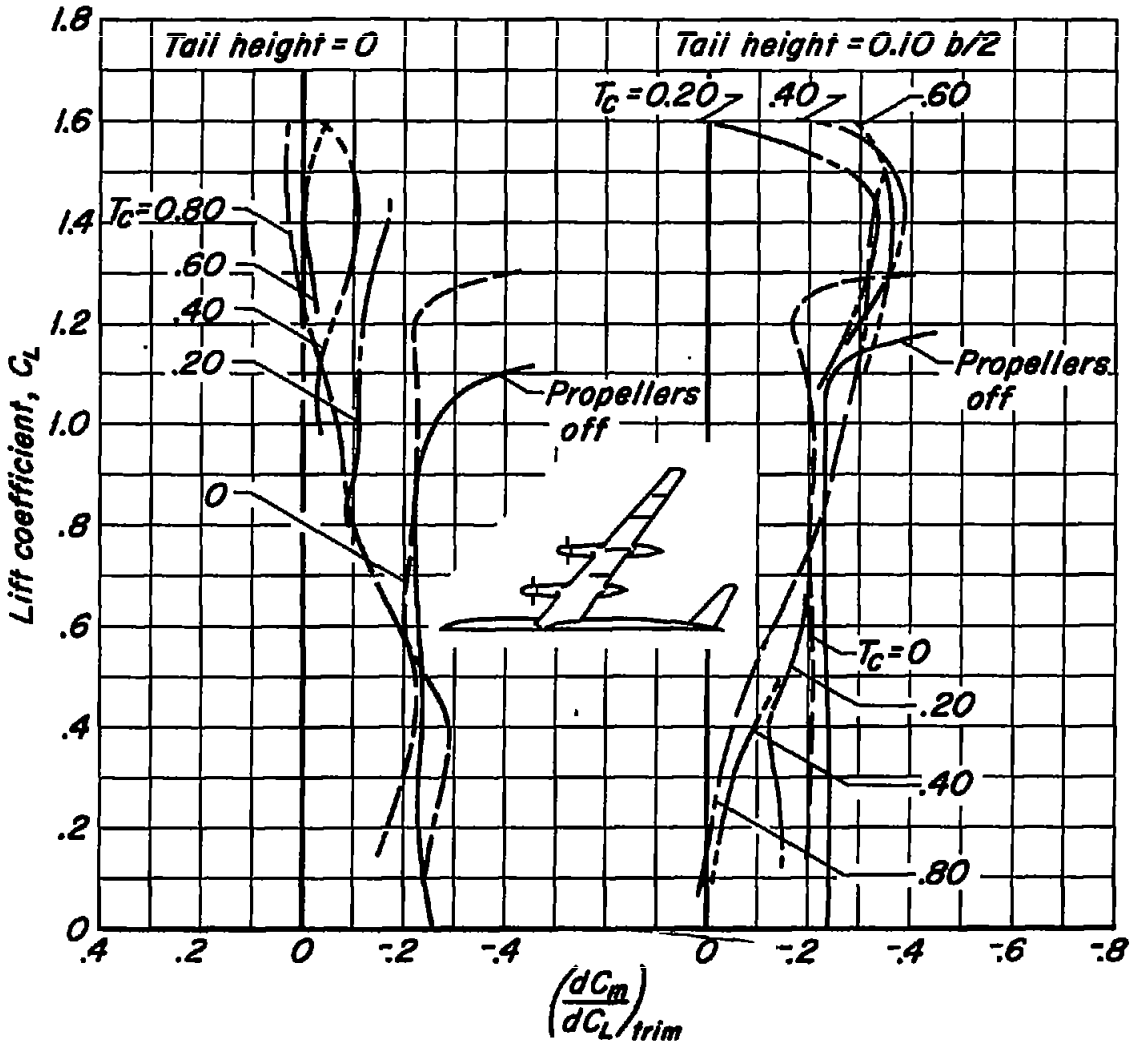

(b) $\left(\frac{dC_m}{dC_L}\right)_{trim}$ vs. C_L

Figure 44.- Continued.

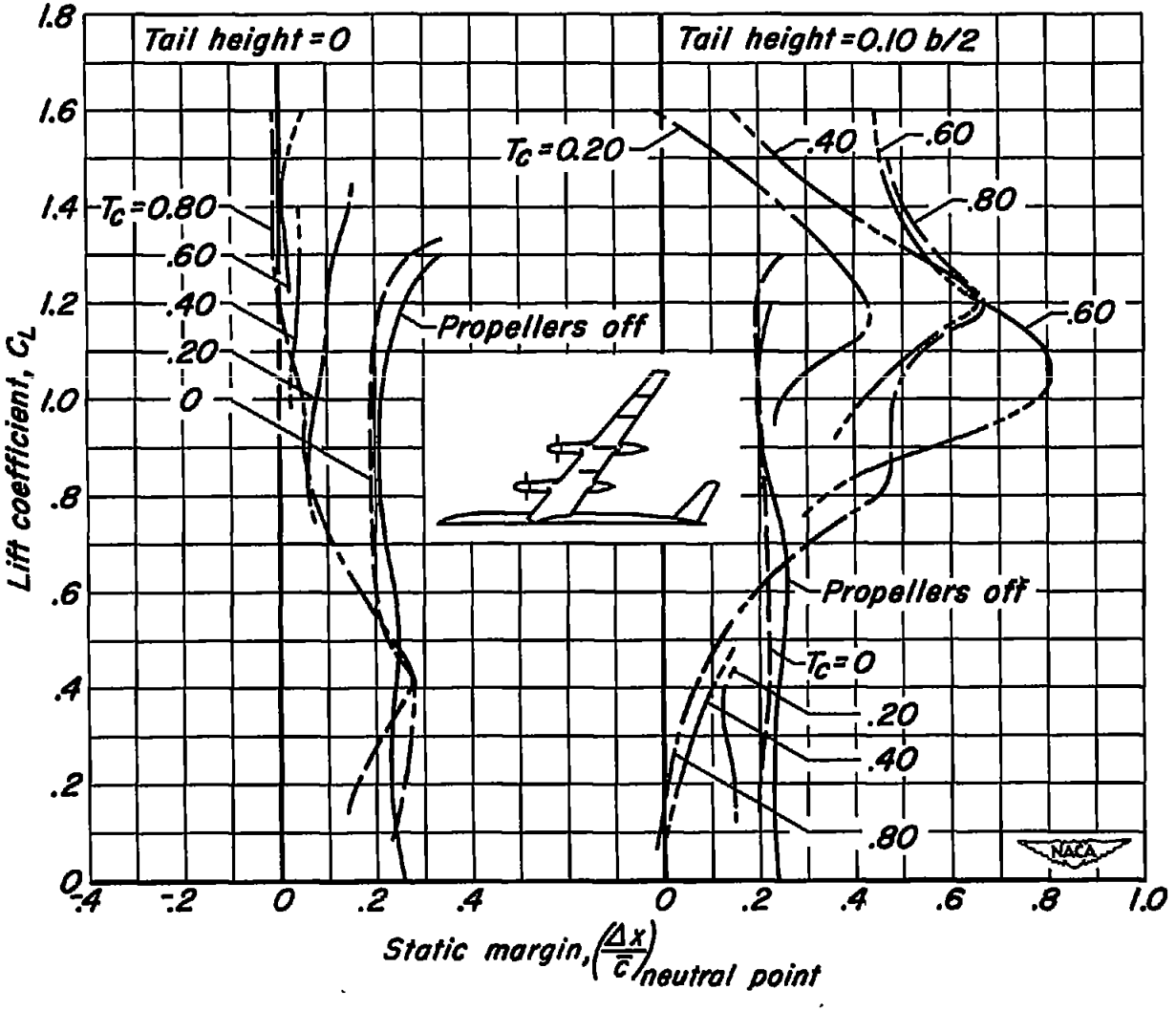

(c) Static margin vs. C_L.

Figure 44.- Concluded.

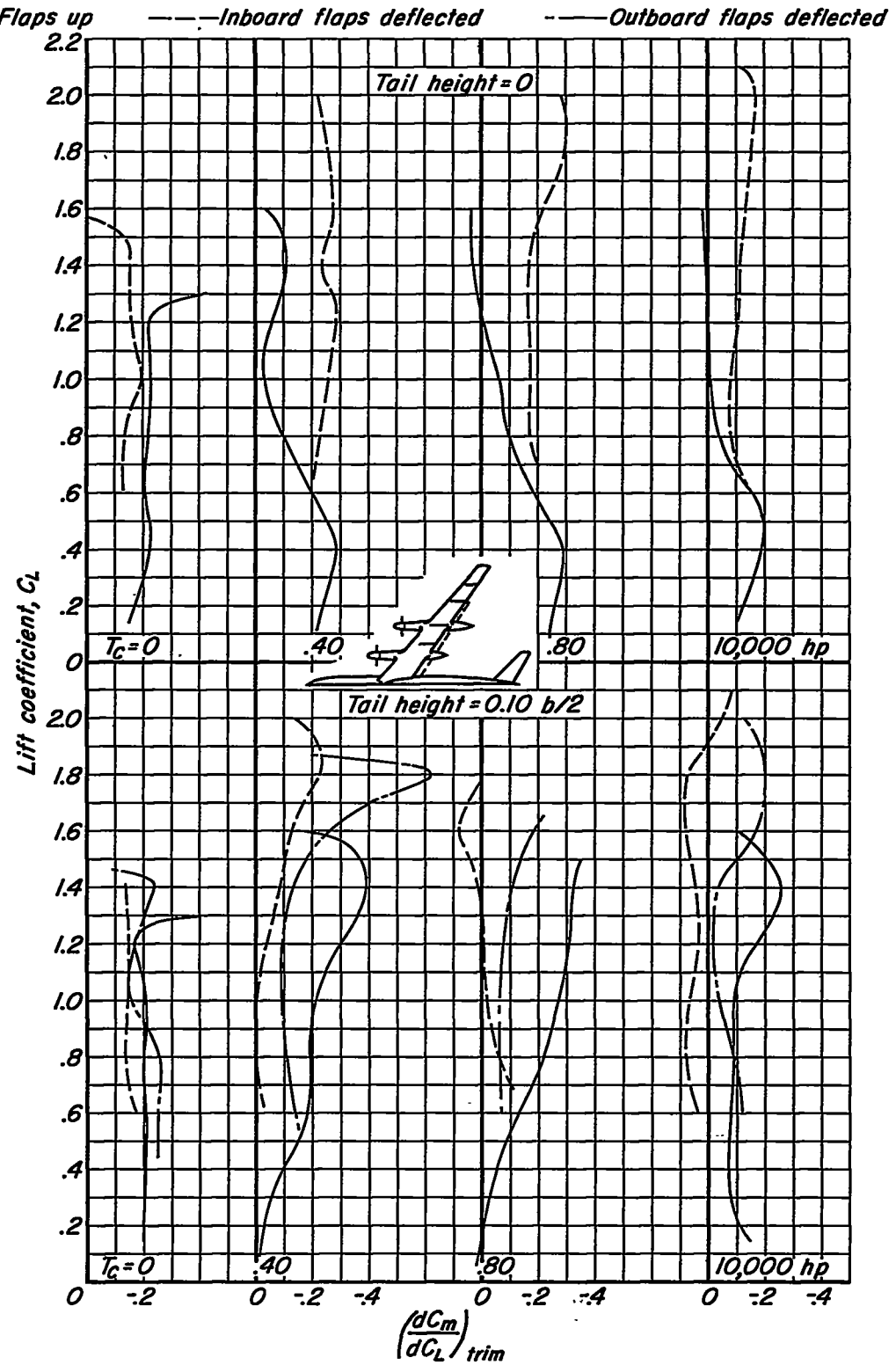

Figure 45.- The effects of flaps on the longitudinal stability of the model; M = 0.082; R = 4,000,000; $\beta = 26^{\circ}$.

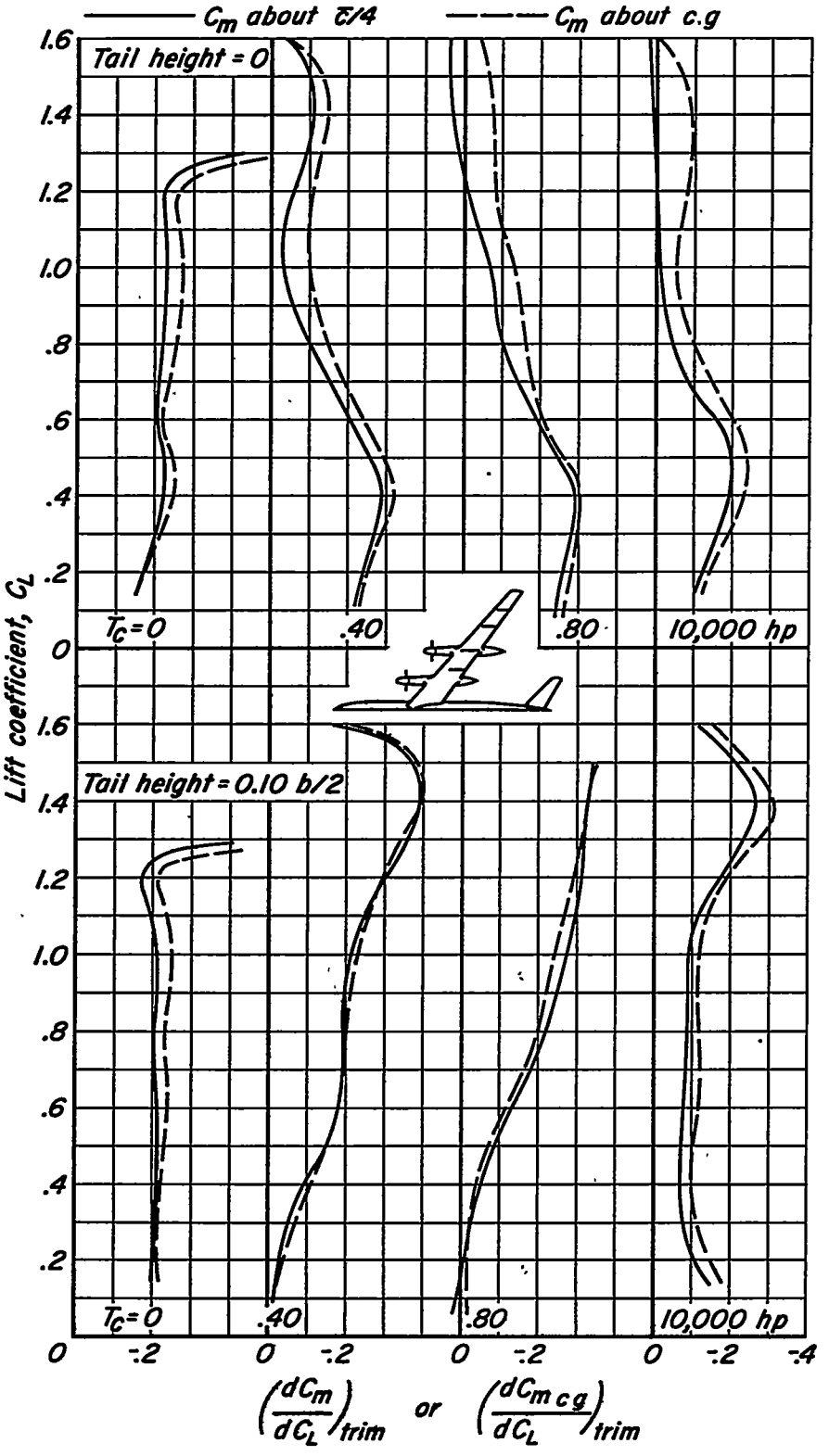

Figure 46.- The effects of vertical displacement of the center of moments on the longitudinal stability of the model; flaps up; M = 0.082; R = 4,000,000; $\beta = 26^{\circ}$.

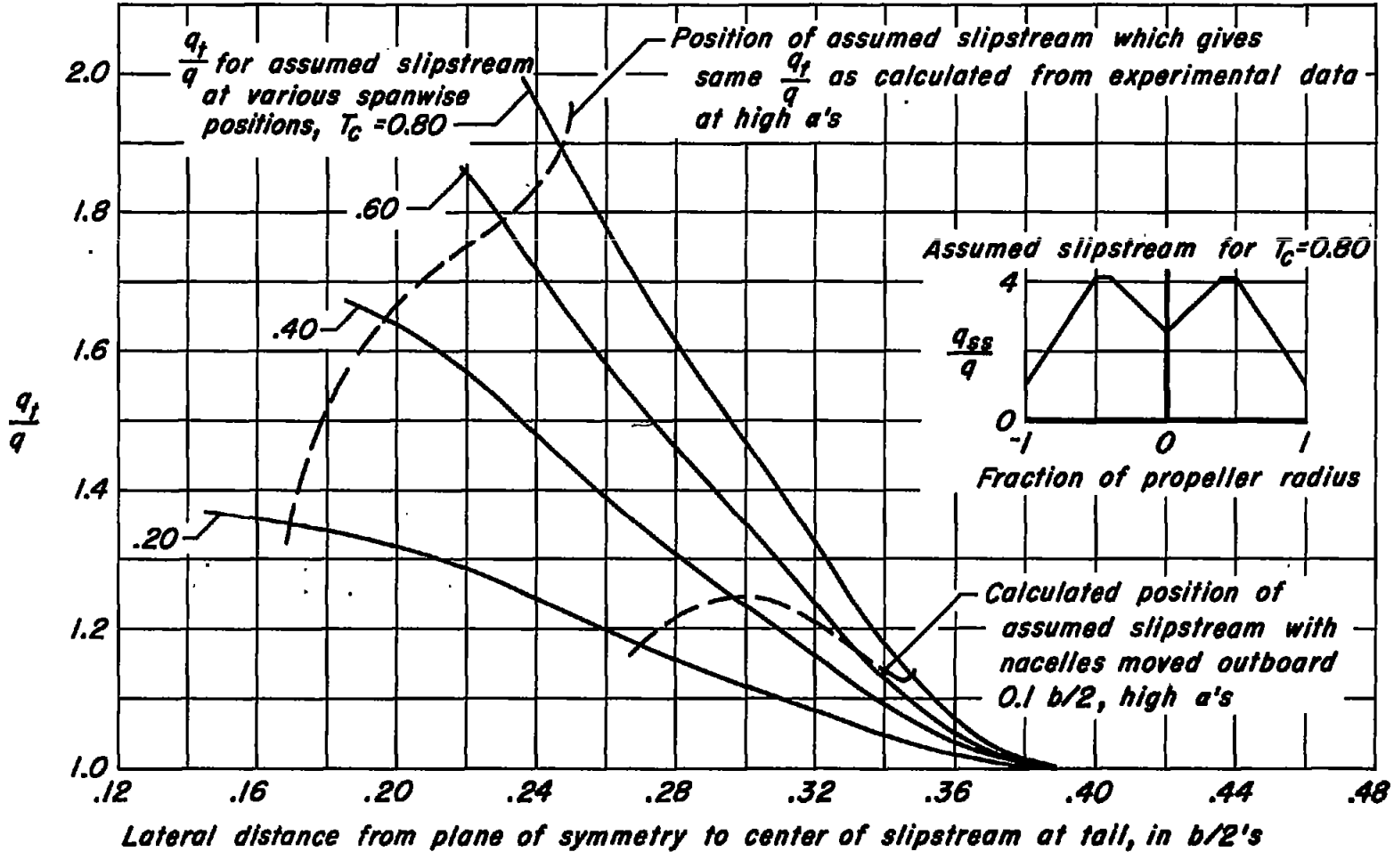

Figure 47.- The estimated maximum effective dynamic pressure at the tail with the nacelles moved outboard; flaps up or inboard flaps deflected; M = 0.082; R = 4,000,000; β = 26°.

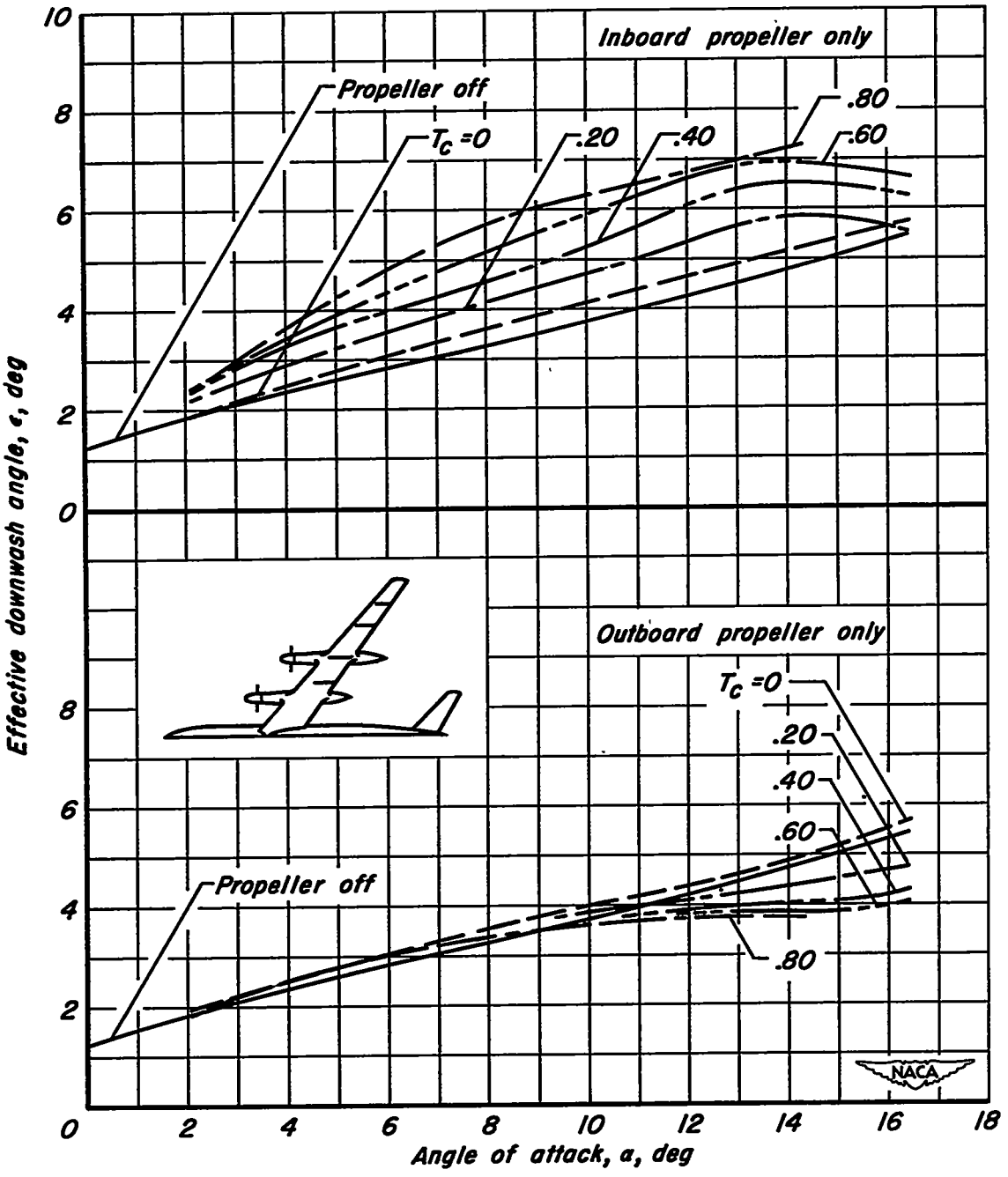

Figure 48.- The estimated effective downwash at the tail due to operation of each propeller; tail height = 0.10 b/2; flaps up; M = 0.082; R = 4,000,000; $\beta = 26^{\circ}$.

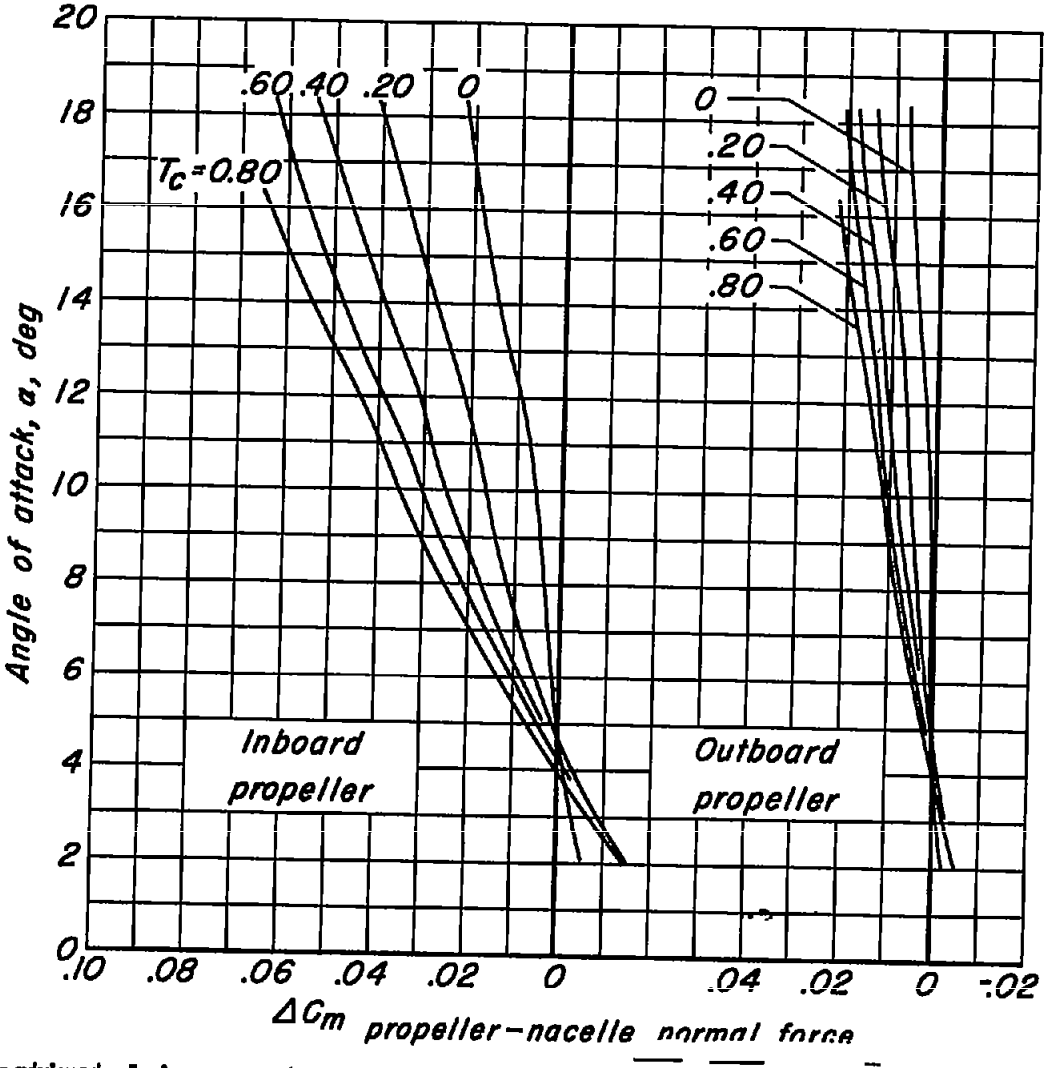

Figure 49.- The estimated increments of pitching-moment coefficient of the model due to the normal force of each propeller with the nacelles moved 0.1 b/2 outboard of their original positions; flaps up or deflected; M = 0.082; R = 4,000,000; $\beta = 26^{\circ}$.

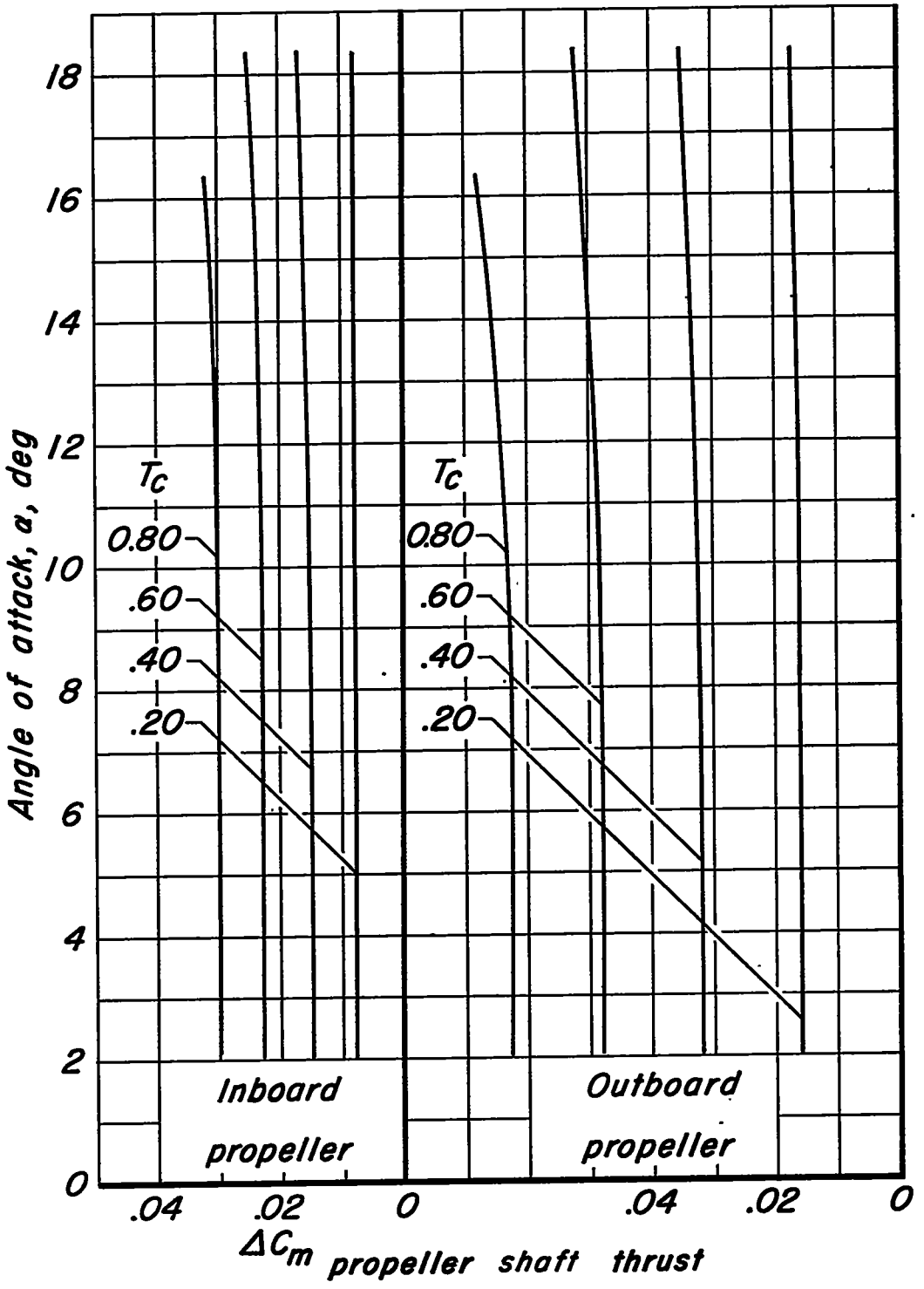

Figure 50.- The estimated increments of pitching-moment coefficient of the model due to the shaft thrust of each propeller with the nacelles moved 0.1 b/2 outboard of their original positions; M = 0.082; R = 4,000,000; $\beta = 26^\circ$.

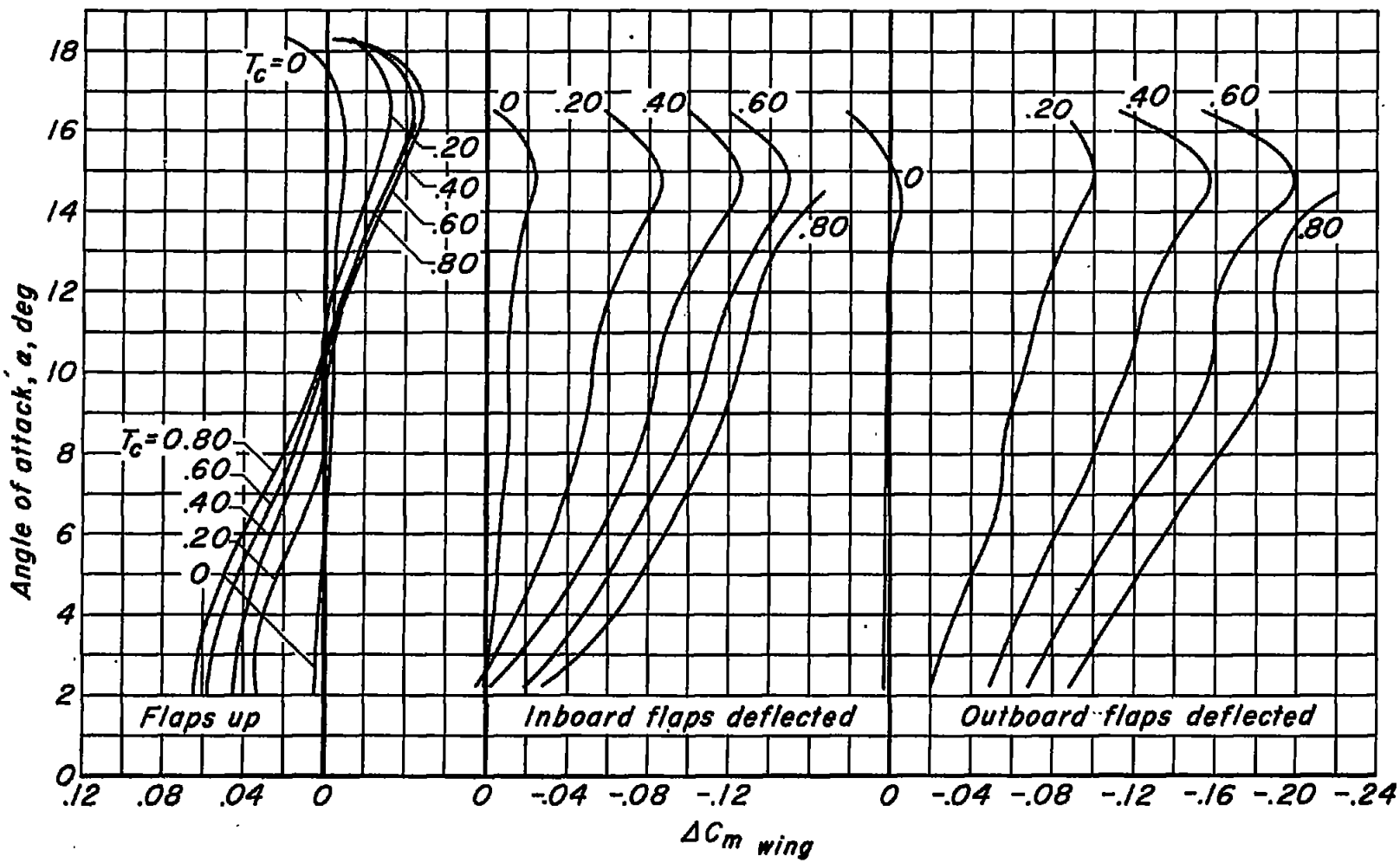

Figure 51.- The estimated increments of pitching-moment coefficient of the model due to the slipstreams on the wing with the nacelles moved 0.1 b/2 outboard of their original positions; M = 0.082; R = 4,000,000; $\beta = 26^{\circ}$.

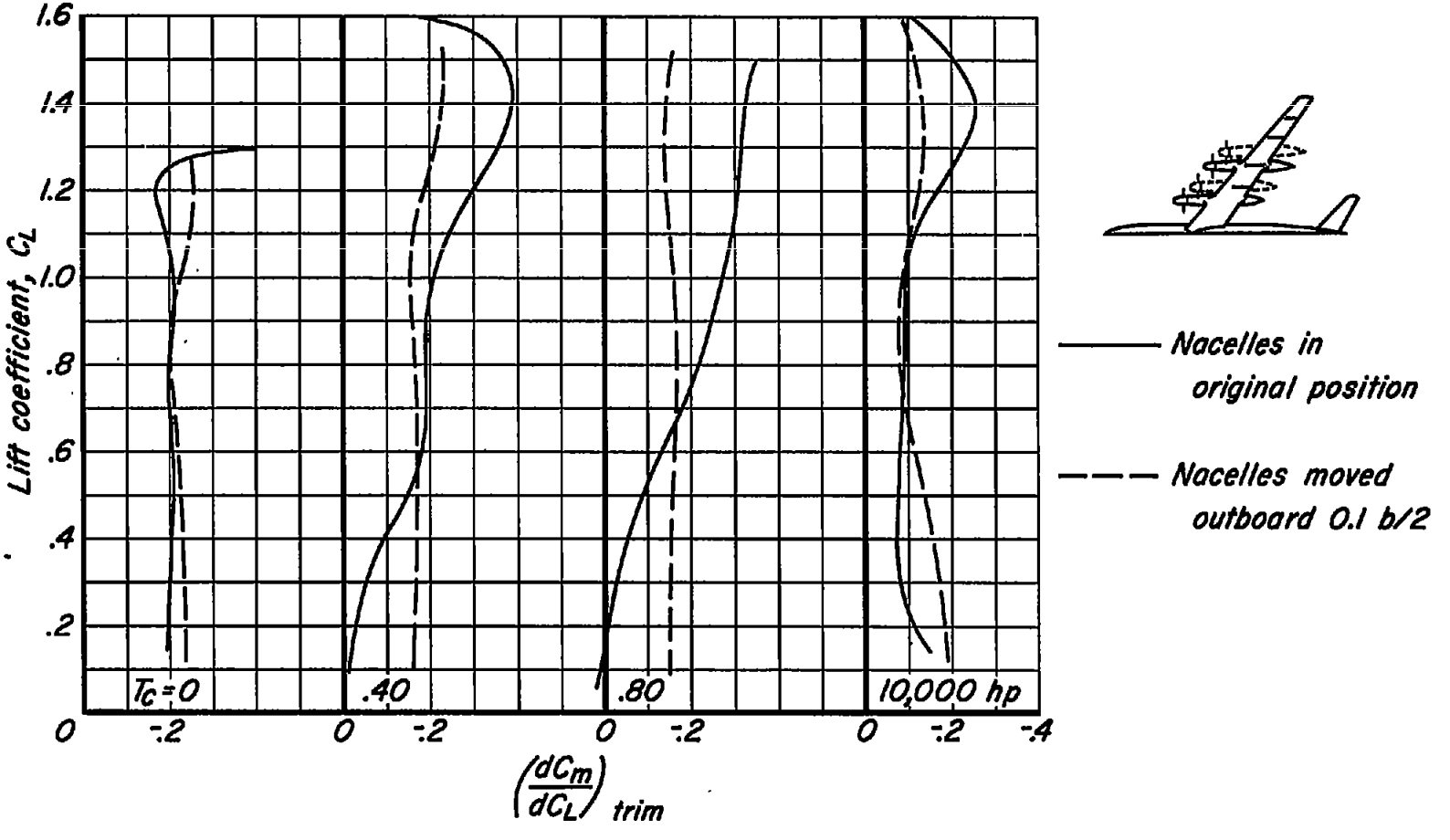

(a) Flaps up.

Figure 52.- The estimated effects on the longitudinal stability of the model of moving the nacelles 0.1 b/2 outboard of their original positions; tail height = 0.10 b/2; M = 0.082; R = 4,000,000; $\beta = 26^{\circ}$.

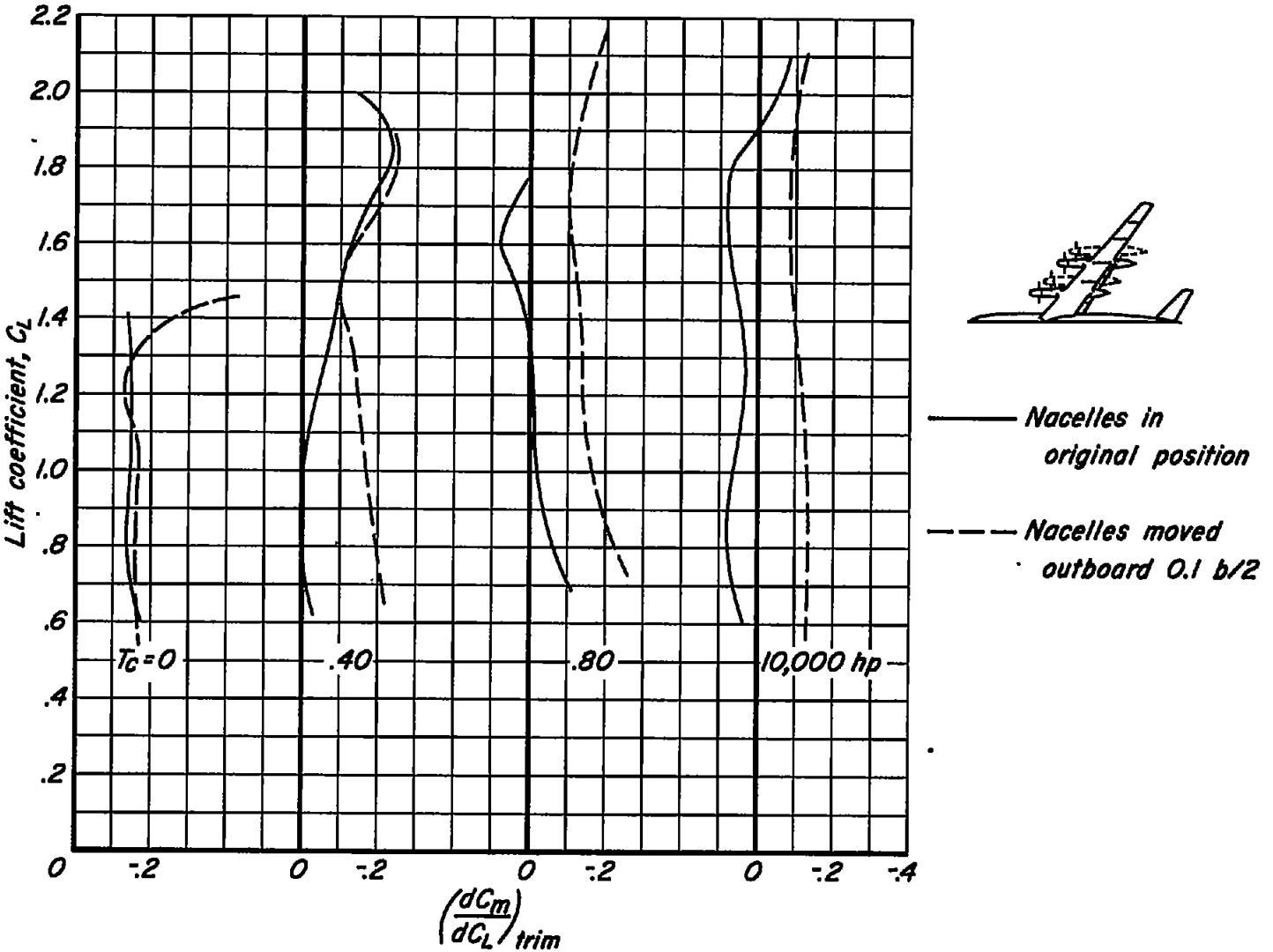

(b) Inboard flaps deflected.

Figure 52.- Continued.

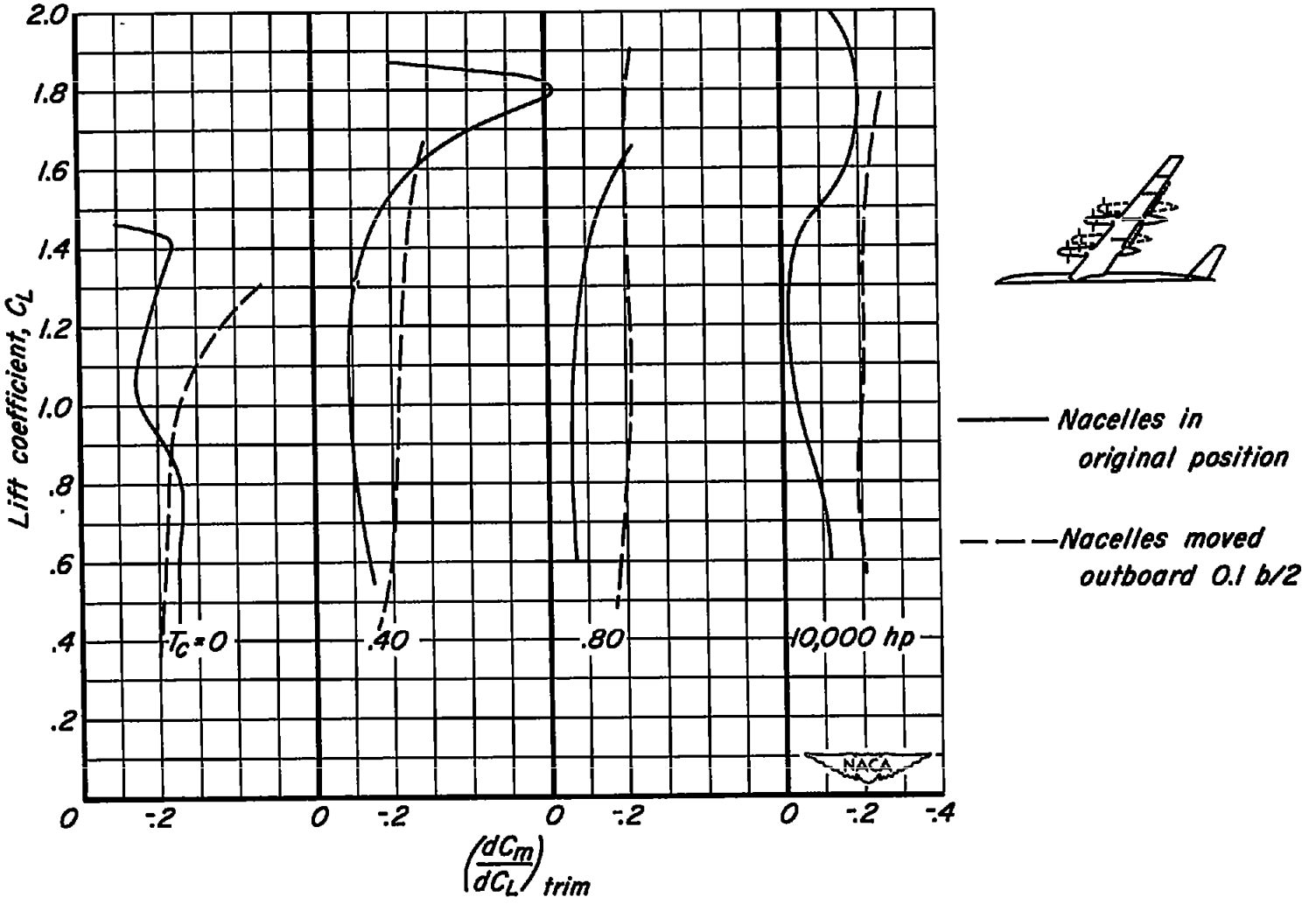

(c) Outboard flaps deflected.

Figure 52.- Concluded.

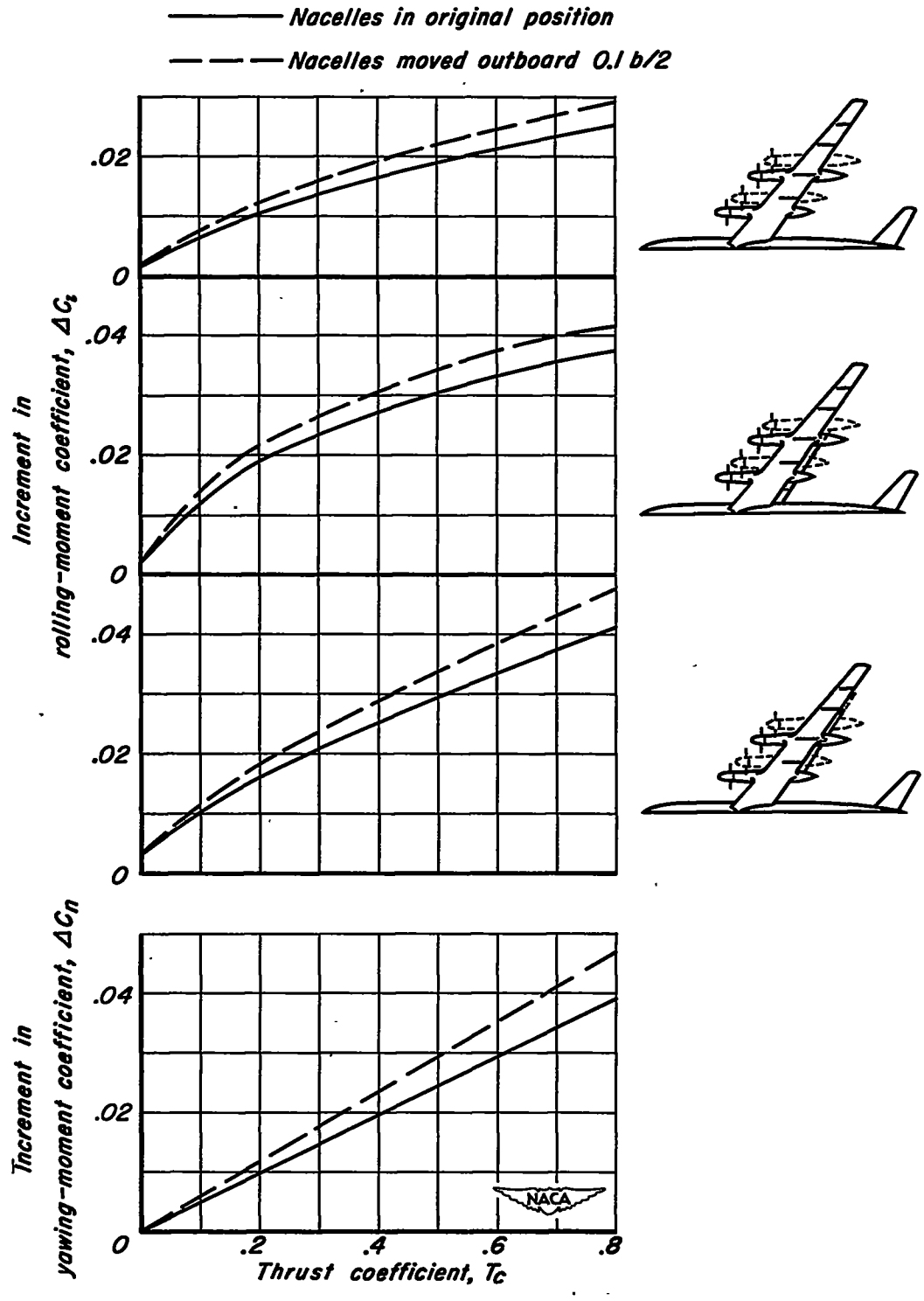

Figure 53.- The estimated increments of rolling-moment coefficient and yawing-moment coefficient resulting from loss of thrust on the right outboard propeller; M = 0.082; R = 4,000,000; $\beta = 26^\circ$; $\alpha = 14^\circ$.

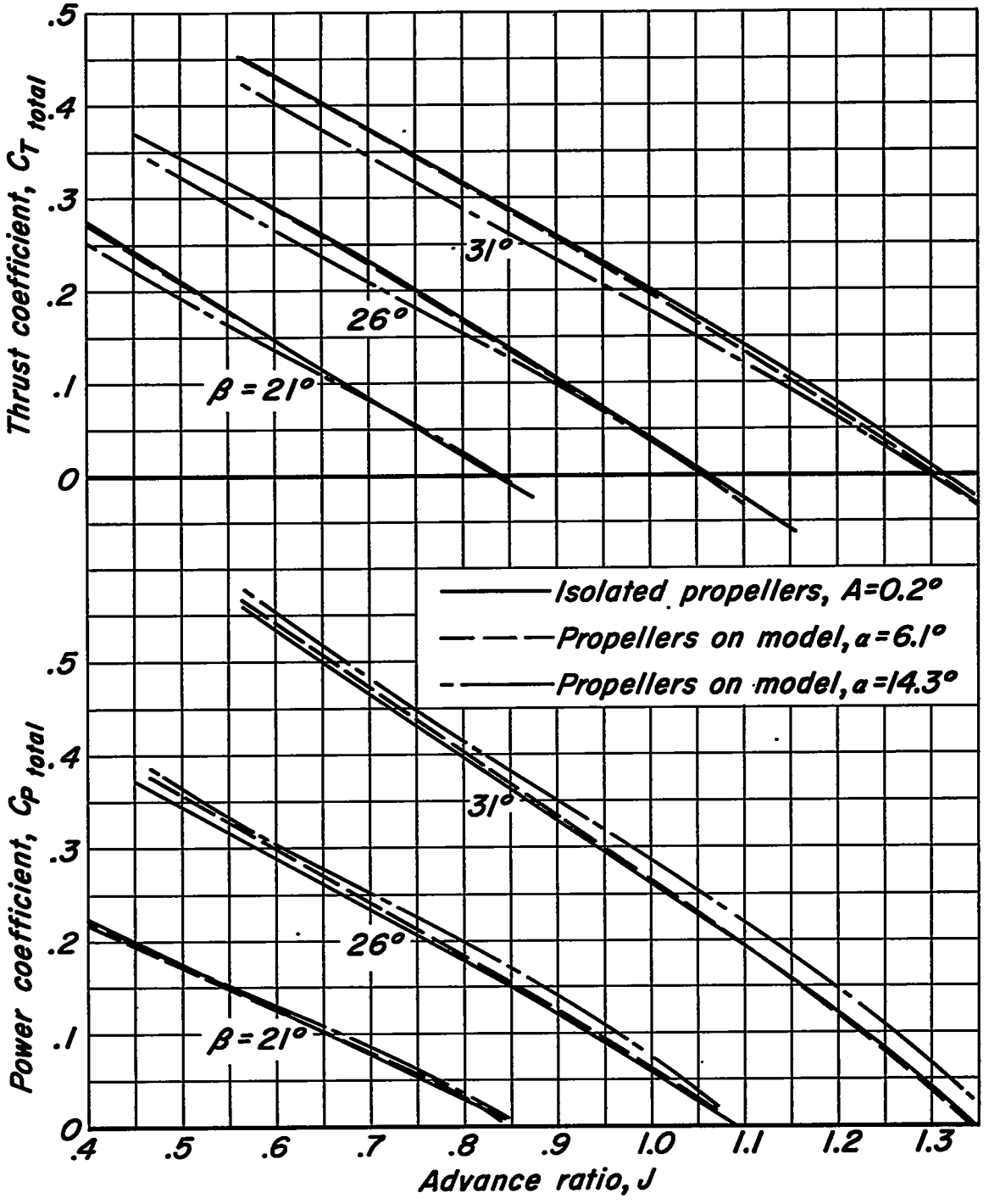

(a) Thrust and power characteristics.

Figure 54.- A comparison of propulsive characteristics of the model with isolated-propeller characteristics; NACA 1.167-(0)(05)-058 propeller; tail removed; flaps up; M = 0.082; R = 4,000,000.

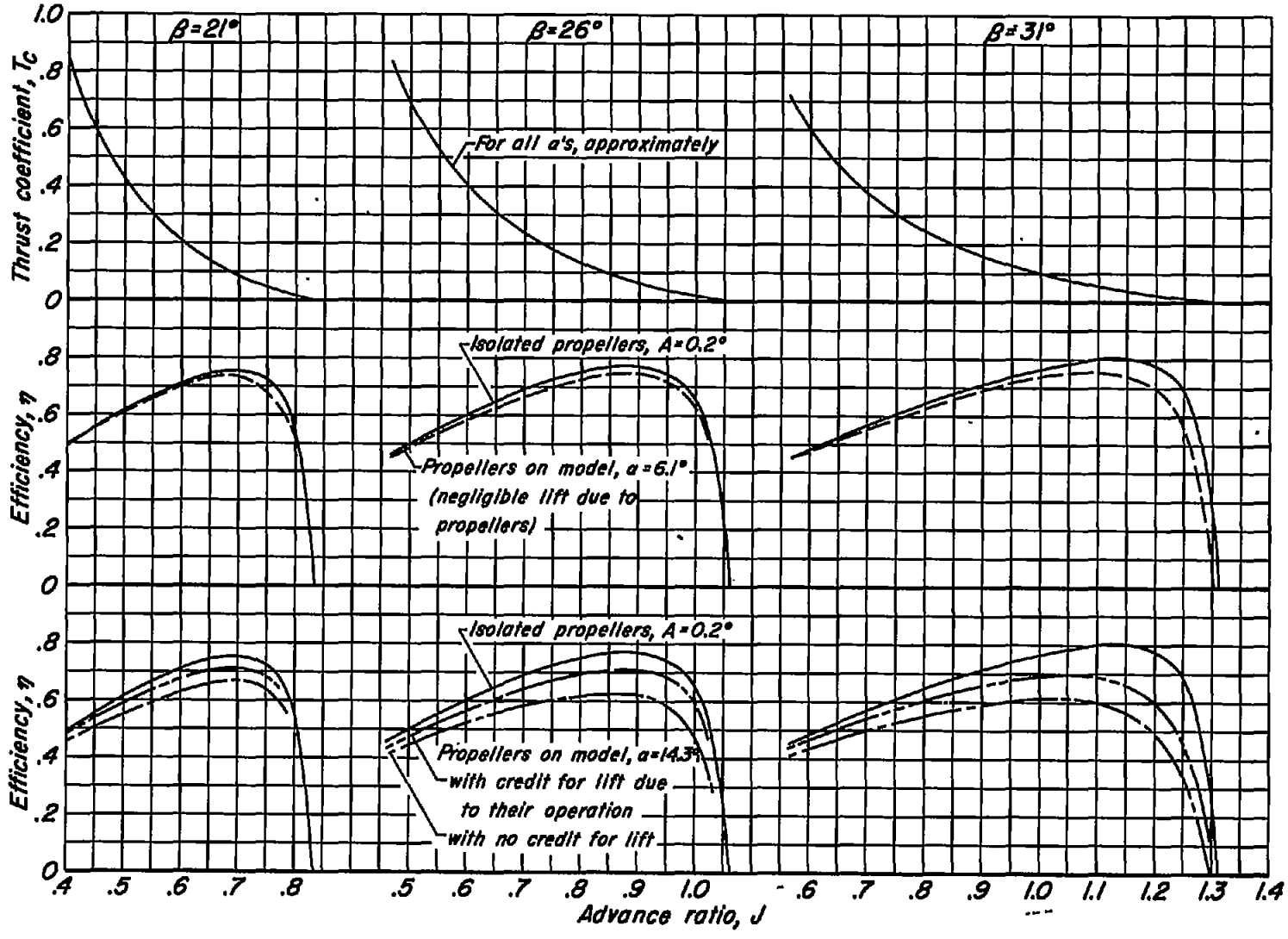

(b) η and T_c vs. J

Figure 54.- Continued.

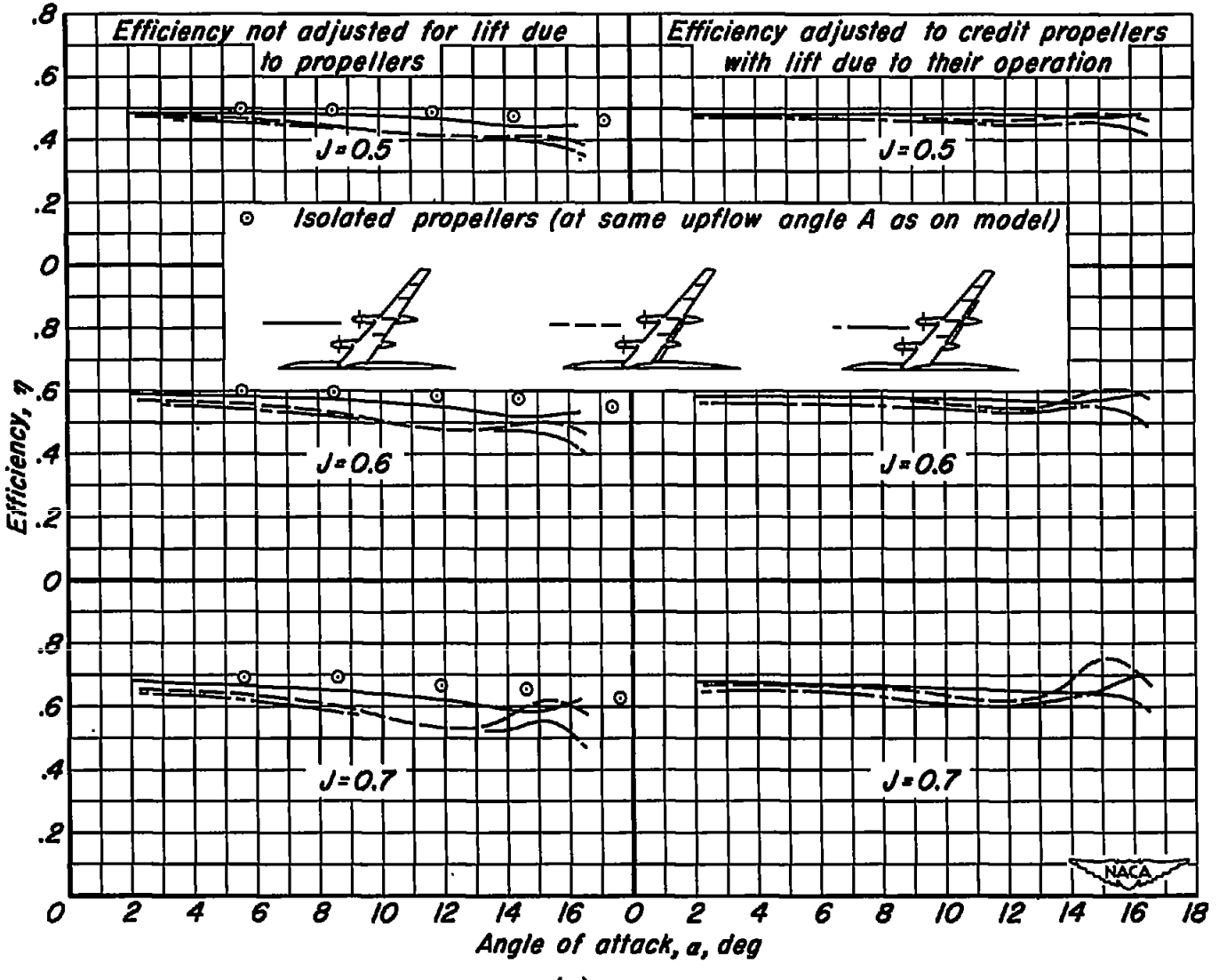

(c) η vs. α

Figure 54.- Concluded.

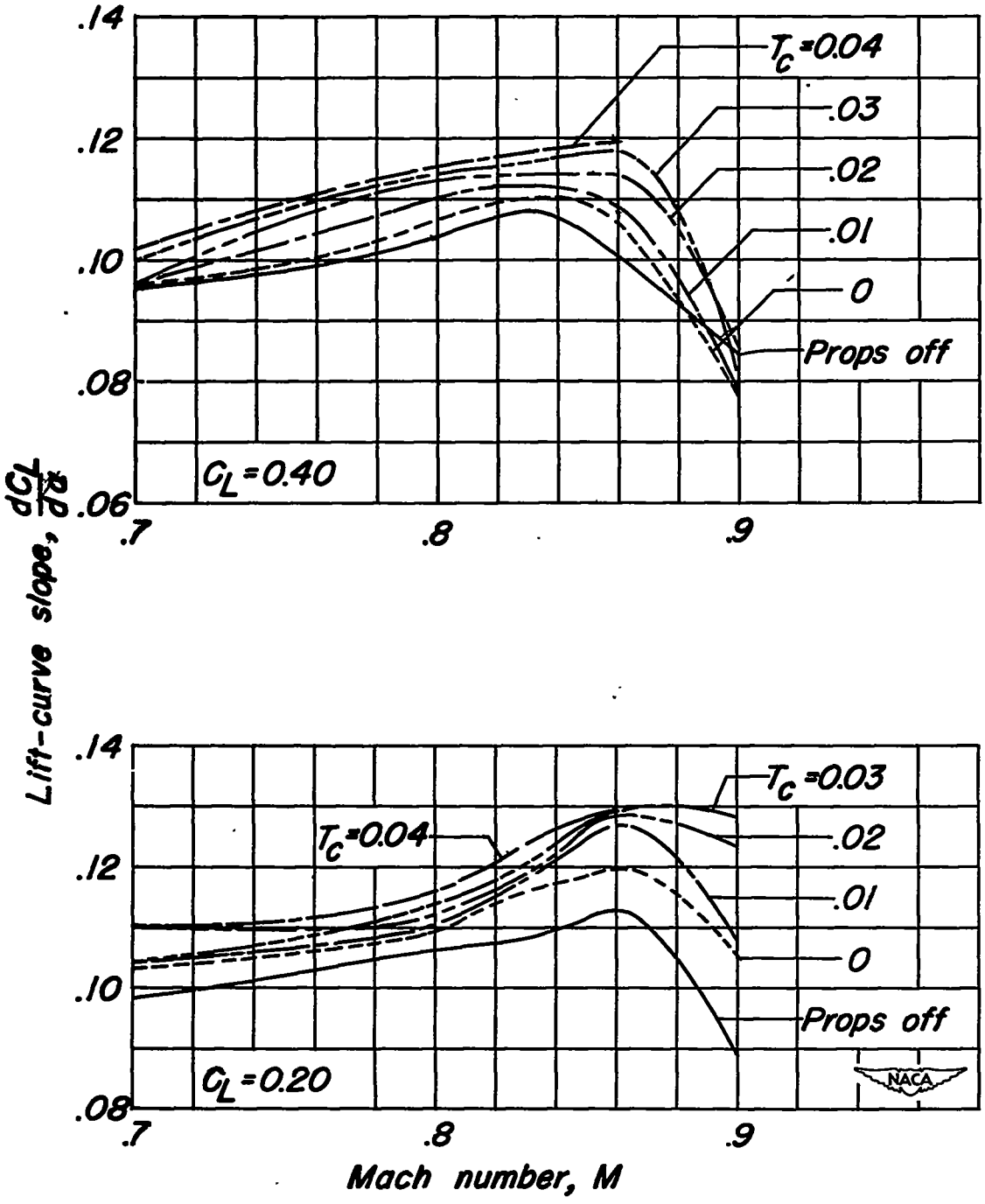

(a) Tail height = 0 b/2, $i_t = -4^\circ$.

Figure 55.- The effect of Mach number on the lift-curve slopes of the model at constant lift coefficient with and without operating propellers. $\beta = 51^\circ$, R = 1,000,000.

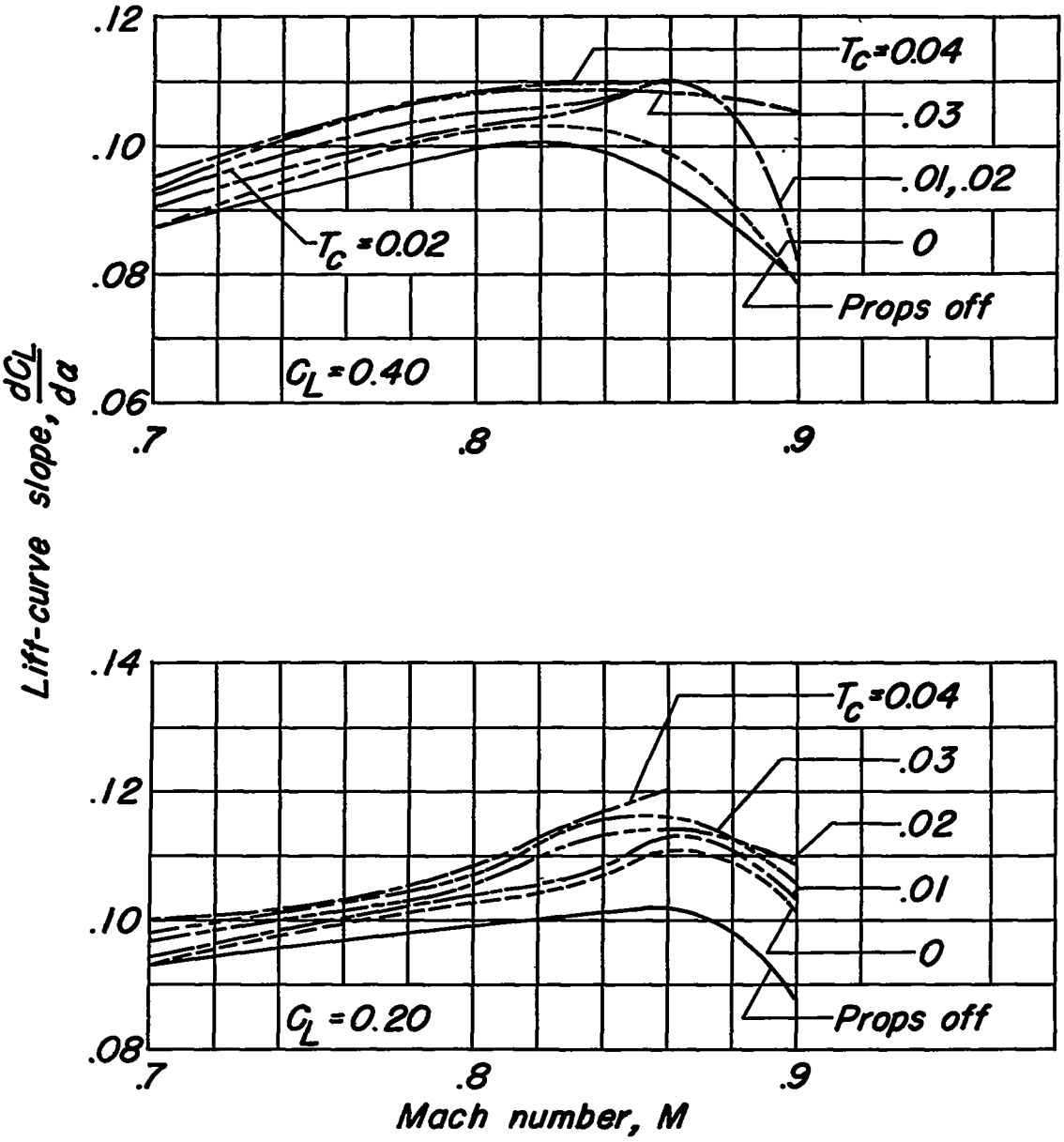

(b) Tail off.

Figure 55.- Concluded.

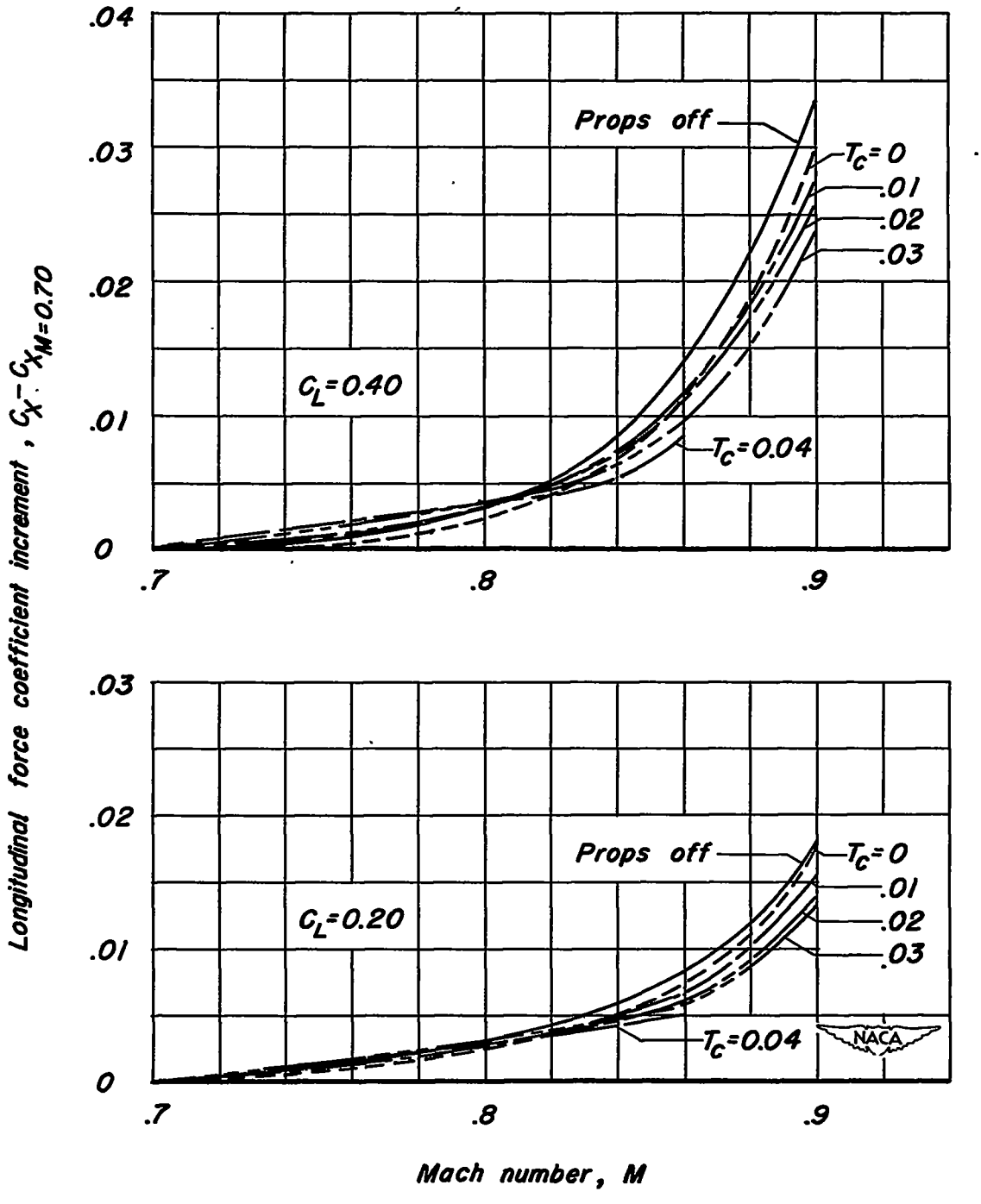

Figure 56.- The effect of Mach number on the longitudinal force coefficient increment of the model at constant lift coefficient with and without operating propellers. Tail height = 0 b/2, $i_t = -4^\circ$, $\beta = 51^\circ$, R = 1,000,000.

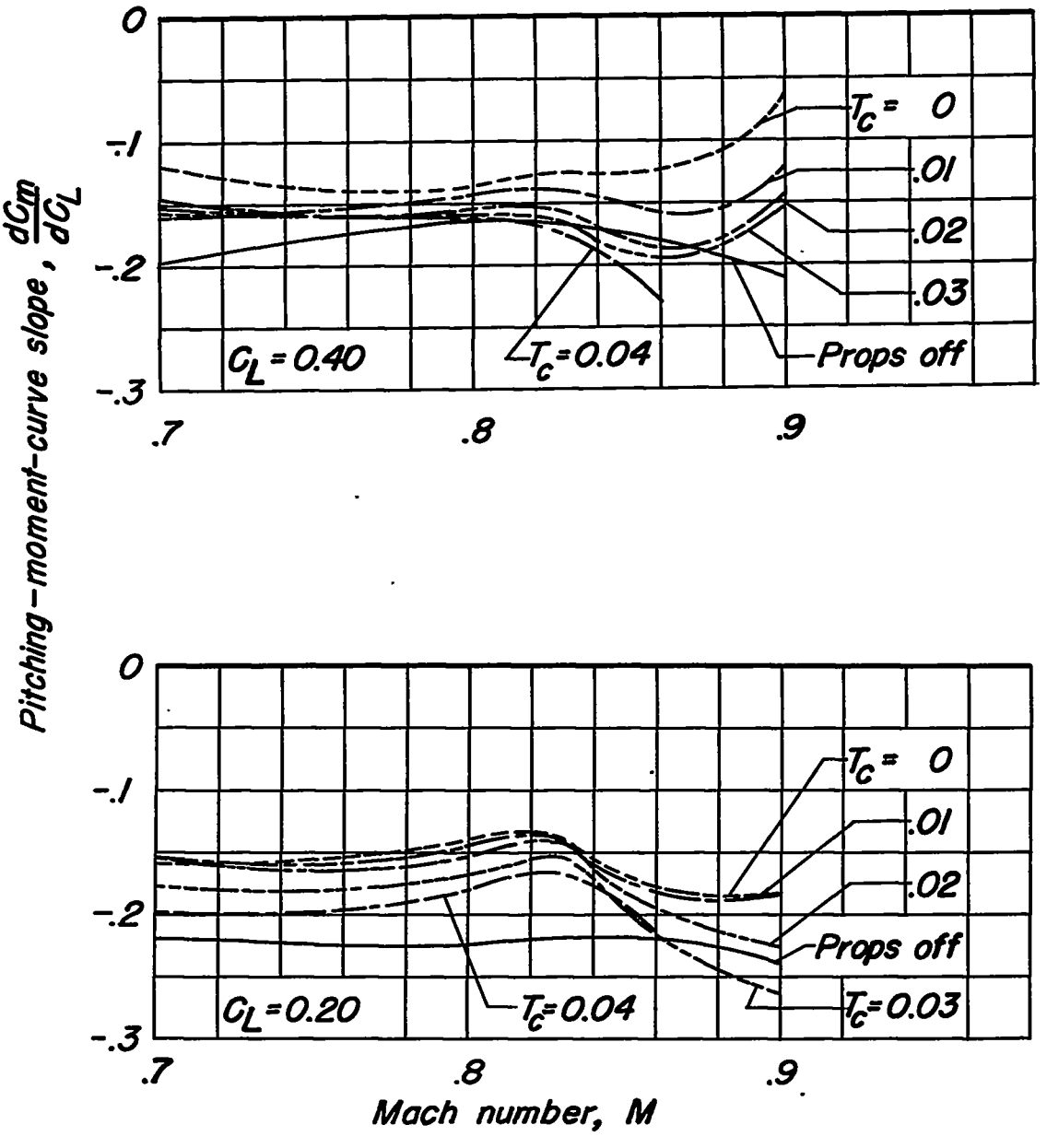

(a) Tail height = 0 b/2, $i_t = -4^\circ$.

Figure 57.- The effect of Mach number on the pitching-moment-curve slopes of the model at constant lift coefficient with and without operating propellers. $\beta = 51^\circ$, R = 1,000,000.

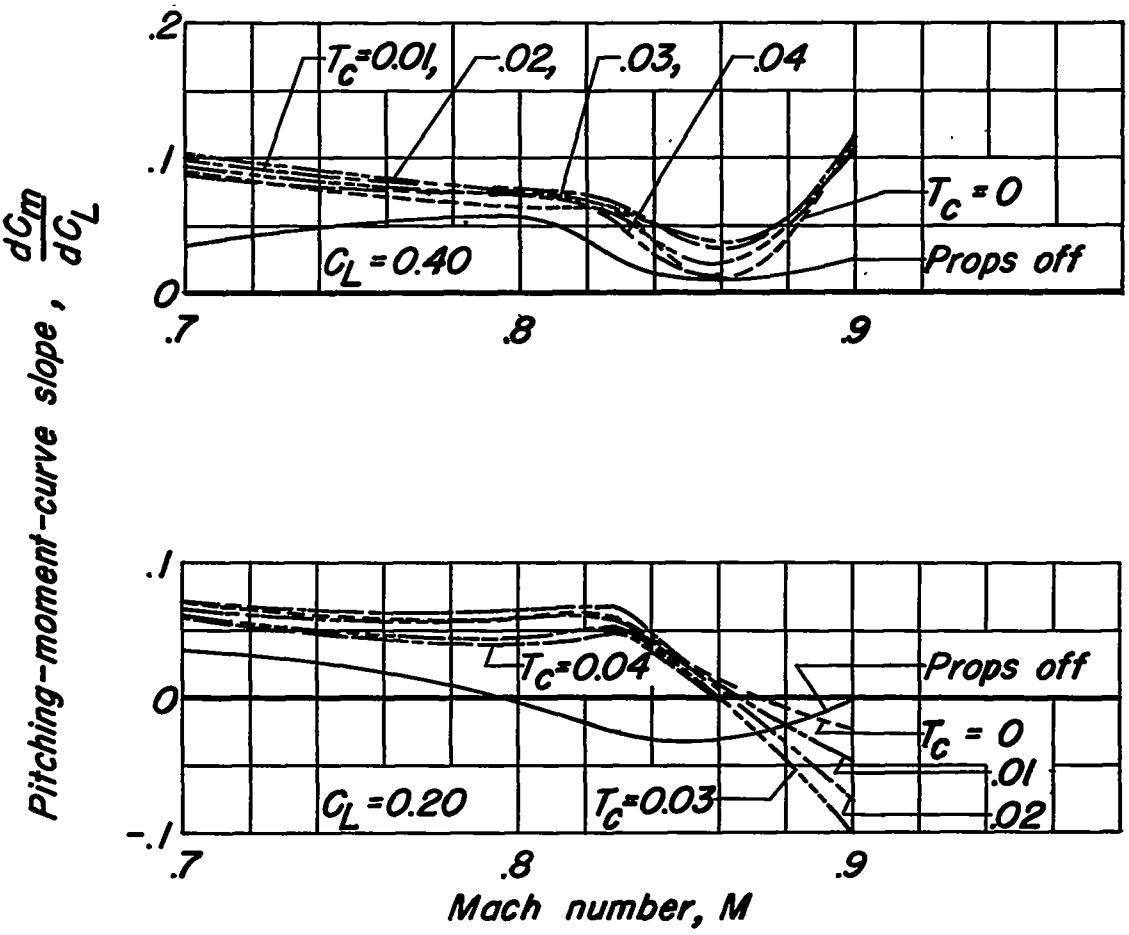

(b) Tail off.

Figure 57.- Concluded.

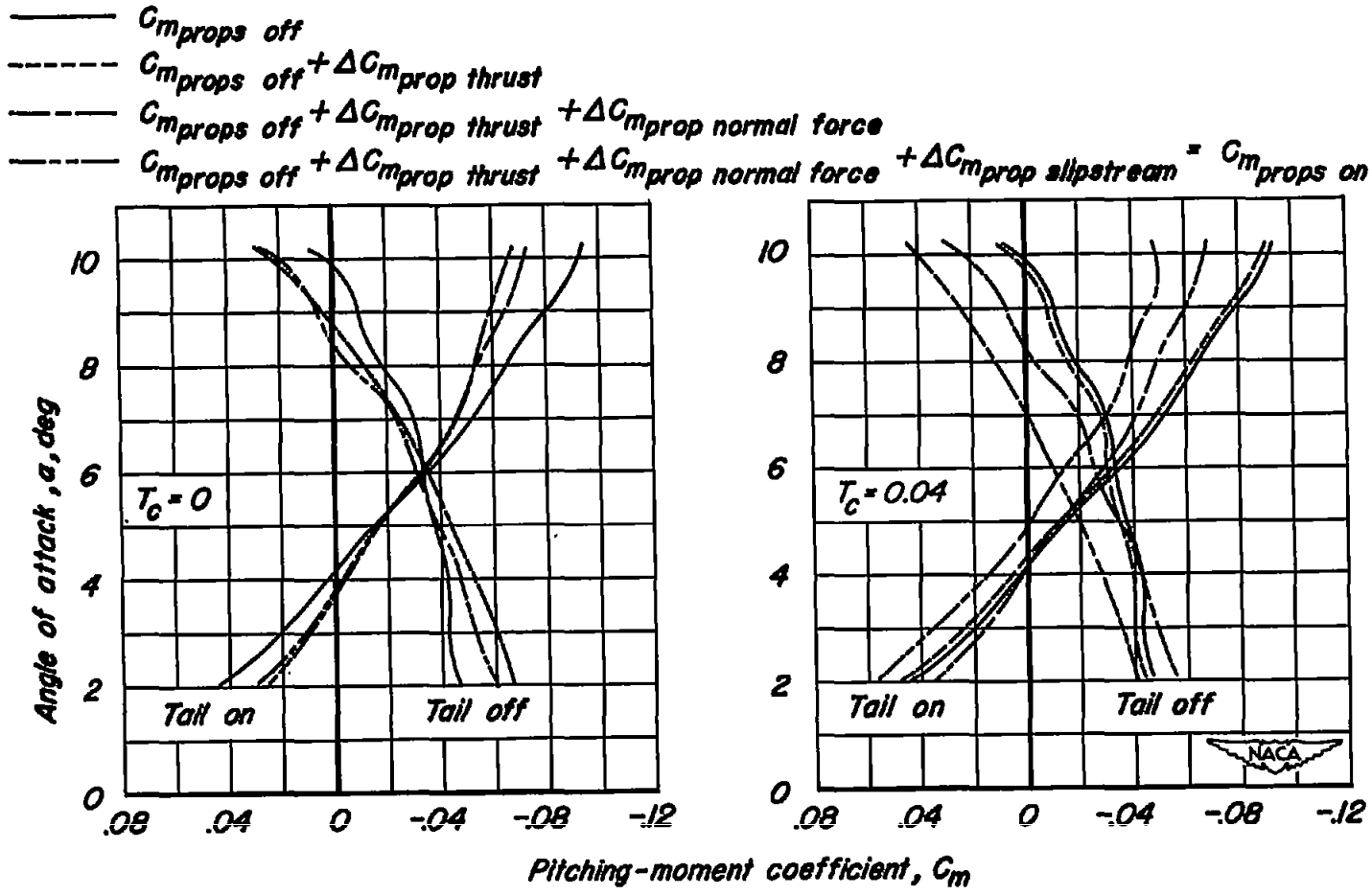

(a) M = 0.70

Figure 58.- The various effects of operating propellers at constant thrust on the pitching-moment characteristics of the model. Tail height = 0 b/2, $i_t = -4^\circ$, $\beta = 51^\circ$, R = 1,000,000.

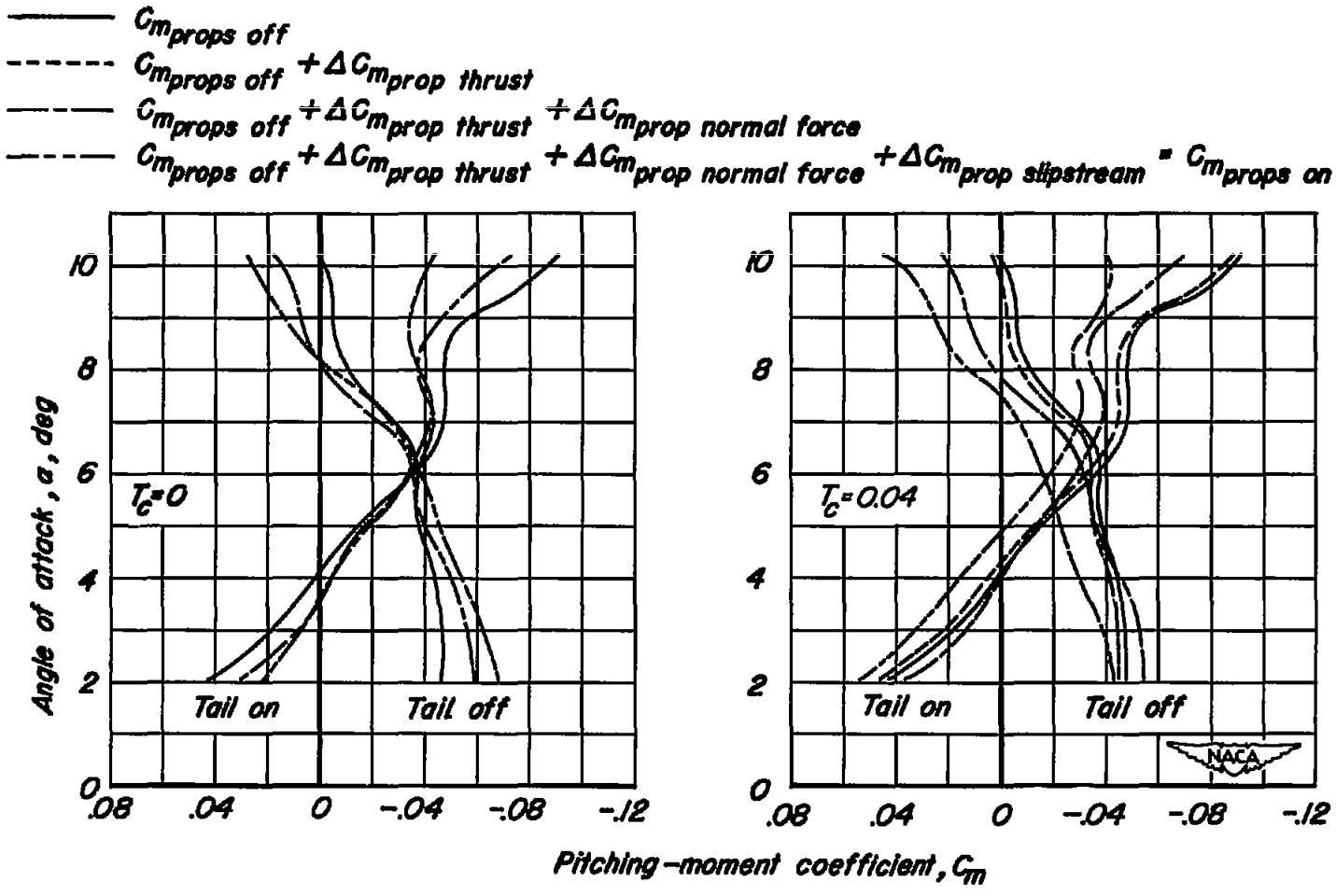

(b) M = 0.80

Figure 58.- Continued.

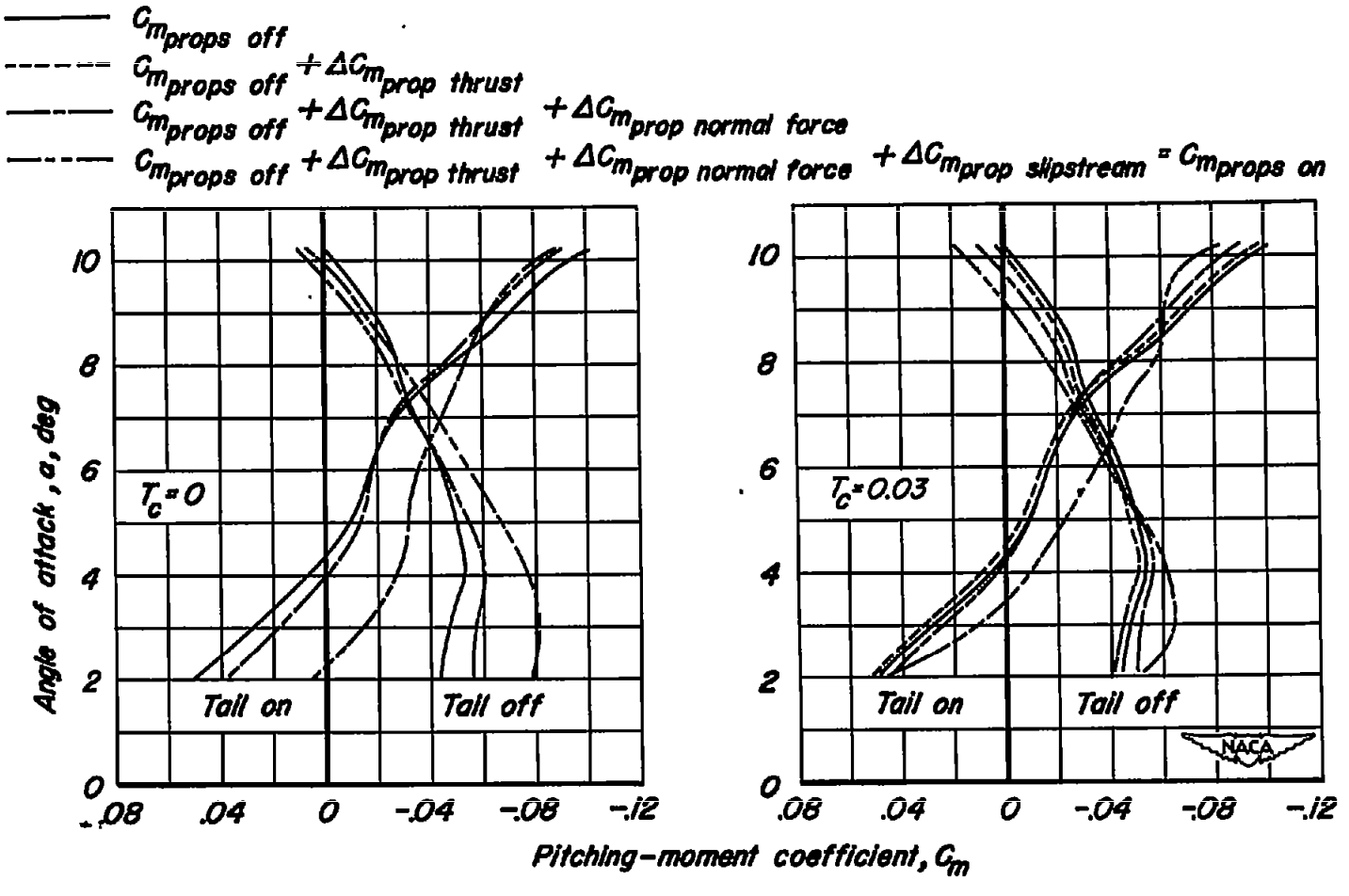

(c) M = 0.90

Figure 58.- Concluded.

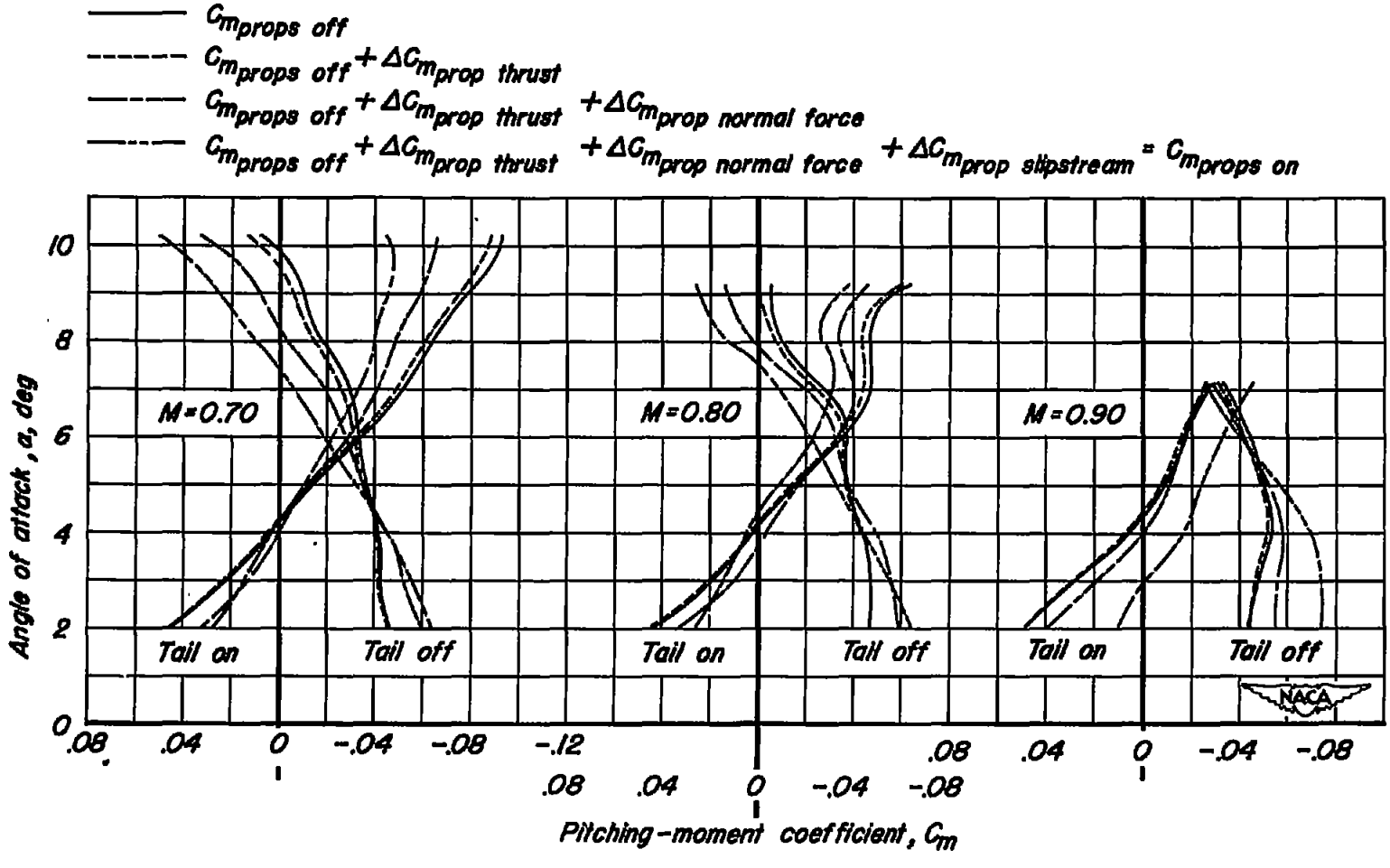

(a) 2500 hp per engine.

Figure 59.- The various effects of operating propellers at constant simulated horsepower on the pitching-moment characteristics of the model. Tail height = 0 b/2, $i_t = -4^\circ$, $\beta = 51^\circ$, R = 1,000,000.

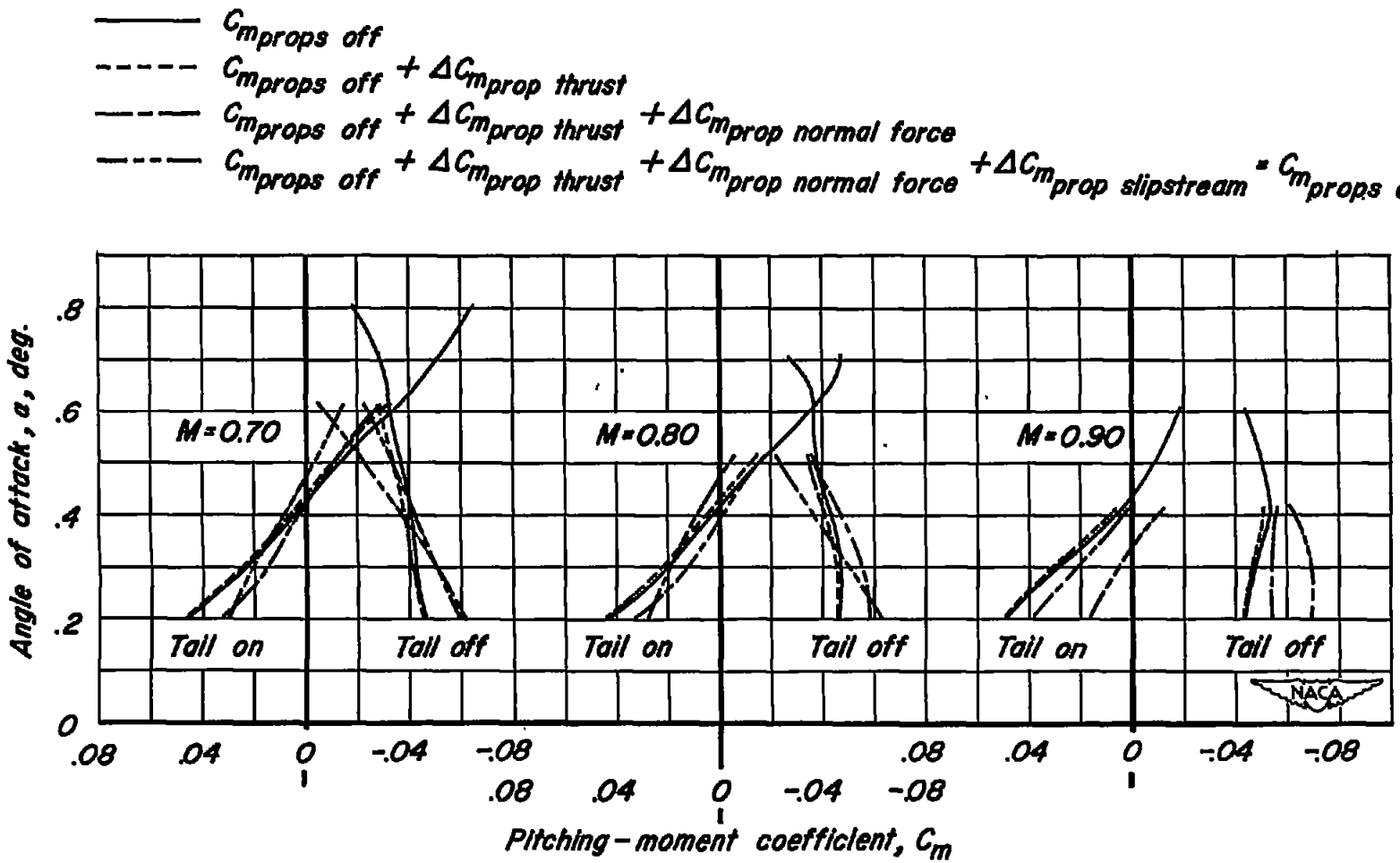

(b) 5000 hp per engine.

Figure 59.- Concluded.

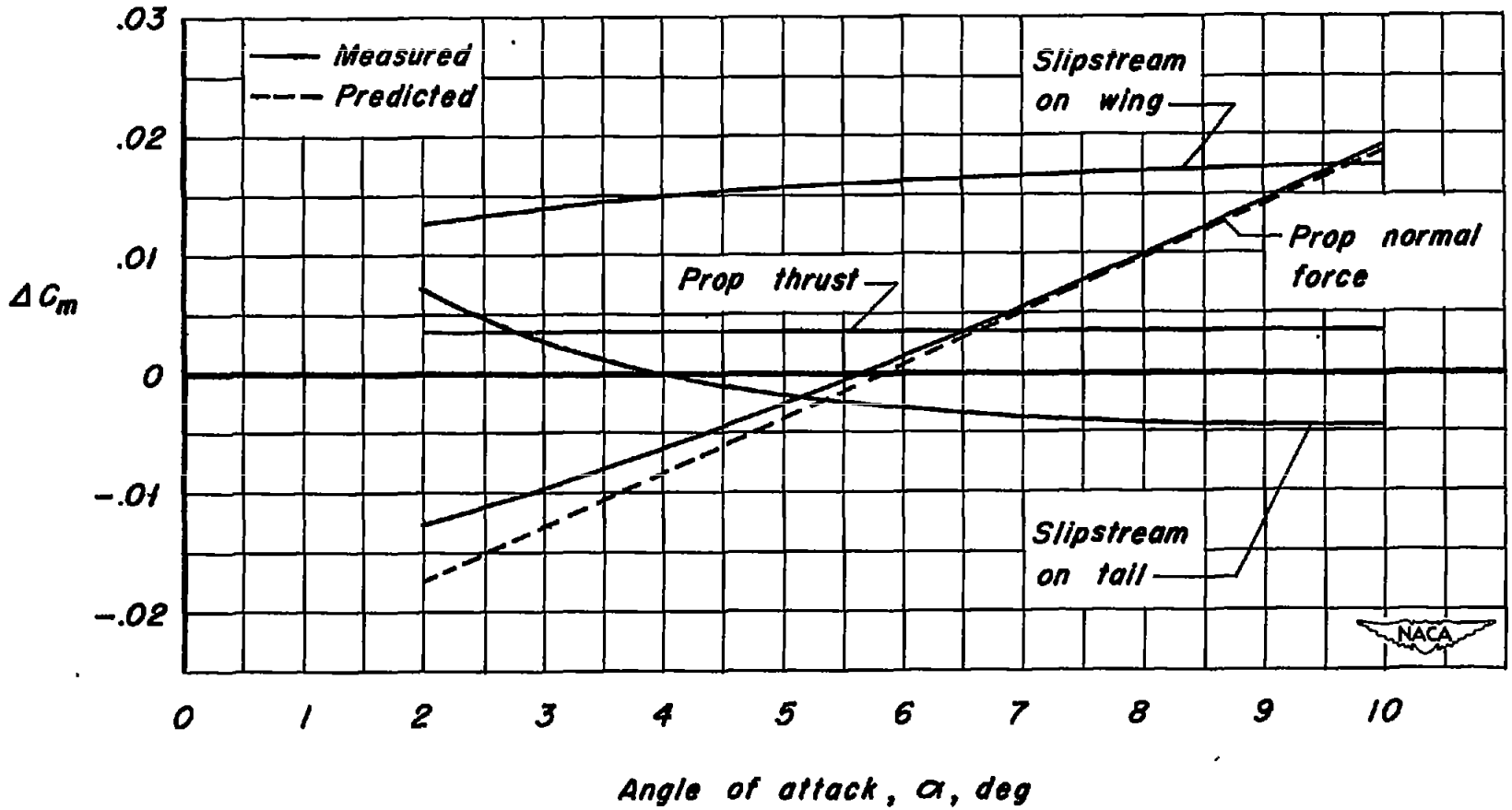

Figure 60.- Comparison of the measured and predicted effects of propeller normal force on increment of pitching moment and the measured effects of propeller thrust and slipstream on increment of pitching moment. M = 0.80, T_c = 0.04, tail height = 0 b/2, i_t = -4°, β = 51°, R = 1,000,000.

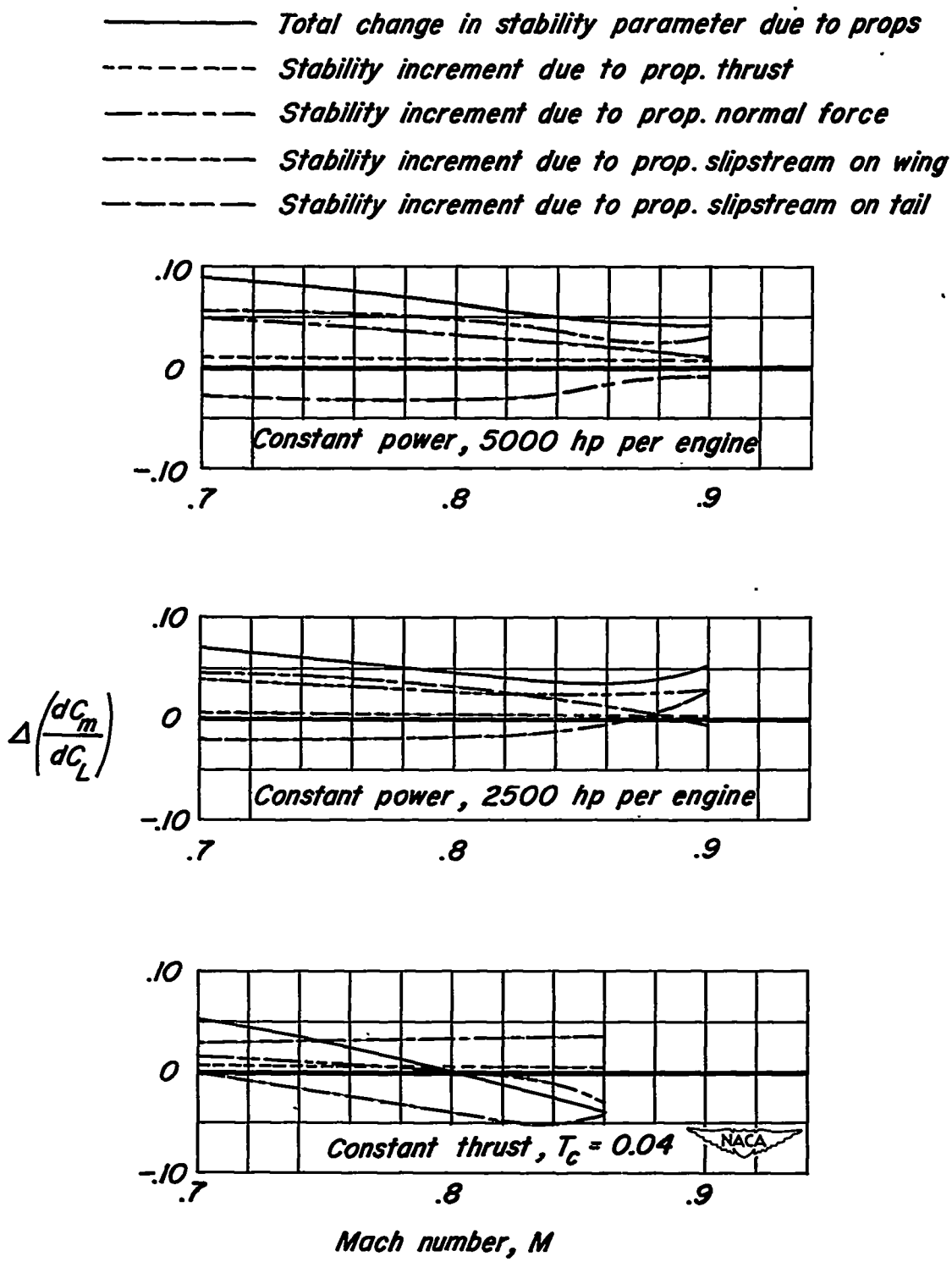

Figure 61.- The variation with Mach number of the various effects of operating propellers on increment of pitching-moment-curve slope. C_L = 0.40, tail height = 0 b/2, i_t = -4°, β = 51°, R = 1,000,000.

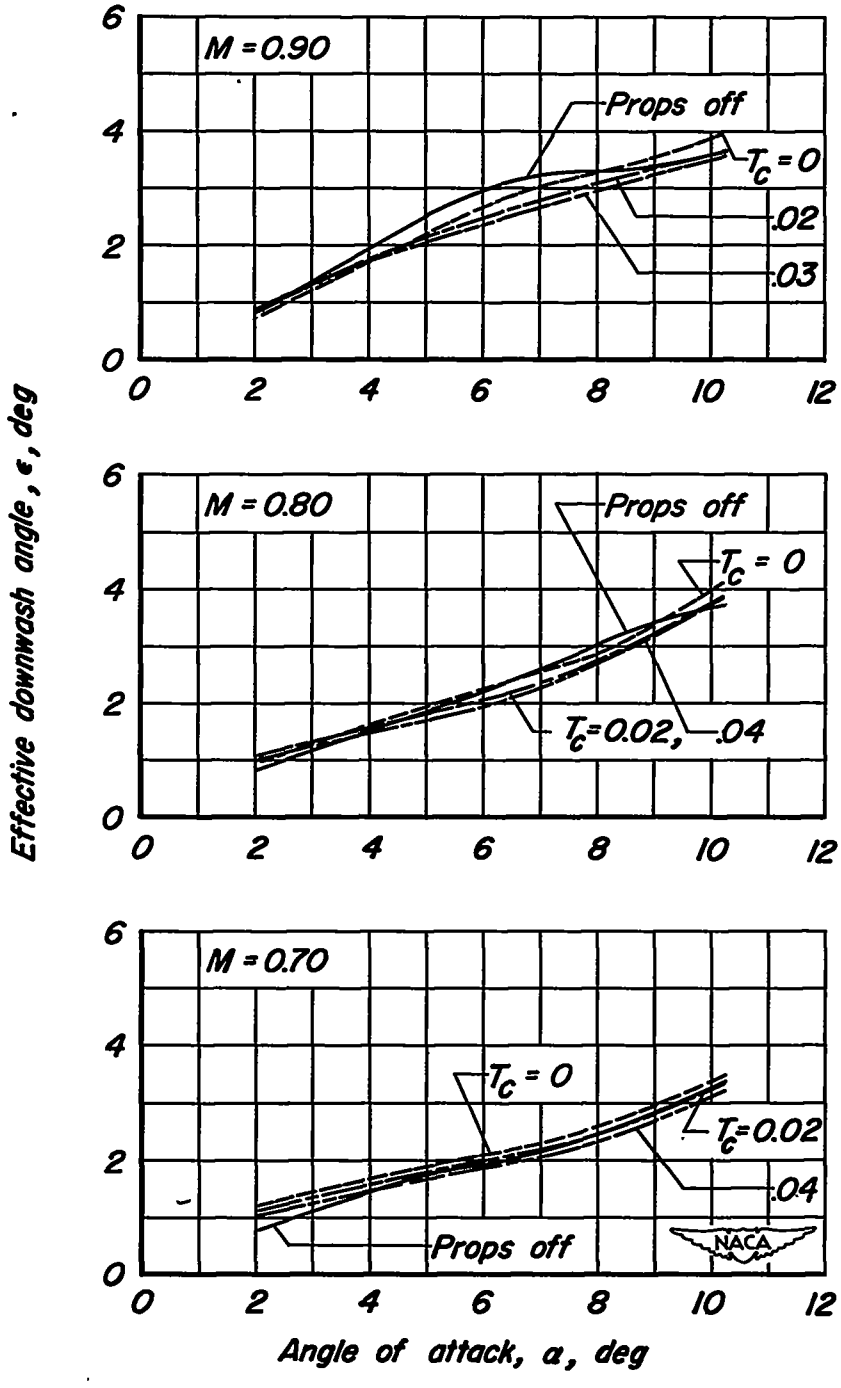

Figure 62.- The effect of operating propellers on the variation of downwash angle with angle of attack. Tail height = 0 b/2, $\beta = 51^{\circ}$, R = 1,000,000.

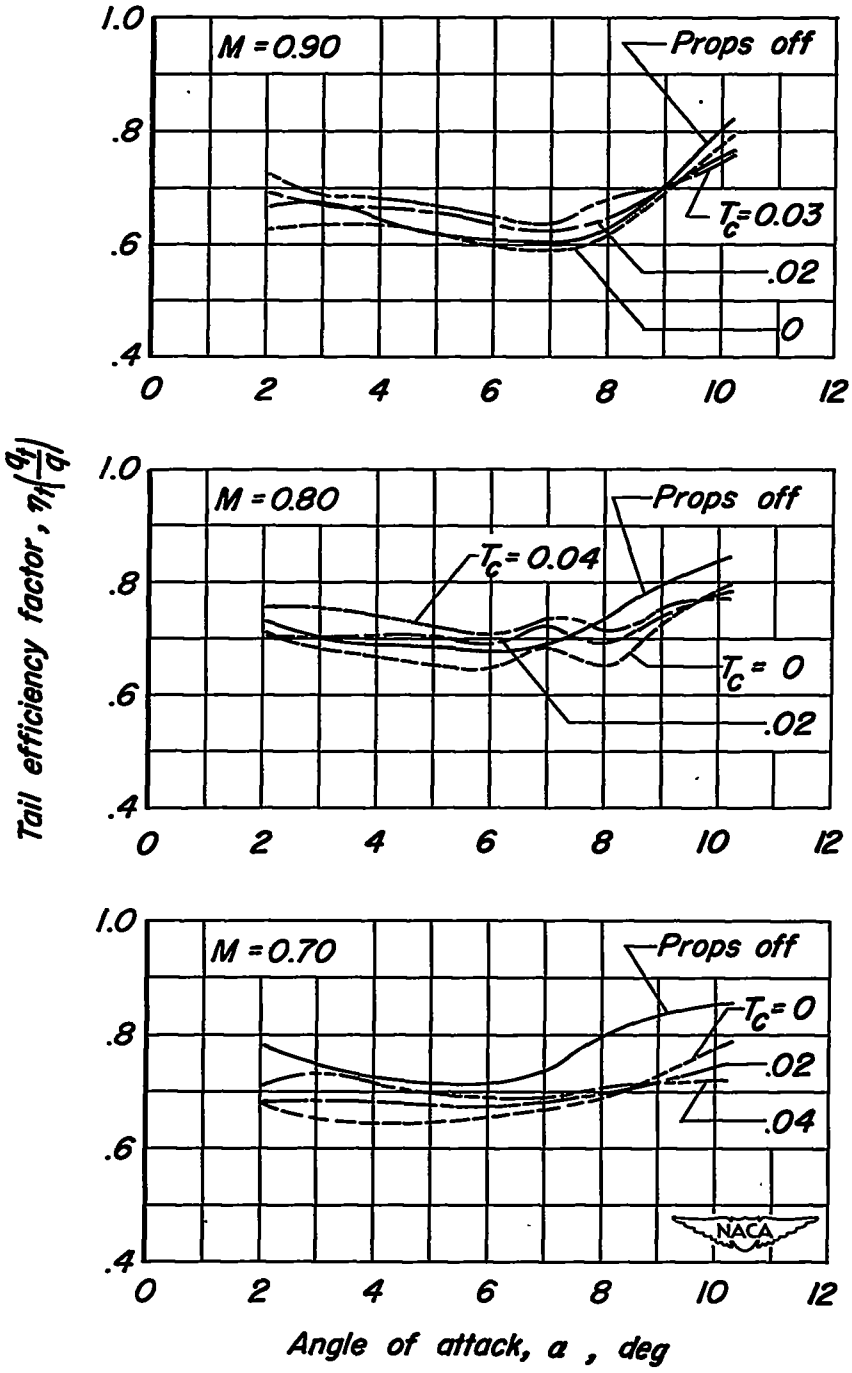

Figure 63.- The effect of operating propellers on the variation of tail-efficiency factor with angle of attack. Tail height = 0 b/2, $\beta = 51^{\circ}$, R = 1,000,000.

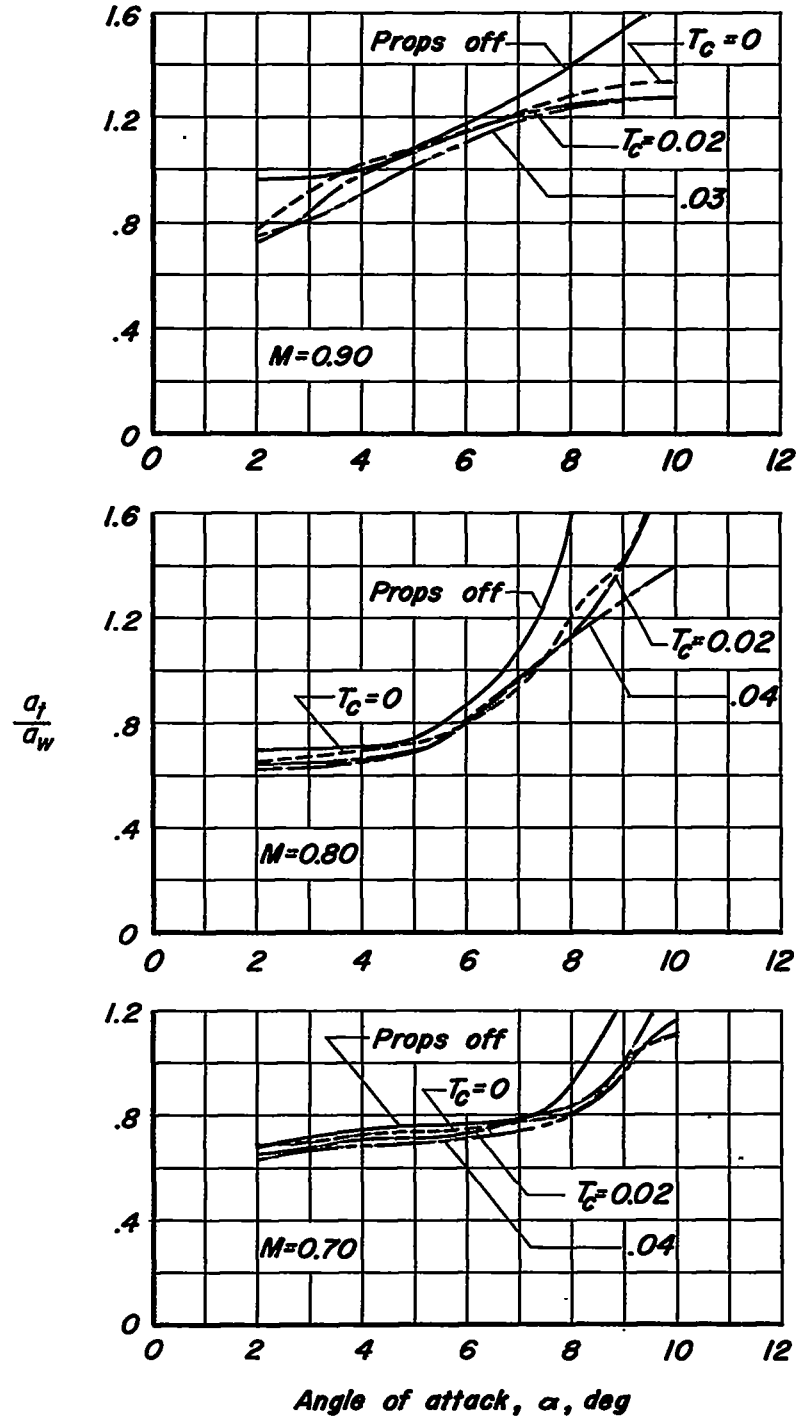

Figure 64.- The effect of operating propellers on the variation with angle of attack of the ratio of isolated horizontal tail lift-curve slope to tail-off lift-curve slope. $\beta = 51^{\circ}$, R = 1,000,000.

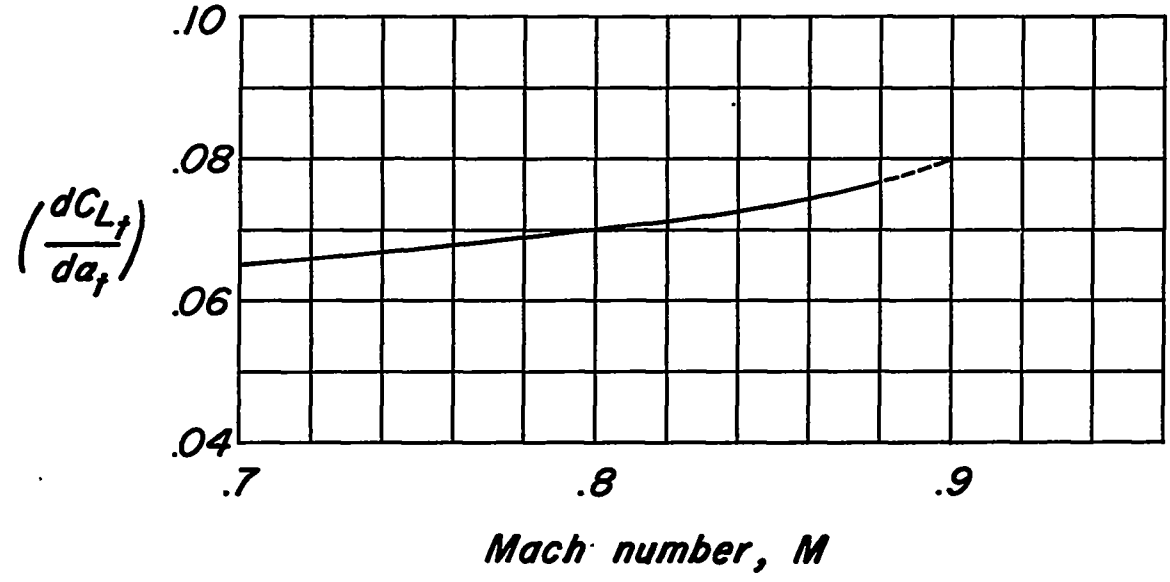

Figure 65.- The effect of Mach number on the lift-curve slope of the isolated horizontal tail. $\alpha_t = 4^\circ$, R = 2,000,000.

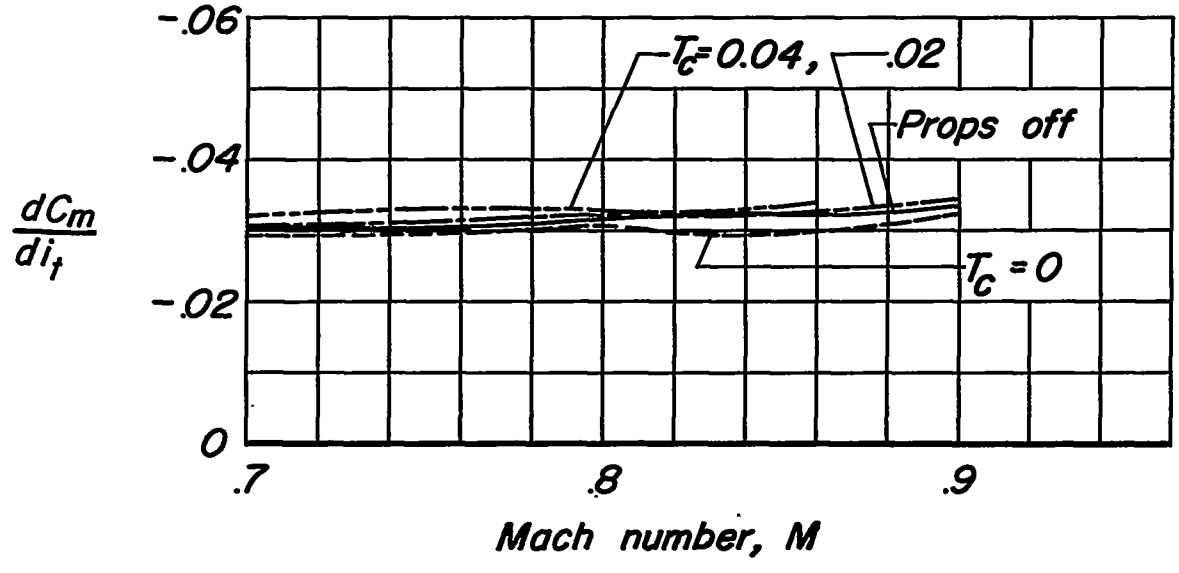

Figure 66.- The effect of Mach number on the effectiveness of the horizontal tail with and without operating propellers. $\alpha = 4^\circ$, tail height = 0 b/2, $\beta = 51^\circ$, R = 1,000,000.

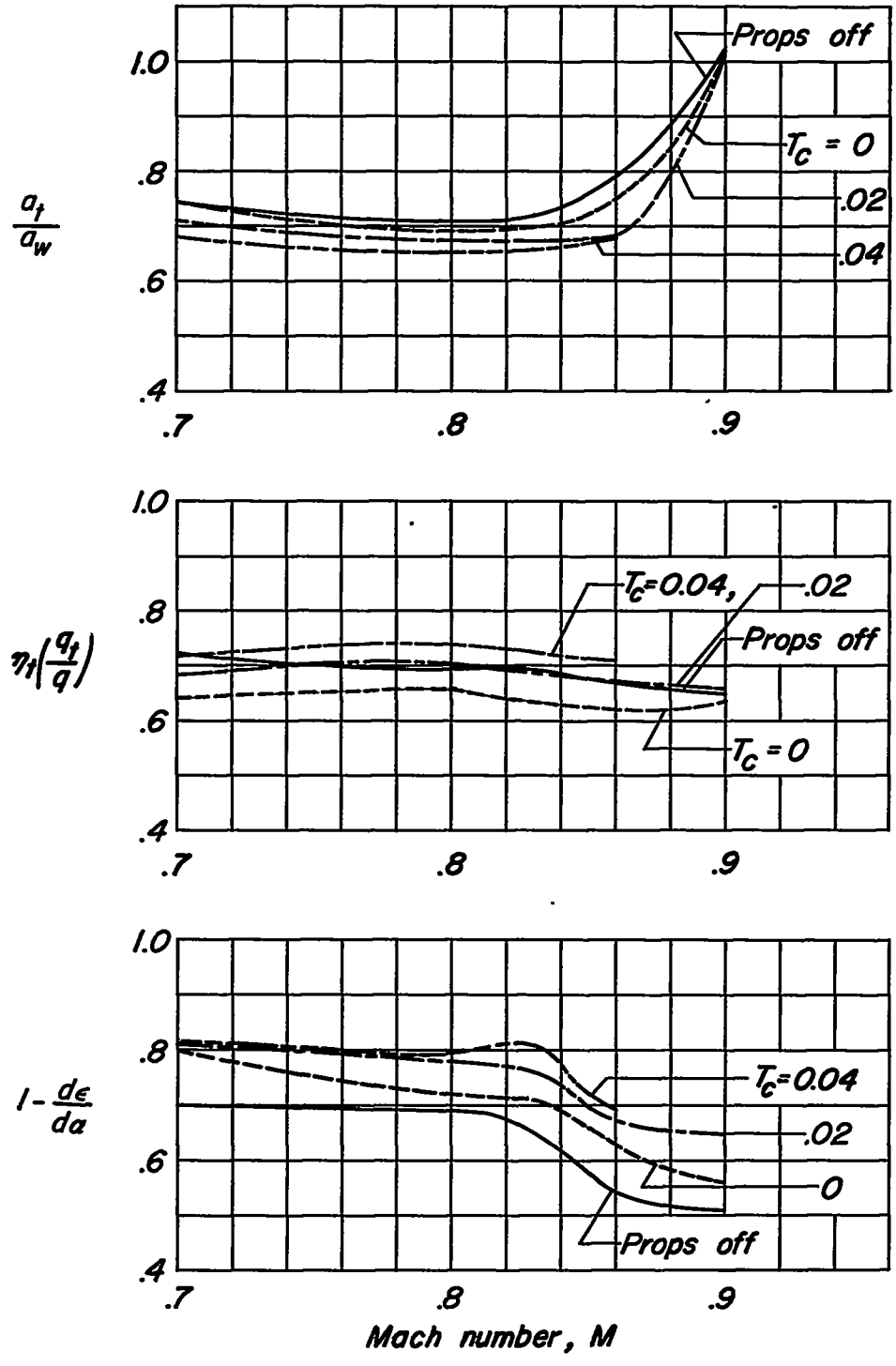

Figure 67.- The variation with Mach number with and without operating propellers of the factors affecting the stability contribution of the horizontal tail. $\alpha = 4^\circ$, tail height = 0 b/2, $\beta = 51^\circ$, R = 1,000,000.

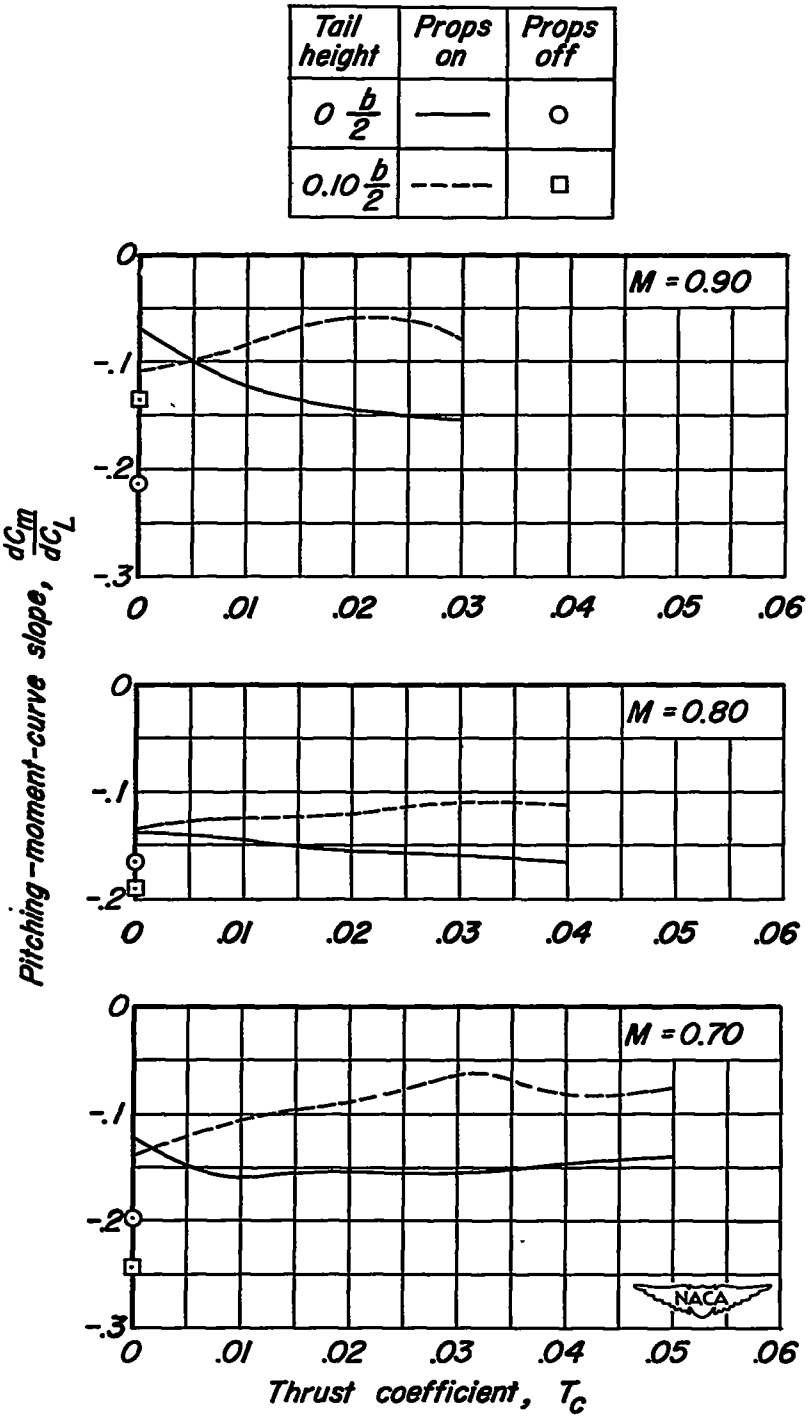

Figure 68.- The effect of horizontal-tail height on the pitching-moment-curve slopes of the model with and without operating propellers. $C_L = 0.40$, $i_t = -4^\circ$, $\beta = 51^\circ$, R = 1,000,000.

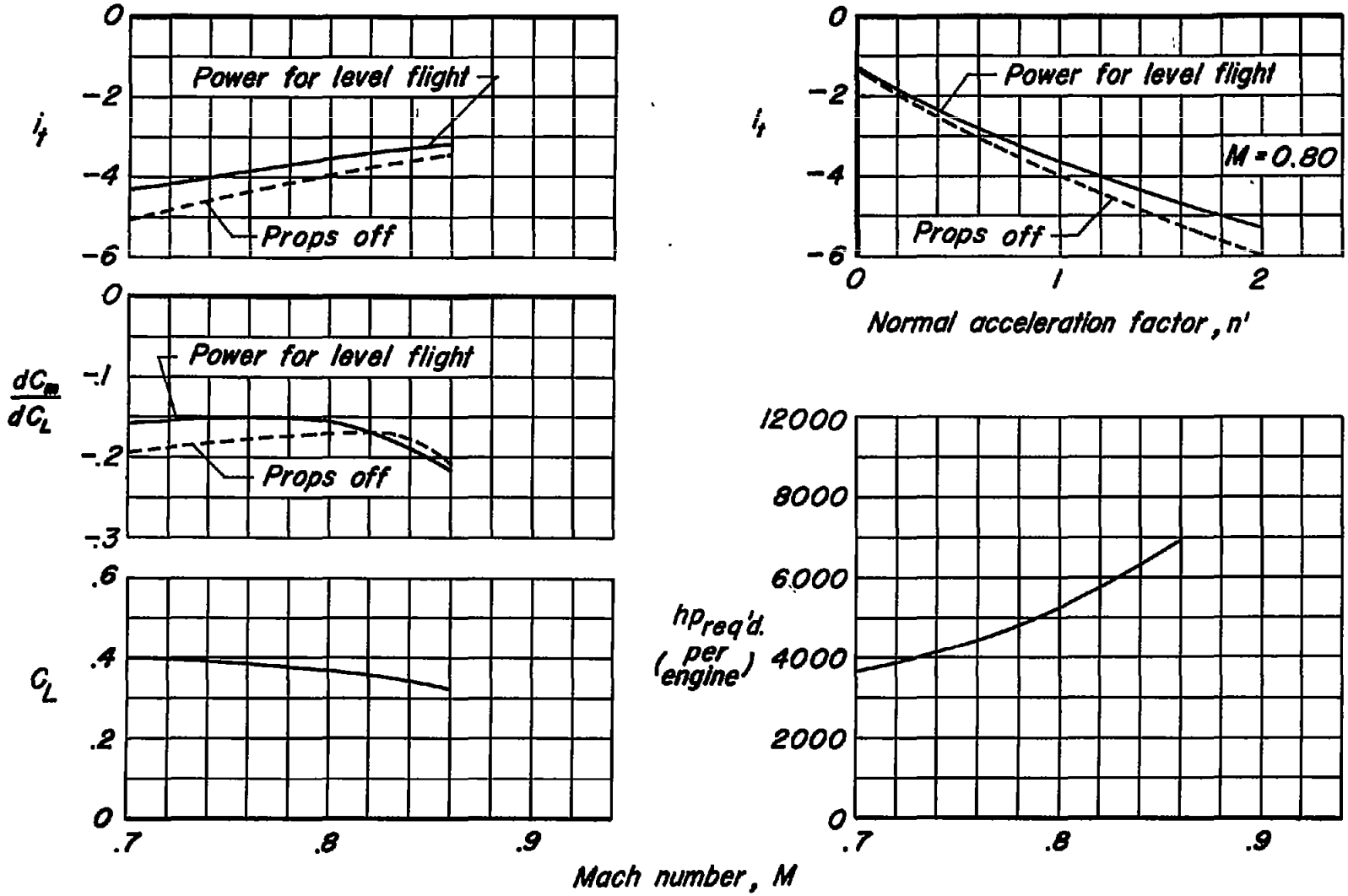

Figure 69.- Summary of the aerodynamic characteristics of a hypothetical four-engine airplane in level flight at 40,000 feet. Tail height = 0 b/2, $\eta_{assumed}$ = 0.65, W/S = 65 lb/sq ft.

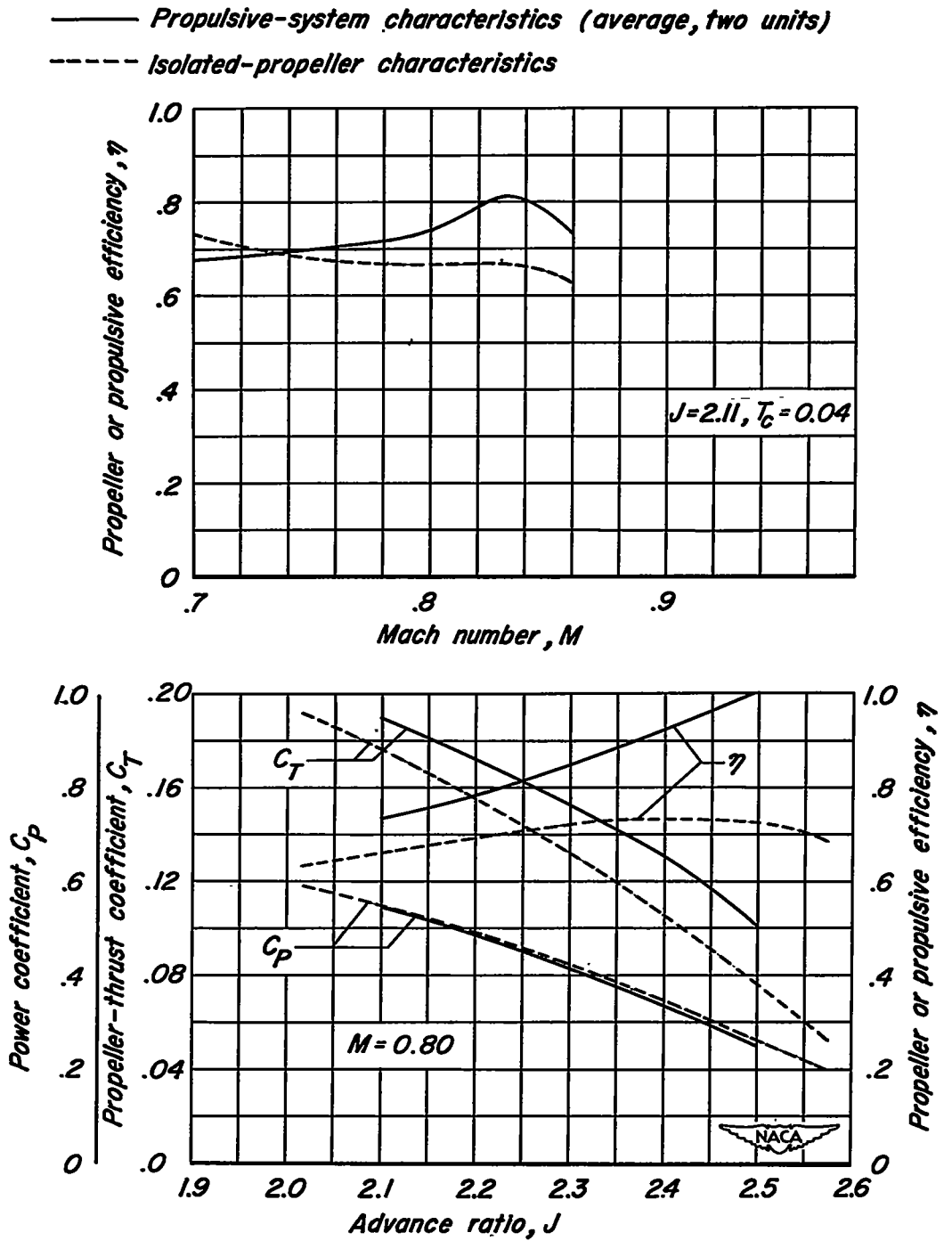

Figure 70.- Comparison of propulsive characteristics with isolated propeller characteristics. NACA 1.167-(0)(03)-058 propeller; A = 0°, β = 51°, R = 1,000,000.